The tyrocidines in the creation of antimicrobial cellulose and sterilising materials

by

Wilma van Rensburg
Master of Science (Biochemistry)

March 2020

Dissertation approved for the degree
Doctor of Philosophy (Biochemistry)

in the
Faculty of Science
at the
University of Stellenbosch

Supervisor: Prof. Marina Rautenbach
Department of Biochemistry
University of Stellenbosch

Declaration

By submitting this thesis electronically, I ***Wilma van Rensburg*** declare that the entirety of the work contained therein is my own, original work, that I am the sole author thereof (save to the content explicitly stated otherwise), that reproduction and publication thereof by Stellenbosch University will not infringe any third party rights and that I have not previously in its entirety or in part submitted it for obtaining any qualification.

Wilma van Rensburg — Name

March 2020 — Date

Summary

The rising resistance of pathogenic bacteria is of great concern, especially since resistance has been reported for five of the six common hospital acquired infections. Furthermore, continual infections occurring in the food industry can become costly to the companies and negatively impact consumers. Modified antimicrobial and antifouling materials and surfaces can be used limit the propagation of microorganisms on various surfaces and minimise the occurrence of infection and spoilage. These materials can prevent pathogenic cell adhesion or kill cells with the release of active compounds or kill cells on contact. Active compounds used to functionalise materials can include silver nanoparticles, antimicrobially active polymers, antibiotics, enzymes and chemically synthesised peptides. Due to the increased demand for more environmentally friendly practises, naturally produced antimicrobial peptides are considered. Antimicrobial peptides have a broad spectrum of activity and resistance is less likely to develop due to their membranolytic mode of action. Tyrocidines and analogues (Trcs) are antimicrobial cyclodecapeptides with a potent broad spectrum of activity against Gram-positive bacteria, filamentous fungi, human pathogens *Candida albicans* and malaria parasite *Plasmodium falciparum*. The peptides have been shown to adsorb onto various surfaces while maintaining activity, with a selectivity towards cellulose. The goal for this study was therefore to determine the application in commercial materials, the robustness of the cellulose-peptide material and conditions that dictate the cellulose-peptide interaction, as well as the molecular descriptors in peptide interaction.

In order to facilitate antimicrobial screening of Trcs treated materials, a high throughput solid surface assay was developed that gave comparable results to that observed with an industrial standard assay. The assay was developed for detection of antimicrobial activity within four hours, by utilising a cell viability or metabolic active dye, resazurin. A key factor that allowed for the fast detection was the use of ten times more cells per cm^2 as what is used in other solid surface assays, which allowed for the selection of only the best performing antimicrobial materials. Optimisation was confirmed with four model organisms *Listeria monocytogenes*, *Escherichia coli*, *Staphylococcus aureus* and *Pseudomonas aeruginosa* against materials that contained five different antimicrobial agents (gentamicin, bacitracin, ampicillin, gramicidin S and tetracycline).

Screening of association of a Trc mixture containing 11 cyclodecapeptides (Trc mix) to laboratory and commercial materials showed that the peptides in this mixture maintained activity and showed full inhibition of *L. monocytogenes* by peptide treated cellulose-based materials and

plastics. Trc mix treated cellulose proved to be robust in terms of cell exposure (killing up to 90% of 10^7 cells/cm^2 within 10 minutes of contact time), temperature and solvents. The only solvents that resulted in decreased activity were 1% *m/v* SDS and 70% *v/v* acetonitrile. Comparison between cellulose treated with tyrocidine and other antimicrobial peptides, showed the tyrocidine-cellulose outperforming the other peptides in terms of inhibition of *L. monocytogenes* and *E. coli.*

Study into the aggregation of Trcs using different percentages acetonitrile, as a denaturant of larger hydrophobic driven oligomers, showed the formation of two distinct types of oligomer groups: one group stabilised with hydrogen bonding formed at higher acetonitrile concentrations and one driven by hydrophobic interactions formed in aqueous solutions. The hydrophobic driven self-assembly structures were temperature stable and attributed to the temperature and solvent stability of the Trc-treated cellulose. It was also proposed to be a key factor in the association between Trc and cellulose, apart from the possible Maillard reaction that drive covalent linkages of some of the peptides in the initial seeding layer on the cellulose. Trcs showed a concentration dependent association linked to the formation of an optimal aggregate size that allows for association. Interaction with various cellulose derivates (glucose, cellobiose, hydropropyl cellulose) showed conformational changes of the peptide resulting in higher activity against *L. monocytogenes* and higher haemolytic activity. Studies into the molecular interaction, using FTIR and NMR, between cellulose and Trcs with the cellulose derivatives as cellulose models showed the amino acids exposed to the solvent environment to be most effected by the presence of the saccharides and therefore involved in the peptide:cellulose interaction.

The hypothesis is that the peptide forms self-assembled structures driven by hydrophobic interactions in aqueous solutions allowing the formation of hydrogen bonds between the hydroxyl groups on cellulose and Orn^9, Asn^5, and Gln^6 followed by Trp^4 and Tyr^7. Upon association the peptide oligomers would form a layered sheet like structure on the cellulose surface with above mentioned amino acids associated to the cellulose and exposed to the solvent environment. Thereby allowing for further self-assembly and/or antimicrobial activity as Orn^9 and Trp^4 are both key residues in the activity of Trcs. Furthermore, the peptide can arrange and re-arrange its conformation based on the environment to better suit association.

The creation of functional materials by harnessing Trcs' natural ability to associate to surfaces is more environmentally friendly but also creates an antimicrobial material that is robust in terms of activity and solvent/environment exposure. Therefore, materials functionalised with Trcs hold great promise in preventing surface colonization by resistant pathogens while still being "green" in its environmental footprint.

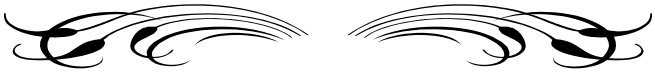

I am always doing that which I cannot do,

in order that I may learn how to do it.

Pablo Picasso

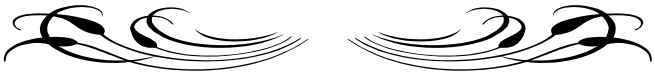

Acknowledgements

It is said that it takes a village to raise a child, and in some way the same counts for this degree. I would therefore like to express thanks and gratitude to my 'village':

I would like to thank Prof. Marina Rautenbach, my supervisor and promoter, for having the vision for this project and allowing me to fill in the details. Also, for her guidance and advise during the writing of this thesis and for all the financial support that came from the BioPEP funding.

I would like to thank the NRF for providing the necessary financial support for my degree.

Then I would like to thank Dr. Marietjie Stander, Malcolm Taylor (Central Analytical Facility, University of Stellenbosch) for their assistance with the mass spectrometry and seemingly endless patience.

I would like to thank the BIOPEP group of the past seven years for making coming to the lab an absolute joy, especially on days were the science did not feel worth it. Thank you for being my sanity in the last months of this degree, for being the perfect soundboards and the sushi. Thank you to the "De Rautenstrauss" lab for the coffee time and the chats. A special thanks to Dr. Helba Bredell for downplaying all the melodrama and being super honest when I needed to hear it.

To my friends, family and church community, whether you've joined the journey in the last month or were there from the beginning of my post-graduate studies; thank you for the encouragement and for never tiring of asking when this thesis would be done. I would like to thank my godparents, Nico and Sue Theron, for all their love and support. I would like to thank Teresa Collins for being with me every step of the way since my second year. It's been a ten-year journey where you've seen the worst and best days; thank you for holding me accountable to a higher standard of being than what I some days would have liked to. Thank you for having my back and your continual prayers and encouragement.

To my siblings, for matching my crazy and being the perfect distraction when I needed it.

I would like to thank my parents for walking this out with me, for creating the environment that allowed me to go after my dreams, for setting up the work boundaries when I was too close to everything to make good decisions for me. Thank you for all your love - I truly stood on the shoulders of giants.

My heavenly Father, for being my strength, my quiet place and for showing me that valleys can be crossed, and mountains can be conquered.

Table of Contents

CHAPTER 3: CREATING ROBUST ANTIMICROBIAL MATERIALS WITH STICKY TYROCIDINES

CHAPTER 4: ELUCIDATION OF TYROCIDINE-CELLULOSE INTERACTION

CHAPTER 6: CONCLUSIONS AND FUTURE STUDIES

Abbreviations and Acronyms

$[M+H]^+$	singly charged monomeric molecular ion
$[M+2H]^{2+}$	doubly charged monomeric molecular ion
$[2M+2H]^{2+}$	doubly charges dimeric molecular ion
ATR	attenuated total reflectance
ACN	acetonitrile
ANS	8-anilinonaphthalene-1-sulfonic acid
AgNPs	silver nanoparticles
AU	Arbitrary units
BHI	brain heart infusion
C. albicans	*Candida albicans*
CCS	collision cross section
CD	circular dichroism
CFU	colony forming units
CL	cellulose
E. coli	*Escherichia coli*
Ems	emission
ESMS	electrospray ionisation mass spectrometry
Ex	excitation
FTIR	Fourier transform infrared spectroscopy
GENT	gentamicin
GS	gramicidin S
GRAS	Generally Recognised As Safe
IM-MS	ion-mobility mass spectrometry
K_d^{app}	apparent dissociation constant
L. monocytogenes	*Listeria monocytogenes*
M_r	relative molar mass
m/z	mass over charge ratio
NMR	nuclear magnetic resonance
OD	optical density
Orn	ornithine
O	ornithine

PBS	phosphate buffered saline
Phc A	phenycidine A
Phc(s)	phenycidine(s)
RP-HPLC	reverse phase high performance liquid chromatography
SD	standard deviation
SE	standard error of the mean
SEM	Scanning electron microscopy
S/N	signal to noise ratio
TFA	trifluoroacetic acid
TFE	trifluoroethanol
Tpc A	tryptocidine A
Tpc B	tryptocidine B
Tpc B1	tryptocidine B_1
Tpc C	tryptocidine C
Tpc C1	tryptocidine C_1
Tpc(s)	tryptocidines(s)
Trc A	tyrocidine A
Trc A1	tyrocidine A_1
Trc B/B’	tyrocidine B/B’
Trc B1	tyrocidine B_1
Trc C	tyrocidine C
Trc C1	tyrocidine C_1
Trc(s)	tyrocidine(s)
Trc mix	tyrocidine mixture (tyrocidines purified from commercial tyrothricin)
UPLC-MS	ultra-performance liquid chromatography linked to mass spectroscopy

Preface

Bacterial colonisation of surfaces affects the medical and food industries alike which is of great concern due to the continual rise of resistance to commonly used antibiotics. As a result, much research is focused on creating materials that either prevent adhesion or result in cell death. Materials are functionalised with active compounds either by graft-on, graft-from or mixing approaches. However, current methods of determining the efficacy of the materials are time-consuming and laborious which limits screening of new materials. Active compounds used to create materials that lead to pathogenic cell death can include silver nanoparticles, antimicrobial polymers, enzymes, antibiotics and synthetic antimicrobial peptides etc. Naturally produced antimicrobial peptides are favoured for their broad spectrum of activity and decreased resistance development potential but also due to the increased demand for environmentally friendly practises.

Antimicrobial peptides produced by the soil organism *Bacillus brevis*, tyrocidines and tyrocidine analogues (Trcs), have a broad spectrum of activity against Gram positive bacteria, filamentous fungi, human pathogens *Candida albicans* and malaria parasite *Plasmodium falciparum*. Their membrane-oriented mode of action combined with multiple other targets makes the development of resistance less likely but also makes them ideal candidates for surface functionalisation since they can be associated to a surface and still elicit its antimicrobial response. Previous research on the creation of Trcs containing materials showed the peptide to be associated to various materials while still maintaining activity against *M. luteus.* Trcs showed a selectivity towards cellulose, and the resulting active material was found to be quite robust. Investigation into the scope of materials and conditions required for association can lead to a greater range of application but also define the parameters that determines association in the light of industrial scale production of Trcs-containing materials.

The main goal of this project was to screen commercial surfaces to determine the commercial viability of tyrocidine-materials, determine the robustness of the active materials and elucidate the interactions between tyrocidine (Trc) and cellulose that allow for its unique association and activity. The following objectives had to be completed in order to reach this goal:

1. Production and purification of commercial Trc mix, tyrocidine extract produced from unsupplemented and amino acid supplemented media and isotopically labelled peptides

followed by ESI-MS characterization to determine identity and purity. (Chapter 3 and Chapter 4 – Supplementary data)

2. Optimization of a resazurin based solid surface assay with four model organisms for the quick high-throughput screening of peptide functionalized materials. (Chapter 2)
3. Creation of tyrocidine-based antimicrobial materials (Chapter 3)
    a. Treatment of various laboratory acquired and commercial surfaces with Trc mix, assessing the amount bound in terms of fluorescence and activity against *Listeria monocytogenes*.
    b. Determining the robustness of the tyrocidine:cellulose association with changes in the association and dissociation environment including a range of acetonitrile concentrations, pH ranges, water washes and other solvents
    c. Treatment of cellulose with different antibiotics to determine the uniqueness of the cellulose:Trc mix interaction
4. Investigation of molecular and activity aspects of tyrocidine-cellulose interaction (Chapter 4)
    a. Ascertaining the kinetics of tyrocidine association to cellulose as a model surface, in competition with simple saccharides, using fluorescence
    b. Monitoring changes in peptide conformation with circular dichroism in the presence of glucose
    c. Determining the association of peptide to cellulose in competition with simple saccharides regarding its activity towards *L. monocytogenes* and red blood cells
    d. Defining the molecular interactions between the peptides and soluble saccharides through FTIR
    e. Confirming the direct interaction of peptide with cellulose utilising solid state NMR
5. Investigation of oligomerisation and activity aspects of tyrocidine-cellulose interaction (Chapter 5)

a. Determining the effect of acetonitrile on peptide oligomerization and stability with ion-mobility mass spectrometry, circular dichroism, fluorescence and melting temperature determinisations

b. Assessing the change in oligomerisation due to acetonitrile changes on peptide association and dissociation to cellulose with fluorescence and activity against *Listeria monocytogenes*

c. Visualisation of tyrocidine oligomers on surfaces with the use of scanning electron microscopy

This thesis consists of a total of six chapters: a literature review (Chapter 1), followed by four experimental chapters (Chapter 2-5) and lastly a concluding chapter that includes suggestions for future studies (Chapter 6). Each of the experimental chapters are written as independent units to ease future publication. Inevitable repetition of methodologies was kept to a minimum.

Outputs of PhD study

Oral Presentations

- Van Rensburg, W. (2017) Non-covalent functionalization of polymeric materials with antimicrobial peptides to create antimicrobial surfaces, Biochemistry Forum, University of Stellenbosch, Oral presentation. Ph.D Progress Talk
- Van Rensburg, W. (2017) Antimicrobial surfaces and films. Oral presentation, Tyrocidine Workshop, University Stellenbosch, Stellenbosch, South-Africa
- Van Rensburg, W. (2020), Biochemistry Forum, University of Stellenbosch, The tyrocidines in the creation of antimicrobial cellulose and sterilising materials. Oral defence of Ph.D. thesis (February 2020)

Conference outputs

- Van Rensburg, W, Rautenbach, M. (2018) Tyrocidines and the creation of antimicrobial cellulose. Poster, European Peptide Symposium (EPS), Dublin, Ireland
- Van Rensburg, W, Rautenbach, M. (2018) Tyrocidines and the creation of antimicrobial cellulose. Poster, International Meeting on Antimicrobial Peptides (IMAP), Edinburgh, Scotland
- Van Rensburg W, Rautenbach M (2018) Tyrocidines and the creation of antimicrobial cellulose. Journal of Peptide Science 24, S107-S107

Patent

- Rautenbach M, van Rensburg, W. (2015-06-02, PCT/IB2015/054166; 2015-12-10, WO2015186058A1). Method for preventing or treating microbial growth on a manufactured product. Patent registered in South Africa 2016 (SA2016/08601), Australia 2019 (Patent 2015270120). Patent accepted in USA (Patent 15/315,755) and China (Patent 201580040786.2) and registration to be finalised in 2020.

Industrial outputs

- Rautenbach, M, Vosloo, JA, Van Rensburg W (2017) Assay validation of MicCon kit for microbial contamination detection in industrial samples. Technical Report for Kensai-Plascon (work based on chapter 2)
- Licencing of the patented technology to FlexiGreen for incorporation in biodegradable/ compostable plastic bags and plastic ware (based on results from Chapter 3)

Peer-reviewed articles

- Juhl, DW, Van Rensburg, W, Bossis, X, Vosloo, JA, Rautenbach, M, Bechinger, B. (2019) Tyrocidine A interactions with saccharides investigated by CD and NMR spectroscopies. Journal of Peptide Science, 25 (5) 1-11, DOI: 10.1002/psc.3163
- Wenzel, M., Rautenbach, M., Vosloo, J.A., Siersma, T., Aisenbrey, C.H., Zaitseva, E., Laubsher, W.E., van Rensburg, W., Behrends, J.C., Bechinger, B. and HAmoen, L.W. (2018) The multifaceted antibacterial mechanisms of the pioneering peptide antibiotics Tyrocidine and Gramicidin S. *MBio*, 9 (5), 802 -818, DOI: 10.1128/mBio.00802-18
- Vosloo, J.A., Beims, H., Allsopp, M.H., van Rensburg, W., von der Ohe, W., Steinert, M., Rautenbach, M. (2017) Tolerance of honey-bee adults and larvae toward tyrothricin peptides derived from *Brevibacillus parabrevis.* Apidologie, 48(6), 833-844, DOI:10.1007/s13592-017-0528-0

Expected outputs

- Van Rensburg, W., Rautenbach, M. Fast throughput method to determine the activity of antimicrobial polymeric materials. Manuscript in preparation for Journal of Microbiological Methods. (Chapter 2)
- Van Rensburg, W., Rautenbach, M. Creating robust antimicrobial materials with sticky tyrocidines. Manuscript in preparation for Biomaterials (Chapter 3)
- Van Rensburg, W., Rautenbach, M. Biophysical characterization of tyrocidine-cellulose interaction (manuscript to be drafted from Chapters 4, 5 and 6)

Chapter 1
Literature Review

1.1 Introduction

It is estimated that 300 million people could die by 2050 due to antimicrobial resistance (Vikesland et al., 2019). Resistance development is generally attributed to continual use of antibiotics in medicine as well as agriculture. According to the World Health Organisation there are currently 12 organisms for which new antibiotics are needed: *Mycobacterium tuberculosis*, *Acinetobacter baumannii*, *Pseudomonas aeruginosa*, *Enterobacteriaceae*, *Enterococcus faecium*, *Staphylococcus aureus*, *Helicobacter pylori*, *Campylobacter spp*., *Salmonella spp*., *Neisseria gonorrhoeae*, *Streptococcus pneumoniae*, *Haemophilus influenzae* and *Shigella spp*. (Tacconelli et al., 2018). Five of these are part of the ESKAPE pathogens (*E. faecium, S. aureus, Klebsiella pneumoniae, A. baumannii, P. aeruginosa* and *Enterobacter spp.*) which are hospital acquired infections known for increased virulence and antimicrobial resistance (Mulani et al., 2019).

In the USA alone about 90 000 people die per year due to hospital acquired infections (Weinstein, 1998) by antibiotic resistant pathogens such as *S. aureus*, *E. faecalis* and *M. tuberculosis* (Levy and Marshall, 2004). To counter/prevent possible infections, hospitals are required to frequently replace catheters, wound dressings and medical ventilators which comes at a greater cost and inconvenience to the patient (Noimark et al., 2009). Great care is taken with the likes of implants and prosthesis, however, when infection does occur the 'cure' in most cases is removal (Ramsden et al., 2007). Furthermore, the surfaces surrounding the patient (work surfaces, drains, door handles etc.) plays a vital role in secondary spreading of pathogens and is commonly overlooked or disregarded (Noimark et al., 2009). Though hospitals take all precautions in ensuring the cleanliness of a patient's environment it simultaneously creates a selective stress for resistant pathogens through constant exposure to antimicrobial agents. Moreover, patients have a lower functioning immune system increasing the risk of infection (Angele and Faist, 2002). Therefore, the question then becomes not whether a patient will obtain a resistant infection but rather when.

Persistent infections are not only a concern in the medical sector, but also in the food/agricultural industries (Srey et al., 2013), especially with processed foods or exported crops subjected to long periods of storage where the food is more susceptible to infection. In the USA, microbial contamination of ready-to-eat food accounts for most of the microbial class

I recalls, two thirds of which can be traced back to product mishandling and faulty packaging (Cagri et al., 2004). The shelf-life of fresh-cut fruit and vegetables which are minimally processed (peeling, shredding, slicing and dicing) are shortened due to their vulnerability to microbial and sensory spoilage (Curutchet et al., 2014; Finnegan and O'Beirne, 2015; Mantilla et al., 2013). Of the total cases reported of foodborne illness in the USA, *Listeria* spp. has been listed as the fifth highest pathogen (Barakat and Harris, 1999; Grower et al., 2004). In 2017, a *Listeria monocytogenes* outbreak in a meat factory in South Africa caused a country wide recall of processed meats which led to great financial losses. The outbreak led to the recorded deaths of 200 people, the largest ever reported for one single outbreak (Boatemaa et al., 2019; Olanya et al., 2019). Moreover, a study on simulated factory conditions showed resistance development of *L. monocytogenes* to conventional cleaning routines (Pan et al., 2006). This poses a threat as the pathogen can be reintroduced to processing plants if the surrounding surfaces are not kept clean. Infection of food processing plants are not limited to Gram-positive bacteria, but can also include infections by Gram-negative *Pseudomonas* spp., *Klebsiella* spp. and *Aeromonas* spp. (Hood and Zottola, 1997).

It is evident that from the wide-spread occurrence of continual infection by pathogenic organisms that the initial surface infection and subsequent surface colonization is at the core of the problem. It would therefore be prudent to try to limit the propagation of microbes on surfaces thereby preventing microbial related product losses and human infection. This can be achieved with the use of active materials that kill pathogens or prevent adhesion.

1.2 Part I: Antimicrobial surfaces and materials

There has been a surge in the development of antimicrobial surfaces that either aim at preventing microbial adhesion or with adhesion aim at killing cells on contact or entrapment that would lead to cell death. This can be done by modification of surfaces to have antimicrobial properties or at the very least prevent adhesion/attachment. Colonization-prevention surfaces can be grouped into, but not limited to, two categories based on their functionality. Antifouling surfaces are surfaces that repel cells and/or prevent cell adhesion by creating unfavourable conditions for association. Antimicrobial surfaces prevent surface colonisation by killing the cells either on contact (contact killing surfaces), or by slowly releasing an active compound into the surrounding (slow release surfaces). Categorising active materials or surfaces depends greatly on the base material, intended active compound (antibiotics, antimicrobial agents, anti-fouling agents etc.) and method of attachment or containment of the active compound to the

base material. Though contact killing surfaces and slow release surfaces are two different types of surfaces in theory, they are difficult to be practically confirmed as such and will be discussed simultaneously. Furthermore, surface developments that make use of both antifouling and antimicrobial approaches have been reported (Cao et al., 2012). A distinction must be made between coatings, intrinsically active materials (refer to a review by Campoccia *et al.* (2013)) and materials functionalised with an active compound. The latter will be the focus of this literature overview.

The two groups of active materials, antibiofouling and antimicrobial, have vastly different methods of efficacy testing. Antimicrobial surfaces are the focus of this study and therefore only methods pertaining to these materials will be discussed, briefly. The methods used to determine the efficacy of materials include disk diffusion (Abou-Yousef and Kamel, 2015; De Moura et al., 2012; Gemili et al., 2009; Imran et al., 2010; Isquith et al., 1972; Rouabhia et al., 2014; Sayanjali et al., 2011), gel-overlay diffusion (Nguyen et al., 2008), aerosol cells covered material (Lin et al., 2003), 'sandwich' technique (bacterial culture is placed between two pieces of solid surface) (Ren et al., 2008), suspension in bacterial broth with CFU counts (Barbiroli et al., 2012; Pedrosa et al., 2014), surface incubation with inoculum with CFU counts (Pivec et al., 2017). The two main methods to determine the functional activity of the active surfaces among these methods are diffusion vs. numeration of surviving cells. The first requires diffusion of the active compound from the base material into the agar which is difficult with non-polar compounds (Elshikh et al., 2016; Sánchez and Kouznetsov, 2010). Moreover, the use of linkers in the creation in active materials with covalently attached antimicrobial compounds typically results in a lower active compound density which upon release, if it takes place, it would result in a smaller halo formation in comparison to a material with non-covalently absorbed or coated active compound (Green et al., 2011). The numeration of surviving cells in combination with a contact-based assay gives a better evaluation of the surface activity of an active material, however, this can become time consuming, expensive and laborious regarding the screening of active materials.

The main concern with having multiple methods is that there is no overlap in methods between studies, therefore no real comparison can be made and no clear definition of what constitutes 'good' activity of antimicrobial surfaces. Fortunately, recent reviews have been published (Sjollema et al., 2018; van de Lagemaat et al., 2017) to highlight pitfalls between methods and aid in selecting the best method for efficacy testing relating to the intended application. The best performing method (Japanese Industrial standard - JIS 2801 Z) allowed for surface activity

determination were the cells are in direct contact with the surface followed by numeration of surviving cells after incubation. As for the differentiation between contact surfaces and slow-release surfaces, a three-day water wash before testing was proposed (van de Lagemaat et al., 2017). Improvements on this method would be scaling to function within a high-throughput environment to screen multiple materials in a short time frame. Such an improvement can greatly assist in the development of antimicrobial materials. This has been addressed in this thesis in the development of a novel high throughput assay for the determination of surface antimicrobial activity is presented in Chapter 2.

1.2.1 Methods of material modification to create antimicrobial material and surfaces

The attachment or immobilization of an active compound to the base material can occur in three ways (1) 'graft-to' or adsorption (2) 'graft-from' or (3) incorporated in the initial step of creating the base material (Green et al., 2011). Selected examples of antimicrobial surfaces and materials and the methods employed to create these matrixes are given in Table 1.1. 'Graft-to' (Figure 1.1: A) broadly entails an activation step of the base material (oxidation, UV radiation, atmospheric plasma, ozonation etc.) creating functional groups such as amines, carboxylic acids, aldehydes or thiols (Felgueiras and Amorim, 2017; Green et al., 2011). Following activation, the already existing active compound can be covalently attached with or without a linker molecule. Practical examples are pre-treatment of cellulose with NaOH followed by a heating step with $AgNO_3$ which allows for the creation of silver nanoparticles (AgNPs) directly on the fibres (Pivec et al., 2017). Polymers such as *N*-alkylated high-molecular-weight polyetylenimine (PEI) can be graft-to textiles (cotton, wool, nylon and polyester) to give it an antimicrobial functionality (Lin et al., 2003). Furthermore, antimicrobial peptides such as the human cathelicidin, LL-37, can be graft-to titanium with the use of linkers such as polyethylene glycol (PEG) (Gabriel et al., 2006). Adsorption is the non-covalent attachment of an active compound to the base material through ionic bonds, hydrogen bonds or entanglement within the base material polymers during the solvent swelling step (Green et al., 2011). Two antimicrobial peptides, Tet-124 and Tet-124-Br, was attached to a PEI film by the electrostatic interactions between the peptide C-terminal carboxylic groups of tryptophan and glycine and the amino groups found on polyethylenimine (Hernandez-Montelongo et al., 2018). Adsorption of the bacteriocin nisin to porous silica has been achieved by prolonged incubation (Bower et al., 1995; Daeschel et al., 1992).

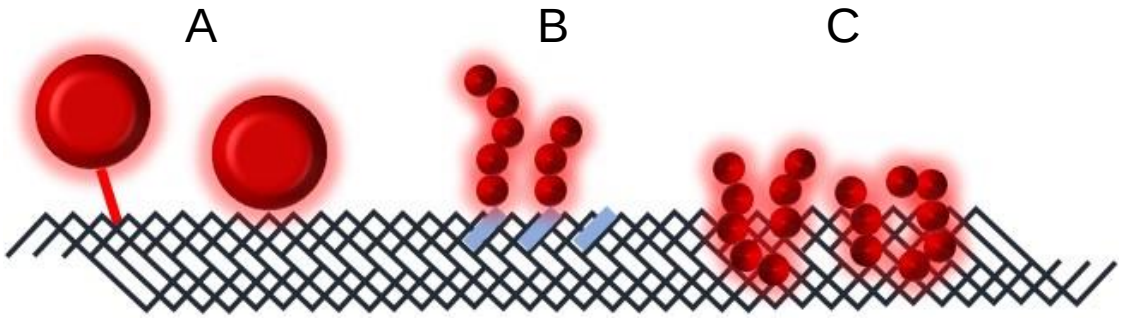

Figure 1.1: Representation of the methods of attachment in the creation of active materials (A) 'Graft-on' by means of covalent attachment or adsorption (B) 'Graft-from' as the creation of an active polymer directly on the material with the use of a initiator (blue) (C) Addition during solvent swelling/mixing step as the active compound is dispersed throughout the material.

'Graft-from' (Figure 1.1: B), also known as surface-initiated polymerisation, entails the creation of an active compound/polymer by using initiators on the base material. This method allows for a more controlled active compound density, compared to the 'graft-to' method, since the density of the initiator on the base material can be controlled (Felgueiras and Amorim, 2017). Atom transfer radical polymerization (ATRP), one of the most popular 'graft from' methods, was used to attach poly(tert-butyl acrylate) brushes onto cellulose, which was changed to poly(acrylic acid) with trifluoroacetic acid in order to form silver nano particles through the chelation of Ag^{+} with poly(acrylic acid)(Tang et al., 2009). Active materials can also be created with multiple rounds of ATRP by first attaching PEG monomethacrylate to polypropylene, followed by the attachment of 2-(dimethylamino)ethyl methacrylate (Yao et al., 2008).

The last method of attachment is the incorporation of an active compound during the creation of the active material (Figure 1.1: C). Some base material polymers require a swelling step in a pre-set solvent system, before it is cast into a film or electrospun into a fibrous mat. This can be taken advantage of for the incorporation of an active compound. AgNPs are either mixed into the base material (e.g. hydroxypropyl methylcellulose) before it is cast in a film (De Moura et al., 2012) or added to the material (e.g. cellulose acetate) before is it electrospun (Son et al., 2006, 2004). It is also achieved by soaking the material in a solution of active compound that is absorbed into the material such as nisin being adsorbed into bacterial cellulose (Nguyen et al., 2008).

Table 1.1: Selected examples of methods employed in the creation of antimicrobial surfaces and materials

Method	Base material	Active compound
Graft-on		
Pre-treatment of cellulose with NaOH followed by a heating step with $AgNO_3$	cellulose fibres	silver nanoparticles
Functional groups created on textile treated with 4-bromobutyrylchloride	cotton, wool, nylon and polyester	*N*-alkylated high-molecular-weight polyethylenimine (PEI)
Covalent attachment with hydrophilic PEG spacer	titanium	antimicrobial peptide LL-37
Electrostatic interactions between base and active compound	polyethylenimine	antimicrobial peptide Tet-124
Graft-from		
ATRP attachment of poly(tert-butyl acrylate) brushes	cellulose	silver nanoparticles
ATRP attachment of PEG monomethacrylate and 2-(dimethylamino)ethyl methacrylate brushes	polypropylene	quaternary amine salt
Incorporated		
Added during the dissolving and heating step required to make films	hydroxypropyl methylcellulose	silver nanoparticles
Added to fibre preparation before electrospinning	cellulose acetate	silver nanoparticles
Absorbed into cellulose	cellulose	antimicrobial peptide nisin

1.2.2 Antifouling surfaces

Anti-adhesion surfaces or antifouling surfaces work based on preventing adhesion of microorganisms by modification of the surface to create less favourable conditions for adhesion. The application thereof is typically aimed at preventing biofilm formation which occurs in three stages: attachment, the formation of microcolonies followed by the maturation of the biofilm (Costerton et al., 1995; Donlan, 2000). Maturation of a biofilm includes the production of an exopolysaccharide matrix that can both protect the biofilm and adhere it to the infected surface (Costerton et al., 1995; Dunne, 2002). The exopolysaccharide serves a method to provide nourishment to the cells within the biofilm by concentrating nutrients from the environment (Carpentier and Cerf, 1993; Costerton et al., 1987), but more importantly capture antimicrobial agents thereby contributing to the observed biofilm resistance (Donlan,

2000). Surfaces colonized by one microbial species usually leads to the attachment of other microbial species creating a mixed biofilm containing anything from bacteria, yeasts and fungi which contributes to the observed resistance (Donlan, 2000). Once formed, biofilms are very difficult to remove (Shirtliff et al., 2002) which emphasises the importance of preventing attachment.

Attachment occurs in two stages: an initial reversible attachment and irreversible docking (Garrett et al., 2008). An intermediate factor between the initial attachment and docking is surface coating or film formation by the surrounding media or environment that could either hamper or promote adhesion (Garrett et al., 2008). The initial attachment of cells is influenced by the surface roughness (Ivanova et al., 2011; Mrabet et al., 2009) and hydrophobicity of abiotic material (Fadeeva et al., 2011). Electrostatic interactions can influence the attachment, but the main determining factor has been shown to be hydrophobicity (Liu et al., 2004; Garrett et al., 2008). Research into altering surface roughness to prevent adhesion has been shown to be difficult since different species react differently (Ivanova et al., 2011; Variola et al., 2014).

The hydrophobicity of surfaces is altered by creating nature mimicking structures or the addition of a hydrophobic compounds. Selected examples of antifouling surfaces and the methods employed to create these matrixes are given in Table 1.2. Laser modification has been used to mimic the micro- and nano-scale structures found on *Nelumbo nucifera* leaf on superhydrophobic titanium which was able to prevent the adhesion of *P. aeruginosa* (Fadeeva et al., 2011). A hydrophilic hybrid material of poly(2-hydroxyethyl methacrylate), PHEMA, brushes grafted onto silanized glass, prevented the adhesion of *Sa. typhimurium* (Mrabet et al., 2009). PHEMA is commonly used as a coating for cell culture flasks to prevent adhesion of cells. PEG grafted onto polyurethane surface prevented the adhesion of *S. epidermidis* and *E. coli* (Park et al., 1998). A combination of agents can also be attached as with acrylate and PEG grafted onto silica nanoparticles which prevented the adhesion of *S. epidermidis* (Holmes et al., 2009). There has also been research in to surfaces that have both anti-fouling and bactericidal activity. Dual function material containing *N*,*N*-dimethyl-2-morpholinone (CB-ring) that is hydrolysed to a zwitterionic carboxy betaine (CB-OH) when killing *E. coli*. CB-OH prevents bacterial adhesion and can be regenerated to CB-ring in an acidic environment (Cao et al., 2012).

Table 1.2: Selection of surface modifications in the creation of antifouling materials

	Base	Target Organism
Nature mimetics		
Laser to create structures found on *Nelumbo nucifera* leaf	titanium	*P. aeruginosa*
Active compounds		
PHEMA brushes	silanised glass	*Sa. typhimurium*
PEG	polyurethane	*S. epidermidis, E. coli*
acrylate + PEG	silica nanoparticles	*S. epidermidis*
N,*N*-dimethyl-2-morpholinone	gold	*E. coli*

1.2.3 Antimicrobial surfaces and materials

The basic principle behind slow release surfaces and materials is the release of either a fast, high burst of antimicrobial agent followed by a tail end of slower release of agent over time or the continual slow release of an antimicrobial agent. These matrices normally operate in a two-pronged system, killing bacteria on the surface as well as the surrounding planktonic cells which lends the technology to medical implants where the area operated is as susceptible to infection as the implant. However, common problems faced with the implementation of these functional matrices includes the development of resistance, lack of long-term activity, inflammatory responses and cytotoxicity (Glinel et al., 2012). Therefore, much of the research is focussed on controlling the release of the active agents. This can be done by either modification of the surface or material and compound to alter the rate of release or to create a base surface polymer that only releases active compound when presented with a pre-determined stimulus. Surfaces and materials can also be altered to release different active compounds at different time points (Holzapfel et al., 2013) to include both a slow release and contact killing mode of action (Li et al., 2006) or anti-adhesion properties (Ho et al., 2004; Hu et al., 2013; Yu et al., 2015) and to include various application specific properties such as bone- and tissue-integration and anticoagulation (Chua et al., 2008; Cloutier et al., 2014; Goodman et al., 2013; Jin et al., 2014; Zhao et al., 2011).

Contact killing surfaces differ from slow release matrices in that the active compounds must remain active while attached to the material. This can be detrimental to compounds that have intracellular targets in that direct attachment to the surface or material limits the mobility of the compound which would render it inactive (Lewis and Klibanov, 2005). Therefore, membranolytic compounds are more suitable to use for the creation of contact killing surfaces

(Bagheri et al., 2012; Green et al., 2011). There is no clear way to distinguish between contact active and slow release materials, except for antimicrobial materials where the active compound is absorbed into the base material. Practical examples include a slow release surface of carboxymethyl cellulose paper containing lactoferrin and lysozyme that could inhibit the growth of *E. coli* and *L. innocua* on veal strips over a two-day period (Barbiroli et al., 2012). Furthermore, nisin absorbed (>6 hours) into bacterial cellulose (produced by *Gluconacetobacter xylinus*) was reported to prevent *L. monocytogenes* growth on frankfurter sausages (Nguyen et al., 2008). As for the contact killing or possible slow release systems cellulose fibres with covalent attached AgNPs that could inhibit the growth of *S. aureus*, *K. pneumoniae* and *Candida albicans* (Pivec et al., 2017). Silver nanoparticles attached to poly(carboxybetaine methacrylate) (pCBMA) polymers on glass were able to inhibit growth of *E. coli* (Hu et al., 2013). Covalently attached gentamicin to Arg-Gly-Asp-Cys (RGDC)-functionalised bacterial cellulose (produced from *Acetobacter xylinum*) showed activity against *Streptococcus mutans* and can be used in a wound dressing application, since it was found to be non-toxic towards human dermal fibroblasts (Rouabhia et al., 2014). The modification of RGDC was to promote cell adhesion, spreading and wound healing. Textiles (cotton, wool, nylon and polyester) with covalently bound N-alkylated high-molecular-weight polyethylenimine (PEI) showed activity against *S. aureus*, *S. epidermis*, *E. coli* and *P. aeruginosa* (Lin et al., 2003). Selected examples of non-covalent and triggered release antimicrobial matrices and the methods employed to create these matrixes are given in Table 1.3.

Table 1.3: Examples of a selection of surface modifications in the creation of non-covalent and triggered release antimicrobial matrices

Active compound	Base	Target Organism
Absorbed		
lactoferrin and lysozyme	cellulose paper	*E. coli* and *L. innocua*
nisin	bacterial cellulose	*L. monocytogenes*
Contact or slow release		
Covalent attachment of AgNPs	textiles	*S. aureus*, *K. pneumoniae* and *C. albicans*
Silver nanoparticles attached to pCBMA	Glass	*E. coli*
Gentamycin	cellulose	*Str. mutans*
N-alkylated high-molecular-weight PEI	textiles	*S. aureus*, *S. epidermis*, *E. coli* and *P. aeruginosa*

1.3 Part II: Antimicrobial peptides derived materials and surfaces

Active compounds used in the creation of antimicrobial materials are quite diverse with comprehensive reviews published by Campoccia *et al.* (2013) and Hasan *et al*. (2013). Incorporation of silver nanoparticles (AgNPs) into materials is the most popular (De Moura et al., 2012; Hu et al., 2013; Pivec et al., 2017; Son et al., 2006, 2004), however, the use of TiO_2 nanoparticles as carriers for antimicrobial peptides has been reported (Li et al., 2017). Antimicrobially active polymers (Muñoz-Bonilla and Fernández-García, 2012) are also used to functionalise existing materials such as N-alkylated high-molecular-weight polyethylenimine (Lin et al., 2003). Other active compounds used to modify materials are quaternary ammonium silanes and polymers (Green et al., 2011), antibiotics (Muñoz-Bonilla and Fernández-García, 2012; Rouabhia et al., 2014), enzymes (Barbiroli et al., 2012) and synthetic antimicrobial peptides (Hilpert et al., 2009; Jeong et al., 2018; Li et al., 2017; Patch and Barron, 2002).

Considering the increased demand for environmentally friendly products (Sobrino-López and Martín-Belloso, 2008; Tharanathan, 2003), antimicrobial peptides have the potential to be the next generation of active agents for antimicrobially active surfaces. As multiple reviews have been written on antimicrobial peptides (Ageitos et al., 2017; Bahar and Ren, 2013; Rautenbach et al., 2016a; Reddy et al., 2004; Wimley and Hristova, 2011), this group of antimicrobial compounds will only be discussed in brief. They are ubiquitous in nature with sources spreading over multiple species as they form part of the innate immune system. They can be found in lactic acid bacteria producing Class I lantibiotics (e.g. nisin)(Bierbaum and Sahl, 2009) and Class II lantibiotics (e.g. pediocin)(Willey and van der Donk, 2007), soil bacteria (e.g. gramicidin S)(Tamaki et al., 1996), fungi (e.g. copsin or sillucin)(Bradley and Somkuti, 1979; Essig et al., 2014), plants (e.g. circulin A&B) (Tam et al., 1999), amphibians (e.g. magainin and PGLa) (Soravia et al., 1988; Van Belkum and Stiles, 1995), fish (e.g. pleurocidin)(Tam et al., 1999), reptiles (e.g. cathelicidin BF)(Wang et al., 2008), birds (e.g. fowlicidin 1)(Xiao et al., 2006) and mammals (e.g. cathelicidin LL-37)(Dürr and Sudheendra, U.S. Ramamoorthy, 2006; Hell et al., 2010). The linear peptides have a predominantly α-helical structures and most of the N-C cyclic peptides tend to form β-sheets. The disulphide-bonded peptides (e.g. defensins) and thio-ether containing peptides (bacteriocins) tend to have mixed structures. Despite the structural diversity, a shared characteristic of the antimicrobial peptides is an amphipathic structure, with the majority being cationic peptides (Reddy et al., 2004) although a few anionic peptides have been reported (Bahar and Ren, 2013).

Antimicrobial peptides often have a broad spectrum of activity against bacteria, fungi and viruses (Bahar and Ren, 2013; Reddy et al., 2004). These peptides are generally membrane active, but some have activity against intracellular targets such as DNA, RNA and protein synthesis as well as other modes of action (Bahar and Ren, 2013; Reddy et al., 2004; Rautenbach et al., 2016a). Membrane activity can be through a detergent-like membrane disruption, insertion into the membrane resulting in the destabilisation of the membrane or by pore formation (Wimley and Hristova, 2011). It is this membrane activity that makes them ideal for the development of active materials, especially when the material design requires covalent attachment or adsorption of the peptide. Therefore, prior knowledge of the mode of action of any compound is key in the development of active surfaces (Bagheri et al., 2012). The combination of both membrane activity and intracellular targets, makes the development of resistance less likely and antimicrobial peptides the ideal candidates to combat the rising resistance of pathogens against commonly used antibiotics.

Currently most research has been focussed on the incorporation of nisin to create active materials (Table 1.4) (Aveyard et al., 2017; Barbosa et al., 2013; Ercolini et al., 2010; Imran et al., 2010; Mauriello et al., 2005; Nguyen et al., 2008; Qi et al., 2011), especially since it has been approved as GRAS (Generally Recognised As Safe) for food preservation (Carmona-Ribeiro and Carrasco, 2014; Sung et al., 2013). A few studies have been done on other natural antimicrobial peptides magainin I (Héquet et al., 2011; Pedrosa et al., 2014), magainin II (Cao et al., 2018) and LL-37 (Gabriel et al., 2006; Pedrosa et al., 2014) but the full potential of natural antimicrobial peptides as active agents have yet to be fully explored. Furthermore, research is either focussed on covalent attachment of the antimicrobial or absorption into the material, adsorption to the base material with minimal leaching was not reported. The research on nisin adsorption to silica makes use of disk diffusion for activity determination that requires desorption (leaching) of nisin from the silica (Bower et al., 1995; Daeschel et al., 1992) which over time would render the material ineffective.

Previous studies on tyrocidines (Trcs), an antimicrobial peptide complex produced by a soil bacterium, showed the peptide complex maintaining activity against *Micrococcus luteus* after adsorption to various surfaces including cellulose, cellulose esters, cellulose nitrate, polyvinylidene fluoride, polypropylene and polystyrene (Rautenbach and Van Rensburg, 2017)(Van Rensburg, 2015).

Table 1.4: Selection of natural antimicrobial peptides involved in the creation of active surfaces.

Peptide	Origin	Mode of action	Size	Attachment	Activity	Reference
Nisin	*Lactococcus lactis*	Permeabilizes the membrane, inhibits the cell wall synthesis	3354	Mixed with material (hydropropyl methylcellulose/ cellulose acetate)	*S. aureus*, *L. monocytogenes*, *B. cereus*, *E. faecalis*, *Alicyclobacillus acidoterrestris*	(Imran et al., 2010). (Barbosa et al., 2013)
				Absorbed into bacterial cellulose	*L. monocytogenes*	(Nguyen et al., 2008).
				Covalent attachment to multi-walled carbon nanotubes with poly(ethylene glycol) linker	*E. coli*, *P. aeruginosa*, *S. aureus*, *B. subtilis*	(Qi et al., 2011)
				Grafted induced with atmospheric pressure plasma onto polystyrene	*S. aureus*, *L. monocytogenes*	(Aveyard et al., 2017)
				Covalent attachment to stainless steel	*L. ivanovii*	(Héquet et al., 2011)
LL-37	Human defence peptide	Membranolytic	4493.3	Covalent attachment to titanium with hydrophilic poly(ethylene glycol) spacer	*E. coli*	(Gabriel et al., 2006)
				Covalent attachment to cotton	*K. pneumoniae* & *S. aureus*	(Pedrosa et al., 2014)
Magainin I	*Xenopus laevis*	Membrane active	2409.9	Covalent attachment to cotton	*S. aureus*	(Pedrosa et al., 2014)
				Covalent attachment to stainless steel	*L. ivanovii*	(Héquet et al., 2011)
				Covalent attachment to silanized slides	*Sa. typhimurium*, *E. coli*	(Kulagina et al., 2006)
Magainin II	*Xenopus laevis*	Membrane active	2466.9	Covalent attachment to stainless steel	*S. aureus*, *E. coli*	(Cao et al., 2018)
Polymyxin B&E	*Paenibacillus polymyxa*	Cell wall and membrane active	1 301,6 1 155,5	Covalent attachment to silanized slides	*Sa. typhimurium*, *E. coli*	(Kulagina et al., 2006)
Cecropin A	*Hyalophora cecropia*	Membrane active	4003.8	Covalent attachment to silanized slides	*Sa. typhimurium*, *E. coli*	(Kulagina et al., 2006)
Tyrocidines	*Brevibacillus parabrevis*	Membrane active	1269.7 – 1347.7	Adsorption to various surfaces	*L. monocytogenes*, *M. luteus*	(Rautenbach and van Rensburg, 2017)

The Trc-cellulose material proved to be robust maintaining activity after multiple washes, temperature increases in water, pH ranges and solvent exposures. This natural cyclic decapeptide group's ability to associate to seemingly every material and robustness of the peptide-treated material created great interest in its mode of association and retained activity, as well as possible application Trc-derived antimicrobial materials. These peptides are therefore the focus of the studies reported here (Chapters 3-5) and will be discussed in more detail below.

1.3.1 The tyrocidines and analogues as antimicrobial peptides for the creation of antimicrobial materials and surfaces

In 1939 a bactericidal complex was isolated from a Gram-positive soil organism and upon characterization was found to be haemolytic, stable at high temperatures and wide pH ranges (Dubos, 1939). The bactericidal complex was later named tyrothricin due to the presence of tyrosine in most of the analogues. Tyrothricin is produced by the soil bacteria *Brevibacillus parabrevis*, formerly denoted as *Bacillus brevis* and *Bacillus aneurinolyticus* (Danders et al., 1982; Hansen et al., 1982; Katz and Demain, 1977; Seddon and Fynn, 1972; Troskie et al., 2014a) and consists of two groups of peptides: neutral linear gramicidins (±40%) and cationic cyclic decapeptides originally denoted the tyrocidines or Trcs (±60%) (Hotchkiss and Dubos, 1941b). Tyrothricin was the first antibiotic in clinical use even though it was discovered a decade after penicillin. The use of tyrothricin was limited to topical applications due to its haemolytic and leukocytolytic activity (Rammelkamp and Weinstein, 1942; Van Epps, 2006). Even with its limited application it has been found to have a broad spectrum of activity against Gram-positive bacteria (Dubos, 1939; Dubos et al., 1942; Spathelf and Rautenbach, 2009), nanomolar selective activity against the human malaria parasite *Plasmodium falciparum* (Rautenbach et al., 2007), synergistic activity with caspofungin and amphotericin B against biofilm forming *C. albicans* (Troskie et al., 2014b) and broad spectrum activity against filamentous fungi (Mach and Slayman, 1966; Rautenbach et al., 2016b; Troskie et al., 2014a). Interest in these peptides with regards to antimicrobial solid surface development lies with the ability of these peptides to attach to seemingly any type of surface. Previous research (Dubos, 1939) and our group have observed a loss of peptide over the purification steps and loss of peptide activity with the preparation of the peptides for microdilution assays. This led to a pilot study proving that the Trcs bind to various surfaces, while maintaining activity, with a preference to cellulose type surfaces (Van Rensburg, 2015). As this innovation has been patented (Rautenbach and van Rensburg, 2017) and in development, the tyrocidines and

tyrocidine analogues are the focus of this study and it will be discussed in more detail in the sections to follow.

1.3.1.1 Structure of tyrocidines

The general Trc cyclic decapeptide structure is *cyclo*-(f^{1}P^{2}X^{3}x^{4}N^{5}Q^{6}X^{7}V^{8}O^{9}L^{10}) where the lowercase abbreviations denote the D-enantiomer of the amino acid residue (Figure 1.2).

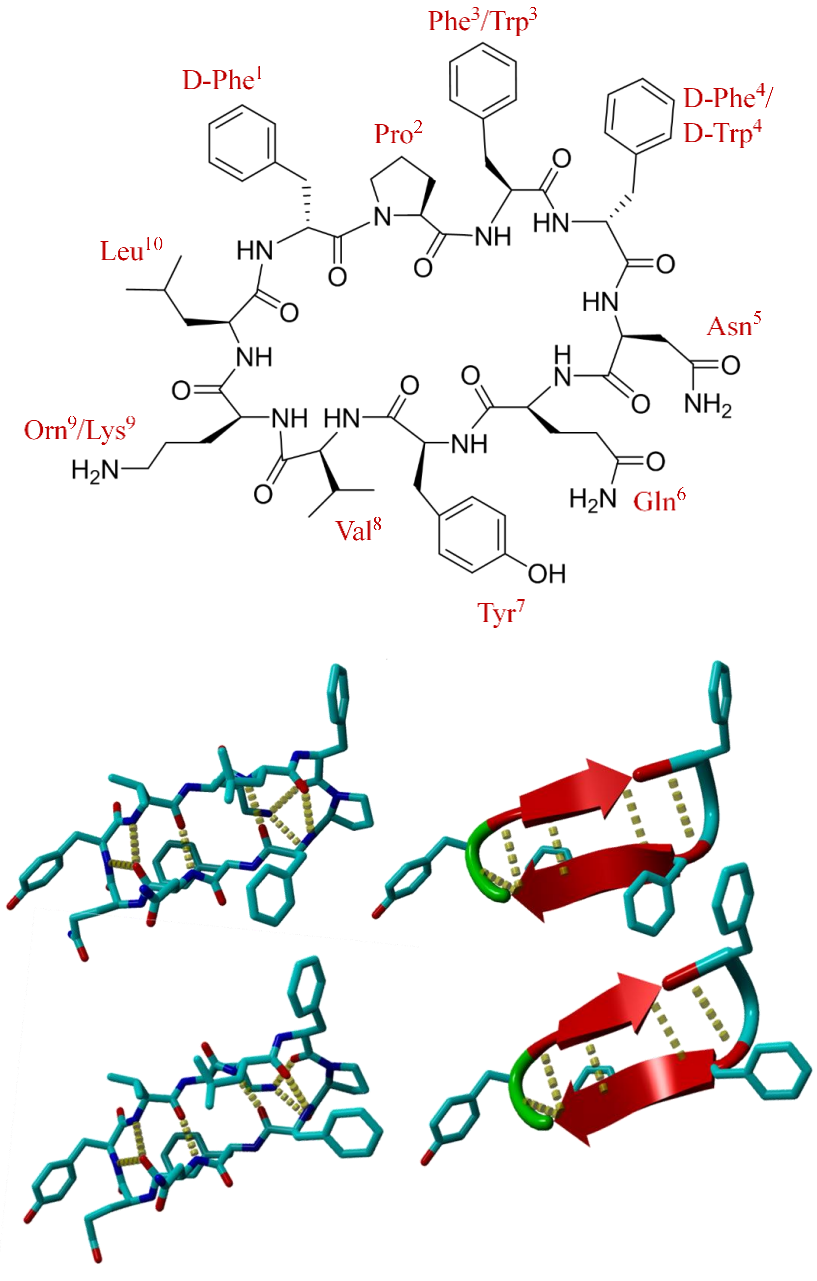

Figure 1.2: The primary structure of tyrocidine A (top), showing possible variable residues of Trp^{4}Phe^4 and Phe^{3}Trp^4 denoting tyrocidine B and B' respectively, Trp^{3}Trp^4 for tyrocidine C and Lys^9 denoting tyrocidine A_1, tyrocidine B_1 and tyrocidine C_1. Stick models of two conformers of tyrocidine A (bottom left), with their corresponding ribbon structures, indicating the aromatic residues (bottom right). The model structures are courtesy V. Kumar and were derived from those of Munyuki et al., 2013, utilising Yasara 11.3.2.

There are three main variable residues for tyrocidines: the variable dipeptide moiety at position 3 and 4 (X^3x^4 = $Phe^{3,4}$, $Trp^{3,4}$), position 7 (X^7 = Tyr^7/Phe^7/Trp^7) and at position 9 (O^9 = Orn^9/Lys^9)(Dubos et al., 1942; Paladini and Craig, 1954; Tang et al., 1992). Variance that occurs at the dipeptide unit denotes the A- (Phe^3Phe^4), B- (Phe^3Trp^4 or Trp^3Phe^4) or C-analogues (Trp^3Trp^4). Substitution at position 7 denote tyrocidines (Tyr^7), phenycidines (Phe^7) and tryptocidines (Trp^7), whereas the substitution at position 9 denote tyrocidines A, B and C (Orn^9) and tyrocidine A_1, B_1 and C_1 (Lys^9). The tyrocidines and tyrocidines analogues (Trcs) commonly found in extracts are summarized in Table 1.5.

The Trcs in aqueous solution have an antiparallel β-sheet secondary structure between Trp^3-Asn^5 and Val^8-Leu^{10} separated with a type I β-turn (Gln^6-Tyr^7) and type II' β-turn (D-Phe^1-Pro^2) (Kuo and Gibbons, 1980, 1979, Loll et al., 2014; Munyuki et al., 2013). The β-sheet structure is stabilised with four intramolecular hydrogen-bonds between Phe^3 O-NH Leu^{10} and Asn^5 NH-O Val^8, also Phe^3 NH-O Leu^{10} and Asn^5 O-NH Val^8 (Beyer et al., 1974; Gibbons et al., 1975; Kuo and Gibbons, 1980; Munyuki et al., 2013). The combination of the cyclization, β-sheet secondary structure and intramolecular bonds gives the peptide its solvent and temperature stability (Appleby et al., 1947; Helle et al., 1992). The Orn^9 side chain can also be involved in intermolecular H-bonding (Figure 1.2). The peptide can be split in two, along the β-sheet, having the Phe^4 and Orn^9 in one plane and the remaining amino acids in the other (Beyer et al., 1974; Gibbons et al., 1975) with Gln^6-NH exposed to the solvent environment (Kuo and Gibbons, 1980). This conformation creates the base for the amphipathic character of the peptide (Beyer et al., 1974). However, recent NMR and X-ray studies have shown that the Trcs are only truly amphipathic in their dimeric conformation (Loll et al., 2014; Munyuki et al., 2013). Moreover, the dimerization of these peptides and by extension the amphipathic character have been directly correlated to their antimicrobial activity (Loll et al., 2014; Munyuki et al., 2013; Salgado et al., 2001).

Unfortunately, the Trcs readily aggregate or form oligomers preceded by dimerization, leading to a variety of problems in solubilisation for biophysical analysis and antimicrobial activity testing. Previous studies indicated that tyrocidine A and tyrocidine C prefer the formation of homodimers, whereas tyrocidine B prefers to form heterodimers with tyrocidine A and tyrocidine C (Williams et al., 1972). The more hydrophobic tyrocidine A is more prone to aggregation, since homodimers were more prevalent, but up to pentamers were observed with mass-spectroscopy analysis (Munyuki et al., 2013). An increased hydrogen bonding in tyrocidines A, required for the higher order aggregation, was confirmed with CD analysis and

corroborated by an electrospray mass spectrometry (ESMS) analysis (Munyuki et al., 2013). In an ESMS analysis, monomers were observed to be the major species of the more polar tyrocidine C, but higher order structures up to trimers were detected (Munyuki et al., 2013).

Table 1.5: Summary of tyrocidines and tyrocidine analogues commonly found in the peptide profile

Identity	Abbreviation	Sequence[a]	Theoretical Monoisotopic M_r
Phenycidine A	Phc A	*cyclo*-(fPFfNQFVOL)	1253.6597
Tyrocidine A	Trc A	*cyclo*-(fPFfNQYVOL)	1269.6546
Tyrocidine A_1	Trc A1	*cyclo*-(fPFfNQYVKL)	1283.6703
Tryptocidine A	Tpc A	*cyclo*-(fPFfNQWVOL)	1292.6706
Tyrocidine B	Trc B	*cyclo*-(fPWfNQYVOL)	1308.6655
Tyrocidine B'	Trc B'	*cyclo*-(fPFwNQYVOL)	1308.6655
Tyrocidine B_1	Trc B1	*cyclo*-(fPWfNQYVKL)	1322.6812
Tyrocidine B_1'	Trc B1'	*cyclo*-(fPFwNQYVKL)	1322.6812
Tryptocidine B	Tpc B	*cyclo*-(fPWfNQWVOL)	1331.6815
Tryptocidine B_1	Tpc B1	*cyclo*-(fPWfNQWVKL)	1331.6815
Tyrocidine C	Trc C	*cyclo*-(fPWwNQYVOL)	1347.6764
Tyrocidine C_1	Trc C1	*cyclo*-(fPWwNQYVKL)	1361.6921
Tryptocidine C	Tpc C	*cyclo*-(fPWwNQWVOL)	1370.6924
Tryptocidine C_1	Tpc C1	*cyclo*-(fPWwNQWVKL)	1384.7080
Val/Ile-Gramicidin A	VGA/IGA	*formyl*-(V/I)GAlAvVvWlWlWlW-(Ea)	1881.0783
Val/Ile-Gramicidin B	VGB/IGA	*formyl*-(V/I)GAlAvVvWlFlWlW-(Ea)	1842.0675
Val-Ile-Gramicidin C	VGC/IGA	*formyl*-(V/I)GAlAvVvWlYlWlW-(Ea)	1858.0624

[a]Peptide sequences, as described by Tang *et. al.* (1992) where the amino acids are represented by conventional one-letter abbreviations except for ornithine which is represented by O; the L-amino acids are in uppercase and the D-amino acids in lowercase; *cyclo*, N-C cyclisation; (*Ea*) , ethanolamine.
[b]The theoretical monoisotopic M_r was calculated by using the residual molecular weights of the constituent amino acids.

As previously mentioned, linear gramicidins are produced with tyrocidine as part of the tyrothricin complex. The general structure of linear gramicidin is formyl-VGAlAvVvWlXlWlW-ethanolamine (lower case abbreviations denote D-amino acids) where X=W at position 11 denotes linear gramicidin A (VGA), X=F denotes linear gramicidin B (VGB) and X=Y denotes linear gramicidin C (VGA)(Table 1.5). Linear gramicidins should not

be confused with gramicidin S (GS) which is produced by another soil organism, *Aneurinibacillus migulanus.* GS is a cyclo-decapeptide with two identical pentapeptides and it shares 50% sequence similarity with Trcs in the VOLfP-moiety. Like the Trcs it has activity against Gram-positive bacteria, but also has activity against Gram-negative bacteria (Kondejewski et al., 1996).

1.3.1.2 Biological activity of tyrocidines

The Trcs have a broad spectrum of activity against Gram-positive bacteria such as *L. monocytogenes* (Spathelf and Rautenbach, 2009), *S. aureus* (Dubos et al., 1942), *Str. hemolyticus* (Dubos et al., 1942), and *M. luteus* (Spathelf and Rautenbach, 2009). It has activity against selected fungi such as *Neurospora crassa* (Mach and Slayman, 1966), and filamentous plant fungi such as: *Fusarium solani*, *F. verticillioides* and *Botrytis cinerea* (Troskie et al., 2014a). The peptides have a greater activity against *F. solani* and *B. cinerea* than the commercial fungicide bifonazole causing slower spore germination and hyperbranching of the hyphae (Troskie et al., 2014a). Activity has also been observed against planktonic and biofilm cells of the yeast *C. albicans* (Troskie et al., 2014b) and the human malaria parasite *P. falciparum* (Rautenbach et al., 2007). The Trcs have also been observed to have different activities against different strains of the same organism (Rammelkamp and Maxon, 1942), but this could possibly be related to the combination of Trcs in the Trc-preparation used in these studies. Though the Trcs are known to be primarily Gram-positive active, there have been isolated reports on its activity against Gram-negative bacteria (Chopra et al., 2010; Dubos and Hotchkiss, 1941; Rautenbach et al., 2015b; Vosloo et al., 2017).

The difference in activity between target organisms and strains can be attributed to the various Trcs analogues found in the tyrocidine extract. The Trcs showed activity in the micromolar range against planktonic *C. albicans* cells, with Phc A having the least activity compared to the other major analogues. It was also observed that Trc A had a higher activity than Trc C. The peptides, Trc A, Trc B and GS were also shown to prevent the formation of biofilms, whereas Phc A, Trp C and Trc C had a 2-fold lower activity. Biofilm eradication activity was also observed for Trc A, Trc B and Trc C (Troskie et al., 2014b). Trc B/B1 and Trc C/C1 have been shown to have a higher activity against Gram-positive *L. monocytogenes* (Spathelf and Rautenbach, 2009). Trc A has been shown be the most active against *F. solani* and *A. fumigatus,* whereas Trp C being the least active (Troskie et al., 2014a)(Vosloo, 2016).

The peptides work at an incredible rate acting as depolarising agents that destroys the membrane potential within 2-4 seconds (Mach and Slayman, 1966, Wenzel *et. al*. 2018). It was observed in *N. crassa* that Trcs (Trc A, B, C and Tpc C being equally active) caused a rapid release of the intracellular contents of the hyphae which included K^+, proteins, nucleic acids, nucleotides, non-dialyzable molecules and ultimately the disruption of the membrane potential (Mach and Slayman, 1966). The rate at which the reaction occurred, regardless of temperature, led to the conclusion that membrane disruption is the primary mode of action concerning hyphae, especially since the concentration needed for permeabilization was similar to the concentration needed to inhibit log-phase growth (Mach and Slayman, 1966). Studies with membrane impermeable dyes, SYTOX green and propidium iodide, against fungi and fungal model membranes (70:30; POPC:Ergosterol ratio) confirmed that membrane disruption was the main mode of action (Troskie et al., 2014a, 2014b). In *L. monocytogenes*, 60% lysis was seen after 30 minutes indicating a strong membranolytic mode of action (Spathelf and Rautenbach, 2009). However, there have been cases were there was no parallel between lysis and bactericidal effect of Trcs which points to the peptides also possibly having intracellular targets and that the lysis observed is a secondary response (Dubos, 1939; Rautenbach et al., 2007). Wenzel *et. al*. (2018) did the first detailed study on the mode of action of the Trcs by using Trc A and Trc C against *B. subtilis*. It was observed that the Trcs influenced the membrane integrity by forming pores, increased membrane fluidity of the membrane resulting in areas of increased rigidity and delocalizing membrane proteins. Furthermore, Trcs led to the dissociation of peripheral flotillin which in turn would affect protein secretion, signal transduction, membrane fluidity, membrane organization, respiration and signal transduction. Trcs were also shown to affect DNA-packaging and membrane synthesis. This combination of activities was attributed as the reason as to why Trcs can kill persister cells (not possible by ampicillin and chloramphenicol) and why resistance development against Trcs is highly unlikely. Studies of the effect of the Trcs on respiration and fermentation showed that the peptides inhibited both processes in *S. aureus*, *Str. hemolyticus* and baker's yeast (Dubos et al., 1942; Woodward and Hudson, 1957). Since data between target organisms differs in terms of whether membrane lysis is the primary mode of action, it is possible that the peptides change mode of action based on the target cell or target membrane, as well as their higher order conformation in the formulation or preparation used in the study.

Primarily bactericidal in its mode of action against bacteria, it has been reported that their activity is completely lost in the presence of blood or serum even when in direct contact with

the target cells (Robinson and Graessle, 1942). Similarly, it has been reported that activity seen against Gram-negative bacteria in buffer, was completely negated in the presence of media or some of the media constituents (Dubos and Hotchkiss, 1941). In contrast the linear gramicidins, which is bacteriostatic in their mode of action, does not lose its activity in blood and serum and neither does tyrothricin complex. However, both linear gramicidin and the tyrothricin complex need to be in direct contact with the cells to elicit its response in blood or serum (Robinson and Graessle, 1942). This loss of activity *in vivo* was also seen with a reported case of resistance of *S. aureus* found in an ulcer of a patient (Rammelkamp and Maxon, 1942) and that of tumours found in rats models even though the peptides where found to be active against tumour slices (Woodward and Hudson, 1957). Linear gramicidin A was found to negate the membranolytic activity of the Trcs (Aranda and de Kruijff, 1988), as well as surfactin inhibiting the activity of Trc C more than Trc B (Eyéghé-Bickong, 2011). Similar results were observed with surfactin and GS, which shares sequence similarity with Trcs, making it inactive and even protecting non-surfactin producers from the membranolytic effect of GS (Rautenbach et al., 2012). The activity of Trcs have also been reported to be hampered by Ca^{+}, but not effected by Mg^{2+}, K^{+} and Na^{+} (Troskie et al., 2014a). It could be that the Trc oligomerisation state can influence its mode of action and target specificity. In the early stages of discovery it was established that though the Trcs have a very broad spectrum of activity which is ideal for clinical application, the peptide complex is very haemolytic and leukocytolytic (Dubos, 1939; Hotchkiss and Dubos, 1941a; Rammelkamp and Weinstein, 1942). Its application was therefore limited to topical application due to the toxicity when injected intravenously (Hotchkiss & Dubos 1941). Trcs are specific haemolysins eliciting their activity binding to a component in the cell membrane and causing subsequent lysis (Seeman, 1966).

The Trcs biological effect on its producer, *B. parabrevis*, hangs on a delicate balance depending on the concentration of the peptide. High concentrations of peptide lead to tightly packed nuclease resistant DNA-peptide complexes, by binding to G+C rich regions, which in turn inhibits RNA synthesis (Bohg and Ristow, 1987, 1986; Chakraborty et al., 1978; H Ristow et al., 1975; H. Ristow et al., 1975b, 1975a) whereas low levels of the peptide allow for DNA uncoiling (Chakraborty et al., 1978; Hansen et al., 1982). The former can be undone by the presence of linear gramicidin. (Chakraborty et al., 1978; Hansen et al., 1982; H Ristow et al., 1975; H. Ristow et al., 1975b, 1975a). Linear gramicidin inhibits RNA synthesis, but not through DNA-complex formation (H Ristow et al., 1975). The Trcs have also been identified as a key aspect in the induction of sporulation. Growth can be suspended by the inhibition of

RNA synthesis which, as mentioned above, can be caused and to some extent reversed by Trcs and linear gramicidins (H. Ristow et al., 1975a). The Trcs cause a slower growth rate with sporadic growth lapses and depletion of cellular nucleotides (Fynn and Davison, 1976). A study done by Ristow and Paulus (1982) showed that an exponential *Bacillus brevis* culture that was suddenly deprived of a nitrogen source could not continue growing or sporulate. However, the latter could be induced by the addition of Trcs which in turn lead to the production of linear gramicidins showing that both peptides are important to the induction of sporulation (Pschorn et al., 1982). Trcs levels needed for sporulation under these circumstances were concentration dependent (ideal 5 µM: under 5 µM did not cause sporulation, above cause a delay in the reactions leading to sporulation) and had to be added within a critical window of 1-3 minutes after transfer to nitrogen deprived media. The addition of Trcs to the media had a range of observed results: the first being a depletion of intracellular ATP and other nucleotides (Ristow and Paulus, 1982). On the contrary, other studies have noted that a reduction of intracellular ATP did not occur during Trcs production and sporulation (Fynn and Davison, 1976). GS, that shares both surfactant properties and structure with Trcs, had no effect on sporulation or RNA polymerase but caused a loss in intracellular ATP (Sarkar and Paulus, 1972). Thus, it is possible that the reduction of ATP is merely due to the membranolytic activity of the peptide, and not as a result of sporulation or as a precursor for sporulation. The second observation was that the addition of Trcs was accompanied by the increased use of extracellular nucleotide precursors (Ristow and Paulus, 1982). Lastly, it caused an overall decrease in RNA synthesis which is a key step in sporulation (Ristow and Paulus, 1982).

1.3.1.3 Structure relation to activity

Recent studies that included the single Trcs analogues showed that certain analogues showed better results against certain target cells. Trc A/A1 had the least activity against *L. monocytogenes*, whereas the activity observed for TrcB/B1 and TrcC/C1 was strain dependent (Spathelf and Rautenbach, 2009). Since all the Trcs tested shared the same Tyr and Orn residue it could be concluded that the dipeptide moiety was the determining factor for activity. The Lys-containing peptides Trc A1 and Trc C1 had a slightly lower activity compared to the Orn-containing counterparts, whereas the opposite was observed with Trc B1 and Trc B (Spathelf and Rautenbach, 2009). It was shown, against the human malaria parasite, that the main activity determining factor was the hydrophobicity and the side chain surface area of the dipeptide moiety (X^3x^4) (Rautenbach et al., 2007). Therefore, Trc A was shown to have the best activity and the most polar tyrocidine, Trc C1, the worst activity against *P. falciparum*. It

was observed that Phe in the third position would yield the best result, whereas the presence of Trp/Phe at position four made no difference (Rautenbach et al., 2007). It was also observed that the Orn-containing peptides had much better activities compared to their Lys counterparts (Leussa and Rautenbach, 2014; Rautenbach et al., 2007). However, neither the identity of the aromatic residues on position 3 & 4 nor that of the cationic residue on position 7 determines the haemolytic activity (Leussa and Rautenbach, 2014; Spathelf and Rautenbach, 2009). This could point to two 'activity conformations', each responsible for a different characteristic of the peptide.

The hypothesis of the mode of action of Trcs is dependent on two assumptions: that the first crucial step is the membrane association of the cationic residue through electrostatic interactions followed by membrane integration through hydrophobic interactions (Spathelf and Rautenbach, 2009). There can therefore only be two factors that determine and/or influence activity. The first being the cationic charge: compared to Orn, Lys has a longer tail (butylene group) that will 'snorkel' into the membrane and associate stronger to the membrane (Danders et al., 1982; Rautenbach et al., 2007). In dipeptide unit it can only be Phe or Trp as aromatic residues. Phe inserts deeper into the membrane (Kelkar and Chattopadhyay, 2006), whereas Trp, due to its large size and amphipathic character will insert shallower in the bilayer. Trp can be anchored with hydrogen bonds between the fatty-acyl carbonyl groups of the membrane and the NH-group in the tryptophan side chain (Norman and Nymeyer, 2006; Strøm et al., 2002). Furthermore, $Trp^{3}Trp^{4}$ (C analogues) have bulkier side chains compared to $Phe^{3}Phe^{4}$ (A analogues) which was proposed to result in higher pore formation due to an increased spreading of membrane lipids (Wenzel et al., 2018). The aromatic amino acids have also been implicated in the Trcs' ability to interfere with DNA-packaging (Wenzel et al., 2018). Based on these attributes it is evident that the Trcs' activity is dependent on an optimal amphipacity to obtain the best conformation in terms of self-assembly, membrane integration and translocation into the target cell (Spathelf and Rautenbach, 2009).

Chemically synthesized Trc A with substitutions showed that disruption of the structure led to a decrease in biological activity. A chemical Trcs analogue TrcA-Val^{3} showed a two-fold decrease in its ability to inhibit active membrane transport and transcription against *B. subtilis* whereas TrcA-Gly^{3} substitution led to five-fold decrease in activity (Danders et al., 1982). This points to the importance of a hydrophobic amino-acid at position 3 (Danders et al., 1982). A TrcA-Orn^{4} analogue, creating a peptide similar to GS, showed a complete loss of activity with no inhibition of active transport, inhibition of transcription or spore growth (Danders et al.,

1982). Chemical modification of the Trc A structure has found that the substitution of D-Phe^4 and Gln^6 with charged amino acids Orn, Arg and Lys, increased the therapeutic index (Qin et al., 2003). An increase was observed up to 140-fold in activity against *B. subtilis* for the Gln^6 substitutions (Qin et al., 2003). In another chemical modification (Trc A) it was found that the substitution of Lys^{4,6} yielded a peptide that had activity against Gram-negative *E. coli* with improvement of activity against Gram-positive bacteria (except *En. faecalis*) (Marques et al., 2007). Substitution of Lys^4 alone showed a loss of activity whereas substitution of Lys^6 showed the best activity across the board against all the target organisms tested (Marques et al., 2007). Thus, the substitution/modification of the Trcs is not just dependent on an increase in charge but also where the extra charge is located within the hydrophobic plane of the peptides (Marques et al., 2007). Substitutions at position 4 with Orn/Lys lead to the complete destruction of activity whereas substitutions at position 6 always led to an increase in activity. Therefore, as long as the structural topography of a hydrophobic and hydrophilic regions needed for the Trcs to elicit its biological response is not disrupted the peptide will remain active (Danders et al., 1982). This in turn points to the importance of the amphipathic character needed for dimerization, which is vital to the peptides activity, as described above.

1.3.1.4 Tyrocidines in application

As previously mentioned, the Trcs have a very broad spectrum of activity but are haemolytic and toxic when injected into the bloodstream (Hotchkiss and Dubos, 1941a). Tyrothricin is ineffective and non-toxic when taken orally (Robinson, H.J. & Molitor, 1941) and was originally used topically (Van Epps, 2006) since it is not toxic when applied to skin (Hotchkiss and Dubos, 1941a) and does not cause skin irritations (Robinson, H.J. & Molitor, 1941). Tyrothricin was suggested to be used for topical applications such as sinusitis, mastoiditis, dental abscesses, superficial infections with predominant Gram-positive bacteria, thrombophlebitic ulcers and certain ophthalmic infections (Lask, 1948). Tyrothricin has been used in lozenges and as a gel, Tyrosur® gel created by Engelhard Arneimittel GmbH and Co. (Niederdorfelden, Germany), where the peptides neither hindered growth or caused cell irritation (Wigger-Alberti et al., 2013). Added to the possibility of application the peptides are incredibly stable; remaining active at 90 ^{o}C, pH 2.0, pH 9.0 (although it precipitates) and are resistant to pepsin, crystalline trypsin, chymotrypsin and crude trypsin (Dubos, 1939; Hotchkiss, 1941).

Previous research has shown the possibility of Trcs to be implemented as part of an antimicrobial surface (Van Rensburg, 2015, Rautenbach and Van Rensburg, 2017). Surfaces

tested for the peptide to adsorb and maintain activity included cellulose, an acetate cellulose and nitrocellulose mixture, cellulose acetate, polyvinylidene fluoride and polycarbonate. The best activity was observed for the cellulose based surface fully inhibiting growth of $3.7x10^5$ cells/cm^2 *M. luteus*. The cellulose-surface maintained activity after multiple water washes, pH ranges and temperatures. The only point where loss of activity was observed was at pH 13, which was attributed to the cellulose surface disintegrating. The cellulose surfaces were tested in application for the germination of tomato plants and it was found that the peptide containing cellulose promoted root growth which correlated with previous research (Rautenbach et al., 2015a).

The Trcs therefore hold great potential in the creation of antimicrobial materials for commercial use. These Trcs-functionalized materials would be able to combat the propagation of resistant pathogens on materials/surfaces without fear of resistance development against Trcs (Wenzel et al., 2018). Furthermore, previous research suggested a unique mode of adsorption that results in the peptides' ability to associate to the various materials and have a robust activity and stability (Van Rensburg, 2015). It is therefore key to extend research into screening of commercial surfaces, determine the robustness Trcs-treated materials but more importantly elucidate the unique mode of association that allow the association of Trcs to various materials.

1.4 References

Abou-Yousef, H., Kamel, S., 2015. High efficiency antimicrobial cellulose-based nanocomposite hydrogels. J. Appl. Polym. Sci. 132, 1–9.

Ageitos, J.M., Sánchez-Pérez, A., Calo-Mata, P., Villa, T.G., 2017. Antimicrobial peptides (AMPs): Ancient compounds that represent novel weapons in the fight against bacteria. Biochem. Pharmacol. 133, 117–138.

Angele, M.K., Faist, E., 2002. Clinical review: immunodepression in the surgical patient and increased susceptibility to infection. Crit. Care 6, 298.

Appleby, J.C., Knowles, E., Pearson, J., White, T., 1947. A preliminary study of the formation, assay and stability of tyrothricin. J. Gen. Microbiol. 1, 137–44.

Aranda, F.J., de Kruijff, B., 1988. Interrelationships between tyrocidine and gramicidin A' in their interaction with phospholipids in model membranes. Biochim. Biophys. Acta - Biomembr. 937, 195–203.

Aveyard, J., Bradley, J.W., McKay, K., McBride, F., Donaghy, D., Raval, R., D'Sa, R.A., 2017. Linker-free covalent immobilization of nisin using atmospheric pressure plasma induced grafting. J. Mater. Chem. B 5, 2500–2510.

Bagheri, M., Beyermann, M., Dathe, M., 2012. Mode of action of cationic antimicrobial peptides defines the tethering position and the efficacy of biocidal surfaces. Bioconjug. Chem. 23, 66–74.

Bahar, A.A., Ren, D., 2013. Antimicrobial peptides. Pharmaceuticals 6, 1543–1575.

Barakat, R.K., Harris, L.J., 1999. Growth of *Listeria monocytogenes* and *Yersinia enterocolitica* on cooked modified-atmosphere-packaged poultry in the presence and absence of a naturally occurring microbiota. Appl. Environ. Microbiol. 65, 342–345.

Barbiroli, A., Bonomi, F., Capretti, G., Iametti, S., Manzoni, M., Piergiovanni, L., Rollini, M., 2012. Antimicrobial activity of lysozyme and lactoferrin incorporated in cellulose-based food packaging. Food Control 26, 387–392.

Barbosa, A.A.T., de Araújo, H.G.S., Matos, P.N., Carnelossi, M.A.G., de Castro, A.A., 2013. Effects of nisin-incorporated films on the microbiological and physicochemical quality of minimally processed mangoes. Int. J. Food Microbiol. 164, 135–140.

Beyer, C.F., Gibbons, W.A., Craig, L.C., Longworth, J.W., 1974. Heterogeneous tryptophan environments in the cyclic peptides tyrocidines B and C. Phosphorescence studies. J. Biol. Chem. 249, 3204–3211.

Bierbaum, G., Sahl, H.G., 2009. Lantibiotics: mode of action, biosynthesis and bioengineering. Curr. Pharm. Biotechnol. 10, 2–18.

Boatemaa, S., Barney, M., Drimie, S., Harper, J., Korsten, L., Pereira, L., 2019. Awakening from the listeriosis crisis: Food safety challenges, practices and governance in the food retail sector in South Africa. Food Control 104, 333–342.

Bohg, A., Ristow, H., 1987. Tyrocidine-induced modulation of the DNA conformation in *Bacillus brevis*. Eur. J. Biochem. 170, 253–258.

Bohg, A., Ristow, H., 1986. DNA-supercoiling is affected in vitro by the peptide antibiotics tyrocidine and gramicidin. Eur. J. Biochem. 160, 587–591.

Bower, C.K., McGuire, J., Daeschel, M.A., 1995. Suppression of *Listeria monocytogenes* colonization following adsorption of nisin onto silica surfaces. Appl. Environ. Microbiol. 61, 992–997.

Bradley, W.A., Somkuti, G.A., 1979. The primary structure of sillucin and antimicrobial peptide from mucor pusillus. FEBS Lett. 97, 81–83.

Cagri, A., Ustunol, Z., Ryser, E.T., 2004. Antimicrobial edible films and coatings. J. Food Prot. 67, 833–848.

Campoccia, D., Montanaro, L., Arciola, C.R., 2013. A review of the biomaterials technologies for infection-resistant surfaces. Biomaterials 34, 8533–8554.

Cao, P., Yuan, C., Xiao, J., He, X., Bai, X., 2018. A biofilm resistance surface yielded by grafting of antimicrobial peptides on stainless steel surface. Surf. Interface Anal. 50, 516–521.

Cao, Z., Mi, L., Mendiola, J., Ella-Menye, J.R., Zhang, L., Xue, H., Jiang, S., 2012. Reversibly switching the function of a surface between attacking and defending against bacteria. Angew. Chemie Int. Ed. 51, 2602–2605.

Carmona-Ribeiro, A.M., Carrasco, L.D. de M., 2014. Novel formulations for antimicrobial peptides. Int. J. Mol. Sci. 15, 18040–18083.

Carpentier, B., Cerf, O., 1993. Biofilms and their consequences, with particular reference to hygiene in the food industry. J. Appl. Bacteriol. 75, 499–511.

Chakraborty, T., Hansen, J., Schazschneider, B., Ristow, H., 1978. The DNA-Tyrocidine complex and its dissociation in the presence of gramicidin D. Eur. J. Biochem. 90, 261–270.

Chopra, S., Torres-Ortiz, M., Hokama, L., Madrid, P., Tanga, M., Mortelmans, K., Kodukula, K., Galande, A.K., 2010. Repurposing FDA-approved drugs to combat drug-resistant *Acinetobacter baumannii*. J. Antimicrob. Chemother. 65, 2598–2601.

Chua, P., Neoh, K., Kang, E., Wang, W., 2008. Surface functionalization of titanium with hyaluronic acid/chitosan polyelectrolyte multilayers and RGD for promoting osteoblast functions and inhibiting bacterial adhesion. Biomaterials 29, 1412–1421.

Cloutier, M., Tolouei, R., Lesage, O., Lévesque, L., Turgeon, S., Tatoulian, M., Mantovani, D., 2014. On the long term antibacterial features of silver-doped diamondlike carbon coatings deposited via a hybrid plasma process. Biointerphases 9, 1–9.

Costerton, J.W., Cheng, K.J., Geesey, G.G., Ladd, T.I., Nickel, J.C., Dasgupta, M., Marrie, T.J., 1987. Bacterial biofilms in nature and disease. Annu. Rev. Microbiol. 41, 435–464.

Costerton, J.W., Lewandowski, Z., Caldwell, D.E., Korber, D.R., Lappin-Scott, H.M., 1995. Microbial biofilms. Annu. Rev. Microbiol. 49, 711–745.

Curutchet, A., Dellacassa, E., Ringuelet, J.A., Chaves, A.R., Viña, S.Z., 2014. Nutritional and sensory quality during refrigerated storage of fresh-cut mints (*Mentha* x *piperita* and *M. spicata*). Food Chem. 143, 231–238.

Daeschel, M.A., McGuire, J., Al-Makhlafi, H., 1992. Antimicrobial activity of nisin adsorbed to hydrophilic and hydrophobic silicon surfaces. J. Food Prot. 55, 731–735.

Danders, W., Marahiel, M.A., Krause, M., Kosui, N., Kato, T., Izumiya, N., Kleinkauf, H., 1982. Antibacterial action of gramicidin S and tyrocidines in relation to active transport, in vitro transcription, and spore outgrowth. Antimicrob. Agents Chemother. 22, 785–790.

De Moura, M.R., Mattoso, L.H., Zucolotto, V., 2012. Development of cellulose-based bactericidal nanocomposites containing silver nanoparticles and their use as active food packaging. J. Food Eng. 109, 520–524.

Donlan, R.M., 2000. Role of biofilms in antimicrobial resistance. ASAIO J. 46, S47–S52.

Dubos, R.J., 1939. Studies on a bactericidal agent extracted from a soil bacillus. I. Preparation of the agent. Its activity in vitro. J. Exp. Med. 70, 1–10.

Dubos, R.J., Hotchkiss, R.D., 1941. The production of bactericidal substances by aerobic sporulating bacilli. J. Exp. Med. 73, 629–640.

Dubos, R.J., Hotchkiss, R.D., Coburn, A.F., 1942. The effect of gramicidin and tyrocidine on bacterial metabolism. J. Biol. Chem. 146, 421–426.

Dunne, M.W., 2002. Bacterial Adhesion: Seen Any Good Biofilms Lately? Clin. Microbiol. Rev. 15, 155–166.

Dürr, U.H., Sudheendra, U.S. Ramamoorthy, A., 2006. LL-37, the only human member of the cathelicidin family of antimicrobial peptides. Biochim. Biophys. Acta - Biomembranes 1758, 1408–1425.

Elshikh, M., Ahmed, S., Funston, S., Dunlop, P., McGaw, M., Marchant, R., Banat, I.M., 2016. Resazurin-based 96-well plate microdilution method for the determination of minimum inhibitory concentration of biosurfactants. Biotechnol. Lett. 38, 1015–1019.

Ercolini, D., Ferrocino, I., La Storia, A., Mauriello, G., Gigli, S., Masi, P., Villani, F., 2010. Development of spoilage microbiota in beef stored in nisin activated packaging. Food Microbiol. 27, 137–143.

Essig, A., Hofmann, D., Münch, D., Gayathri, S., Künzler, M., Kallio, P.T., Sahl, H.G., Wider, G., Schneider, T., Aebi, M., 2014. Copsin, a novel peptide-based fungal antibiotic interfering with the peptidoglycan synthesis. J. Biol. Chem. 289, 34953–34964.

Eyéghé-Bickong, H.A., 2011. Role of surfactin from *Bacillus subtillis* in protection against antimicrobial peptides produced by *Bacillus* species. Stellenbosch University, Department of Biochemistry, Stellenbosch, South Africa. PhD.Thesis, http://scholar.sun.ac.za/handle/10019.1/6773.

Fadeeva, E., Truong, V.K., Stiesch, M., Chichkov, B.N., Crawford, R.J., Wang, J., Ivanova, E.P., 2011. Bacterial retention on superhydrophobic titanium surfaces fabricated by femtosecond laser ablation. Langmuir 27, 3012–3019.

Felgueiras, H.P., Amorim, M.T.P., 2017. Functionalization of electrospun polymeric wound dressings with antimicrobial peptides. Colloids Surfaces B Biointerfaces 156, 133–148.

Finnegan, E., O'Beirne, D., 2015. Characterising deterioration patterns in fresh-cut fruit using principal component analysis. II: Effects of ripeness stage, seasonality, processing and packaging. Postharvest Biol. Technol. 100, 91–98.

Fynn, G.H., Davison, J.A., 1976. Adenine nucleotide pool and energy charge during growth of a tyrothricin-producing strain of *Bacillus brevis*. J. Gen. Microbiol. 94, 68–74.

Gabriel, M., Nazmi, K., Veerman, E.C., Nieuw Amerongen, A.V., Zentner, A., 2006. Preparation of LL-37-grafted titanium surfaces with bactericidal activity. Bioconjug. Chem. 17, 548–550.

Garrett, T.R., Bhakoo, M., Zhang, Z., 2008. Bacterial adhesion and biofilms on surfaces. Prog. Nat. Sci. 18, 1049–1056.

Gemili, S., Yemenicioglu, A., Altinkaya, S.A., 2009. Development of cellulose acetate based antimicrobial food packaging materials for controlled release of lysozyme. J. Food Eng. 90, 453–462.

Gibbons, W.A., Beyer, C.F., Dadok, J., Sprecher, R.F., Wyssbrod, H.R., 1975. Studies of individual amino acid residues of the decapeptide tyrocidine A by proton double-resonance difference spectroscopy in the correlation mode. Biochemistry 14, 420–429.

Glinel, K., Thebault, P., Humblot, V., Pradier, C.M., Jouenne, T., 2012. Antibacterial surfaces developed from bio-inspired approaches. Acta Biomater. 8, 1670–1684.

Goodman, S.B., Yao, Z., Keeney, M., Yang, F., 2013. The future of biologic coatings for orthopaedic implants. Biomaterials 34, 3174–3183.

Green, J.D., Fulghum, T., Nordhaus, M.A., 2011. A review of immobilized antimicrobial agents and methods for testing. Biointerphases 6, MR13–MR28.

Grower, J.L., Cooksey, K., Getty, K.J., 2004. Development and characterization of an antimicrobial packaging film coating containing nisin for inhibition of *Listeria monocytogenes*. J. Food Prot. 67, 475–479.

Hansen, J., Pschorn, W., Ristow, H., 1982. Functions of the peptide antibiotics tyrocidine and gramicidin: Induction of conformational and structural changes of superhelical DNA. Eur. J. Biochem 126, 279–284.

Hasan, J., Crawford, R.J., Ivanova, E.P., 2013. Antibacterial surfaces: the quest for a new generation of biomaterials. Trends Biotechnol. 31, 295–304.

Hell, É., Giske, C.G., Nelson, A., Römling, U., Marchini, G., 2010. Human cathelicidin peptide LL37 inhibits both attachment capability and biofilm formation of *Staphylococcus epidermidis*. Lett. Appl. Microbiol. 50, 211–215.

Helle, S.S., Zandstra, P.W., Cooper, D.G., 1992. Unusual surface tension behavior of an aqueous solution of gramicidin S. J. Colloid Interface Sci. 151, 130–135.

Héquet, A., Humblot, V., Berjeaud, J.M., Pradier, C.M., 2011. Optimized grafting of antimicrobial peptides on stainless steel surface and biofilm resistance tests. Colloids Surfaces B Biointerfaces 84, 301–309.

Hernandez-Montelongo, J., Ureña, Y.C., Machado, D., Lancelloti, M., Pinheiro, M.P., Rischka, K., Lisboa-Filho, P.N., Cotta, M.A., 2018. Electrostatic immobilization of antimicrobial peptides on polyethylenimine and their antibacterial effect against *Staphylococcus epidermidis*. Colloids Surfaces B Biointerfaces 164, 370–378.

Hilpert, K., Elliott, M., Jenssen, H., Kindrachuk, J., Fjell, C.D., Körner, J., Winkler, D.F., Weaver, L.L., Henklein, P., Ulrich, A.S., Chiang, S.H., 2009. Screening and characterization of surface-tethered cationic peptides for antimicrobial activity. Chem. Biol. 16, 58–69.

Ho, C.H., Tobis, J., Sprich, C., Thomann, R., Tiller, J.C., 2004. Nanoseparated polymeric networks with multiple antimicrobial properties. Adv. Mater. 16, 957–961.

Holmes, P.F., Currie, E.P.K., Thies, J.C., Van der Mei, H.C., Busscher, H.J., Norde, W., 2009. Surface-modified nanoparticles as a new, versatile, and mechanically robust nonadhesive coating: Suppression of protein adsorption and bacterial adhesion. J. Biomed. Mater. Res. 91, 824–833.

Holzapfel, B.M., Reichert, J.C., Schantz, J.T., Gbureck, U., Rackwitz, L., Nöth, U., Jakob, F., Rudert, M., Groll, J., Hutmacher, D.W., 2013. How smart do biomaterials need to be? A translational science and clinical point of view. Adv. Drug Deliv. Rev. 65, 581–603.

Hood, S.K., Zottola, E.., 1997. Isolation and identification of adherent gram-negative microorganisms from four meat-processing facilities. J. Food Prot. 60, 1135–1138.

Hotchkiss, D., 1941. The chemical nature of gramicidin and tyrocidine. J. Biol. Chem. 141, 171–185.

Hotchkiss, R.D., Dubos, R., 1941a. The isolation of bactericidal substances from cultures of *Bacillus brevis*. J. Biol. Chem. 141, 155–162.

Hotchkiss, R.D., Dubos, R.J., 1941b. Bactericidal fractions from an aerobic sporulation bacillus. J. Biol. Chem. 136, 803–804.

Hu, R., Li, G., Jiang, Y., Zhang, Y., Zou, J.J., Wang, L., Zhang, X., 2013. Silver-zwitterion organic-inorganic nanocomposite with antimicrobial and antiadhesive capabilities. Langmuir 29, 3773–3779.

Imran, M., El-Fahmy, S., Revol-Junelles, A.M., Desobry, S., 2010. Cellulose derivative based active coatings: Effects of nisin and plasticizer on physico-chemical and antimicrobial properties of hydroxypropyl methylcellulose films. Carbohydr. Polym. 81, 219–225.

Isquith, A.J., Abbott, E.A., Walters, P.A., 1972. Surface-bonded antimicrobial activity of an organosilicon quaternary ammonium chloride. Appl. Environ. Microbiol. 24, 859–863.

Ivanova, E.P., Truong, V.K., Webb, H.K., Baulin, V.A., Wang, J.Y., Mohammodi, N., Wang, F., Fluke, C., Crawford, R.J., 2011. Differential attraction and repulsion of *Staphylococcus aureus* and *Pseudomonas aeruginosa* on molecularly smooth titanium films. Sci. Rep. 1, 165.

Jeong, G.M., Seong, H., Im, S.G., Sung, B.H., Kim, S.C., Jeong, K.J., 2018. Coating of an antimicrobial peptide on solid substrate via initiated chemical vapor deposition. J. Ind. Eng. Chem. 58, 51–56.

Jin, G., Qin, H., Cao, H., Qian, S., Zhao, Y., Peng, X., Zhang, X., Liu, X., Chu, P.K., 2014. Synergistic effects of dual Zn/Ag ion implantation in osteogenic activity and antibacterial ability of titanium. Biomaterials 35, 7699–7713.

Katz, E., Demain, A., 1977. The peptide antibiotics of *Bacillus*: chemistry, biogenesis, and possible functions. Bacteriol. Rev. 41, 449–474.

Kelkar, D.A., Chattopadhyay, A., 2006. Membrane interfacial localization of aromatic amino acids and membrane protein function. J. Biosci. 31, 297–302.

Kondejewski, L.H., Farmer, S.W., Wishart, D.S., Hancock, R.E., Hodges, R.S., 1996. Gramicidin S is active against both Gram-positive and Gram-negative bacteria. Int. J. Pept. Protein Res. 47, 460–466.

Kulagina, N. V, Shaffer, K.M., Anderson, G.P., Ligler, F.S., Taitt, C.R., 2006. Antimicrobial peptide-based array for *Escherichia coli* and *Salmonella* screening. Anal. Chim. Acta 575, 9–15.

Kuo, M.-C., Gibbons, W.A., 1980. Nuclear Overhauser effect and cross-relaxation rate determinations of dihedral and transannular interproton distances in the decapeptide tyrocidine A. Biophys. J. 32, 807–36.

Kuo, M.-C., Gibbons, W.A., 1979. Determination of individual side-chain conformations, tertiary conformations, and molecular topography of tyrocidine A from scalar coupling constants and chemical shifts. Biochemistry 18, 5855–5867.

Lask, S., 1948. Tyrothricin as an antibiotic. Arch. Surg. 56, 475–83.

Leussa, A.N.N., Rautenbach, M., 2014. Detailed SAR and PCA of the tyrocidines and analogues towards leucocin A-sensitive and leucocin A-resistant *Listeria monocytogenes*. Chem. Biol. Drug Des. 84, 543–557.

Levy, S.B., Marshall, B., 2004. Antibacterial resistance worldwide: causes, challenges and responses. Nat. Med. 10, S122.

Lewis, K., Klibanov, A.M., 2005. Surpassing nature: rational design of sterile-surface materials. Trends Biotechnol. 23, 343–348.

Li, T., Wang, N., Chen, S., Lu, R., Li, H., Zhang, Z., 2017. Antibacterial activity and cytocompatibility of an implant coating consisting of TiO2 nanotubes combined with a GL13K antimicrobial peptide. Int. J. Nanomedicine 12, 2995–3007.

Li, Z., Lee, D., Sheng, X., Cohen, R.E., Rubner, M.F., 2006. Two-level antibacterial coating with both release-killing and contact-killing capabilities. Langmuir 22, 9820–9823.

Lin, J., Qiu, S., Lewis, K., Klibanov, A.M., 2003. Mechanism of bactericidal and fungicidal activities of textiles covalently modified with alkylated polyethylenimine. Biotechnol. Bioeng. 83, 168–172.

Liu, Y., Yang, S.F., Li, Y., Xu, H., Qin, L., Tay, J.H., 2004. The influence of cell and substratum surface hydrophobicities on microbial attachment. J. Biotechnol. 110, 251–256.

Loll, P.J., Upton, E.C., Nahoum, V., Economou, N.J., Cocklin, S., 2014. The high resolution structure of tyrocidine A reveals an amphipathic dimer. Biochim. Biophys. Acta - Biomembr. 1838, 1199–1207.

Mach, B., Slayman, C.W., 1966. Mode of action of tyrocidine on *Neupospora*. Biochim. Biophys. Acta 124, 351–361.

Mantilla, N., Castell-Perez, M.E., Gomes, C., Moreira, R.G., 2013. Multilayered antimicrobial edible coating and its effect on quality and shelf-life of fresh-cut pineapple (*Ananas comosus*). LWT-Food Sci. Technol. 51, 37–43.

Marques, M.A., Citron, D.M., Wang, C.C., 2007. Development of Tyrocidine A analogues with improved antibacterial activity. Bioorganic Med. Chem. 15, 6667–6677.

Mauriello, G.D.L.E., De Luca, E., La Storia, A., Villani, F., Ercolini, D., 2005. Antimicrobial activity of a nisin-activated plastic film for food packaging. Lett. Appl. Microbiol. 41, 464–469.

Mrabet, B., Nguyen, M.N., Majbri, A., Mahouche, S., Turmine, M., Bakhrouf, A., Chehimi, M.., 2009. Anti-fouling poly(2-hydoxyethyl methacrylate) surface coatings with specific bacteria recognition capabilities. Surf. Sci. 603, 2422–2429.

Mulani, M.S., Kamble, E.E., Kumkar, S.N., Tawre, M.S., Pardesi, K.R., 2019. Emerging strategies to combat ESKAPE pathogens in the era of antimicrobial resistance: a review. Front. Microbiol. 10, 1–24.

Muñoz-Bonilla, A., Fernández-García, M., 2012. Polymeric materials with antimicrobial activity. Prog. Polym. Sci. 37, 281–339.

Munyuki, G., Jackson, G.E., Venter, G.A., Kövér, K.E., Szilágyi, L., Rautenbach, M., Spathelf, B.M., Bhattacharya, B., Van Der Spoel, D., 2013. β-sheet structures and dimer models of the two major tyrocidines, antimicrobial peptides from *Bacillus aneurinolyticus*. Biochemistry 52, 7798–7806.

Nguyen, V.T., Gidley, M.J., Dykes, G.A., 2008. Potential of a nisin-containing bacterial cellulose film to inhibit Listeria monocytogenes on processed meats. Food Microbiol. 25, 471–478.

Noimark, S., Dunnill, C.W., Wilson, M., Parkin, I.., 2009. The role of surfaces in catheter-associated infections. Chem. Soc. Rev. 38, 3435–3448.

Norman, K.E., Nymeyer, H., 2006. Indole localization in lipid membranes revealed by molecular simulation. Biophys. J. 91, 2046–2054.

Olanya, O.M., Hoshide, A.K., Ijabadeniyi, O.A., Ukuku, D.O., Mukhopadhyay, S., Niemira, B.A., Ayeni, O., 2019. Cost estimation of listeriosis (*Listeria monocytogenes*) occurrence in South Africa in 2017 and its food safety implications. Food Control 102, 231–239.

Paladini, A., Craig, L.C., 1954. The chemistry of tyrocidine. III. The structure of tyrocidine A. J. Am. Chem. Soc. 76, 688–692.

Pan, Y., Breidt, F., Kathariou, S., 2006. Resistance of *Listeria monocytogenes* biofilms to sanitizing agents in a simulated food processing environment. Appl. Environ. Microbiol. 72, 7711–7717.

Park, K.D., Kim, Y.S., Han, D.K., Kim, Y.H., Lee, E.H.B., Suh, H., Choi, K.S., 1998. Bacterial adhesion on PEG modified polyurethane surfaces. Biomaterials 19, 851–859.

Patch, J.A., Barron, A.E., 2002. Mimicry of bioactive peptides via non-natural, sequence-specific peptidomimetic oligomers. Curr. Opin. Chem. Biol. 6, 872–877.

Pedrosa, M., Mouro, C., Nogueira, F., Vaz, J., Gouveia, I., 2014. Comparison of the antibacterial activity of modified-cotton with magainin I and LL-37 with potential as wound-dressings. J. Appl. Polym. Sci. 131, 1–8.

Pivec, T., Hribernik, S., Kolar, M., Kleinschek, K.S., 2017. Environmentally friendly procedure for in-situ coating of regenerated cellulose fibres with silver nanoparticles. Carbohydr. Polym. 163, 92–100.

Pschorn, W., Paulus, H., Hansen, J., Ristow, H., 1982. Induction of sporulation in *Bacillus brevis*. 2. Dependence on the presence of the peptide antibiotics tyrocidine and linear gramicidin. Eur. J. Biochem. 129, 403–407.

Qi, X., Poernomo, G., Wang, K., Chen, Y., Chan-Park, M.B., Xu, R., Chang, M.W., 2011. Covalent immobilization of nisin on multi-walled carbon nanotubes: superior antimicrobial and anti-biofilm properties. Nanoscale 3, 1874–1880.

Qin, C., Zhong, X., Bu, X., Ng, N.L.J., Guo, Z., 2003. Dissociation of antibacterial and hemolytic activities of an amphipathic peptide antibiotic. J. Med. Chem. 46, 4830–4833.

Rammelkamp, C.H., Maxon, T., 1942. Resistance of *Staphylococcus aureus* to the action of penicillin. Exp. Biol. Med. 51, 386–389.

Rammelkamp, C.H., Weinstein, L., 1942. Toxic effects of tyrothricin, gramicidin and tyrocidine. J. Infect. Dis. 71, 166–173.

Ramsden, J.J., Allen, D.M., Stephenson, D.J., Alcock, J.R., Peggs, G.N., Fuller, G., Goch, G., 2007. The design and manufacture of biomedical surfaces. CIRP Ann. 56, 687–711.

Rautenbach, M., de Beer, A., Troskie, A.M., Vosloo, J.A., 2015a. Antimicrobial peptide compositions for plants. WO/2013/150394 A1, P2366CN00 China (TBA, 21/10/2014); P2366EP00 Europe (13717558.4, 22/09/2014); P2366IN00 India (1963/KOLNP/2014; 16/09/2014); P2366US00 United States (14380518, 22/08/2014); P2366ZA01 South Africa (2014/06499; 04/09/2014).

Rautenbach, M., Eyéghé-Bickong, H.A., Vlok, N.M., Stander, M., de Beer, A., 2012. Direct surfactin-gramicidin S antagonism supports detoxification in mixed producer cultures of *Bacillus subtilis* and *Aneurinibacillus migulanus*. Microbiology 158, 3072–3082.

Rautenbach, M., Troskie, A.M., Vosloo, J.A., 2016a. Antifungal peptides: To be or not to be membrane active. Biochimie 130, 132–145.

Rautenbach, M., Troskie, A.M., Vosloo, J.A., Dathe, M.E., 2016b. Antifungal membranolytic activity of the tyrocidines against filamentous plant fungi. Biochimie 130, 122–131.

Rautenbach, M., van Rensburg, W., 2017. Method for preventing or treating microbial growth on a manufactured product. South Africa 2016 (SA2016/08601), Australia 2019 (Patent 2015270120), USA 2020 (Patent 15/315,755), China 2020 (Patent 201580040786.2).

Rautenbach, M., Vlok, N.M., Stander, M., Hoppe, H.C., 2007. Inhibition of malaria parasite blood stages by tyrocidines, membrane-active cyclic peptide antibiotics from *Bacillus brevis*. Biochim. Biophys. Acta - Biomembr. 1768, 1488–1497.

Rautenbach, M., Vosloo, J.A., van Rensburg, W., Engelbrecht, Y., 2015b. Natural antimicrobial peptides as green microbicides in agriculture. Green Economy Research Report, Green Fund, Development Bank of Southern Africa, Midrand. https://www.researchgate.net/publication/303538333.

Reddy, K.V.R., Yedery, R.D., Aranha, C., 2004. Antimicrobial peptides: Premises and promises. Int. J. Antimicrob. Agents 24, 536–547.

Ren, X., Kou, L., Liang, J., Worley, S.D., Tzou, Y.M., Huang, T.S., 2008. Antimicrobial efficacy and light stability of N-halamine siloxanes bound to cotton. Cellulose 15, 593–598.

Ristow, H., Paulus, H., 1982. Induction of sporulation in *Bacillus brevis* .1. Biohemical events and modulation of RNA synthesis during induction by tyrocidine. Eur. J. Biochem. 129, 395–401.

Ristow, H, Schazschneider, B., Bauer, K., Kleinkauf, H., 1975. Tyrocidine and the linear gramicidin. Do these peptide antibiotics play an antagonistic regulative role in sporulation? Biochim. Biophys. Acta 390, 246–252.

Ristow, H., Schazschneider, B., Kleinkauf, H., 1975a. Effects of the peptide antibiotics tyrocidine and the linear gramicidin on RNA synthesis and sporulation of *Bacillus brevis*. Biochem. Biophys. Res. Commun. 63, 1085–1092.

Ristow, H., Schazschneider, B., Vater, J., Kleinkauf, H., 1975b. Some characteristics of the DNA - tyrocidine complex and a possible mechanism of the gramicidin action. Biochim. Biophys. Acta 414, 1–8.

Robinson, H.J. & Molitor, H., 1941. Some toxicological and pharmacological properties of gramicidin, tyrocidine and tyrothricin. J. Pharmacol. Exp. Ther. 74, 75–82.

Robinson, H.J., Graessle, O.E., 1942. In vitro and in vivo studies of gramicidin, tyrothricin and tyrocidine. J. Pharmacol. Exp. Ther. 76, 316–325.

Rouabhia, M., Asselin, J., Tazi, N., Messaddeq, Y., Levinson, D., Zhang, Z., 2014. Production of biocompatible and antimicrobial bacterial cellulose polymers functionalized by RGDC grafting groups and gentamicin. ACS Appl. Mater. Interfaces 6, 1439–1446.

Salgado, J., Grage, S.L., Kondejewski, L.H., Hodges, R.S., McElhaney, R.N., Ulrich, A.S., 2001. Membrane-bound structure and alignment of the antimicrobial β-sheet peptide gramicidin S derived from angular and distance constraints by solid state ^{19}F-NMR. J. Biomol. NMR 21, 191–208.

Sánchez, J.G.., Kouznetsov, V.V., 2010. Antimycobacterial susceptibility testing methods for natrual products reseach. Brazilian J. Microbiol. 41, 270–277.

Sarkar, N., Paulus, H., 1972. Function of peptide antibiotics in sporulation. Nat. New Biol. 239, 228.

Sayanjali, S., Ghanbarzadeh, B., Ghiassifar, S., 2011. Evaluation of antimicrobial and physical properties of edible film based on carboxymethyl cellulose containing potassium sorbate on some mycotoxigenic *Aspergillus species* in fresh pistachios. LWT - Food Sci. Technol. 44, 1133–1138.

Seddon, B., Fynn, G.H., 1972. Energetics of growth in a tyrothricin-producing strain of *Bacillus brevis*. J. Gen. Microbiol. 74, 305–314.

Seeman, P., 1966. III. A method for distinguishing specific from nonspecific hemolysins. Biochem. Pharmacol. 15, 1767–1774.

Shirtliff, M.E., Mader, J.T., Camper, A.K., 2002. Molecular interactions in biofilms. Chem. Biol. 9, 859–871.

Sjollema, J., Zaat, S.A., Fontaine, V., Ramstedt, M., Luginbuehl, R., Thevissen, K., Li, J., van der Mei, H.C., Busscher, H.J., 2018. In vitro methods for the evaluation of antimicrobial surface designs. Acta Biomater. 70, 12–24.

Sobrino-López, A., Martín-Belloso, O., 2008. Use of nisin and other bacteriocins for preservation of dairy products. Int. Dairy J. 18, 329–343.

Son, W.K., Youk, J.H., Lee, T.S., Park, W.H., 2004. Preparation of antimicrobial ultrafine cellulose acetate fibers with silver nanoparticles. Macromol. Rapid Commun. 25, 1632–1637.

Son, W.K., Youk, J.H., Park, W.H., 2006. Antimicrobial cellulose acetate nanofibers containing silver nanoparticles. Carbohydr. Polym. 65, 430–434.

Soravia, E., Martini, G., Zasloff, M., 1988. Antimicrobial properties of peptides from *Xenopus* granular gland secretions. FEBS Lett. 228, 337–340.

Spathelf, B.M., Rautenbach, M., 2009. Anti-listerial activity and structure-activity relationships of the six major tyrocidines, cyclic decapeptides from *Bacillus aneurinolyticus*. Bioorganic Med. Chem. 17, 5541–5548.

Srey, S., Jahid, I.K., Ha, S. Do, 2013. Biofilm formation in food industries: A food safety concern. Food Control 31, 572–585.

Strøm, M.B., Haug, B.E., Rekdal, Ø., Skar, M.L., Stensen, W., Svendsen, J.S., 2002. Important structural features of 15-residue lactoferricin derivatives and methods for improvement of antimicrobial activity.

Sung, S.Y., Sin, L.T., Tee, T.T., Bee, S.T., Rahmat, A.R., Rahman, W.A.W.A., Tan, A.C., Vikhraman, M., 2013. Antimicrobial agents for food packaging applications. Trends Food Sci. Technol. 33, 110–123.

Tacconelli, E., Carrara, E., Savoldi, A., Harbarth, S., Mendelson, M., Monnet, D.L., Pulcini, C., Kahlmeter, G., Kluytmans, J., Carmeli, Y., Ouellette, M., 2018. Discovery, research, and development of new antibiotics: the WHO priority list of antibiotic-resistant bacteria and tuberculosis. Lancet Infect. Dis. 18, 318–327.

Tam, J.P., Lu, Y.A., Yang, J.L., Chiu, K.W., 1999. An unusual structural motif of antimicrobial peptides containing end-to-end macrocycle and cystine-knot disulfides. Proc. Natl. Acad. Sci. 96, 8913–8918.

Tamaki, M., Akabori, S., Muramatsu, I., 1996. Properties of synthetic analogs of gramicidin S containing L-serine or L-glutamic acid residue in place of L-ornithine residue. Int. J. Pept. Protein Res. 47, 369–375.

Tang, F., Zhang, L., Zhang, Z., Cheng, Z., Zhu, X., 2009. Cellulose filter paper with antibacterial activity from surface-initiated ATRP. J. Macromol. Sci. Part A Pure Appl. Chem. 46, 989–996.

Tang, X.J., Thibault, P., Boyd, R.K., 1992. Characterisation of the tyrocidine and gramicidin fractions of the tyrothricin complex from *Bacillus brevis* using liquid chromatography and mass spectrometry. Int. J. Mass Spectrom. Ion Process. 122, 153–179.

Tharanathan, R.N., 2003. Biodegradable films and composite coatings: past, present and future. Trends Food Sci. Technol. Technol. 14, 71–78.

Troskie, A.M., de Beer, A., Vosloo, J.A., Jacobs, K., Rautenbach, M., 2014a. Inhibition of agronomically relevant fungal phytopathogens by tyrocidines, cyclic antimicrobial peptides isolated from *Bacillus aneurinolyticus*. Microbiology 160, 2089–2101.

Troskie, A.M., Rautenbach, M., Delattin, N., Vosloo, J.A., Dathe, M., Cammue, B.P.A., Thevissen, K., 2014b. Synergistic activity of the tyrocidines, antimicrobial cyclodecapeptides from *Bacillus aneurinolyticus*, with amphotericin B and caspofungin against *Candida albicans* biofilms. Antimicrob. Agents Chemother. 58, 3697–3707.

Van Belkum, M.J., Stiles, M.E., 1995. Molecular characterization of genes involved in the production of the bacteriocin leucocin A from *Leuconostoc gelidum*. Appl. Environ. Microbiol. 61, 3573–3579.

van de Lagemaat, M., Grotenhuis, A., van de Belt-Gritter, B., Roest, S., Loontjens, T.J.A., Busscher, H.J., van der Mei, H.C., Ren, Y., 2017. Comparison of methods to evaluate bacterial contact-killing materials. Acta Biomater. 59, 139–147.

Van Epps, H.L., 2006. René Dubos: unearthing antibiotics. J. Exp. Med. 203, 259–259.

van Rensburg, W., 2015. Characterization of natural antimicrobial peptides adsorbed to different matrices. Stellenbosch University, Department of Biochemistry, Stellenbosch, South Africa. MSc.Thesis, http://scholar.sun.ac.za/handle/10019.1/97929.

Variola, F., Zalzal, S.F., Leduc, A., Barbeau, J., Nanci, A., 2014. Oxidative nanopatterning of titanium generates mesoporous surfaces with antimicrobial properties. Int. J. Nanomedicine 9, 2319–2325.

Vikesland, P., Garner, E., Gupta, S., Kang, S., Maile-Moskowitz, A., Zhu, N., 2019. Differential drivers of antimicrobial resistance across the world. Acc. Chem. Res. 52, 916–924.

Vosloo, J.A., 2016. Optimised bacterial production and characterisation of natural antimicrobial peptides with potential application in agriculture. Stellenbosch University, Department of Biochemistry, Stellenbosch, South Africa. PhD.Thesis, http://scholar.sun.ac.za/handle/10019.1/98411

Vosloo, J.A., Beims, H., Allsopp, M.H., van Rensburg, W., von der Ohe, W., Steinert, M., Rautenbach, M., 2017. Tolerance of honey bee adults and larvae toward tyrothricin peptides derived from *Brevibacillus parabrevis*. Apidologie 48, 833–844.

Wang, Y., Hong, J., Liu, X., Yang, H., Liu, R., Wu, J., Wang, A., Lin, D., Lai, R., 2008. Snake cathelicidin from *Bungarus fasciatus* is a potent peptide antibiotic. PLoS One 3, e3217.

Weinstein, R.A., 1998. Nosocomial infection update. Emerg. Infect. Dis. 4, 416–420.

Wenzel, M., Rautenbach, M., Vosloo, J.A., Siersma, T., Aisenbrey, C.H., Zaitseva, E., Laubscher, W.E., van Rensburg, W., Behrends, J.C., 2018. The multifaceted antibacterial mechanisms of the pioneering peptide antibiotics tyrocidine and gramicidin S. Am. Soc. Microbiol. 9, 1–20.

Wigger-Alberti, W., Stauss-Grabo, M., Grigo, K., Atiye, S., Williams, R., Korting, H.C., 2013. Efficacy of a tyrothricin-containing wound gel in an abrasive wound model for superficial wounds. Skin Pharmacol. Physiol. 26, 52–56.

Willey, J.M., van der Donk, W.A., 2007. Lantibiotics: peptides of diverse structure and function. Annu. Rev. Microbiol. 61, 447–501.

Williams, R.C., Yphantis, D.A., Craig, L.C., 1972. Noncovalent association of tyrocidine B. Biochemistry 11, 70–77. doi:10.1021/bi00751a013

Wimley, W.C., Hristova, K., 2011. Antimicrobial peptides: Successes, challenges and unanswered questions. J. Membr. Biol. 239, 27–34.

Woodward, G.E., Hudson, M.T., 1957. Effect of tyrocidine on the carbohydrate metabolism of yeast and tumor tissue, and on the growth of tumors in mice. J. Franklin Inst. 264, 147–152.

Xiao, Y., Cai, Y., Bommineni, Y.R., Fernando, S.C., Prakash, O., Gilliland, S.E., Zhang, G., 2006. Identification and functional characterization of three chicken cathelicidins with potent antimicrobial activity. J. Biol. Chem. 281, 2858–2867.

Yao, F., Fu, G.D., Zhao, J., Kang, E.T., Neoh, K.G., 2008. Antibacterial effect of surface-functionalized polypropylene hollow fiber membrane from surface-initiated atom transfer radical polymerization. J. Memb. Sci. 319, 149–157.

Yu, Q., Wu, Z., Chen, H., 2015. Dual-function antibacterial surfaces for biomedical applications. Acta Biomater. 16, 1–13.

Zhao, L., Wang, H., Huo, K., Cui, L., Zhang, W., Ni, H., Zhang, Y., Wu, Z., Chu, P.K., 2011. Antibacterial nano-structured titania coating incorporated with silver nanoparticles. Biomaterials 32, 5706–5716.

Chapter 2
High throughput method to determine the activity of antimicrobial polymeric materials

2.1. Introduction

Surface colonization by microorganisms plays a fundamental role in the production problems of various industries. These issues are most prominent in post-harvest infections and spoilage of produce (Chakraborty and Newton, 2011; Srey et al., 2013), especially in the light of international export, shipping or long-term storage. In the food processing industry fresh and ready-to-eat foods are most at risk of infection by pathogens (Ahvenainen, 1996; Gombas et al., 2003; Kaneko et al., 1999; Srey et al., 2013). In medicine, every surface concerning a patient, from operation surfaces to implants and catheters are at risk as a source of infection (Adlhart et al., 2018; Eichner et al., 2019; Otter et al., 2013).

Amidst the alarming rise in resistance of microorganisms against the available antibiotics, and the link between resistance and biofilm formation, much development has gone into preventing surface colonization instead as a preventative measure. Active antimicrobial surfaces are divided into three general categories: anti-adhesion, slow release or contact killing surfaces. Anti-adhesion materials are directly aimed at preventing surface colonization by considering surface roughness (Ivanova et al., 2011; Mrabet et al., 2009), surface hydrophobicity (Fadeeva et al., 2011), and the target organism (Fadeeva et al., 2011). The variety of factors does make the development of a broad-spectrum anti-adhesion material difficult, however, some success had been achieved with mesoporous titanium surface that could prevent adhesion of *E. coli* and *S. aureus* (Variola et al., 2014). In terms of increasing the hydrophobicity of a surface, the incorporation of poly(2-hydroxyethyl methacrylate) onto glass prevented the adhesion of *Salmonella typhimurium* (Mrabet et al., 2009). Slow release or contact killing surfaces are applied to industries where it is beneficial that the microorganisms that encounter the surface are killed rather than just preventing surface colonization. Slow release of an active compound can either be through design, as with medical implants, or through leaching, as with wound dressing and active food packaging. For informative reviews on available technologies from intrinsically active materials, coatings that release nitric oxide, materials that release reactive oxygen species, materials that contain antimicrobial peptides, antibiotics and silver nanoparticles and many others compounds (Campoccia et al., 2013; Muñoz-Bonilla and Fernández-García, 2012).

The research into antimicrobially active solid surfaces has been quite extensive, but there have been limited screening methodologies. Reviews on available methods (Sjollema et al., 2018) indicate that the major limitations are time, cost in terms of consumables, and that these methods can become quite laborious. One of the best performing methods specifically testing solid surface activity, identified in a recent comparative study (van de Lagemaat et al., 2017), is the Japanese industrial standard method JIS Z 2801. However, the well-known disk diffusion type assays are more commonly used by research groups to assess the antimicrobial activity of surfaces and materials (Abou-Yousef and Kamel, 2015; De Moura et al., 2012; Gemili et al., 2009; Imran et al., 2010; Isquith et al., 1972; Rouabhia et al., 2014; Sayanjali et al., 2011).

The JIS Z 2801 method entails the incubation of a microbial culture with the active material for 24 hours after which serial dilutions and plate counts are used to determine the efficacy of the material. Though the method was found to yield repeatable results and truly reflects the surface activity of the material, each sample and organism tested requires multiple dilutions and plating for the numeration of viable cells which can become time and resource consuming.

Disk diffusion and strip diffusion assays are used in the field of antimicrobial solid surface development where either an existing material is chemically modified, or antimicrobial compounds are attached to or absorbed onto selected materials or surfaces. This assay serves as a quick and easy method to determine the optimal conditions and combinations to deliver the wanted antimicrobial response. Diffusion assays are also common in pre-treatment testing in medicine to confirm which antibiotic will have the desired effect and would be a better option for treatment. In both applications the disk diffusion assays are relatively easy but could become laborious when more than one antibiotic/organism needs to be tested (Sarker et al., 2007). The disk diffusion-type assays are also limited to slow release materials and polar compounds that will diffuse through the agar/agarose matrix to enable halo formation in the microbial carpet or microcolony network (Elshikh et al., 2016; Sánchez and Kouznetsov, 2010).

Though both methods require very little infrastructure and training, it takes 20-48 hours before results can be obtained. In order to circumvent the time and laboriousness of the assays, we opted to develop an assay that is dependent on microbial metabolism in 96-well plate format. The resazurin-resorufin type assays utilises vitality/viability chemistry based on the redox status of the cells (Chadha and Kale, 2015). Originally used to detect microbial infections in milk (Erb and Ehlers, 1950; Golding, 1952), it is now also used to determine the efficacy of

novel drugs (Elshikh et al., 2016; Katawera et al., 2014; Sánchez and Kouznetsov, 2010) or hormones (Gutleb et al., 2005; Tsakalozou et al., 2012), as well as their cytotoxicity (Borra et al., 2009; O'Brien et al., 2000). Resazurin (7-hydroxy-10-oxidophenoxazin-10-ium-3-one) is proposed to be taken up by the cell and reduced by the mitochondrial enzymes transferring electrons from appropriate reducing agent, such as NADH, $FADH_2$ $FMNH_2$, $NADPH_2$ and reduced cytochromes leading to the conversion to resorufin (7-hydroxy-3-phenoxazin-10-ium 3-one) (Figure 2.1)(Borra et al., 2009; Chadha and Kale, 2015; O'Brien et al., 2000). Resazurin can also act as a pH indicator and can indicate acidification of a medium due to certain types of microbial contaminants as its neutral form is red at pH<6.5 (Lancaster and Fields, 1996). Furthermore, the irreversible conversion of the resazurin to its fluorescent counterpart by reducing equivalents in cells, resorufin, can be directly correlated to the metabolic activity and vitality/viability of the target cells and by extrapolation, the number of viable cells. The high sensitivity of the dye lies with the increased conversion over time due to the continued cellular metabolism of the viable cells. A drawback is that the resorufin can be lost by conversion to the colourless dihydroresorufin, however, the reaction in reversible over time (Figure 2.1).

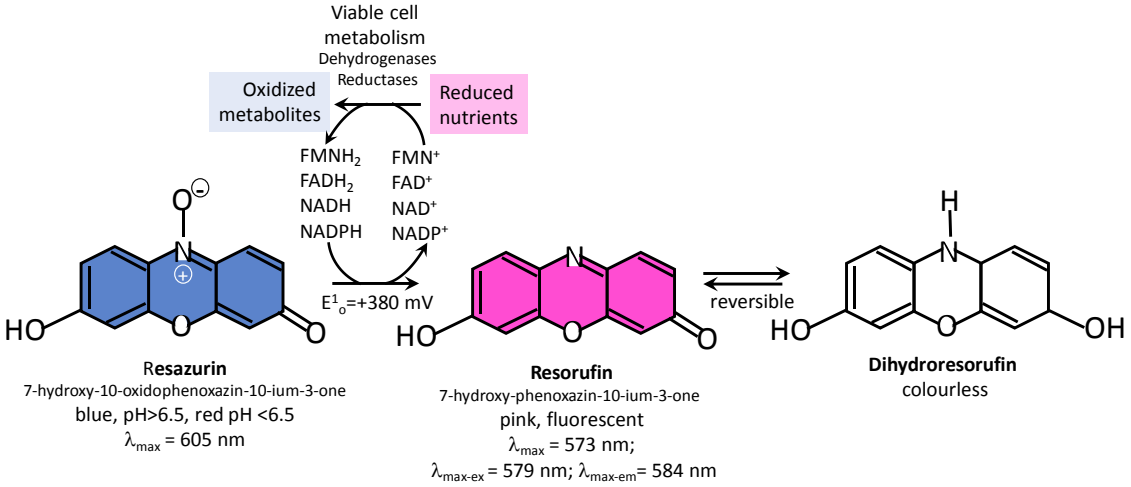

Figure 2.1: Conversion reactions of blue resazurin to its pink fluorescent counterpart, resorufin and colourless dihydroresorufin, upon reduction by reducing equivalents in metabolising/viable cells (Borra et al., 2009; Chadha and Kale, 2015; O'Brien et al., 2000)

In this study we adapted the JIS Z 2801 assay into 96-well format to make use of the smaller sample size and ease of disk diffusion, and combined it with the detection sensitivity of resazurin dye into a high throughput hybrid assay to determine the solid surface activity of newly developed active materials. The two conventional assays and our adapted resazurin assay were evaluated by testing antibiotic-containing cellulose, as reference polymeric matrix,

against four human pathogens *Escherichia coli*, *Pseudomonas aeruginosa*, *Staphylococcus aureus* and *Listeria monocytogenes*.

2.2 Materials

Tetracycline was obtained from Boehringer Mannheim GmbH/Roche Diagnostics GmbH (Germany). Gentamicin, erythromycin, ampicillin, bacitracin, resazurin sodium salt and KCl was supplied by Sigma (St. Louis, MA, USA). Cellulose filters (Paper) (MN 615/No 1) were obtained from Macherey-Nagel (Düren, Germany). Acetonitrile, HPLC-grade far UV cut-off was supplied by Romil Ltd (Cambridge, UK). Merck (Darmstadt, Germany) supplied agar, yeast extract, tryptone, Na_2HPO_4, KH_2PO_4 and Merck (Wadeville, SA) supplied sodium chloride. Petri dishes were provided by Greiner bio-one (Frickenhausen, Germany). The 96-well polystyrene plates were acquired from Corning (Kennebunk, ME, USA) and Whatman Filter paper 1 from GE Healthcare Life Sciences supplied by Sigma-Aldrich (Darmstadt, Germany). Analytical grade water (milliQ) was obtained by filtering water in a reverse osmosis plant through Millipore Milli-Q® water purification system (Milford, USA).

2.3. Methods

2.3.1 Creating antibiotic discs

The antibiotic containing disks were utilised as antimicrobial material models for a proof of concept study, therefore the concentrations used were not selected to mimic any therapeutic values. The selection of agents was chosen as representatives of possible active agents on solid surfaces. Amounts of 0.25 µg to 8.0 µg per active compound per cellulose disk was used for the diffusion assay. Based on the results obtained, 1.0 µg of the respective compounds per disk was used for the JIS Z 2801 and resazurin assay. All the antibiotics were dissolved in water and disks prepared in a 96-well plate to ease with the process.

Accurately assessing the contact killing ability of a novel solid surface would entail ensuring that leachable compounds are accounted for which can be achieved by washing the materials in water (van de Lagemaat et al., 2017). However, since the antibiotics were not actively attached to the cellulose the materials were not washed prior to testing.

2.3.2 Culturing of target organisms

A freezer stock of *Listeria monocytogenes* B73 was streaked out onto BHI agar plates (brain heart infusion) and incubated at 37 ºC for 48 hours until colonies were visible. *Escherichia coli* K12, *Staphylococcus aureus* RN 4220 and *Pseudomonas aeruginosa* ATCC 27853 were

streaked out from freezer stocks onto LB agar plates (1% *m/v* NaCl, 1% *m/v* tryptone, 0.5% *m/v* yeast extract, 1.5% *m/v* agar in water) and incubated at 37ºC for 24 hours. Overnight starter cultures were made by selecting three to five colonies of the target organism and inoculating 1 mL of the respective growth medium. From the starter culture a subculture was made into 6 mL of fresh media and grown until mid-exponential growth phase was reached for each organism. All cultures were incubated at 37 ºC by shaking at 150 RPM at an angle. The mid exponential growth phase and cell concentration for each organism was determined with classical plate counts as: *S. aureus* (OD= 0.3; ± 1.4 x 10^8 cells/mL), *P. aeruginosa* (OD= 0.5; ± 2.9 x 10^8 cells/mL), *L. monocytogenes* (OD= 0.4; 1.3 x 10^8 cells/mL) and *E. coli* (OD= 0.4; 4 x 10^7 cells/mL). Optical density (OD) was determined at 600 nm with path length of 1 cm.

2.3.3 Disk-diffusion method

A culture of target organism (1 mL) with 1 x 10^8 cells/mL was used to cover each square pre-poured agar plate (10 x10 cm) with a cotton tip. Once the plates were dried, the antibiotic containing disks were transferred to the plate, incubated for 20 hours and inspected for halo formation. NBT (nitroblue tertrazolium, 200 µg/mL in water) was incubated for 5 minutes with the *L. monocytogenes* plate to better visualize the halo formation. This visualisation was not deemed necessary for the other three organisms.

2.3.4 Japanese industrial standard method JIS Z 2801

The assay was performed based on a standardised methodology (Cleophas et al., 2014; *Japanese Industrial Standard Jis Z 2801, Test for Antibacterial Activity and Efficacy*, 2010; van de Lagemaat et al., 2017). A solid surface sample with antibiotic was inoculated with 10 µL of a 1.4x10^5 cells/mL cell culture, equivalent to the industrial standard of 5x10^5 cells/cm^2 and incubated for 24 hours at 37°C in a humidity chamber to limit evaporation. Following the incubation, the material disk and incubated culture were transferred to a microcentrifuge tube and 1.00 mL of PBS added. The sample was vortexed for 60 seconds to dislodge any surviving cells from the surface after which the solution was serially diluted, plated onto agar plates and incubated at 30°C for 20-24 hours. Based on the cell count the log reduction of cell number and thus the efficacy of the solid surface could be calculated by using the following equation:

$$Log\ reduction = log_{10}\ \frac{A}{B}$$

Where *A* is the number of CFU determined from the control sample and *B* the number of CFU determined from the antibiotic-containing materials. A cellulose disk containing no antibiotic was used as the growth control.

2.3.5 Resazurin disc method

The standard cell number used to challenge solid surface assays to confirm antimicrobial activity is $5x10^5$ cells/cm^2 with an inoculation volume of 10 µL to ensure surface activity (van de Lagemaat et al., 2017). Three cells concentrations were used for the resazurin assay: $5x10^4$ cells/cm^2, $5x10^5$ cells/cm^2, $5x10^6$ cells/cm^2. Mid-exponential growth cultures of the respective target organisms were diluted to the necessary cell concentration, transferred to a 96-well plate containing the antimicrobial disks and incubated for 1 hour at 37°C. Antibiotic containing discs were placed in 96-well plates in triplicate for each cell concentration, including three controls for each of the antibiotics and three growth controls. After the hour incubation 90µL PBS (phosphate buffer saline: 0.8% *w/v* NaCl, 0.04% *w/v* KCl, 0.144% *w/v* Na_2HPO_4, 0.02% *w/v* KH_2PO_4; pH 7.4) and 10 µL resazurin (3.0, 0.3 and 0.03 mg/mL in PBS) solution were added to each well. The concentration typically used in resazurin based cell viability assays are 10 µL of a 0.3 mg/mL stock solution or variations thereof e.g. 20 µL of 0.15 mg/mL (Riss et al., 2004). Variations on the standard concentration were chosen to increase the sensitivity of the assay. A ten times diluted resazurin concentration (0.03 mg/mL) was chosen to detect low cell numbers ($<10^4$), whereas a ten times concentrated dye solution (3.0 mg/mL) was chosen to improve linearity between the higher cell numbers by prolonging the time to full conversion. After the addition of the PBS and resazurin, the plate was incubated at 37ºC and read on the hour for four hours, which is the suggested stability of the resazurin dye. Fluorescence readings were taken at Ex_{530} and Ems_{590} with the Tecan Spark 10M Multimode Microplate Reader and controlled by the Spark Control™ software, both provided by Tecan Group Ltd (Mennedorf, Switzerland). The percentage inhibition, based on fluorescence (F), was calculated from the following calculation:

$$\%\ \boldsymbol{Inhibition\ of\ Target\ organism} = \frac{\boldsymbol{F\ of\ well - F\ of\ average\ blank}}{\boldsymbol{F\ of\ growth\ control - F\ of\ average\ blank}}$$

2.4. Results

The study represents a proof of concept method for a range of solid surfaces with different active compounds thus the antibiotics were selected to represent a wide range of antimicrobial agents with different modes of action. The activity of each of the antibiotics were not the focus

of the study, but they merely served as test compounds in the creation of model antimicrobial materials used to compare the three methods of activity determination. Five antibiotics were chosen to represent different classes, namely gentamicin (aminoglycoside), ampicillin (penicillin), bacitracin (cyclic branched peptide), gramicidin S (cyclic antibiotic peptide) and tetracycline (polyketide). They differ in size, chemistry (water solubility), in mode of action and target(s). By extension these differences influence the rate of activity and type of activity, which will highlight shortcomings within each of the two existing methods compared with our new method based on the ability of the assays to detect the activity of different antimicrobial compounds.

2.4.1 Disk-Diffusion

Disk diffusion is probably one of the oldest methods used to determine the antimicrobial activity of new compounds (Biemer, 1973; Heatley, 1944). The basis of the method relies on the diffusion of an active compound that has been previously dried onto a disk or strip, to diffuse through a media agar plate and inhibit the growth of the target microorganism around the disk or strip. Since the ability of the assay to detect microbially active materials is in question, activity will be defined as any halo formation regardless of size. However, a halo in a disk diffusion assay would indicate that the compound was no longer attached to the material and diffused into the agar or agarose in order to inhibit microbial growth. As some compounds cannot leach or diffuse in and through the agar, the disks where removed to inspect any microbial growth inhibition under the disks (Figure 2.2). Comparing the active compound containing disks with the control disks, the presence of the disks on the microbial lawn inhibits the growth of the target organism in both cases confirming that detection of surface activity is limited to the formation of halos. This limits the disk diffusion assay to materials with slow release antibiotics and only antibiotics that can diffuse into the gel matrix. Materials with covalently bound antibiotics or antimicrobials and materials with antimicrobials that do not diffuse will yield false negatives in this assay. The appearance of lighter areas under the antibiotic containing disks were due to the disturbance of the agar and not residual growth of the target organism.

Gentamicin, ampicillin and tetracycline are all active against Gram-positive and Gram-negative bacteria, with the MIC of each antibiotic varying depending on the target organism. (Rakic-Martinez et al., 2011). Gramicidin S has both activity against Gram-positive and Gram-negative bacteria, however it loses all activity against Gram-negative bacteria in the presence of agar (Kondejewski et al., 1996). Bacitracin only has Gram-positive activity. This holds true

for the activity against *E. coli* (Figure 2.2), as an example: gentamicin and tetracycline shows good activity and gramicidin S and bacitracin shows no activity, as expected. There is however detectable resistance of *E. coli* against ampicillin.

Based on the results obtained (Table 2.1) the gentamicin (GENT) containing material had the best overall activity, inhibiting all the target organisms at low amounts of the active agent. This was followed by the tetracycline containing material which inhibited the growth of all the organisms, except for *P. aeruginosa* for which it had low level of activity. The gramicidin S (GS) containing material mainly worked against Gram-positive bacteria, whereas the bacitracin and ampicillin containing material had very little to no activity against the target organisms at the range of concentrations for the active agents tested. The conclusion would therefore be that the gentamicin and tetracycline containing material would hold promise for application, the gramicidin S containing material was either limited to applications against Gram-positive bacteria or in need of formulation with another active agent to combat Gram-negative infection. The bacitracin and ampicillin containing material would either be re-evaluated in terms of concentrations or be regarded as ineffective.

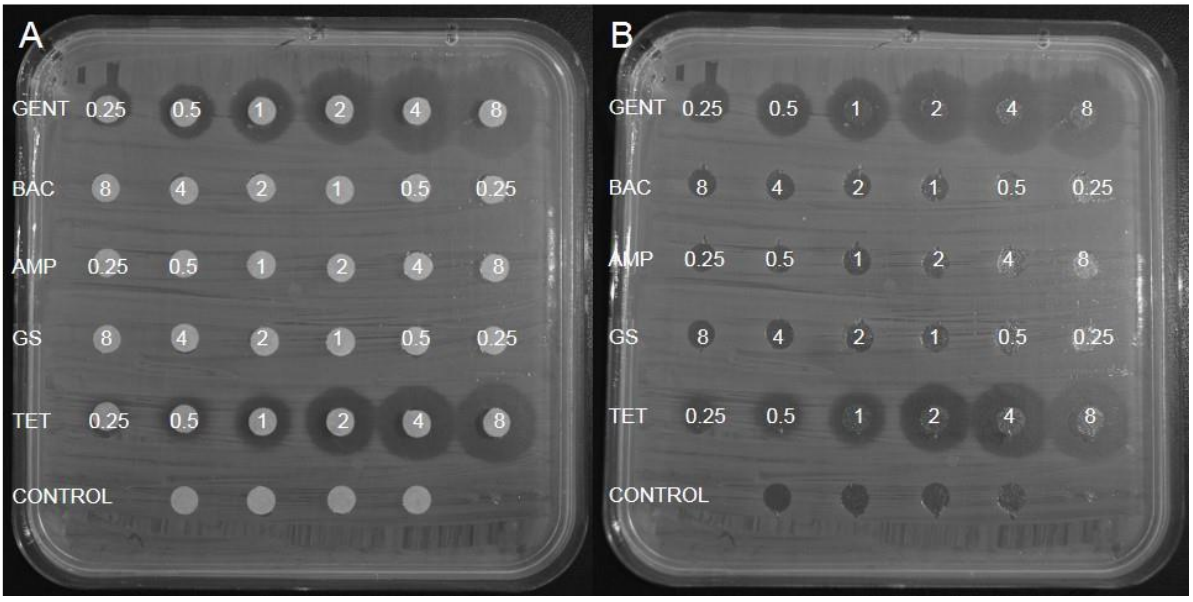

Figure 2.2: Examples of halo formation observed with disk diffusion, after 20 hours of gentamicin (GENT), bacitracin (BAC), ampicillin (AMP), gramicidin S (GS), tetracycline (TET) against *E. coli* **(A)** with and **(B)** with the disks removed. Note that the *E. coli* strain is known to be resistant to AMP, while GS and BAC has weak activity towards Gram negative bacteria

Table 2.1: Summary of the lowest halo-inducing concentration (µg per disk) for each of the antibiotic compounds against the selected organisms as determined by disk diffusion. The data represents two biological repeats.

Compound/ Organism	*L. monocytogenes*	*S. aureus*	*E. coli*	*P. aeruginosa*	*Comments*
Gentamicin	< 0.25	1	< 0.25	1	Broad spectrum of activity
Bacitracin	> 8	> 8	> 8	> 8	Not active
Ampicillin	> 8	8	> 8	> 8	Little activity against *S. aureus*
Gramicidin S	2	1	> 8	> 8	Only active against Gram-positive bacteria
Tetracycline	< 0.25	< 0.25	1	8	Broad spectrum activity except against *P. aeruginosa*

2.4.2 Japanese Industrial Standard method

The Japanese Standard Assay JIS Z 2801 is a method used to determine the antimicrobial activity of solid surfaces, based on the count of viable cells after direct contact incubation with the surface. Based on a review published (van de Lagemaat et al., 2017) on the current solid surface activity determination methods, this method is one of the few to have consistent results in terms of detecting log reduction of both Gram-positive and Gram-negative bacteria after exposure to antimicrobially active surfaces. However, the method is resource and time intensive and laborious when testing more than one organism and a variety of active matrices. As a result, only three antibiotic-containing materials were tested based on the results obtained between the disk diffusion assay and resazurin assay namely gramicidin S, gentamicin and bacitracin. Gentamicin proved to be active in both assays and served as the 'positive control'. On the other hand, bacitracin showed to have very little or no activity and served as the 'negative control'. Gramicidin S showed very little activity against Gram-negative bacteria in the disk diffusion assay but had a much higher activity when tested with the resazurin assay (refer to discussion later). Also, only *L. monocytogenes* and *P. aeruginosa* were selected as the target organisms because of their role in surface contamination in the health and food processing industries as well as both being human pathogens (Otter et al., 2013; Scallan et al., 2011; Srey et al., 2013).

The active materials were incubated overnight with $5x10^5$ cells/cm^2 of each target organism. Flowing the incubation, the disks with the incubated culture were placed in 1.0 mL PBS and vortexed to dislodge the cells from the material. Seven 10-fold dilutions were made, plated onto agar plates and incubated overnight followed by inspection for colony formation. As previously mentioned, this method relies heavily on the successful detachment of single cells and subsequent CFU counts. Based on the observed cell counts the log reduction of each of the materials could be calculated and are summarised in Table 2.2. Important to note: the log reduction reported for the control sample indicates the maximum possible number of cells killed by the active material, based on the cell count observed for the control sample. A cellulose disk containing no antibiotic was used as a control sample for full growth.

The gentamicin-containing material could fully inhibit the growth of *L. monocytogenes* followed by gramicidin S-containing material. The bacitracin-containing material did result in some activity, but it is not considered a viable option in terms of active material. Ideally, considering that development of active materials aims to eradicate or control microbial infection, materials are expected to at least result in a log reduction of 1 (90% inhibition) of the target cell. Activity tests against *P. aeruginosa* showed only gentamicin having activity against the pathogen and resulting in full inhibition. No activity was observed for the bacitracin- and gramicidin S-containing materials.

Table 2.2: Comparison of the log reduction in cell counts (as log_{10} values) determined from the JIS Z 2801 assay to evaluate the activity of gramicidin S-, gentamicin- and bacitracin-containing solid surfaces (paper disks). Efficacy of the disks are expressed as a log reduction, with the control showing the highest possible log reduction as calculated from the full growth observed. A cellulose disk containing no antibiotic was used to determine the growth control. The data represents three technical and one biological repeat.

Compound/ Organism	***L. monocytogenes***	***P. aeruginosa***	***Comments***
Gentamicin	6.4 ±0.1	6.4 ±1.3	Broad spectrum of activity
Bacitracin	0.8 ±0.3	No activity	Some activity against *L. monocytogenes*
Gramicidin S	5.6 ±1.2	No activity	Only active against *L. monocytogenes*
Control	6.4 ±0.1	7.4 ±0.1	Not applicable

Based on the results obtained, as summarized in Table 2.2, the gentamicin-containing material would hold the most promise in terms of preventing solid surface contamination. The gramicidin S-containing materials would also have some application even though it is just active against Gram-positive bacteria. Overall the antibiotic-containing materials were deemed in general more active than determined by the disk diffusion assay where the recorded MIC value was 2 µg compared to the 1 µg tested with the JIS Z 2801 method.

2.4.3 Resazurin solid surface assay

Resazurin was originally developed and used in milk to detect the presence of actively metabolising cells (Erb and Ehlers, 1950; Golding, 1952). The dye is reduced by the cells to its pink fluorescent counterpart, resorufin, but can be further reduced to dihydroresorufin (refer to Figure 2.1) which is translucent and non-fluorescent (O'Brien et al., 2000). The reduction of the dye can be caused by sugars in media and certain antibiotics with reducing character, as was observed in this study at high concentrations of tetracycline. The dye also auto-reduces in light, and therefore the maximum suggested time for incubation with the dye is four hours. Other than the controls of media and solid surfaces, the conversion of resazurin by the organism should be optimised to ensure the best results possible which was done for all the target organisms (supplementary data). As in choosing the best incubation times it is imperative to select a time point that is both sensitive to the lowest cells/cm^2 without sacrificing the linearity of detection. The active materials were incubated with three cell counts: 5x10^5 cells/cm^2 (which is the industry standard), 5x10^4 cells/cm^2 and 5x10^6 cells/cm^2 (which are 10-fold less and more than the standard, respectively). An optimum incubation time was selected for each of the cells counts for each of the organisms. It was observed that the cellulose paper alone did inhibit some growth leading to slightly lower conversion and resorufin fluorescence detected. However, incubation time points were still selected based on the original growth curves in the absence of the cellulose matrix. Furthermore, with some antibiotics greater than 100% inhibition was reported. This is possibly due to entrapment of the resazurin either within cells at low cell numbers or within the cell debris. Such cases were considered as full inhibition of the target organism.

The incubation time selected for *L monocytogenes* based on the best resazurin conversion were at 30 minutes, 1 hour and 3 hours for 5x10^6 cells/cm^2, 5x10^5 cells/cm^2 and 5x10^4 cells/cm^2 respectively (Figure 2.3: A-C). Complete inhibition was observed for gentamicin-, gramicidin S- and tetracycline-containing materials at a cell number of 5x10^4 cells/cm^2. At the same cell number ampicillin-containing materials elicited 90% inhibition and bacitracin inhibited about

50% of the *L monocytogenes* growth. All the materials, except for gramicidin S, were affected by the increase in cell number. At the highest cell number $5x10^6$ cells/cm^2, (Figure 2.3: C) gramicidin S fully inhibited the growth of *L. monocytogenes*, followed by tetracycline and gentamicin. Ampicillin had low activity, whereas bacitracin could be considered to have no activity.

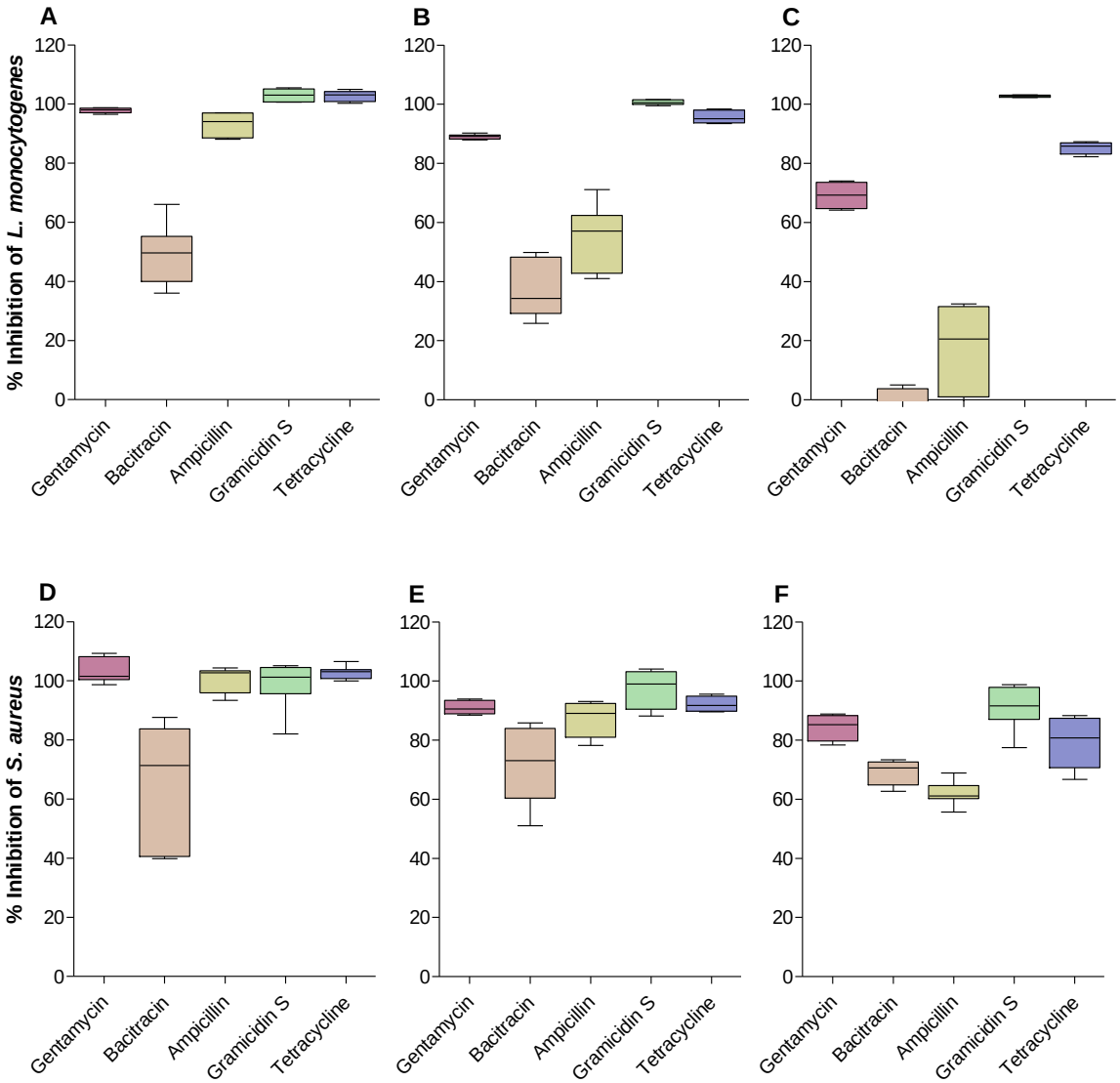

Figure 2.3: Percentage inhibition of 1.0 µg active compound against *L. monocytogenes* at **(A)** $5x10^4$ **(B)** $5x10^5$ **(C)** $5x10^6$ cells/cm^2. Percentage inhibition of 1.0 µg active compound against *S. aureus* at **(D)** $5x10^4$ **(E)** $5x10^5$ **(F)** $5x10^6$ cells/cm^2. The data bars are representative of mean of 8 repeats with error bars showing SD.

Incubation time points selected for *S. aureus* based on the best resazurin conversion were at 1 hour, 2 hours and 4 hours for $5x10^6$ cells/cm^2, $5x10^5$ cells/cm^2 and $5x10^4$ cells/cm^2 respectively

(Figure 2.3: D-F). At a cell number $5x10^4$ cells/cm^2 all the antibiotic-containing materials, except for the bacitracin-containing material, fully inhibited or nearly fully inhibited *S. aureus* metabolism. As was expected the activity of the active materials decreased as the number of cells increased with ampicillin being the most effected. Gramicidin S-, tetracycline- and gentamicin-containing materials would be considered as good choices for inhibition of *S. aureus*. Interestingly the percentage inhibition elicited by the bacitracin-containing material stayed at an average of 70% inhibition regardless of the increase of cell number, possibly linked to the metabolic stress effect the antibiotic has on *S aureus.*

The incubation time selected for *E coli* based on the best resazurin conversion was 1 hour, 2 hours and 4 hours for $5x10^6$ cells/cm^2, $5x10^5$ cells/cm^2 and $5x10^4$ cells/cm^2 respectively (Figure 2.4: A-C). Gentamicin- and tetracycline-containing materials fully inhibited the growth of *E. coli* at $5x10^4$ cells/cm^2, with an expected decrease in activity as the number of cells increased. The results obtained for bacitracin, ampicillin and gramicidin S overall showed a low level of metabolism inhibition and did not show a decrease in the activity with an increase in cell number and has large variances between repeats, thus it would appear that these surfaces do not have a direct antimicrobial impact towards this target organism. Overall the tetracycline material would be considered the most active against *E. coli*.

The incubation time point selected for *P. aeruginosa* was at 4 hours after incubation due to the slow conversion of resazurin by the organism (Figure 2.4: D&E) and no inhibition data could be recorded at $5x10^4$ cells/cm^2, indicating that the assay may be insensitive towards this cell count with *P. aeruginosa* as target. At $5x10^5$ cells/cm^2 (Figure 2.4: D) gentamicin and tetracycline fully inhibits the *P. aeruginosa* growth, activity which remain unaffected at the higher cell number of $5x10^6$ cells/cm^2 (Figure 2.4: E). Some inhibition activity is observed against *P. aeruginosa* for bacitracin, ampicillin and gramicidin S, but completely lost with an increase in cell number.

In terms of assessing the overall activity of each of the materials (Table 2.3), it is clear that gentamicin- and tetracycline-containing materials have good broad spectrum activity, inhibiting either 90% or 100% of the target organism metabolism. Gramicidin S-materials only have activity against Gram-positive bacteria *L. monocytogenes* and *S. aureus*. Ampicillin-materials have mainly Gram-positive activity and is more effective against inhibiting *S. aureus.* Bacitracin-materials overall had very low activity at the concentration of compound tested with some activity against *S. aureus* and *L. monocytogenes*. Thus, the activity of the materials can

be ranked from most effective to least effective as gentamicin/tetracycline> gramicidin S> ampicillin> bacitracin.

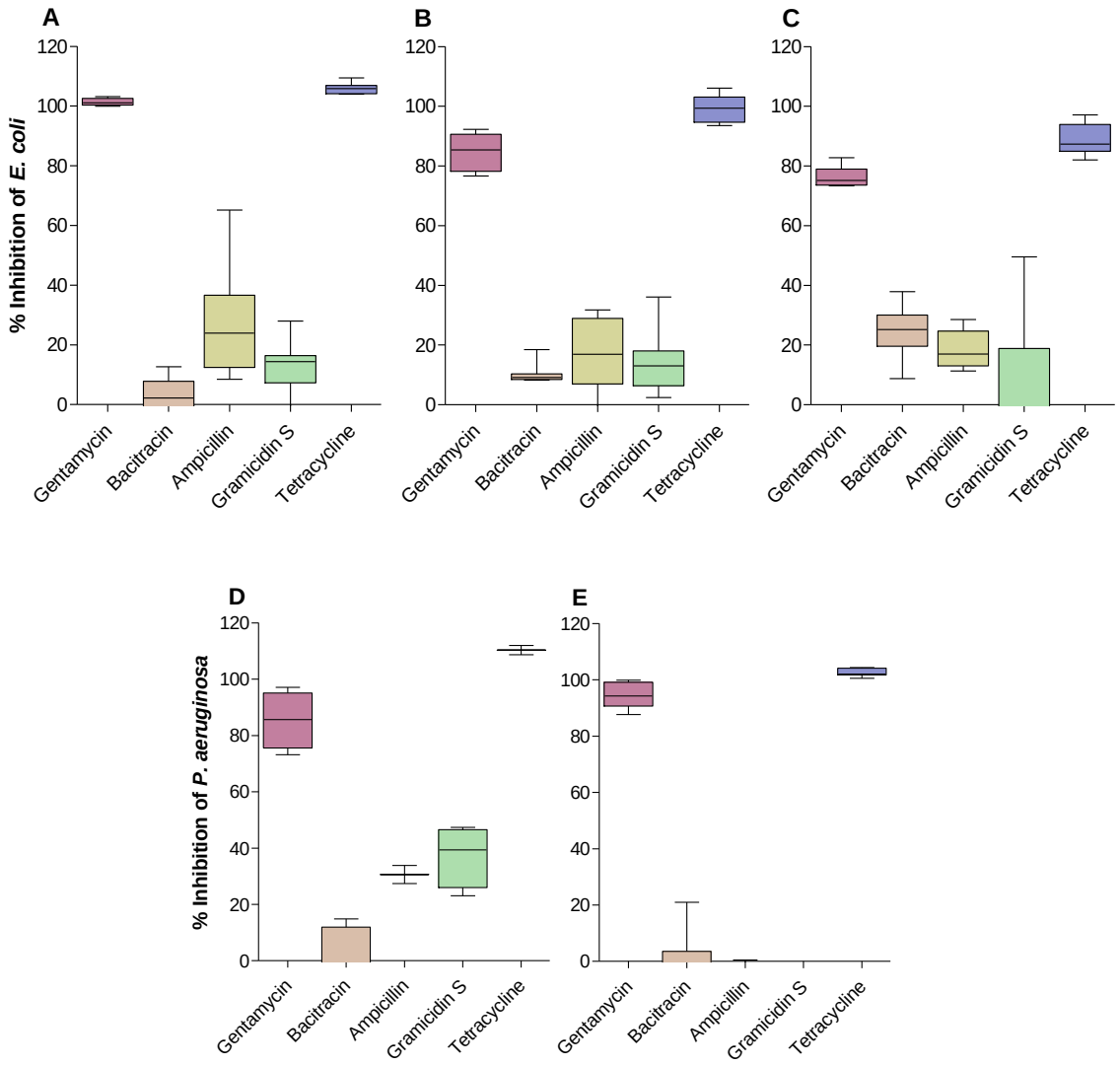

Figure 2.4: Percentage inhibition of 1.0 µg active compound against *E. coli* at **(A)** $5x10^4$ **(B)** $5x10^5$ **(C)** $5x10^6$ cells/cm^2. Percentage inhibition of 1.0 µg active compound against *P. aeruginosa* at **(D)** $5x10^5$ **(E)** $5x10^6$ cells/cm^2. The data bars are representative of mean of 8 repeats with error bars showing SD.

Table 2.3: Comparison of the percentage growth inhibition of each of target organisms at a cell count of $5x10^5$ cells/cm^2 by the active materials. The data is representative of 8 repeats with the mean and SD. Best performing materials for each organism are highlighted in bold.

Compound/ Organism	*L. monocytogenes*	*S. aureus*	*E. coli*	*P. aeruginosa*	*Comments*
Gentamicin	89 ±0.8	**91 ±2.3**	**85 ±6.2**	**85 ±10**	Broad spectrum activity
Bacitracin	37 ±9.6	72 ±13	10 ±3.4	0 ±15	Some activity against *S. aureus* and *L. monocytogenes*
Ampicillin	55 ±11	87 ±5.9	17 ±12	11 ±19	Some activity against *S. aureus* and *L. monocytogenes*
Gramicidin S	**100 ±0.8**	**97 ±6.7**	14 ±10	5.6 ±35	Gram-positive activity
Tetracycline	**96 ±2.1**	**92 ±2.4**	**99 ±4.8**	**110 ±1.6**	Broad spectrum of activity

2.5. Discussion

The widespread effect of surface colonization and subsequent biofilm formation, product spoilage or patient infection is a global issue. Much focus is placed on the development of new and better surfaces to prevent adhesion all together. However, current methods to screen these active materials are lacking in that they are time consuming, costly and laborious which ultimately limits material development and screening. We set out to compare disk diffusion, a Japanese industrial standard for solid surface activity detection and our new resazurin containing method. Disk diffusion and the resazurin assay were evaluated with four target organisms (*E. coli*, *P. aeruginosa*, *S. aureus* and *L. monocytogenes*) and five active compounds (gentamicin, bacitracin, ampicillin, gramicidin S and tetracycline). Due to the laborious nature of the Japanese industrial test JIS Z 2801 test, only three active compounds (gentamicin, bacitracin and gramicidin S) were tested against *L. monocytogenes* and *P. aeruginosa*. The effectiveness of each assay was determined by both comparing the observed sensitivity of the assays to detect the activity of the active polymers and the technical aspects of each of the assays. As each method makes use of different cell concentrations, the methods could not be directly compared in terms of detected killed cells/cm^2. The results are summarised in Table 2.4, in terms of whether the surfaces would have been considered effective by each respective method

All three assays showed that the gentamicin-containing material would hold promise as an antibiotic in a material or on a surface. However, what is interesting is that tetracycline was shown to have little activity against *P. aeruginosa* in the disk diffusion assay but resulted in full inhibition of the organism in the resazurin assay. Gramicidin S was shown to have very good activity against the Gram-positive bacteria but was observed to be much more active in the JIS Z 2801 and resazurin assay compared to the disk diffusion. This can be linked to the gramicidin S not properly diffusing though the agar to elicit a bacterial response. Ampicillin-containing material only had little activity at high concentrations against *S. aureus* as determined by the disk diffusion assay, however 1 µg of ampicillin in the resazurin assay could inhibit 10^4 cells/cm^2 and had activity against *L. monocytogenes* determined with the resazurin assay. Similar results were reported for bacitracin: with the disk diffusion assay the bacitracin-containing material was considered ineffective compared to the resazurin assay where the material had activity against both Gram-positive bacteria at low cell numbers.

Table 2.4: Comparison of the results for each of the active surfaces as determined by the different solid surface assays

Compound/ Assay	***Disk diffusion***	***JIS Z 2801***	***Resazurin Assay***
Gentamicin	Broad spectrum of activity	Broad spectrum of activity	Broad Spectrum activity
Bacitracin	Not active	Some activity against *L. monocytogenes*	Some activity against *S. aureus* and *L. monocytogenes*
Ampicillin	Little activity against *S. aureus*	-	Some activity against *S. aureus* and *L. monocytogenes*
Gramicidin S	Only active against Gram-positive bacteria	Only active against *L. monocytogenes* (Gram-positive)	Gram-positive activity
Tetracycline	Broad spectrum activity except against *P. aeruginosa*	-	Broad Spectrum of activity

Thus, comparison of the three methods: the disk diffusion is only suited to detect slow release active materials where the active compound can easily diffuse through agar whereas the JIS Z 2801 method could detect the true solid surface activity of the materials. The resazurin assay could detect all the activities as seen with JIS Z 2801 and could test more surfaces and organisms due to it being a high throughput method.

Regarding methodology (Table 2.5), the disk diffusion assay has the benefit of being a fully optimized method with clear activity guidelines/thresholds for a range of organisms and compounds that requires very little training and infrastructure. However, as previously mentioned this assay cannot be used to accurately assess the activity of contact killing surfaces but is more suited to slow-release and leaching from materials. Admittedly, the current study did not select for non-leaching materials since the active compounds where not covalently attached to the cellulose disks, however, this can be circumvented by soaking the materials in water for three days, replacing the water every 24 hours (van de Lagemaat et al., 2017). Comparing the two remaining assays the main factors to consider are the time and labour involved obtaining the results (Table 2.5). Both conventional assays gave similar results regarding the activity of the active materials, but results could be obtained with the resazurin assay within 3-8 hours after incubation. In the JIS Z 2801 the activity of the solid surfaces is determined through CFU counts which is a laborious manual exercise. This is overcome in the resazurin assay by directly correlating cell metabolism to number of viable cells on the surface of the material which is then converted to the effectivity of the active material. The assay is also performed in a 96-well plate which enables a broader range of materials and target cells to be tested with a larger number of controls and technical repeats. This high-throughput adaptation allows for quicker screening of materials with less consumables used, ultimately resulting in a similar assay to JIS Z 2801, but cheaper and faster. Furthermore, due to the assay being performed in a 96-well plate it can be easily automated by using a robot dispenser.

2.6. Conclusion

We optimised a method containing resazurin to determine the antimicrobial activity of an active solid surface. This method yields similar results as an industrial standard method, JIS Z 2801, in a shorter time frame and at lower cost. Due to the use of a 96-well plate, the assay is high throughput and can be used to screen multiple samples at a time. This would enable the testing multiple parameters within the creation of antimicrobial materials and surfaces. The use of higher cell counts (ten times higher) than the standard of $5x10^5$ cells/cm^2 allows for faster detection of inhibition but more importantly selects for highly active materials. Furthermore, it can be used as a substitute for the disk diffusion assay in the medical sector were the assay can determine the suitability of antibiotics for treatment. The assay makes use of both disk diffusion and broth assay methodologies and can therefore be adapted to low cost sterility testing in environments that have low infrastructure.

Table 2.5: Comparative summary of advantages, disadvantages and time to results of the disk diffusion, JIS Z 2801 and resazurin assay

	Disk Diffusion	**JIS Z 2801**	**Resazurin Assay**
Advantages	– Established method, requires no optimisation – Inexpensive – Requires little instrumentation – Medium throughput – Requires little sample	– True measure of solid surface activity – Direct contact with cells – Not limited by type of active compound tested	– True measure of solid surface activity – Direct contact with cells – Not limited by type of active compound tested – Can test different cell ranges – High throughput – Requires little sample
Disadvantages	– Limited to active compounds that can diffuse through agar – Limited to slow release materials	– Limited by effectivity of removing cells from surface and CFU plate count – Laborious and costly – Not high throughput – Requires large amounts of sample	– Need to determine conversion of resazurin by target organism – Cell stress can cause false negatives
Time from incubation to results	20-24 hours	40-48 hours	3-8 hours

2.7. References

Abou-Yousef, H., Kamel, S., 2015. High efficiency antimicrobial cellulose-based nanocomposite hydrogels. J. Appl. Polym. Sci. 132, 1–9.

Adlhart, C., Verran, J., Azevedo, N.F., Olmez, H., Keinänen-Toivola, M.M., Gouveia, I., Melo, L.F., Crijns, F., 2018. Surface modifications for antimicrobial effects in the healthcare setting: a critical overview. J. Hosp. Infect. 99, 239–249.

Ahvenainen, R., 1996. New approaches in improving the shelf life of minimally processed fruit and vegetables. Trends Food Sci. Technol. 7, 179–187.

Biemer, J.J., 1973. Antimicrobial susceptibility testing by the Kirby-Bauer disc diffusion method. Ann. Clin. Lab. Sci. 3, 135–140.

Borra, R.C., Lotufo, M.A., Gagioti, S.M., Barros, F.D.M., Andrade, P.M., 2009. A simple method to measure cell viability in proliferation and cytotoxicity assays. Braz. Oral Res. 23, 255–262.

Campoccia, D., Montanaro, L., Arciola, C.R., 2013. A review of the biomaterials technologies for infection-resistant surfaces. Biomaterials 34, 8533–8554.

Chadha, S., Kale, S.P., 2015. Simple fluorescence-based high throughput cell viability assay for filamentous fungi. Lett. Appl. Microbiol. 61, 238–244.

Chakraborty, S., Newton, A.C., 2011. Climate change, plant diseases and food security: An overview. Plant Pathol. 60, 2–14.

Cleophas, R.T., Sjollema, J., Busscher, H.J., Kruijtzer, J.A., Liskamp, R.M., 2014. Characterization and activity of an immobilized antimicrobial peptide containing bactericidal PEG-hydrogel. Biomacromolecules 15, 3390–3395.

De Moura, M.R., Mattoso, L.H., Zucolotto, V., 2012. Development of cellulose-based bactericidal nanocomposites containing silver nanoparticles and their use as active food packaging. J. Food Eng. 109, 520–524.

Eichner, A., Holzmann, T., Eckl, D., Zeman, F., Koller, M., Huber, M., Pemmerl, S., Schneider-Brachert, W., Bäumler, W., 2019. Novel photodynamic coating reduces the bioburden on near-patient surfaces thereby reducing the risk for onward pathogen transmission: a field study in two hospitals. J. Hosp. Infect. doi:10.1016/j.jhin.2019.07.016

Elshikh, M., Ahmed, S., Funston, S., Dunlop, P., McGaw, M., Marchant, R., Banat, I.M., 2016. Resazurin-based 96-well plate microdilution method for the determination of minimum inhibitory concentration of biosurfactants. Biotechnol. Lett. 38, 1015–1019.

Erb, R.E., Ehlers, M.H., 1950. Resazurin reducing time as an indicator of bovine semen fertilizing capacity. J. Dairy Sci. 33, 853–864.

Fadeeva, E., Truong, V.K., Stiesch, M., Chichkov, B.N., Crawford, R.J., Wang, J., Ivanova, E.P., 2011. Bacterial retention on superhydrophobic titanium surfaces fabricated by femtosecond laser ablation. Langmuir 27, 3012–3019.

Gemili, S., Yemenicioglu, A., Altinkaya, S.A., 2009. Development of cellulose acetate based antimicrobial food packaging materials for controlled release of lysozyme. J. Food Eng. 90, 453–462.

Golding, N.S., 1952. Resazurin test for milk. U.S. Patent 2,609,275.

Gombas, D.E., Chen, Y., Clavero, R.S., Scott, V.N., 2003. Survey of *Listeria monocytogenes* in ready-to-eat foods. J. Food Prot. 66, 559–569.

Gutleb, A.C., Meerts, I.A.T.M., Bergsma, J.H., Schriks, M., Murk, A.J., 2005. T-Screen as a tool to identify thyroid hormone receptor active compounds. Environ. Toxicol. Pharmacol. 19, 231–238.

Heatley, N.G., 1944. A rapid method for the assay of penicillin. Biochem. J. 38, 61–65.

Imran, M., El-Fahmy, S., Revol-Junelles, A.M., Desobry, S., 2010. Cellulose derivative based active coatings: Effects of nisin and plasticizer on physico-chemical and antimicrobial properties of hydroxypropyl methylcellulose films. Carbohydr. Polym. 81, 219–225.

Isquith, A.J., Abbott, E.A., Walters, P.A., 1972. Surface-bonded antimicrobial activity of an organosilicon quaternary ammonium chloride. Appl. Environ. Microbiol. 24, 859–863.

Ivanova, E.P., Truong, V.K., Webb, H.K., Baulin, V.A., Wang, J.Y., Mohammodi, N., Wang, F., Fluke, C., Crawford, R.J., 2011. Differential attraction and repulsion of *Staphylococcus aureus* and *Pseudomonas aeruginosa* on molecularly smooth titanium films. Sci. Rep. 1, 165.

Japanese Industrial Standard Jis Z 2801, Test for Antibacterial Activity and Efficacy, 2010. . Japanese Standards Association, Tokyo, Japan, www.jsa.or.jp.

Kaneko, K.I., Hayashidani, H., Ohtomo, Y., Kosuge, J., Kato, M., Takahashi, K., Shiraki, Y., Ogawa, M., 1999. Bacterial contamination of ready-to-eat foods and fresh products in retail shops and food factories. J. Food Prot. 62, 644–649.

Katawera, V., Siedner, M., Boum, Y., 2014. Evaluation of the modified colorimetric resazurin microtiter plate-based antibacterial assay for rapid and reliable tuberculosis drug susceptibility testing. BMC Microbiol. 14, 1–4.

Kondejewski, L.H., Farmer, S.W., Wishart, D.S., Hancock, R.E., Hodges, R.S., 1996. Gramicidin S is active against both Gram-positive and Gram-negative bacteria. Int. J. Pept. Protein Res. 47, 460–466.

Lancaster, M.V., Fields, R.D., 1996. Antibiotic and cytotoxic drug susceptibility assay using resazurin and poising agents. U.S. Patent 5,501,959.

Mrabet, B., Nguyen, M.N., Majbri, A., Mahouche, S., Turmine, M., Bakhrouf, A., Chehimi, M.., 2009. Anti-fouling poly(2-hydoxyethyl methacrylate) surface coatings with specific bacteria recognition capabilities. Surf. Sci. 603, 2422–2429.

Muñoz-Bonilla, A., Fernández-García, M., 2012. Polymeric materials with antimicrobial activity. Prog. Polym. Sci. 37, 281–339.

O'Brien, J., Wilson, I., Orton, T., Pognan, F., 2000. Investigation of the Alamar Blue (resazurin) fluorescent dye for the assessment of mammalian cell cytotoxicity. Eur. J. Biochem. 267, 5421–5426.

Otter, J.A., Yezli, S., Salkeld, J.A.G., French, G.L., 2013. Evidence that contaminated surfaces contribute to the transmission of hospital pathogens and an overview of strategies to address contaminated surfaces in hospital settings. Am. J. Infect. Control 41, S6.

Rakic-Martinez, M., Drevets, D.A., Dutta, V., Katic, V., Kathariou, S., 2011. *Listeria monocytogenes* strains selected on ciprofloxacin or the disinfectant benzalkonium chloride exhibit reduced susceptibility to ciprofloxacin, gentamicin, benzalkonium chloride, and other toxic compounds. Appl. Environ. Microbiol. 77, 8714–8721.

Riss, T.L., Moravec, R.A., Niles, A.L., Benick, H.A., Worzella, T.J., Minor, L., 2004. Assay guidance manual. Eli Lilly & Company and the National Center for Advancing Translational Sciences.

Rouabhia, M., Asselin, J., Tazi, N., Messaddeq, Y., Levinson, D., Zhang, Z., 2014. Production of biocompatible and antimicrobial bacterial cellulose polymers functionalized by RGDC grafting groups and gentamicin. ACS Appl. Mater. Interfaces 6, 1439–1446.

Sánchez, J.G.., Kouznetsov, V.V., 2010. Antimycobacterial susceptibility testing methods for natrual products reseach. Brazilian J. Microbiol. 41, 270–277.

Sarker, S.D., Nahar, L., Kumarasamy, Y., 2007. Microtitre plate-based antibacterial assay incorporating resazurin as an indicator of cell growth , and its application in the in vitro antibacterial screening of phytochemicals. Methods 42, 321–324.

Sayanjali, S., Ghanbarzadeh, B., Ghiassifar, S., 2011. Evaluation of antimicrobial and physical properties of edible film based on carboxymethyl cellulose containing potassium sorbate on some mycotoxigenic *Aspergillus species* in fresh pistachios. LWT - Food Sci. Technol. 44, 1133–1138.

Scallan, E., Hoekstra, R.M., Angulo, F.J., Tauxe, R. V, Widdowson, M., Roy, S.L., Jones, J.L., Griffi, P.M., 2011. Foodborne illness acquired in the United States—major pathogens. Emerg. Infect. Dis. 17, 7–15.

Sjollema, J., Zaat, S.A., Fontaine, V., Ramstedt, M., Luginbuehl, R., Thevissen, K., Li, J., van der Mei, H.C., Busscher, H.J., 2018. In vitro methods for the evaluation of antimicrobial surface designs. Acta Biomater. 70, 12–24.

Srey, S., Jahid, I.K., Ha, S. Do, 2013. Biofilm formation in food industries: A food safety concern. Food Control 31, 572–585.

Tsakalozou, E., Eckman, A.M., Bae, Y., 2012. Combination effects of docetaxel and doxorubicin in hormone-refractory prostate cancer cells. Biochem. Res. Int.

van de Lagemaat, M., Grotenhuis, A., van de Belt-Gritter, B., Roest, S., Loontjens, T.J.A., Busscher, H.J., van der Mei, H.C., Ren, Y., 2017. Comparison of methods to evaluate bacterial contact-killing materials. Acta Biomater. 59, 139–147.

Variola, F., Zalzal, S.F., Leduc, A., Barbeau, J., Nanci, A., 2014. Oxidative nanopatterning of titanium generates mesoporous surfaces with antimicrobial properties. Int. J. Nanomedicine 9, 2319–2325.

2.8 Supplementary data

Disk diffusion

Pictures of the remaining disk diffusion results can be found for *P. aeruginosa* (Figure S2.1), for *S. aureus* (Figure S2.2) and *L. monocytogenes* (Figure S2.3).

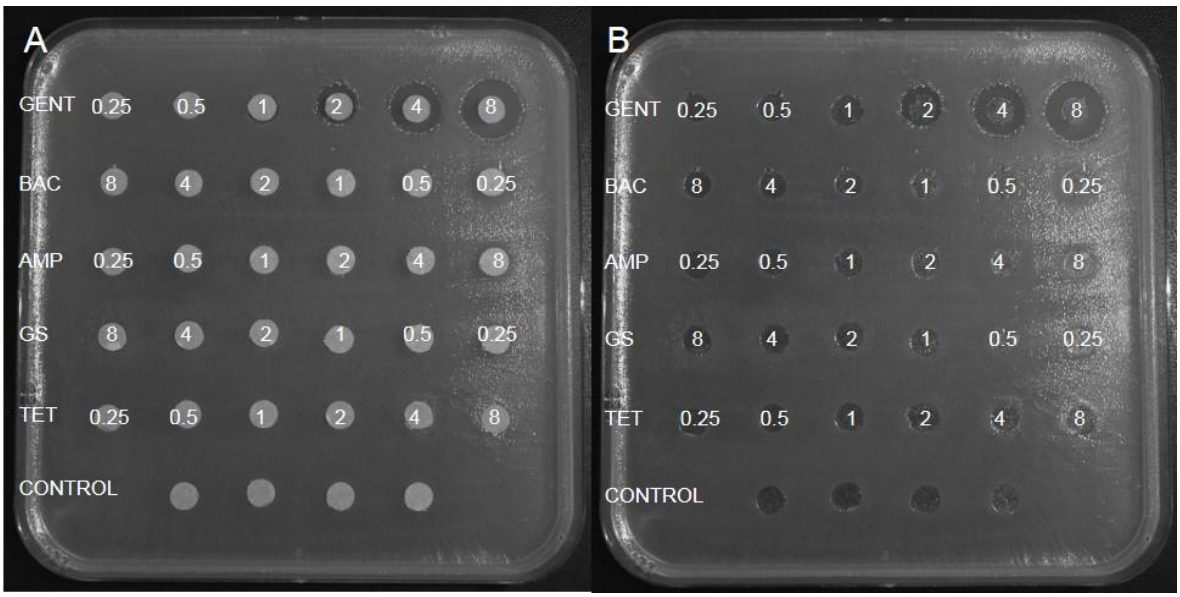

Figure S2.1: An example of halo formation observed with disk diffusion, after 20 hours of gentamicin (GENT), bacitracin (BAC), ampicillin (AMP), gramicidin S (GS), tetracycline (TET) against *P. aeruginosa* **(A)** with and **(B)** without the disks. Note that only activity is observed for gentamicin.

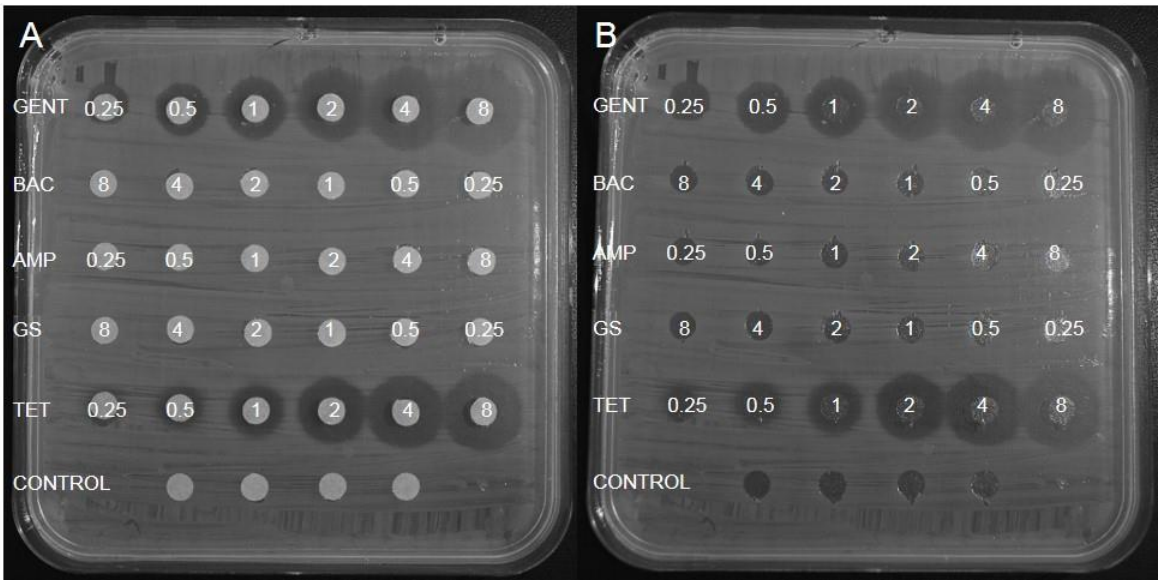

Figure S2.2: An example of halo formation observed with disk diffusion, after 20 hours of gentamicin (GENT), bacitracin (BAC), ampicillin (AMP), gramicidin S (GS), tetracycline (TET) against *S. aureus* **(A)** with and **(B)** without the disks. Note the activity of gentamicin and tetracycline.

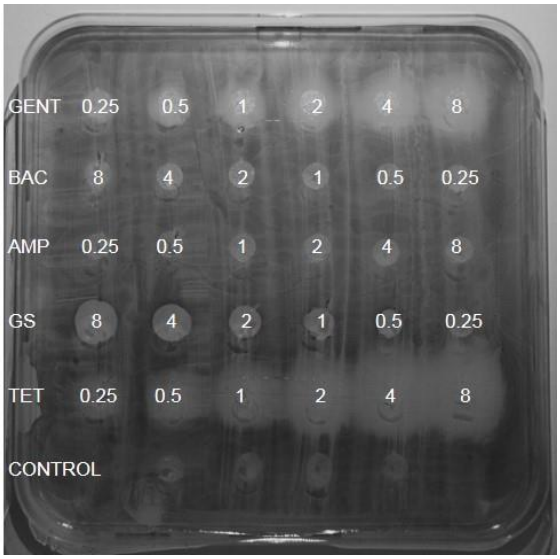

Figure S2.3: An example of halo formation observed with disk diffusion, after 20 hours of gentamicin (GENT), bacitracin (BAC), ampicillin (AMP), gramicidin S (GS), tetracycline (TET) against *L. monocytogenes* without the disks. Halo visualisation was dependent on the NBT conversion of L. monocytogenes. Note the activity of gentamicin, gramicidin S and tetracycline.

Optimisation of the resazurin solid surface assay

Resazurin is used to detect the activity of compounds by directly correlating the amount of resorufin (fluorescent counterpart of resazurin) to the metabolism of viable cells. It is therefore first important to determine the linearity of the dye conversion to cell number to fully ascertain the percentage of inhibition caused by the active compound. Second, to determine the repeatability between cultures in terms of lowest detectable cell count within four hours which will ultimately affect the sensitivity of the assay. The target cells were cultured as previously described, a dilution of cells incubated with three concentrations of resazurin, and the fluorescence read every hour for four hours. Due to the fast conversion of resazurin by *L. monocytogenes* readings were taken at 30 minutes and then every hour. Conversion of cells/mL to cells/cm^2 was done by calculating the number of cells added to each well in 10 µL culture divided by the surface area of the well/disk (0.28cm^2).

Incubation of *E. coli* showed good linearity after one hour of incubation for all three concentrations of resazurin (Figure S2.4), with the lowest cell number detected as 10^4 cells/cm^2. The presence of 10^3 cells/cm^2 can be confirmed after 4 hours, but due to the maximum dye conversion at the growth control this could only be confirmed as growth or as not full inhibition. A study of the conversion curves at the higher cell numbers at three and four hours of incubation shows the plateau that forms due to the maximum dye that is converted. When comparing the concentrations of resazurin, it is clear the 0.03 mg/mL solution (Figure S2.4: A) is too sensitive to changes in cell metabolism and could very easily lead to false conclusions. The results for 0.3 mg/mL and 3.0 mg/mL (Figure S2.4: B and C, respectively) showed similar results in repeatability, however 0.3 mg/mL is more sensitive in the amount of relative fluorescence units (RFU) detected. This is crucial to better distinguish between cell metabolism, by extension cell counts and ultimately percentage inhibition when in contact with the active materials. Similar results were observed with *S. aureus* (Figure S2.5): 0.03 mg/mL yields similar results, but 0.3 mg/mL is more sensitive in RFU. The best incubation time to read the fluorescence is at one hour due to the linearity of cells/cm^2 and detected fluorescence. The lowest confirmed cell count is at 10^4 cells/cm^2 after one hour which could not be improved with a longer incubation time. The fluorescence detected at 3.0 mg/mL for all the organisms were similar to the low fluorescence at 0.03 mg/mL. The low fluorescence detected at 3.0 mg/ml resazurin is possibly due to masking of the resorufin (pink) by the excess resazurin (blue) whereas the low fluorescence detected 0.03 mg/mL resazurin is possibly a combination

between low amount of resorufin formed and the formation of the non-fluorescent dihydroresorufin.

As previously mentioned, *L. monocytogenes* converts the resazurin very quickly giving the best growth curve in terms of cell concentration to conversion at 30 minutes of incubation time for each of the dye concentrations (Figure S2.6). Regarding resazurin concentrations, 0.03 mg/mL is too sensitive and results in inconsistent growth curves. The higher 3.0 mg/mL resazurin has good repeatability between biological repeats but is not sensitive enough to distinguish between the different concentrations with the lowest detection being 10^3 cells/cm^2 after 3 hours. The best concentration of resazurin is 0.3 mg/mL since it gives both a good linearity at 30 minutes incubation, is sensitive enough to detect the range of cell concentrations and can confirm the presence of 10 cells/cm^2 after 3 hours of incubation.

P. aeruginosa converts resazurin very slowly (Figure S2.7), even with the low concentration 0.03 mg/mL resazurin gives low fluorescence results. All three concentrations of resazurin gives the same trend in cell number to fluorescence and can only detect 10^4 cells/cm^2 after 4 hours of incubation. Based on the sensitivity and highest fluorescence signal, 0.3mg/mL resazurin gave the best results.

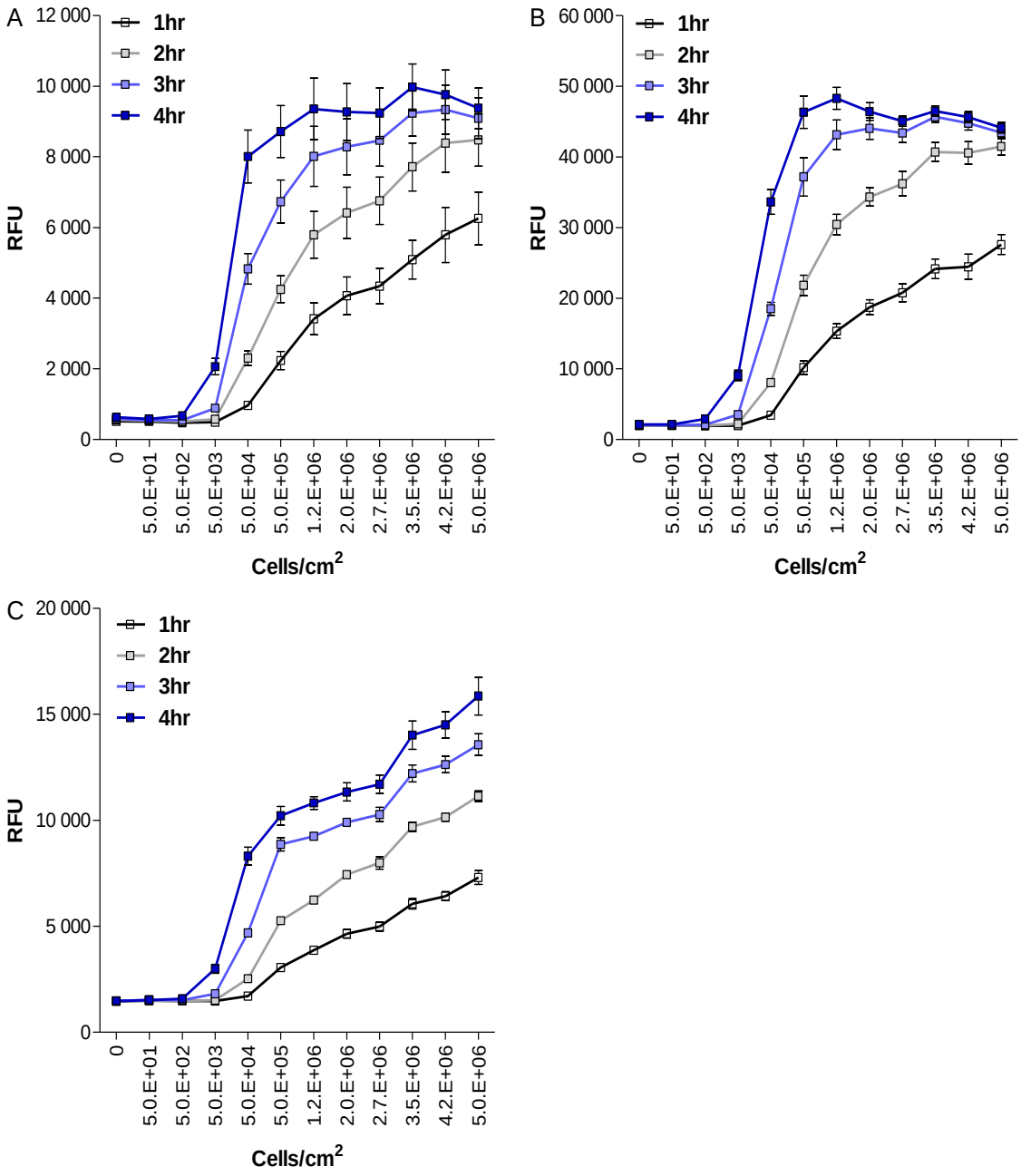

Figure S2.4: Fluorescence observed for a dilution of *E. coli* cells over four hours at resazurin concentrations of **(A)** 0.03mg/mL **(B)** 0.3mg/mL and **(C)** 3mg/mL. The data points represent the mean of three technical and three biological repeats with error bars showing the standard error of the mean (SE).

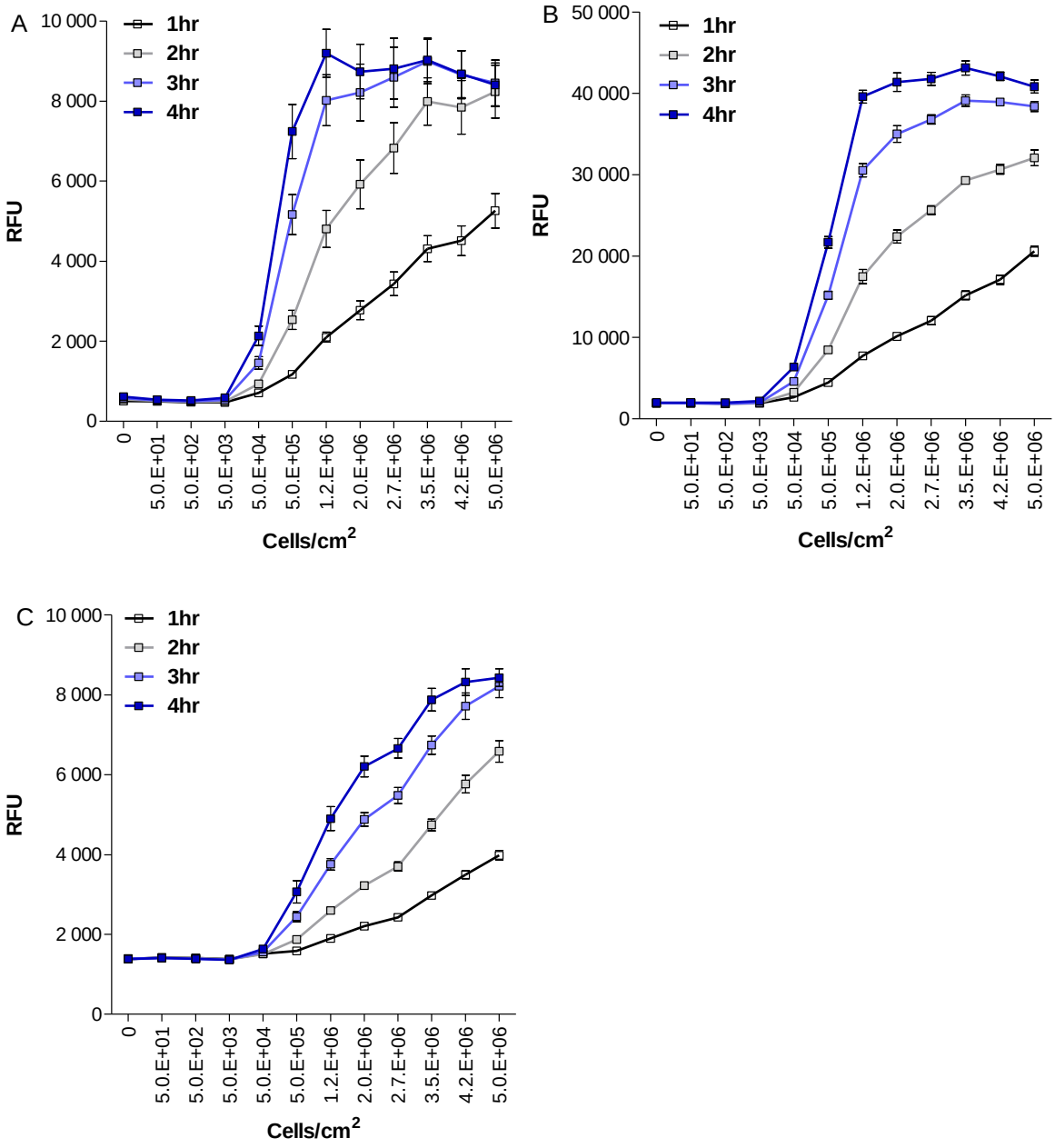

Figure S2.5: Fluorescence observed for a dilution of *S. aureus* cells over four hours at resazurin concentrations of **(A)** 0.03mg/mL **(B)** 0.3mg/mL and **(C)** 3mg/mL. The data points represent the mean of three technical and three biological repeats with error bars showing the standard SE.

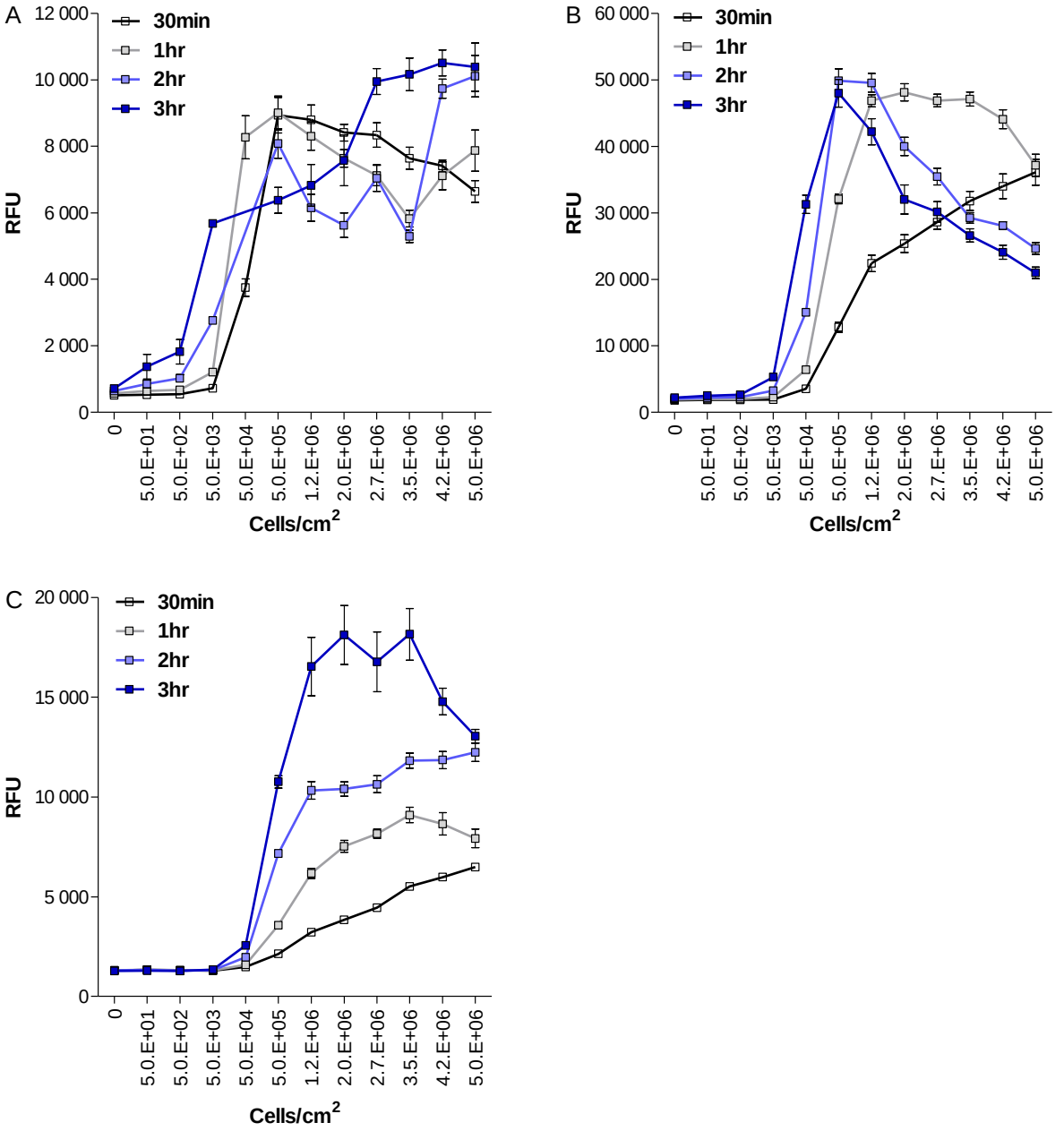

Figure S2.6: Fluorescence observed for a dilution of *L. monocytogenes* cells over three hours at resazurin concentrations of **(A)** 0.03mg/mL **(B)** 0.3mg/mL and **(C)** 3mg/mL. The data points represent the mean of three technical and three biological repeats with error bars showing the standard SE.

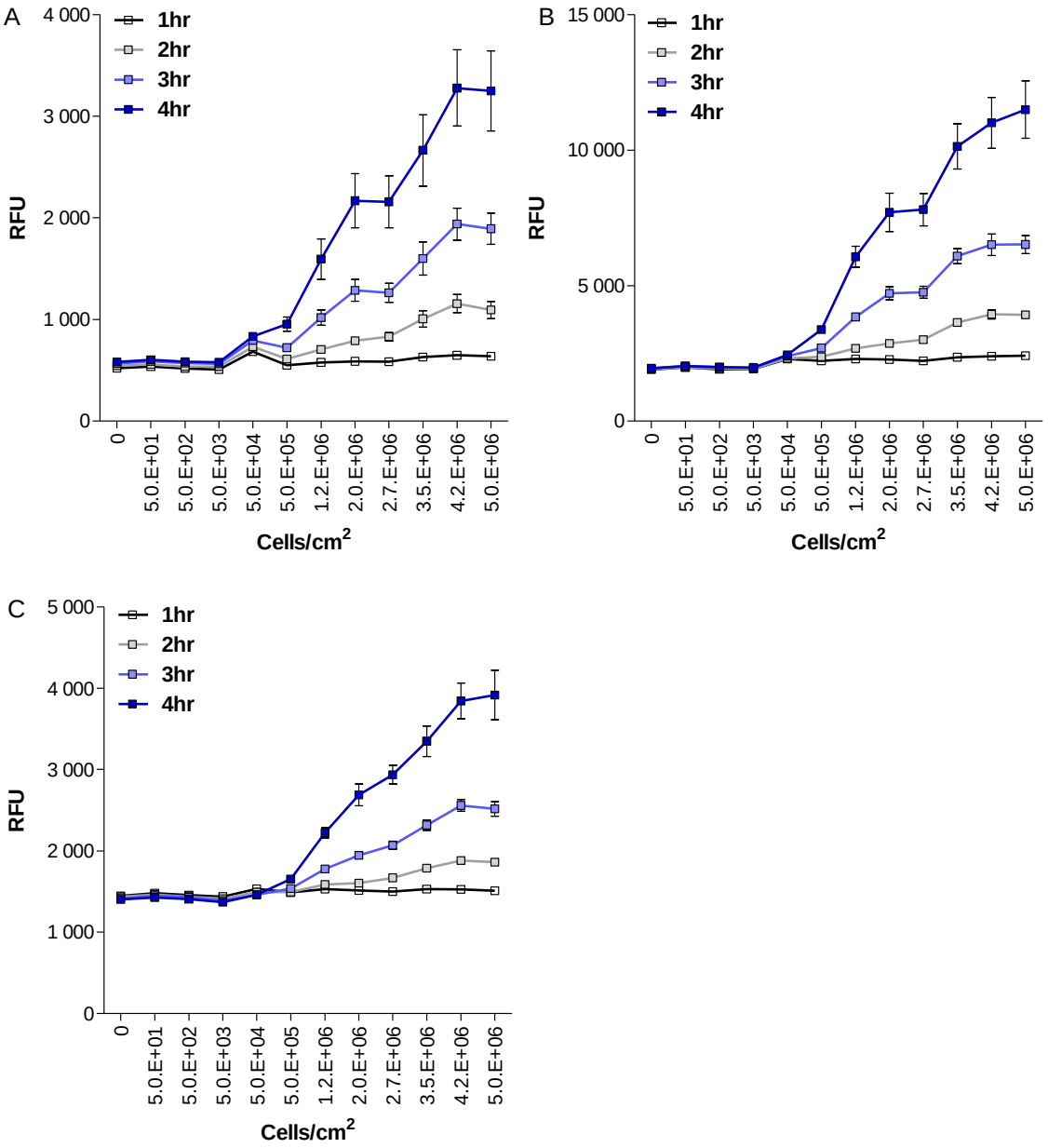

Figure S2.7: Fluorescence observed for a dilution of *P. aeruginosa* cells over four hours at resazurin concentrations of **(A)** 0.03mg/mL **(B)** 0.3mg/mL and **(C)** 3mg/mL. The data points represent the mean of three technical and three biological repeats with error bars showing the standard SE.

Chapter 3
Creating robust antimicrobial materials with sticky tyrocidines

3.1 Introduction

Surface contamination with microorganisms affects multiple industries throughout the production and supply chain. Persistent microbial contamination results in product losses and the inadequate treatments can promote resistance in plant and human pathogens with increased health risks, which in totality can put financial strain on any industry. It is therefore crucial to limit surface microbial contamination as much as possible as this leads to secondary transfer and spread of microbial pathogens. However, the affected 'surface' and possible preventative measures differ from industry to industry.

As an example: the fruit industry faces a list of post-harvest problems such as bacterial and fungal infections, spoilage, drying/shrivelling and moisture loss. Fortunately, most of these concerns are addressed with the use of edible coating for fruits (Cuq et al., 1995; Gol et al., 2013; Murmu and Mishra, 2017). In addition to the protective coatings, fruits are packaged to prevent bruising and to some extent moisture loss (Opara and Fadiji, 2018; Sung et al., 2013). The concern, however, is that a baseline of infection in these packaging materials would lead to the spoilage of the very fruit it is supposed to protect. A large amount of fruits produced in the Southern hemisphere are exported to European markets (SHAFFE, 2018) with an increasing demand for environmentally friendly or 'green' products (Gol et al., 2013; Haws et al., 2014; Rautenbach et al., 2015). There is therefore a need for an antimicrobial agent that would continually sterilize the packing material, that is not a harsh and/or leaching chemical but falls within the scope of a 'green biocide'. Recent environmental studies have also stressed the hazardous impact plastic consumables have regarding the manufacturing of plastic as well as the negative effect of waste on wildlife, especially marine animals (Gall and Thompson, 2015; Kühn et al., 2015). Possible solutions include biodegradable plastic-mimicking substitutes, however, due to their biodegradable nature these materials are susceptible to microbial contamination that would affect the integrity of the materials. As previously mentioned, legislation is moving towards the implementation of 'green solutions' and therefore it is beneficial if a green biocide can prolong the use of these materials. Antimicrobial peptides are likely candidates to be used in the protection of food and creation of novel solid surfaces. Nisin is one of the few antimicrobial peptides with GRAS (Generally Recognised As Safe)

approval for food preservation (Carmona-Ribeiro and Carrasco, 2014; Sung et al., 2013) and at the centre of antimicrobial surface development research, especially cellulose based packaging and wound dressings (Barbosa et al., 2013; Ercolini et al., 2010; Imran et al., 2010; Mauriello et al., 2005; Nguyen et al., 2008). Following the success of nisin, other antimicrobial peptides are being considered for similar applications (Rydlo et al., 2006).

The tyrocidines and tyrocidine analogues (Trcs) are antimicrobial cyclodecapeptides produced by the soil bacterium *Brevibacillus parabrevis* during the late logarithmic growth phase (Federn and Ristow, 1987; Fujikawa et al., 1968b; Okuda et al., 1963; Oyama and Kubota, 1990) as part of a peptide complex with linear gramicidins (gramicidin D) collectively known as tyrothricin. Trcs has a broad-spectrum activity against Gram-positive bacteria such as *Listeria monocytogenes* (Spathelf and Rautenbach, 2009), *Staphylococcus aureus* (Dubos et al., 1942), *Streptococcus hemolyticus* (Dubos et al., 1942), *Micrococcus luteus* (Spathelf and Rautenbach, 2009) and a broad range of environmental Gram-positive bacteria (Rautenbach et al., 2015). Furthermore, these cyclodecapeptides have activity against the human pathogenic yeast *Candida albicans* (Troskie et al., 2014b) and filamentous fungi such as *Fusarium ssp* (Rautenbach et al., 2015; Troskie et al., 2014a), *Botrytis cinerea* (Troskie et al., 2014a), *Aspergillus fumigatus* (Rautenbach et al., 2016) and a broad range of fungal plant pathogens (Rautenbach et al., 2016, 2015). Trcs are primarily active against Gram-positive bacteria, however, they do have some activity against Gram-negative bacteria (Chopra et al., 2010; Dubos and Hotchkiss, 1941; Rautenbach et al., 2015). These peptides are mainly membrane active (Mach and Slayman, 1966; Troskie et al., 2014a, 2014b), but other intracellular targets have been reported (Dubos, 1939; Seddon and Fynn, 1972). The combination of multiple modes of action and the speed of activity (Mach and Slayman, 1966; Spathelf and Rautenbach, 2009) makes the development of resistance less likely. The peptides are unfortunately haemolytic and leukocytolytic (Rammelkamp and Weinstein, 1942; Van Epps, 2006) limiting them to topical clinical applications. It must be noted that in more than 70 years that it has been used as topical cream and in throat lozenges, no resistance could be found or induced against the peptides in tyrothricin (Wigger-Alberti et al., 2013).

Continual losses in peptide yield during purification and in the preparation of microdilution assays observed by our research group has highlighted the possible association of the Trcs to filters, plastics and chromatography resins. This unwanted adsorption to materials could be harnessed to create broad spectrum antimicrobial surfaces. The peptides themselves are heat stable, pH stable and resistant to degradation (Dubos, 1939; Hotchkiss, 1941) providing the

needed stability for the industrial application of peptide-containing solid surfaces. Their membranolytic mode of action is also perfectly suited for the creation of an antimicrobial solid surface, since they can still come into contact with its target(s) on the cell surface of the microorganism. As such, a membranolytic agent can elicit antimicrobial activity while being associated to a surface which is a key point to consider with the development of antimicrobial surfaces (Bagheri et al., 2011).

In this study, we utilised general laboratory-acquired and commercial materials to test the retention of tyrocidines and their surface-associated antimicrobial activity against a model pathogenic Gram-positive organism, *L. monocytogenes*. Subsequently the robustness of the antimicrobial activity on the filter type materials was determined through multiple rounds of exposure to *L. monocytogenes* and *Escherichia coli*. The stability of these peptides on cellulose were also determined through exposure to heat, pH ranges, salt solutions, acidic solutions, acetonitrile, multiple water washes and the surfactant, sodium dodecyl sulphate. Finally, the uniqueness of tyrocidine association to cellulose was determined by comparison to the activity of cellulose treated with other antimicrobial peptides against *L. monocytogenes* and *E. coli*.

3.2 Materials

Gramicidin S, gramicidin D, tyrothricin, gentamicin, resazurin sodium salt and KCl was supplied by Sigma (St. Louis, MA, USA). Acetonitrile, HPLC-grade far UV cut-off was supplied by Romil Ltd (Cambridge, UK). Merck (Darmstadt, Germany) supplied agar, yeast extract, tryptone, Na_2HPO_4, KH_2PO_4 and Merck (Wadeville, SA) supplied sodium chloride, brain heart infusion broth and black 96-well polystyrene plates. 96-well polystyrene plates were acquired from Corning (Kennebunk, ME, USA) and cellulose filters (Paper) (MN 615/No 1) were obtained from Macherey-Nagel (Düren, Germany). Mixed cellulose ester filters (HAWP, GSWP) were supplied by Waters-Millipore (Milford, USA). Polycarbonate filters were supplied by Nuclepore Corp (Plesanton, CA, USA) and cellulose nitrate was provided by Sartorius (Gottingen, Germany). AcroPrep™ Advance 96 filter plates were sourced from Pall Corporation (Ann Arbor, MI, USA). Analytical grade water was obtained filtering water from a reverse osmosis plant through Millipore Milli-Q® water purification system (Milford, USA). Melittin, magainin 2, leucocin A and PGLa was sourced from of the BIOPEP™ peptide library (Stellenbosch University, South Africa).

3.3 Methods

3.3.1 Selecting base materials

A range of laboratory and commercial materials was selected to study the association and resulting activity of tyrocidines (refer to Table 3.1 under results for details on materials). The laboratory materials included filters commonly used in solvent filtration: mixed cellulose GSWP (0.22 µm) and HAWP (0.45 µm), cellulose nitrate (CN)(0.45 µm), polycarbonate (PC)(0.4 µm) and cellulose (CL). Also included were plates used for peptide preparation and dose-response assays: black polystyrene plate used for fluorescence (BP), clear polystyrene plate (AP), clear round-bottom polypropylene plate (PPR) and clear round-bottom polystyrene plate (PSR). The commercial materials included fruit packaging materials: tissue paper, ripple carton, paper tray and carton box and a plastic tray. Biodegradable materials included: meat packaging paper that has a polylactate layer that is normally in contact with the meat (meat paper & meat paper PL), biodegradable polylactate plastics namely a waste bag marketed for home use (white bag), an industrial grade waste bag (green bag) and cling film that is marketed for both home and catering purposes.

3.3.2 Creation of antimicrobial materials

Circular punches of the base material were created with an office-type paper punch that was sterilised with 70% isopropanol. An aqueous solution of antimicrobial compound (100 µL of 50.0 µg/mL; 5% *v/v* acetonitrile) was incubated for two hours with the base material punch (0.28 cm^2) ensuring that 5.0 µg of compound was available for binding. Following the incubation, the antimicrobial compound solution was removed, and the samples washed twice with 100 µL sterile analytical quality water and dried in a 40 °C oven for 2 hours. The antimicrobial compounds used in this study are given in Table 3.2.

3.3.3 Antimicrobial activity of Trc-containing materials

The antimicrobial activity of the Trc-containing materials and films were determined by the developed resazurin assay described in Chapter 2. *Listeria monocytogenes* B73 was streaked out from freezer stocks onto BHI agar plates (Brain Heart Infusion; 1.5% w/v agar) and incubated for 48 hours at 37°C until colonies were viable. *Escherichia coli* K12 was streaked out from freezer stocks onto LB plates (1% *m/v* NaCl, 1% *m/v* tryptone, 0.5% *m/v* yeast extract, 1.5% *m/v* agar in water) and incubated at 37 ºC for 24 hours. Starter cultures were prepared, by inoculating 1 mL medium with 3-5 colonies and growing the cells overnight at 37 °C at an angle, shaking at 150RPM. The starter culture was sub-cultured into fresh media, grown until

mid-exponential growth phase was reached at at an OD_{600} = 0.4, which is ±1.3 x 10^8 cell/mL for *L. monocytogenes* and 4 x 10^7 cells/mL for *E. coli*. This culture was then pipetted (10 µL) onto the treated and untreated materials in a 96-well polypropylene plate and incubated for one hour at 37°C. Following the incubation, 90 µL PBS (phosphate buffered saline; 0.8% *w/v* NaCl, 0.04% *w/v* KCl, 0.144% w/v Na_2HPO_4, 0.02% *w/v* KH_2PO_4; pH 7.4) and 10 µL resazurin dye (0.3 mg/mL in PBS) was added followed by a further incubation at 37°C. The conversion of the resazurin was measured at Ex_{530} and Em_{590} after 30 minutes, and every hour for three hours using the Tecan Spark 10M Multimode Microplate Reader and controlled by the Spark Control™ software, both provided by Tecan Group Ltd (Mennedorf, Switzerland). Materials remained in the well as it did not interfere with fluorescence measurements. The activity of the material was determined in terms of percentage inhibition by using the acquired fluorescence readings (F), calculated with the following equation:

$$\%\ \boldsymbol{Inhibition\ of\ Target\ organism} = \frac{\boldsymbol{F\ of\ well - F\ of\ average\ blank}}{\boldsymbol{F\ of\ growth\ control - F\ of\ average\ blank}}$$

3.3.4 Determining the amount of Trcs in antimicrobial materials

Previous methods made use of the UV absorption at A_{280} of the incubation solution, before and after treatment, to determine the amount of peptide bound to the solid surface (van Rensburg, 2015). However, background interference from compounds released from cellulose made detection difficult. Therefore, a fluorescence method was developed tracking the naturally occurring fluorophores found in the tyrocidine structure (Trp at position 3 and/or 4 and Tyr at position 7). Optimisation of the method and standard curve used to calculate the amount of peptide bound can be found in the supplementary data. All fluorescence results were background subtracted to remove any effect the materials had on the fluorescence signal.

The incubation step, during the creation of the antimicrobial materials, was used for the Trc mix treated materials to study the rate of association of the peptides to the base material Fluorescence with Ex_{290} and Em_{342} was monitored for two hours. Fluorescence readings were collected by using the Tecan Spark 10M Multimode Microplate Reader and controlled by the Spark Control™ software, both provided by Tecan Group Ltd (Mennedorf, Switzerland).

3.3.5 Filtration experiment

Treated and untreated materials were transferred to a 96-well plate containing 1 µm glass filters and sterilized. A culture of *L. monocytogenes* and *E. coli* was prepared as described above and diluted in PBS to 1.4x10^7 cells/mL. The cultures (100 µL) were then transferred to the filter

plate, allowed a contact time of 2 minutes after which the solution was removed via vacuum in a manifold filtration setup. This process was repeated three times. Following the cell exposure, PBS (90 µL) and resazurin (10 µL) were added to the filter plate whereas only resazurin (10 µL) was added to the plates containing the filtrates. Plates were incubated at 37°C, and the fluorescence monitored as described above.

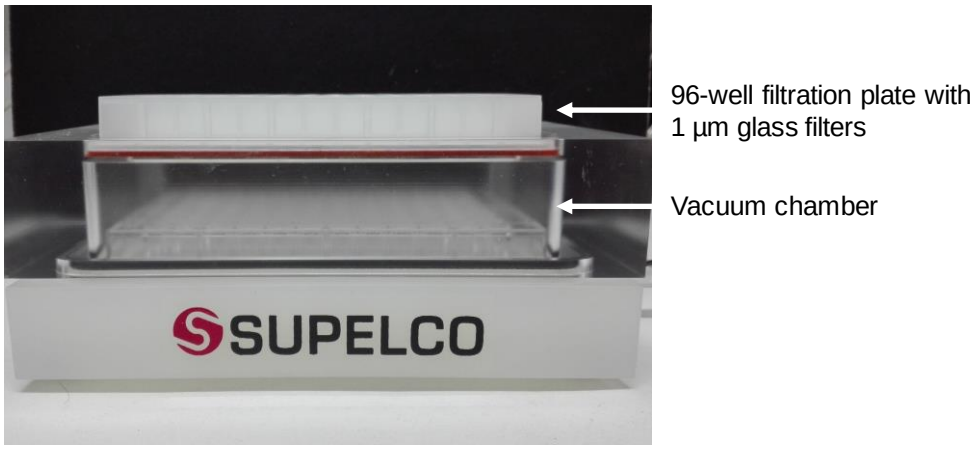

Figure 3.1: Filtration system used to determine the robustness of the Trcs-treated materials. 96-well filtration plate with 1µm glass filters are placed on top of the manifold setup. The filtrate is removed into a new 96-well plate housed in the vacuum chamber

3.3.6 Disk-diffusion method

A culture of target organism (1.0 mL) with 1 x 10^8 cells/mL was used to cover a square pre-poured agar plate (10 x10 cm) with a cotton tip. Once the plates were dried the antibiotic containing disks were transferred to the plate, incubated for 20 hours and inspected for halo formation.

3.3.7 Heat exposure of Trc-cellulose

The effect of 'dry' temperature exposure on the activity of Trcs was done by treating cellulose disks with three different mixtures of peptide: Trc mix (containing a mixture of the primary tyrocidine analogues), a Phe-extract (containing Phe-rich peptides such as Trc A/A1, phenycidine A/A1 and tryptocidine A/A1) and a Trp-extract (containing Trp-rich peptides such as the Trc C/C1, Trc B/B1 and tryptocidine analogues, specifically Tpc C). The characterisation of these peptide complexes is described in supplementary data (Figure S3.1 and Table S3.1). After the disks were created, as described above, the disks were transferred to 4 mL glass vials for heat treatment. Five temperatures (100 °C, 125 °C, 150 °C, 175 °C, 200 °C) and two time points (1 minute and 10 minutes) of exposure were selected. Following heat treatment, the disks were transferred to polystyrene plates in triplicate, including unheated peptide treated

disks and heated untreated disks. The plates were sterilized in chloroform before the use in antimicrobial assays. The same sample preparation was followed for effect of 'wet' heat on Trc mix treated cellulose disks. The only exception is that heat was applied as heated water at five temperatures (25 °C, 40 °C, 60 °C, 80 °C, 100 °C) exposed for 1 minute. After exposure the disks were transferred to polystyrene plates and dried at 40°C.

3.3.8 Solvent exposure of Trc-cellulose

The effect of change in solvent on the adsorption of Trc mix to cellulose was determined in a similar fashion as to how it is created. A solution of Trc mix (100 µL of 50.0 µg/mL) containing the change in solvent (discussed later) was incubated with cellulose for 2 hours. For desorption, pre-treated cellulose disks with Trc mix were treated with the different solvents for 2 hours to allow for passive desorption. Following the incubation, the solutions were removed, and the samples washed three times with 100 µL sterile analytical quality water and dried in a 40°C oven for 2 hours. Solvents tested included a pH range (1-13), $CaCl_2$ (2.5 mM and 7.5 mM), 1% *m/v* sodium dodecyl sulphate (SDS), 5% *m/v* acetic acid, 5mM NaCl, 3% *m/v* citric acid, a range of acetonitrile concentrations in analytical quality water (5-100%, *v/v*). Water washes were done by exposing Trc mix pre-treated cellulose disks with 100 µL sterile-filtered analytical quality water.

3.4 Results

3.4.1 Activity of Trc-mix treated material against L. monocytogenes

Development of antimicrobially active materials first requires the assessment of the effect the base material (untreated or unmodified) has on the growth of the target organism. We selected several materials to utilise as base materials as summarised in Table 3.1

The laboratory materials (Figure 3.2: A) had some effect on the metabolic activity or viability of *L. monocytogenes* (expressed as percentage viability), however, the inhibition caused by cellulose was more pronounced. Similar results were observed for the commercially obtained materials (Figure 3.2: A) where the paper tray resulted in a decrease of viable cells/detectable metabolism. The variability observed can be attributed to the materials moving within the well after PBS and resazurin were added, influencing the bacterial interaction and inhibition/stress and therefore the subsequent fluorescence detected. The viability observed for the different plates could not be compared since some of the plates are not typically suited for fluorescence and the well design influenced the overall fluorescence. It was therefore just used as a growth control.

Table 3.1: Summary of the materials used in this study as base materials.

Material name	Application	Chemical composition	General chemical character
GSWP	Solvent filtration	Mixed cellulose esters	Hydrophilic, porous
HAWP			Hydrophilic, porous
PC	General sterile filtration	Polycarbonate	Hydrophobic, porous
CN		Cellulose nitrate	Hydrophilic, porous
CL		Cellulose	Hydrophilic, porous
BP	Fluorescence assays	Polystyrene	Hard plastic
AP	Micro-dilution assays	Polystyrene	Hard plastic
PPR	Micro-dilution preparation plate	Polypropylene	Hard plastic
PSR		Polystyrene	Hard plastic
Plastic tray	Fruit packaging	Unknown	Hydrophobic, Hard plastic
Tissue paper	Fruit wrapping	Cellulose	Hydrophilic, layered cellulose
Ripple carton	Fruit packaging	Cellulose	Hydrophilic, layered cellulose
Paper tray	Fruit packaging	Cellulose	Hydrophilic, dense cellulose
Carton box	Fruit shipping/transport	Cellulose	Hydrophilic, multiple layered cellulose
Meat paper- PL	Meat wrapping	Cellulose & polylactate	Hydrophobic
Meat paper	Meat wrapping	Cellulose	Hydrophilic
White bag	Waste bag – home use	Polylactate	Hydrophobic
Green bag	Waste bag – industrial use	Polylactate	Hydrophobic
Cling film	Food wrapping	Polylactate	Hydrophobic

Antimicrobial activity of the Trc mix treated materials (expressed as percentage inhibition) was calculated using the growth observed on its untreated counterpart as the growth control. Trc mix (5.0 µg dried in the plate) served as 'full adsorption' and the maximum activity that could be achieved for each of the treated materials. The Trc-treated cellulose fully inhibited the growth of *L. monocytogenes* (Figure 3.3: A), followed by the Trc-treated GSWP, HAWP, CN and PC all having comparable activities.

Interestingly, the Trc-treated BP and PPR showed 80% inhibition and PSR and AP showed 60% inhibition. Though the activity observed increases the application of tyrocidines to a broader scope of materials, it does have some practical implications. The black plate (BP) is used for fluorescence studies of the peptide association to cellulose (will be discussed later and

in Chapter 4 and 5). PSR and AP are used by our group in dose-response assays to determine Trcs' activity against multiple target organisms (Rautenbach et al., 2016; Spathelf and Rautenbach, 2009; Troskie et al., 2014b). The peptides' association to the plates (based on the observed activity) would therefore have an influence on the observed activity within the assay.

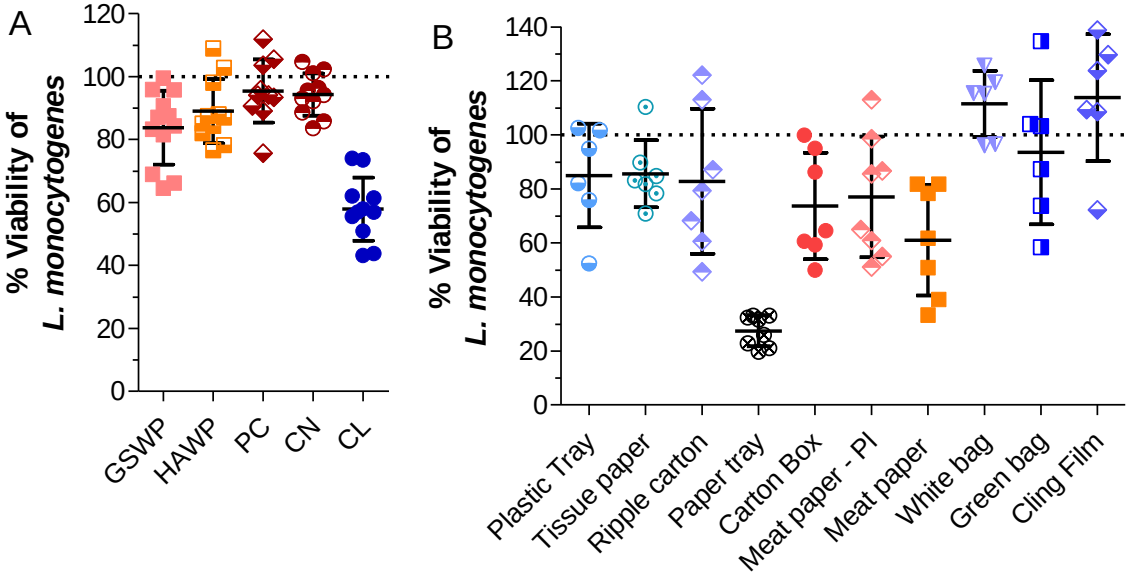

Figure 3.2: Effect of the base material on the metabolic activity of $5x10^6$ cells/cm^2 *L. monocytogenes* expressed as percentage viability. **(A)** Laboratory acquired materials mixed cellulose filters GSWP (0.22 µm) and HAWP (0.45 µm); polycarbonate (PC – 0.4 µm); cellulose nitrate (CN – 0.45 µm) and cellulose (CL) **(B)** Commercially obtained cellulose based and 'plastic' materials. Each data point in a determination is shown and the horizontal line represents the mean of 8 repeats and three and 6 repeats for the laboratory - and commercial materials, respectively. The error bar represents the standard deviation (SD) of the data cluster.

Full inhibition was observed for the Trcs-treated plastic tray, tissue paper, ripple carton, white bag, green bag, cling film (Figure 3.3: B). The carton box showed high inhibition followed by both sides of the meat paper, showing similar results. The paper tray showed very low inhibition and overall performed poorly especially considering the low growth observed for its untreated counterpart. It is possible that the commercial paper tray was pre-treated with a compound that antagonised the activity of the Trcs, as it was the only cellulose-based material that did not give good antimicrobial activity retention.

3.4.2 Determining the amount of Trcs in antimicrobial materials

The amount of peptide associated to the selected materials was determined with the use of a fluorescence method tracking the movement of the fluorophores (Trp and Tyr) that occur in the tyrocidine structure. The full development and optimization of the method is described in supplementary data. The fluorescence signal studied was background subtracted in order to remove any influence on the fluorescence by the materials. It was observed that the fluorescence signal of Trc mix (50 µg/mL) alone decreases over time (Figure 3.4: A) which can be caused by two factors: self-assembly/aggregation and the peptide binding to the plate well surface. Tyrocidines are prone to aggregation, especially in polar solvents (Munyuki et al., 2013; Williams et al., 1972), which would lead to aromatic stacking resulting in fluorescence quenching over time.

The second cause of the fluorescence decrease is the removal of peptide from the solution due to the peptides' association to a surface, in this case the plate. This can be confirmed by the antimicrobial activity observed for the BP (Figure 3.3: A). The addition of a material (e.g. cellulose or tissue paper) showed a much faster decrease in fluorescence that plateaued before or around 60 minutes of incubation (Figure 3.4: A). This time point was therefore selected to estimate the amount of peptide bound to the surfaces. Similar results were found for the other materials in this study. Both the carton box and paper tray (Figure 3.4: B) bound the maximum amount of peptide available that could be quantified based on the sensitivity of the fluorescence method. However, both could not fully inhibit the growth of *L. monocytogenes* with the activity of the paper tray being as low as 50%. Both samples consisted of multiple layers decreasing the true µg/cm^2 coverage of Trc mix below the 3.5 µg/cm^2 needed for full inhibition. The minimum amount needed to result in full inhibition is calculated based on the MIC of 1 µg peptide per 0.28cm^2 of sample size (refer to Chapter 4 – Figure 4.5: A). In the event of industrial application, this could possibly be rectified by increasing the peptide concentration at the incubation step or including the peptide in the manufacturing process.

The remaining results are summarised from the most peptide associated to the least. A comparison between activity of peptide treated material (expressed as percentage inhibition) and peptide bound (µg/cm^2) showed two distinct groups (Figure 3.4: C). The error bars are not included to ease visualisation. The first group has a seemingly linear relationship between peptide bound and activity (red/orange). The second group appears to cluster around 4-8 µg/cm^2 resulting in 95-100% inhibition of *L. monocytogenes* (blue/green). Each of the base materials affected the growth of *L. monocytogenes* differently and therefore no true comparison

can be made regarding peptide association to various surfaces other than that tyrocidines are able to associate and remain active. There was also no clear selection for a type of material (e.g. cellulose materials having the best association and activity) as the two groupings contained both cellulose based materials and plastics.

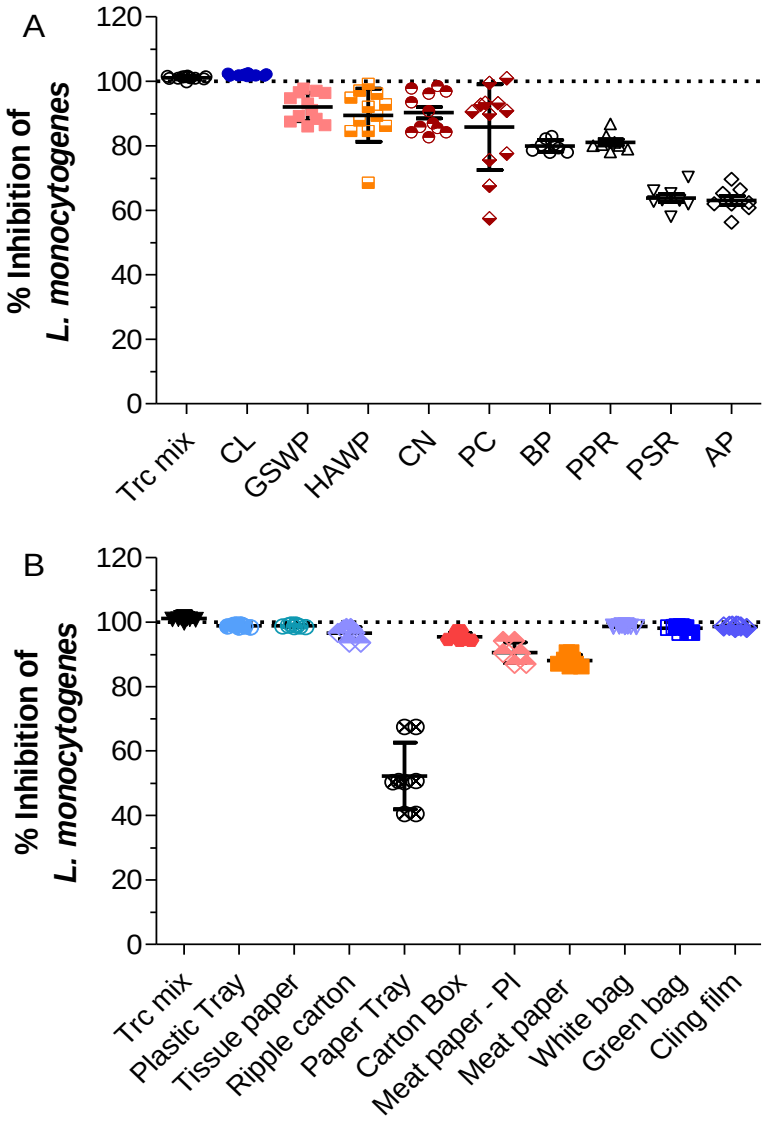

Figure 3.3: Antimicrobial activity against *L. monocytogenes* of Trc mix treated **(A)** laboratory materials and **(B)** commercial materials used in the food industry. Each data set represents the mean of eight and six technical repeats for the laboratory - and commercial materials, respectively. The error bar represents the SD of the data cluster. Abbreviations: cellulose (CL), mixed cellulose filters GSWP (0.22 µm) and HAWP (0.45 µm); cellulose nitrate (CN – 0.45 µm), polycarbonate (PC – 0.4 µm), black polystyrene plate (BP), polypropylene round bottom plate (PPR), polystyrene round bottom plate (PSR) and polystyrene plate (AP). Statistical analysis summary can be found in the supplementary data Table S3.2 & Table S3.3.

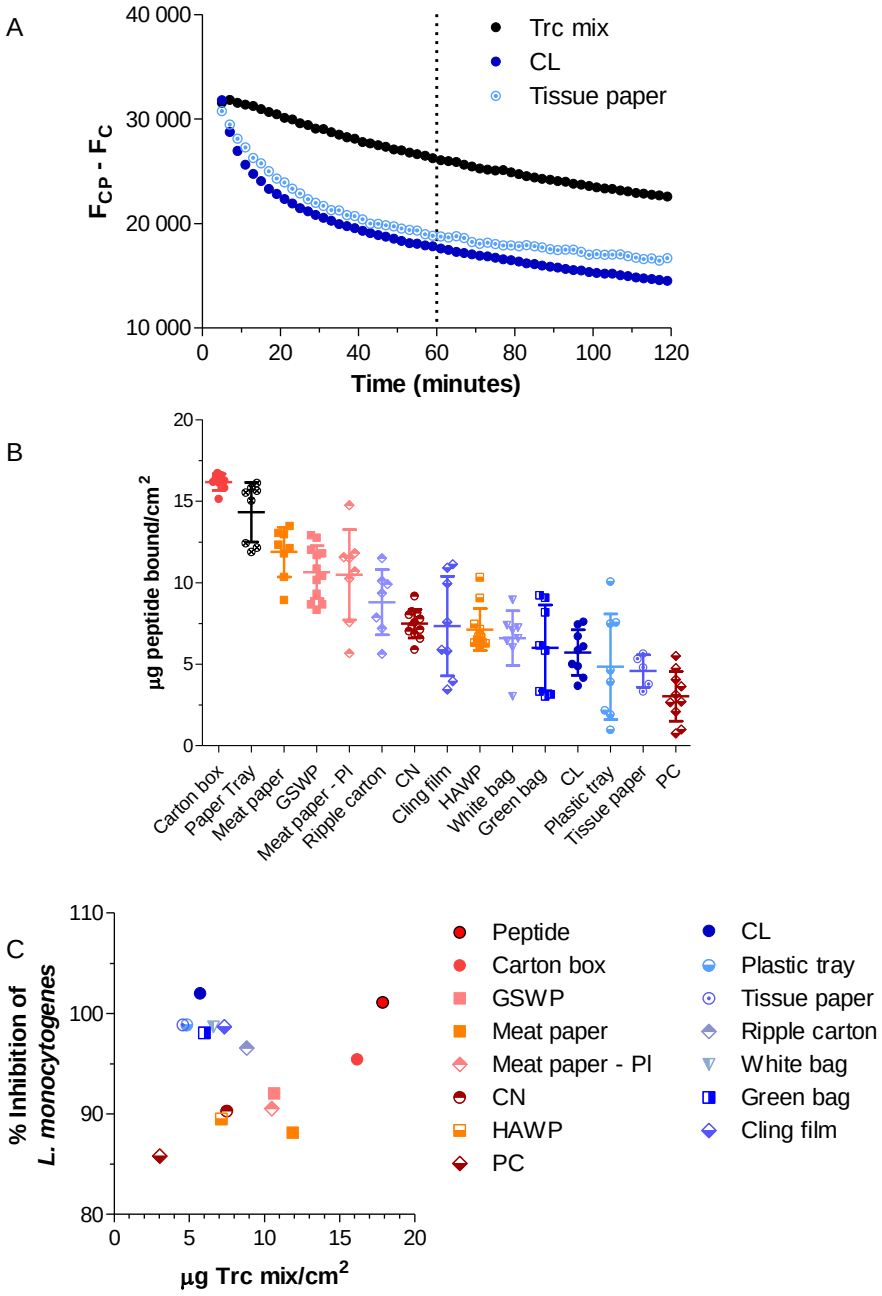

Figure 3.4: **(A)** Fluorescence decrease over time (background subtracted) as observed for Trc mix (50µg/mL), with cellulose and tissue paper as examples. Time point show at 60 minutes as 'end point' based on fluorescence decrease **(B)** Amount of peptide bound (µg/cm^2) to each of the materials as calculated after 60 minutes of association. Each data set represents the mean of at least 6 technical repeats. The error bar represents the SD of the data cluster. Refer to supplementary data for detail on concentration determination, **(C)** Relationship between peptide bound (µg/cm^2) and activity (percentage inhibition of *L. monocytogenes*).

3.4.3 Application of antimicrobial Trc materials in sterile filtering

The laboratory materials are used as filters; therefore, it was crucial to determine whether Trcs association would change the filter character and whether instead of killing the cells on contact, the filters could entrap Gram-negative *E. coli*. Unfortunately, this could not be studied since the filter plate blocked the transfer of bacterial cells to a new 96-well plate, although the supplier indicated that the filters had 1 μm pores that would theoretically allow the passage of bacteria. The passage was further compromised by cell clumping/aggregation caused by cell stress, especially with *L. monocytogenes* as target cell. However, we found that it could be used to study the robustness of the Trcs-containing filters. Exposing the filters to three passages of bacterial cell cultures ($1.4x10^6$ CFUs per passage), which is much higher cell counts than what is normally tested, could put strain on the antimicrobial robustness of the Trc treated filters. Furthermore, since viable cells could be trapped under the treated-filter disks, the incubation time for the organisms were extended to ensure good conversion of resazurin in our solid phase antimicrobial assay (refer to Chapter 2). Therefore, *L. monocytogenes* viability was assessed at 60 minutes, instead of 30 minutes, and *E. coli* at 120 minutes, instead of 60 minutes.

Similar results were observed as before in terms of the effect of the base material on the viability of *L. monocytogenes* where CL caused some inhibition (Figure 3.5: A). With the addition of Trcs, HAWP and PC could inhibit about 20% of the viability after three passages, followed by CN at 40% and CL at 90% inhibition. Previously HAWP, PC and CN could inhibit roughly 80% of the growth at the lower cell count. This decrease in activity can be due to exhausting the available peptide or forming a sediment layer of cells not allowing available peptide to elicit its activity. After three passages CL still had excellent activity, ≥90% inhibition, showing the robustness of the treated paper filter. All the untreated filters also had some inhibitory effect on the growth of *E. coli* (Figure 3.5: B). The Trcs-containing counterparts all showed about 20-40% inhibition and no statistical variance between any of the Trc treated filters.

3.4.4 Leaching of Trcs from cellulose

One of the concerns regarding the perceived robustness of Trc mix-treated cellulose was that the peptide would be removed from the cellulose with each round of filtration or exposure. Therefore, a comparison was made with disk diffusion between Trc mix-treated cellulose, gramicidin S-treated cellulose and gentamicin-treated cellulose to evaluate possible leaching.

Disk diffusion is dependent on the diffusion of an active compound from a disk into the agar, and therefore is also indicative of the active compound leaching from the material.

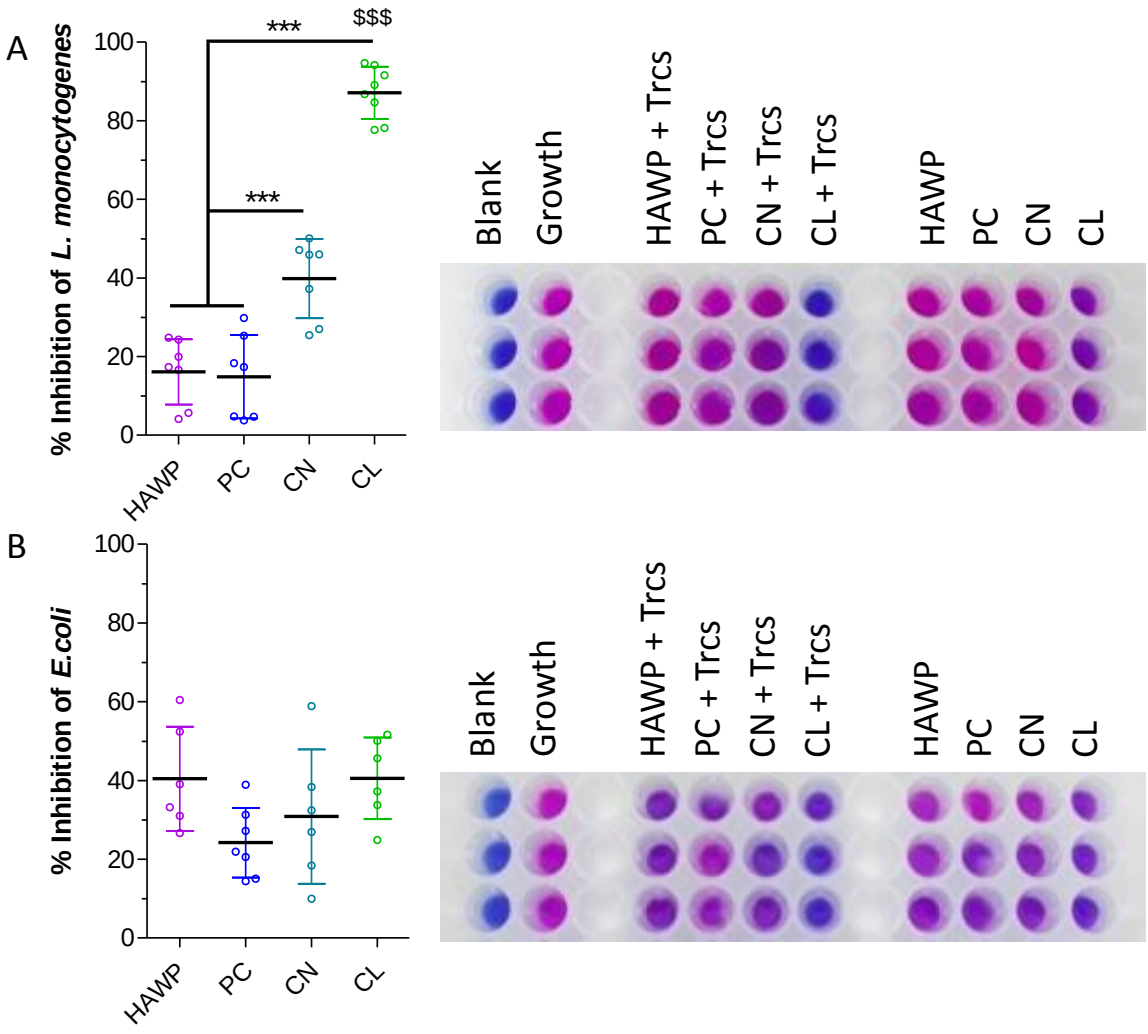

Figure 3.5: Filtering ability and resulting robustness of treated and untreated HAWP, PC, CN and CL exposed to **(A)** *L. monocytogenes* and **(B)** *E. coli*. Data represents 8 technical repeats and one biological repeat. Statistical analysis was performed with One-way Anova (Bonferroni's multiple comparison test) ***/$$$P<0.0001. Visual representation of observed results is displayed next to each respective graph showing resazurin conversion of the blank, growth control, and cells on Trcs treated and untreated materials.

Gentamicin was chosen as a control for compounds that leach and form halos easily, whereas gramicidin S (GS) was chosen as a control that leaches very little (see Chapter 2). GS is also a cyclic decapeptide and shares 50% identity with the Trcs making the comparison of leaching highly relevant. Three concentrations were tested (50 µg, 12 µg and 3 µg) to determine whether halo formation was due to an initial interaction with solvent/agar or due to leaching seen with an increase in halo size with an increase in compound concentration.

As expected, the small polar antibiotic, gentamicin, leached from the cellulose in a concentration dependent manner forming large halos around the cellulose disks (Figure 3.6: A). In comparison, the leaching/diffusion of the much larger gramicidin S was much less, however, it was still concentration dependent as seen with the difference in halo diameter between 50 µg and 3 µg (Figure 3.6: B). The Trc mix-treated materials showed very little leaching that was not influenced by an increase of peptide present on the cellulose (Figure 3.6: C). Therefore, it can be concluded that a small amount of Trc mix can be removed from the cellulose by the initial exposure to an agar/solvent, as seen by the small halo formation, but that there is limited peptide leaching from the cellulose. For leaching an increased halo diameter with increased concentration would have been observed, as with gentamicin and gramicidin S. This stability of Trc mix-treated cellulose after solvent exposure, that could induce release, will be discussed later in this chapter. The observed leaching could possibly be linked to Trcs associating in two manners: an initial stronger association followed by a weaker stacking prone to leaching in the presence of target organisms. The conditions surround Trcs association will be discussed in Chapter 4 and 5.

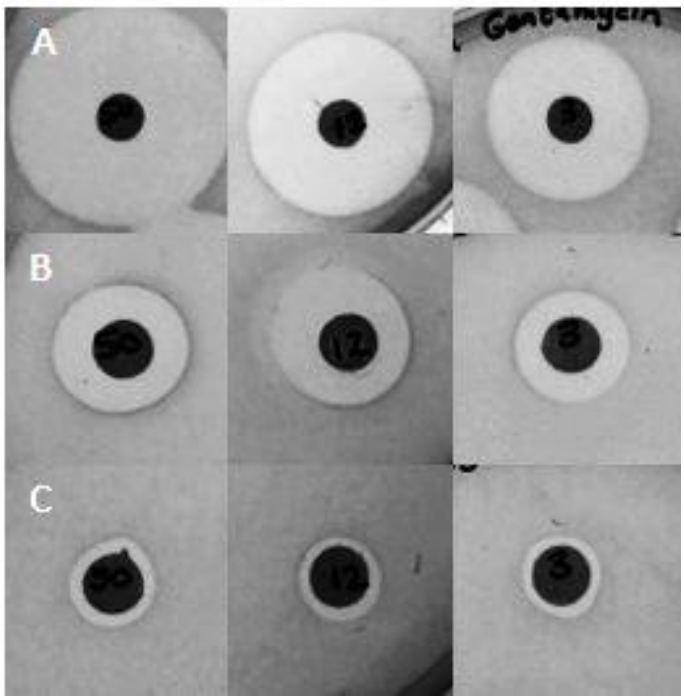

Figure 3.6: Disk diffusion against *L. monocytogenes* of 50 µg, 12 µg and 3 µg (from left to right) of **(A)** gentamicin, **(B)** gramicidin S and **(C)** Trc mix.

3.4.5 Antimicrobial potency of the Trc-cellulose

Knowing that Trc mix does not leach from cellulose, which is very important to future applications, the second factor would be to determine the potency/robustness of these surfaces after exposure to increasing amounts of cells. The activity of the Trc mix-treated cellulose was compared after exposure to three cell concentrations (10^4, 10^5, and 10^6 cells/cm^2) plus the previously discussed filtration experiment (10^7 cells/cm^2)(Figure 3.7). The Trc-mix and cellulose combination is incredible potent, showing only a decrease in activity at 10^7 cells/cm^2, which only had about 10 minutes of contract time with the cells before the resazurin was added. The shorter contact time was due to the experimental design of the filtration/robustness experiment. The cellulose materials used in this study typically result in about 50% inhibition of the target organism adding to appeal to use cellulose in application since the material itself reduces the bacterial load.

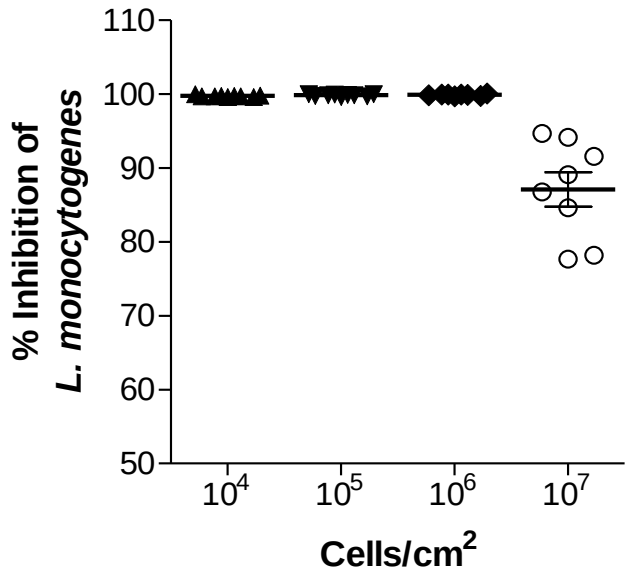

Figure 3.7: Antimicrobial activity (expressed as % Inhibition) of Trc mix (50.0 µg/mL) treated cellulose against increasing cells/cm^2 of *L. monocytogenes*. Each data point is shown with horizontal line and error bar representing the mean of 8 repeats with SD.

3.4.6 How robust is the activity of Trc-cellulose?

Stability is one of the greatest concerns of using a biocide that had been isolated from nature without any further chemical modification in the industrial creation of antimicrobial solid surfaces since these processes can make use of harsh conditions. Just in the paper and packaging industries alone heating steps are used to dry materials before storage and thus any

antimicrobial additive used should be stable at high temperatures. The tyrocidines and tyrocidine analogues are heat stable when exposed to 90°C for 10 minutes (Dubos, 1939) and previous studies have shown that tyrocidine-treated cellulose remains active against *M. luteus* after exposure to up to 100°C wet temperature for a minute (van Rensburg, 2015). This experiment was repeated against *L. monocytogenes* and extended to 'dry' heat exposure. The pre-treated cellulose was exposed to 100°C, 125°C, 150°C, 175°C and 200°C for 1 and 10 minutes. Three peptide mixtures were tested: Trc mix (containing all the main tyrocidine analogues), a Phe supplemented culture extract (containing predominantly Trc A and Phe-rich analogues) and a Trp supplemented culture extract (containing predominantly Tpc C and Trp-rich analogues).

The Trc mix-treated cellulose maintained activity up until 10 minute exposure to 200°C (Figure 3.8: C) which was also observed for the Phe-rich peptide-treated cellulose **(**Figure 3.8: B). The same loss of activity at the 10-minute exposure at 200°C was observed for the Trp-rich peptide-treated cellulose **(**Figure 3.8: A) and even though the effect was not significant, there appears to be some activity loss for the cellulose exposed to a minute at 200°C. Comparing the 10 minute exposure at 200°C of each of the peptide extracts, it appears, though there is no statistical significance, that the Trc mix-treated cellulose is less affected by the high temperatures than the cellulose treated with Phe-rich peptide complexes and Trp-rich peptide complexes (refer to Supplementary data, Figure S3.1 and Table S3.1). The first aspect to consider is that Trp is broken down at high temperatures (Cuq et al., 1983; Cuq and Cheftel, 1983; Mello et al., 2015; Patron et al., 2008) which given the high amount of Trp containing analogues in the Tpcs-extract would explain the decrease in activity at higher temperatures (Figure S3.1 and Table S3.1). However, this does not hold true for the commercial Trc mix and Phe-rich peptide complexes in which 27% and 59% of the respective extracts are Phe-containing peptide (TrcA, TrcA1, Phc A). This would relate to cellulose treated with Phe-rich peptide complex to be more temperature stable, which it is not. The other factor to consider is the abundance of Tyr^7 peptides (tyrocidines) within each extract: Trc mix contains 91% tyrocidines whereas Phe-rich peptide extract contains various Phe containing peptides (Table S3.1). It would therefore appear that heat stability can be attributed to both the presence of Tyr^7 and the identity of the amino acids present in the dipeptide unit. The activity of the 'wet' temperature exposed cellulose remained unaffected in comparison to the control (25°C) against *L. monocytogenes* **(**Figure 3.8: C). This correlates with what has been previously reported (van Rensburg, 2015). We also found that the dried peptide on its own is stable up to 190°C utilising

thermogravimetric analysis (refer to supplementary data, Figure S3.5). It can therefore be concluded that the peptide remains heat stable even though it is associated to cellulose. Furthermore, the peptide would maintain activity with high temperature manufacturing and drying steps when incorporated in the production of antimicrobial cellulose-based materials.

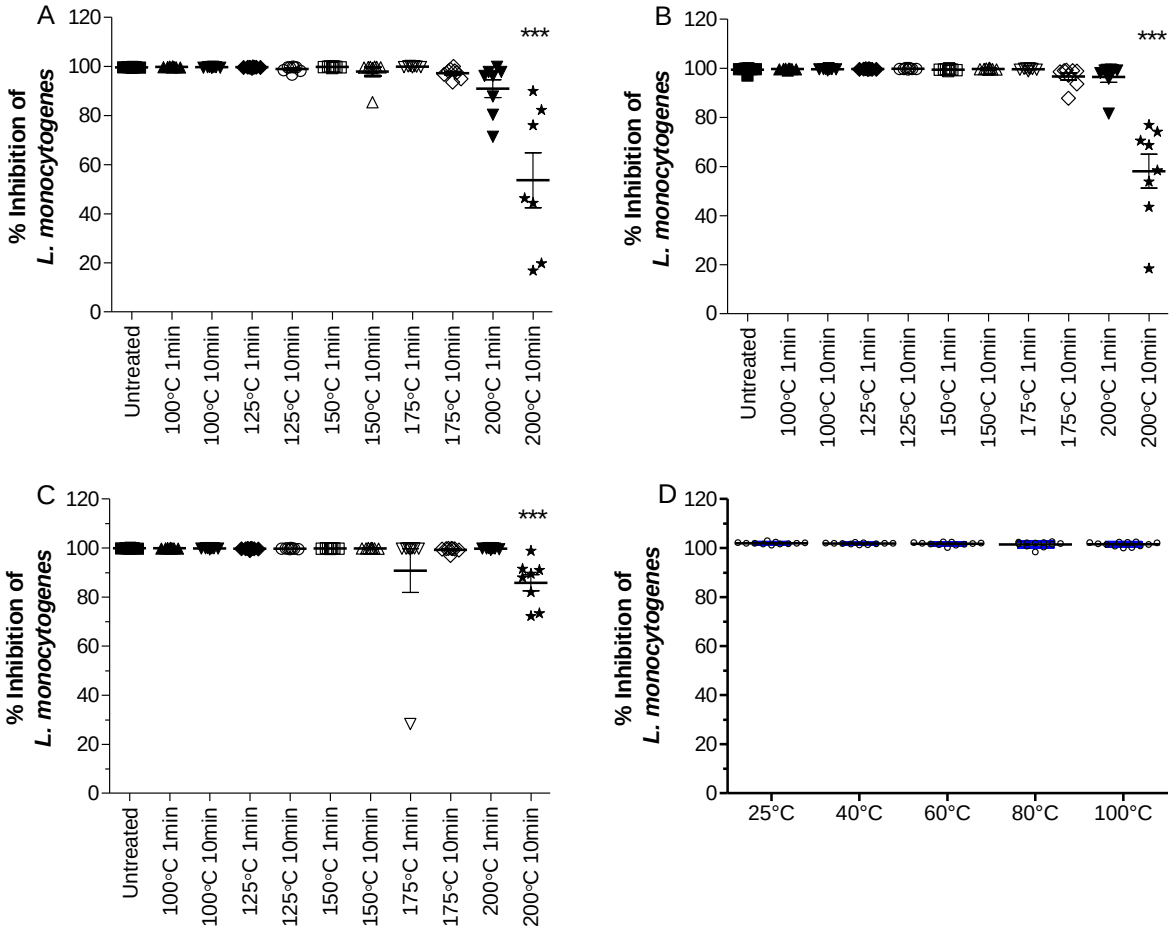

Figure 3.8: Antimicrobial activity of peptide treated cellulose against *L. monocytogenes* ($5x10^6$ cells/cm^2) after exposure to 'dry' temperature ranges at 1 and 10minutes. Three peptide analogue mixtures were tested: **(A)** Trp supplemented culture extract, **(B)** Phe supplemented culture extract and **(C)** Trc mix. **(D)** Antimicrobial activity of Trc mix treated cellulose after exposure to 'wet' temperature ranges. Data represents the mean and SD of 9 repeats. Statistical analysis between untreated as control and the other conditions were determined with One-way Anova and Bonferroni's Multiple comparison post-test; ***P<0.001

Determining solvent stability is dual purpose: it provides the conditions under which the Trcs-cellulose would remain active and offer some insight into the conditions that mediate the peptide-cellulose association. A study into the association between gramicidin S and the exosporium showed that incubation with SDS fully inhibited association, leading to the conclusion that it is a combination of hydrophobic and electrostatic interactions that determines association (Azuma and Demain, 1996). However, the addition of just Ca^{2+} (disrupts electrostatic interactions), ethanol (disrupts hydrophobic interactions) and pH higher than 10 (disrupts ionic and polar interactions) caused some dissociation but not fully (Azuma and Demain, 1996). Tyrocidines share 50% sequence similarity, Val-Orn-Leu-D-Phe-Pro moiety, with gramicidin S and likewise plays a pivotal role in spore germination (Federn and Ristow, 1987; Pschorn et al., 1982) $CaCl_2$ has been shown to increase the activity of Trcs against *L. monocytogenes* (Leussa, 2014; Spathelf, 2010) but reduce the activity against fungi (Troskie, 2013). It has also been shown to change the mode of action of the Trcs from lytic to non-lytic (Leussa, 2014). It was observed that pH did not affect adsorption (Figure 3.9: A) or cause desorption (Figure 3.9: B) of Trcs in terms of a change in activity, neither did $CaCl_2$, acetic acid, NaCl or citric acid (Figure 3.9: C & D). The only observed changes were for 1% SDS, affecting adsorption more than desorption. After ten water washes enough Trc mix remained associated to the cellulose leading to full inhibition of the growth of *L. monocytogenes* (Figure 3.10: A). Exposure to a range of acetonitrile concentrations showed that the activity of Trc mix-treated cellulose was affected by 70% *v/v* acetonitrile and possibly 60% *v/v* acetonitrile (Figure 3.10:B).

It appears that the amphipathic nature of the tyrocidine dimers (Loll et al., 2014; Munyuki et al., 2013) and oligomerisation driven by amphipathic interactions (refer to Chapter 5) could play a key role in association to cellulose since only SDS and 70% *v/v* acetonitrile could affect adsorption/desorption enough to affect the activity against *L. monocytogenes*. The effect of a change in solvent environment on peptide oligomerisation and possibly on the association of peptide to cellulose is therefore specific to the tyrocidines. These exposure studies exemplified the robustness of the Trc-celluloses created in this study. This robustness in maintaining activity on particularly cellulose can also point to the type of interaction, namely interaction in oligomers and with the matrix allowing the release of peptide only in the presence of a target or amphipathic solution.

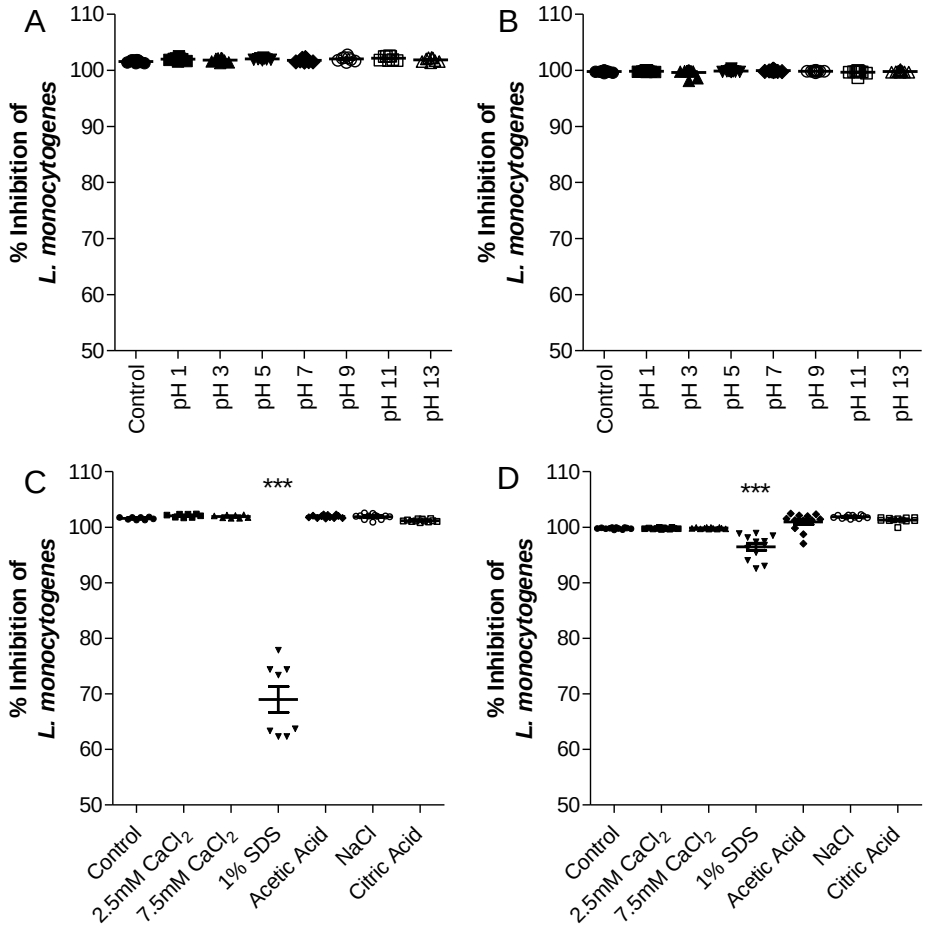

Figure 3.9: Antimicrobial activity, expressed in percentage metabolism inhibition against *L. monocytogenes*, of Trc mix **(A & C)** adsorbed and **(B & D)** desorbed in the presence of pH ranges, salts, 1% SDS and acidic solutions. 5% *m/v* acetic acid, 5mM NaCl and 3% *m/v* citric acid was tested. Data represents the mean and SD of three biological and four technical repeats. Statistical analysis between untreated as control and the other conditions were determined with One-way Anova and Bonferroni's Multiple comparison post-test; ***P<0.001

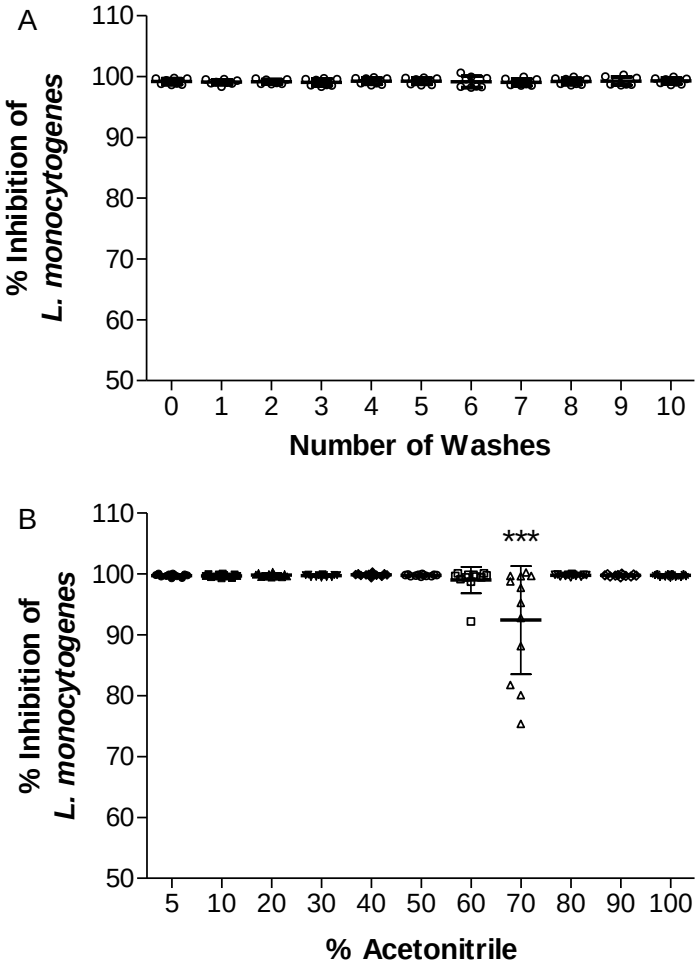

Figure 3.10: Antimicrobial activity of Trcs-treated cellulose, expressed in percentage metabolism inhibition against *L. monocytogenes*, after **(A)** multiple water washes and **(B)** treatment with ranges of percentage (*v/v*) acetonitrile. Each data set is the standard deviation of the mean of four technical repeats; and two biological repeats for (A) and three biological repeats for (B). Statistical analysis was determined with One-way Anova and Bonferroni's Multiple comparison post-test; ***P<0.001

3.4.7 Role of type of active compound on surface activity – Are Trcs unique sticky peptides?

Antimicrobial peptides are favoured for food protection (Rydlo et al., 2006) and in the creation of antimicrobial surfaces with the increased demand for 'green' products (Gol et al., 2013; Haws et al., 2014; Rautenbach et al., 2015). Considering the ability of tyrocidines to associate to cellulose, it was determined whether the same effect would be observed for other antimicrobial peptides if treated the same way. We compiled a representative library of compounds (Table 3.2) and treated celluloses filters in the same way as described for the Trcs.

Table 3.2: Summary of the compounds used to compare with the Trc in creating robust non-covalent antimicrobial materials

Compound	Origin	Mr	Character	Minimum inhibitory concentration (ug/mL)	
				L. monocytogenes	***E coli***
Tcn	Peptide complex produced by *Brevibacillus parabrevis* [a,b]	-	-	21 ± 0.10 [c]	Not available
Trc mix	Purified from Tcn	1269.65 – 1347.67 [d]	Cationic, cyclic decapeptide complex, soluble in ≥50% *v/v* acetonitrile/organic solvents	23 ± 0.63 [c]	>100 [c]
GD	Purified from Tcn	1881.07-1858.06 [d]	Neutral linear pentadecapeptide complex, haemolytic, soluble in organic solvent	19 [e]	9 [e]
GS	*Aneurinibacillus migulanus*	1140.70	Cationic, amphipathic cyclic decapeptide, haemolytic, water soluble	11 ± 0.20 [c]	3-12.5 [f]
Magainin 2	Skin of *Xenopus laevis* [g]	2466.90	23-mer cationic, amphipathic α-helical peptide, water soluble, non-haemolytic, water soluble	Not available	10-50 [g,h]
PGLa	Skin of *Xenopus laevis* [g,i]	1968.50	21-mer cationic, amphipathic α-helical peptide, haemolytic, water soluble	Not available	10-50 [h]
Leucocin A	*Leuconostoc gelidum* UAL187 [j,s]	3930.03 [k]	37-mer cationic, amphipathic disulphide-bonded bacteriocin, non-haemolytic, water soluble	0.98-1.98 [l]	Not available
Melittin	venom of European honey-bee (*Apis mellifera*) [m,n]	2846.46 [m]	26-mer cationic, amphipathic α-helical peptide, haemolytic, water soluble [m-o]	0.315 ± 0.008 [m]	15-42.5 [n,o]
Gentamicin	*Micromonospora purpurea*	477.59	Water soluble aminoglycoside antibiotic	0.5 - 4.0 [p,q]	0.156-1.25 [r]

[a](Seddon and Fynn, 1972); [b](Troskie, de Beer, *et al.*, 2014); [c](Spathelf and Rautenbach, 2009); [d](Tang et al., 1992); [e](Carrasco et al., 2016); [f](Kondejewski et al., 1996); [g](Zasloff, 1988); [h](Soravia et al., 1988); [i](Hartmann et al., 2010); [j](Van Belkum and Stiles, 1995); [k](Balay et al., 2017); [l](Gravesen et al., 2002); [m](Wu et al., 2016); [n](Yang et al., 2018); [o](Picoli et al., 2017); [p](Rakic-Martinez et al., 2011); [q](Adwan and Abu-Hasan, 1998); [r](Moellering et al., 1972); [s](Hastings et al., 1991)

We compared the purified Trc mixture used in this study with tyrothricin (Tcn) from which it was purified and a purified Trc peptide extract from an in-house bacterial culture extract. The first observation was that there is no difference in activity against *L. monocytogenes* between cellulose treated with Tcn, Trc mix and Trc extract (Figure 3.11: A). This holds great promise for the industrial application of Trcs-treated materials, since all the observations made of Trc mix-treated materials should be transferrable to cheaper Tcn and Trc extract-treated materials. Moreover, the linear gramicidins present in Tcn appeared not to have a major influence on association of Trcs to the cellulose, or noticeably inhibit the activity of the treated celluloses. Linear gramicidins (GD) alone resulted in 70% inhibition of *L. monocytogenes* and gramicidin S (GS) resulted in 100% inhibition. The four remaining peptides can be ranked, in terms of activity from most to least, as PGLa, leucocin A, melittin and magainin 2. The activity for the control antibiotic, gentamycin, was comparable to that of leucocin A. Although it appears that some of the peptides are associated to the cellulose, the resulting activity at the low concentrations used for Trcs, it is not comparable to the activity observed for Trcs, except for the related peptide GS. Furthermore, the stability or robustness of the association and activity will have to be confirmed before any more detailed comparison can be made. Previous studies (Rautenbach and van Rensburg, 2017) and results previously discussed showed that the antimicrobial activity of Trc-treated cellulose is highly robust and wash stable to washes at up to 100°C with water, temperatures up to 1 minute at 200°C, up to 12 washes with water, as well as washes with solutions varying in organic solvent composition, pH and salt content.

There was some activity of Tcn, Trc mix, Trc complex and GD observed against *E. coli* (Figure 3.11: B) which correlates to previous reports of the peptides' activity against Gram-negative bacteria (Chopra et al., 2010; Dubos and Hotchkiss, 1941). Interestingly gramicidin S (GS), was the only compound that resulted in full growth inhibition followed by gentamycin. leucocin A and melittin resulted in low levels of inhibition, whereas PGLa and magainin 2 resulted in a stress response that is recorded as "negative" inhibition. A stress response can increase cell metabolism because of stress, such as osmotic stress, that is induced by the antimicrobial peptides (Csonka, 1989).

Overall it can be concluded that Trcs-containing cellulose is unique in terms of high activity against *L. monocytogenes* at low levels of peptide associated to the cellulose. Though only low levels of activity were observed for the Trcs-containing cellulose against *E. coli*, combinations with GS can be formulated to create a material that have broad spectrum of activity against Gram-positive and Gram-negative bacteria. Especially since there is no research into GS-

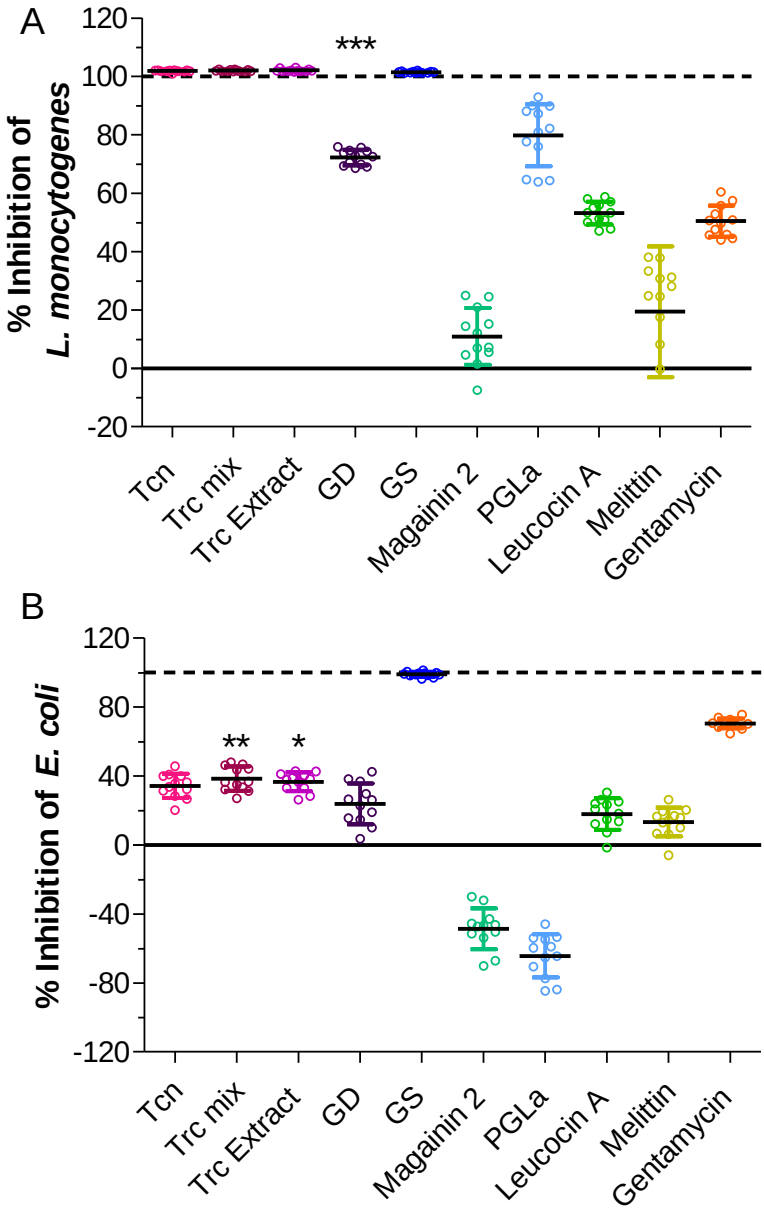

Figure 3.11: Antimicrobial activity (expressed as % Inhibition) of peptide treated cellulose against **(A)** *L. monocytogenes* and **(B)** *E. coli*. % Inhibition is calculated/normalised by the natural activity of the base material cellulose. Gentamycin was used as antibiotic control. Each dataset represents three biological and four technical repeats. Statistical analysis was performed with One-way Anova (Boferroni's multiple comparison test) against GD versus Tcn, Trc mix, Trc extract and for (A) ***P<0.0001 and (B) **P<0.01 and *P<0.05. Full statistical analysis can be found in the supplementary data - Table S3.4 and Table

containing surfaces though cellulose is used as part of a purification method for GS (Gevers et al., 1968; Kanda et al., 1978; Kleinkauf et al., 1968) and the use of GS producing biofilms to prevent pipe corrosion have been reported (Zuo and Wood, 2004). The only other research on the activity of GS on materials were completed by our group, that showed GS having a

comparable activity to Trc mix on cellulose against 10^5 cells/cm^2 *Micrococcus luteus* (van Rensburg, 2015).

3.5 Conclusions

Association and activity of Trc mix was tested on a selection of laboratory and commercial materials. All the materials showed at least 80% inhibition of *L. monocytogenes*, with cellulose and six of the commercial materials (plastic tray, tissue paper, ripple carton, white plastic, green plastic and cling film) resulting in full inhibition. The only underperforming material was the paper tray, but this was possibly due to issues arising from surface area coverage or pre-treatment of the paper with a compound antagonistic to the Trcs. The comparison between activity and amount of associated peptide showed that it does not always equate to activity. Interestingly, the best performing materials in terms of activity could be grouped together based on the amount of peptide associated (5-8 µg/cm^2). Furthermore, this group of materials consists of both hydrophilic and hydrophobic materials, namely cellulose, plastic polymers and polylactate. This points to the peptide possibly changing conformation to better suit initial association to the different surfaces, which could seed further association via oligomerisation (refer to Chapter 5). Once associated, the activity of the material is quite potent as was seen with the filtration experiment. The Trc mix-treated cellulose could fully inhibit the growth of 10^6 cells/cm^2 *L. monocytogenes* (as determined with one-hour contact before resazurin was added) and could inhibit 90% of 10^7 cells/cm^2 within 10 minutes of contact time. The Trcs also did not leach from the cellulose in comparison with gentamicin and GS, showing the stability of the peptide's association but also that the material is most likely a contact-killing material. This is important in the light of application of Trc-treated materials, since the slow-release or leaching of the active compound over time would render the material inactive and ineffective. Additional tests toward the robustness of activity of Trc mix-treated cellulose, showed that the material is very heat stable only showing a decrease in activity at 10 minutes exposure at 200ºC. The peptide also remains associated and active after different solvent challenges which not only shows its stability but also aids in determining the parameters for the possible commercial creation of Trc-containing materials. The only two conditions that resulted in a decrease in activity was 1% *m/v* SDS and 70% *v/v* acetonitrile highlighting that amphipathic nature of the Trcs, and therefore also oligomerisation, play a role in the association with cellulose (Loll et al., 2014; Munyuki et al., 2013; Ruttenberg et al., 1965; Stern et al., 1969; Williams et al., 1972). Finally, the uniqueness of the Trcs association to cellulose was determined by comparing the activity with other peptides at the same conditions. It was found that Trcs (Tcn,

Trc mix and Trc extract) outperformed the other peptides at the low concentrations needed to result in full inhibition of *L. monocytogenes*. GS was the only compound tested that could fully inhibit both the growth of *L. monocytogenes* and *E. coli*. It can therefore be used in conjunction with Trcs to create a broad-spectrum active material.

Moreover, the assay used to assess the activity of these materials makes use of a ten-fold higher cell count compared to other solid surface methods (van de Lagemaat et al., 2017)(Chapter 2). This higher cell count allows for a shorter time frame for results but also allows for the selection of only the most potent surface combinations. Therefore, the full inhibition at 10^6 cells/cm^2 and 90% inhibition of 10^7 cells/cm^2 for Trcs-treated cellulose far outperformed what is expected of a material to be considered active at 10^5 cells/cm^2 (van de Lagemaat et al., 2017).

3.6 References

Adwan, K., Abu-Hasan, N., 1998. Gentamicin resistance in clinical strains of *Enterobacteriaceae* associated with reduced gentamicin uptake. Folia Microbiol. (Praha). 43, 438–440.

Appleby, J.C., Knowles, E., Pearson, J., White, T., 1947. A preliminary study of the formation, assay and stability of tyrothricin. J. Gen. Microbiol. 1, 137–44.

Azuma, T., Demain, A.L., 1996. Interactions between gramicidin S and its producer, *Bacillus brevis*. J Ind Microbiol 17, 56–61.

Bagheri, M., Keller, S., Dathe, M., 2011. Interaction of W-substituted analogs of cyclo-RRRWFW with bacterial lipopolysaccharides: The role of the aromatic cluster in antimicrobial activity. Antimicrob. Agents Chemother. 55, 788–797.

Balay, D.R., Dangeti, R.V., Kaur, K., McMullen, L.M., 2017. Purification of leucocin A for use on wieners to inhibit *Listeria monocytogenes* in the presence of spoilage organisms. Int. J. Food Microbiol. 255, 25–31.

Barbosa, A.A.T., de Araújo, H.G.S., Matos, P.N., Carnelossi, M.A.G., de Castro, A.A., 2013. Effects of nisin-incorporated films on the microbiological and physicochemical quality of minimally processed mangoes. Int. J. Food Microbiol. 164, 135–140.

Carmona-Ribeiro, A.M., Carrasco, L.D. de M., 2014. Novel formulations for antimicrobial peptides. Int. J. Mol. Sci. 15, 18040–18083.

Carrasco, L.D. de M., Bertolucci, R., Ribeiro, R.T., Sampaio, J.L.M., Carmona-Ribeiro, A.M., 2016. Cationic nanostructures against foodborne pathogens. Front. Microbiol. 7, 1804: 1–4.

Chopra, S., Torres-Ortiz, M., Hokama, L., Madrid, P., Tanga, M., Mortelmans, K., Kodukula, K., Galande, A.K., 2010. Repurposing FDA-approved drugs to combat drug-resistant *Acinetobacter baumannii*. J. Antimicrob. Chemother. 65, 2598–2601.

Csonka, L.N., 1989. Physiological and genetic responses of bacteria to osmotic stress. Microbiol. Mol. Biol. Rev. 53, 121–147.

Cuq, B., Gontard, N., Guilbert, S., 1995. Edible films and coatings as active layers, in: Active Food Packaging. Springer, Boston, MA., pp. 111–142.

Cuq, J.C., Cheftel, J.C., 1983. Tryptophan degradation during heat treatments: Part 1—The degradation of free tryptophan. Food Chem. 12, 1–14.

Cuq, J.C., Vié, M., Cheftel, J.C., 1983. Tryptophan degradation during heat treatments: Part 2—Degradation of protein-bound tryptophan. Food Chem. 12, 73–88.

Danders, W., Marahiel, M.A., Krause, M., Kosui, N., Kato, T., Izumiya, N., Kleinkauf, H., 1982. Antibacterial action of gramicidin S and tyrocidines in relation to active transport, in vitro transcription, and spore outgrowth. Antimicrob. Agents Chemother. 22, 785–790.

Dubos, R.J., 1939. Studies on a bactericidal agent extracted from a soil bacillus. I. Preparation of the agent. Its activity in vitro. J. Exp. Med. 70, 1–10.

Dubos, R.J., Hotchkiss, R.D., 1941. The production of bactericidal substances by aerobic sporulating bacilli. J. Exp. Med. 73, 629–640.

Dubos, R.J., Hotchkiss, R.D., Coburn, A.F., 1942. The effect of gramicidin and tyrocidine on bacterial metabolism. J. Biol. Chem. 146, 421–426.

Ercolini, D., Ferrocino, I., La Storia, A., Mauriello, G., Gigli, S., Masi, P., Villani, F., 2010. Development of spoilage microbiota in beef stored in nisin activated packaging. Food Microbiol. 27, 137–143.

Federn, H., Ristow, H., 1987. The GTP pool in *Bacillus brevis* and its significance for sporulation. Eur. J. Biochem. 165, 223–7.

Fujikawa, K., Sakamoto, Y., Suzuki, T., Kurahashi, K., 1968a. Biosynthesis of tyrocidine by a cell-free enzyme system of *Bacillus brevis* ATCC 8185. II. Amino acid substitution in tyrocidine. Biochim. Biophys. Acta 169, 520–533.

Fujikawa, K., Suzuki, T., Kurahashi, K., 1968b. Biosynthesis of tyrocidine by a cell-free enzyme system of *Bacillus brevis* ATCC 8185. I. Preparation of partially purified enzyme system and its properties. Biochim. Biophys. Acta 161, 232–246.

Gall, S.C., Thompson, R.C., 2015. The impact of debris on marine life. Mar. Pollut. Bull. 92, 170–179.

Gevers, W., Kleinkauf, H., Lipmann, F., 1968. The activation of amino acids for biosynthesis of gramicidin S. Proc. Natl. Acad. Sci. U. S. A. 60, 269.

Gol, N.B., Patel, P.R., Rao, T.R., 2013. Improvement of quality and shelf-life of strawberries with edible coatings enriched with chitosan. Postharvest Biol. Technol. 85, 185–195.

Gravesen, A., Ramnath, M., Rechinger, K.B., Andersen, N., Jänsch, L., Héchard, Y., Hastings, J.W., Knøchel, S., 2002. High-level resistance to class IIa bacteriocins is associated with one general mechanism in *Listeria monocytogenes*. Microbiology 148, 2361–2369.

Hansen, J., Pschorn, W., Ristow, H., 1982. Functions of the peptide antibiotics tyrocidine and gramicidin: Induction of conformational and structural changes of superhelical DNA. Eur. J. Biochem 126, 279–284.

Hartmann, M., Berditsch, M., Hawecker, J., Ardakani, M.F., Gerthsen, D., Ulrich, A.S., 2010. Damage of the bacterial cell envelope by antimicrobial peptides gramicidin S and PGLa as revealed by transmission and scanning electron microscopy. Antimicrob. Agents Chemother. 54, 3132–3142.

Hastings, J.W., Sailer, M., Johnson, K., Roy, K.L., Vederas, J.C., Stiles, M.E., 1991. Characterization of leucocin A-UAL 187 and cloning of the bacteriocin gene from *Leuconostoc gelidum*. J. Bacteriol. 173, 7491–7500.

Haws, K.L., Winterich, K.P., Naylor, R.W., 2014. Seeing the world through GREEN-tinted glasses: Green consumption values and responses to environmentally friendly products. J. Consum. Psychol. 24, 336–354.

Hotchkiss, D., 1941. The chemical nature of gramicidin and tyrocidine. J. Biol. Chem. 141, 171–185.

Imran, M., El-Fahmy, S., Revol-Junelles, A.M., Desobry, S., 2010. Cellulose derivative based active coatings: Effects of nisin and plasticizer on physico-chemical and antimicrobial properties of hydroxypropyl methylcellulose films. Carbohydr. Polym. 81, 219–225.

Kanda, M., Hori, K., Kurotsu, T., Miura, S., Nozoe, A., Saito, Y., 1978. Studies on gramicidin S synthetase. J. Biochem. 84, 425–434.

Katz, E., Demain, A., 1977. The peptide antibiotics of *Bacillus*: chemistry, biogenesis, and possible functions. Bacteriol. Rev. 41, 449–474.

Kleinkauf, H., Gevers, W., Lipmann, F., 1968. Interrelation between activation and polymerization in gramicidin S biosynthesis. Proc. Natl. Acad. Sci. 62, 226–233.

Kondejewski, L.H., Farmer, S.W., Wishart, D.S., Hancock, R.E., Hodges, R.S., 1996. Gramicidin S is active against both Gram-positive and Gram-negative bacteria. Int. J. Pept. Protein Res. 47, 460–466.

Kühn, S., Rebolledo, E.L.B., van Franeker, J.A., 2015. Deleterious effects of litter on marine life, in: Marine Anthropogenic Litter. Springer, Cham, pp. 75–116.

Leussa, N.-N.A., 2014. Characterisation of small cyclic peptides with antilisterial and antimalarial activity. Stellenbosch University, Department of Biochemistry, Stellenbosch, South Africa. PhD.Thesis, http://scholar.sun.ac.za/handle/10019.1/86161.

Loll, P.J., Upton, E.C., Nahoum, V., Economou, N.J., Cocklin, S., 2014. The high resolution structure of tyrocidine A reveals an amphipathic dimer. Biochim. Biophys. Acta - Biomembr. 1838, 1199–1207.

Mach, B., Slayman, C.W., 1966. Mode of action of tyrocidine on *Neupospora*. Biochim. Biophys. Acta 124, 351–361.

Mach, B., Tatum, E.L., 1964. Environmental control of amino acid substitutions in the biosynthesis of the antibiotic polypeptide tyrocidine. Proc. Natl. Acad. Sci. 52, 876–884.

Mauriello, G.D.L.E., De Luca, E., La Storia, A., Villani, F., Ercolini, D., 2005. Antimicrobial activity of a nisin-activated plastic film for food packaging. Lett. Appl. Microbiol. 41, 464–469.

Mello, G.D.S., Cardoso, A.D.P., Oliveira, E.W., Siqueira, A.B., 2015. Tryptophan: A proposal of the mechanism of thermal decomposition. J. Therm. Anal. Calorim. 122, 1395–1401.

Moellering, R.C., Medoff, G., Leech, I., Wennersten, C., Kunz, L.J., 1972. Antibiotic synergism against *Listeria monocytogenes*. Antimicrob. Agents Chemother. 1, 30–34.

Munyuki, G., Jackson, G.E., Venter, G.A., Kövér, K.E., Szilágyi, L., Rautenbach, M., Spathelf, B.M., Bhattacharya, B., Van Der Spoel, D., 2013. β-sheet structures and dimer models of the two major tyrocidines, antimicrobial peptides from *Bacillus aneurinolyticus*. Biochemistry 52, 7798–7806.

Murmu, S.B., Mishra, H.N., 2017. The effect of edible coating based on Arabic gum, sodium caseinate and essential oil of cinnamon and lemon grass on guava. Food Chem. 245, 820–828.

Nguyen, V.T., Gidley, M.J., Dykes, G.A., 2008. Potential of a nisin-containing bacterial cellulose film to inhibit Listeria monocytogenes on processed meats. Food Microbiol. 25, 471–478.

Okuda, K., Edwards, G.C., Winnick, T., 1963. Biosynthesis of gramicidin and tyrocidine in the Dubos strain of *Bacillus brevis*. I. Experiments with growing cultures. J. Bacteriol. 85, 329–338.

Opara, U.L., Fadiji, T., 2018. Compression damage susceptibility of apple fruit packed inside ventilated corrugated paperboard package. Sci. Hortic. (Amsterdam). 227, 154–161.

Oyama, M., Kubota, K., 1990. Suppression of tyrocidine production by purine nucleotides and related substances in *Bacillus brevis*. FEMS Microbiol. Lett. 66, 277–279.

Patron, L., Marinescu, G., Culita, D., Diamandescu, L., Carp, O., 2008. Thermal stability of amino acid-(tyrosine and tryptophan) coated magnetites. J. Therm. Anal. Calorim. 91, 627–632.

Picoli, T., Peter, C.M., Zani, J.L., Waller, S.B., Lopes, M.G., Boesche, K.N., Vargas, G.D., Hübner, S. de O., Fischer, G., 2017. Melittin and its potential in the destruction and inhibition of the biofilm formation by *Staphylococcus aureus*, *Escherichia coli* and *Pseudomonas aeruginosa* isolated from bovine milk. Microb. Pathog. 112, 57–62.

Pschorn, W., Paulus, H., Hansen, J., Ristow, H., 1982. Induction of sporulation in *Bacillus brevis*. 2. Dependence on the presence of the peptide antibiotics tyrocidine and linear gramicidin. Eur. J. Biochem. 129, 403–407.

Rakic-Martinez, M., Drevets, D.A., Dutta, V., Katic, V., Kathariou, S., 2011. *Listeria monocytogenes* strains selected on ciprofloxacin or the disinfectant benzalkonium chloride exhibit reduced susceptibility to ciprofloxacin, gentamicin, benzalkonium chloride, and other toxic compounds. Appl. Environ. Microbiol. 77, 8714–8721.

Rammelkamp, C.H., Weinstein, L., 1942. Toxic effects of tyrothricin, gramicidin and tyrocidine. J. Infect. Dis. 71, 166–173.

Rautenbach, M., Troskie, A.M., Vosloo, J.A., Dathe, M.E., 2016. Antifungal membranolytic activity of the tyrocidines against filamentous plant fungi. Biochimie 130, 122–131.

Rautenbach, M., van Rensburg, W., 2017. Method for preventing or treating microbial growth on a manufactured product. South Africa 2016 (SA2016/08601), Australia 2019 (Patent 2015270120), USA 2020 (Patent 15/315,755), China 2020 (Patent 201580040786.2).

Rautenbach, M., Vosloo, J.A., van Rensburg, W., Engelbrecht, Y., 2015. Natural antimicrobial peptides as green microbicides in agriculture. Green Economy Research Report, Green Fund, Development Bank of Southern Africa, Midrand. https://www.researchgate.net/publication/303538333.

Ruttenberg, M.A., King, T., Craig, L.C., 1965. The use of the tyrocidines for the study of conformation and aggregation behavior. J. Am. Chem. Soc. 87, 4196–4198.

Ruttenberg, M.A., Mach, B., 1966. Studies on amino acid substitution in the biosynthesis of the antibiotic polypeptide tyrocidine. Biochemistry 5, 2864–2869.

Rydlo, T., Miltz, J., Mor, A., 2006. Eukaryotic antimicrobial peptides: Promises and premises in food safety. J. Food Sci. 71.

Seddon, B., Fynn, G.H., 1972. Energetics of growth in a tyrothricin-producing strain of *Bacillus brevis*. J. Gen. Microbiol. 74, 305–314.

SHAFFE, 2018. Ranking in volume of exports 2018 https://shaffe.net/ (accessed 1.13.20).

Soravia, E., Martini, G., Zasloff, M., 1988. Antimicrobial properties of peptides from *Xenopus* granular gland secretions. FEBS Lett. 228, 337–340.

Spathelf, B.M., 2010. Qualitative structure-activity relationships of the major tyrocidines , cyclic decapeptides from Bacillus aneurinolyticus. Stellenbosch University, Department of Biochemistry, Stellenbosch, South Africa. PhD.Thesis, http://scholar.sun.ac.za/handle/10019.1/4001.

Spathelf, B.M., Rautenbach, M., 2009. Anti-listerial activity and structure-activity relationships of the six major tyrocidines, cyclic decapeptides from *Bacillus aneurinolyticus*. Bioorganic Med. Chem. 17, 5541–5548.

Stern, A., Gibbons, W.A., Craig, L.C., 1969. Effect of assosiation on the nuclear magnetic resonance spectra of tyrocidine B. J. Am. Chem. Soc. 91, 2794–2796.

Sung, S.Y., Sin, L.T., Tee, T.T., Bee, S.T., Rahmat, A.R., Rahman, W.A.W.A., Tan, A.C., Vikhraman, M., 2013. Antimicrobial agents for food packaging applications. Trends Food Sci. Technol. 33, 110–123.

Tang, X.J., Thibault, P., Boyd, R.K., 1992. Characterisation of the tyrocidine and gramicidin fractions of the tyrothricin complex from *Bacillus brevis* using liquid chromatography and mass spectrometry. Int. J. Mass Spectrom. Ion Process. 122, 153–179.

Troskie, A.M., 2013. Tyrocidines , cyclic decapeptides produced by soil bacilli , as potent inhibitors of fungal pathogens. Stellenbosch University, Department of Biochemistry, Stellenbosch, South Africa. PhD.Thesis, http://scholar.sun.ac.za/handle/10019.1/86162.

Troskie, A.M., de Beer, A., Vosloo, J.A., Jacobs, K., Rautenbach, M., 2014a. Inhibition of agronomically relevant fungal phytopathogens by tyrocidines, cyclic antimicrobial peptides isolated from *Bacillus aneurinolyticus*. Microbiology 160, 2089–2101.

Troskie, A.M., Rautenbach, M., Delattin, N., Vosloo, J.A., Dathe, M., Cammue, B.P.A., Thevissen, K., 2014b. Synergistic activity of the tyrocidines, antimicrobial cyclodecapeptides from *Bacillus aneurinolyticus*, with amphotericin B and caspofungin against *Candida albicans* biofilms. Antimicrob. Agents Chemother. 58, 3697–3707.

Van Belkum, M.J., Stiles, M.E., 1995. Molecular characterization of genes involved in the production of the bacteriocin leucocin A from *Leuconostoc gelidum*. Appl. Environ. Microbiol. 61, 3573–3579.

van de Lagemaat, M., Grotenhuis, A., van de Belt-Gritter, B., Roest, S., Loontjens, T.J.A., Busscher, H.J., van der Mei, H.C., Ren, Y., 2017. Comparison of methods to evaluate bacterial contact-killing materials. Acta Biomater. 59, 139–147.

Van Epps, H.L., 2006. René Dubos: unearthing antibiotics. J. Exp. Med. 203, 259–259.

van Rensburg, W., 2015. Characterization of natural antimicrobial peptides adsorbed to different matrices. Stellenbosch University, Department of Biochemistry, Stellenbosch, South Africa. MSc.Thesis, http://scholar.sun.ac.za/handle/10019.1/97929.

Vosloo, J.A., Stander, M.A., Leussa, A.N.N., Spathelf, B.M., Rautenbach, M., 2013. Manipulation of the tyrothricin production profile of *Bacillus aneurinolyticus*. Microbiology 159, 2200–2211.

Wigger-Alberti, W., Stauss-Grabo, M., Grigo, K., Atiye, S., Williams, R., Korting, H.C., 2013. Efficacy of a tyrothricin-containing wound gel in an abrasive wound model for superficial wounds. Skin Pharmacol. Physiol. 26, 52–56.

Williams, R.C., Yphantis, D.A., Craig, L.C., 1972. Noncovalent association of tyrocidine B. Biochemistry 11, 70–77.

Wu, X., Singh, A.K., Wu, X., Lyu, Y., Bhunia, A.K., Narsimhan, G., 2016. Characterization of antimicrobial activity against *Listeria* and cytotoxicity of native melittin and its mutant variants. Colloids Surfaces B Biointerfaces 143, 194–205.

Yang, Z., Choi, H., Weisshaar, J.C., 2018. Melittin-induced permeabilization, re-sealing, and re-permeabilization of *E. coli* membranes. Biophys. J. 114, 368–379.

Zasloff, M., 1988. Magainins, a class of antimiorobial peptides from *xenopus* skin: Isolation, characterization of two active forms, and partial cDNA sequence of a precursor. J. Occup. Environ. Med. 30, 470.

Zuo, R., Wood, T.K., 2004. Inhibiting mild steel corrosion from sulfate-reducing and iron-oxidizing bacteria using gramicidin-S-producing biofilms. Appl. Microbiol. Biotechnol. 65, 747–753.

3.7 Supplementary data

3.7.1 Purification of tyrocidines and analogues from commercially obtained tyrothricin and amino acid supplemented cultures

Commercial tyrocidines (Trc mix) was purified from commercially available tyrothricin as described previously (Spathelf and Rautenbach, 2009). An optimised method for the large scale production of tyrocidines and supplemented cultures was employed to obtain the Phe- and Trp-containing tyrocidine analogues (Vosloo et al., 2013). Characterization and purity determination of the peptide extracts were performed with a UPLC-MS method previously described (Troskie et al., 2014b; Vosloo et al., 2013).

Electrospray ionisation mass spectrometry (ESI-MS) was used to determine the identity of the peptides present within the purified peptide fractions and the crude produced extracts was prepared of which 3 µL was injected for analysis. ESI-MS analysis was done using a Water Synapt G2 quadrupole TOF mass spectrometer with electrospray ionisation source (Milford, MA, USA). Samples were subjected to a cone voltage of 15V, capillary voltage of 3.0 kV and source temperature of 120ºC. The desolvation gas was set as nitrogen (650 L/hour) with a desolvation temperature of 275ºC. All data was collected in the positive mode scanning over a m/z range of 300-2000. UPLC-MS separation was achieved with a gradient of solvent A (0.1% formic acid, *v/v*) to solvent B (100% acetonitrile, *v/v*) on a Water Acquity UPLC® HSS T3 C18 column (2.1x150 mm; 1.8 µm particle size) at a flow rate of 0.450 mL/minute. The gradient was as follows: 100% solvent A from 0-0.5 minutes, 0-58% solvent B from 0.5-12 minutes and 58-90% solvent B from 12-13 minutes. This was followed by the same analysis used for direct injection MS using a Water Synapt G2 quadrupole TOF mass spectrometer with electrospray ionisation source (Milford, MA, USA). Samples were subjected to a cone voltage of 15V, capillary voltage of 3.0 kV and source temperature of 120ºC. The desolvation gas was set as nitrogen (650 $L.h^{-1}$) with a desolvation temperature of 275ºC. All data was collected in the positive mode scanning over a m/z range of 300-2000.

The linear gramicidins, produced with tyrocidines as the peptide complex tyrothricin, were removed from commercially obtained peptide with the use of an organic solvent extraction to obtain a tyrocidine extract, which is referred to as Trc mix. The main peaks detected, were Trc C1 (1361.6785), Trc C (1347.6694), Trc B1/B1' (1322.6669), Trc B (1308.6517), Trc A1 (1283.6587) and Trc A (1269.6412). Smaller peaks of Trp C (1370.6827), Trc B' (1308.6517), Tpc B1 (1345.6759), Tpc B (1331.6633) and deaminated Trc A (1270.6364) was also detected (Figure S3.1, Table S3.1). No other peaks, other than solvent and machine background was

detected thus the peak areas of each peptide and peptide analogues was used to determine the percentage contribution to the overall sample and subsequently the sample purity. The peptide complex purity was found to be >90%, thus the sample could be used as an assay control and for biophysical experiments (Chapters 4 and 5).

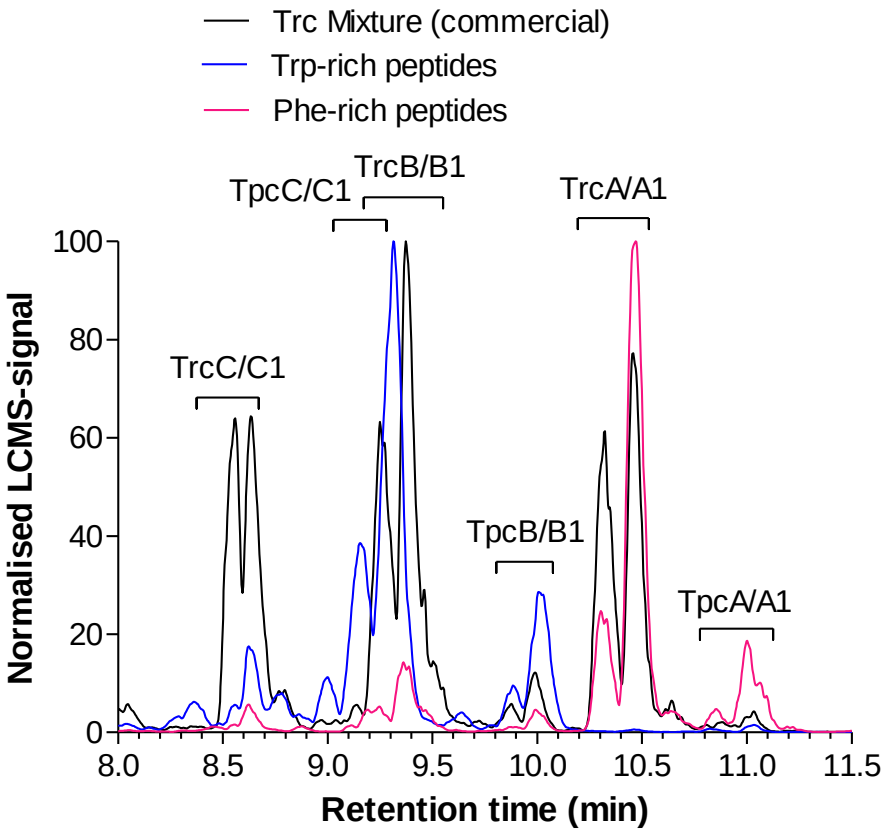

Figure S3.1: UPLC-MS chromatogram overlay in order to compare the difference in analogues present in the commercial Trc mixture, a Trp supplemented culture extract (Trp-rich peptide complex) and a Phe supplemented culture extract (Phe-rich peptide complex). The major tyrocidines groups are indicated to show the profile shift that occurs with amino acid supplementation.

The results obtained for the commercially purified peptides overall compared well to literature in terms of retention times and peptide profile (Tang et al., 1992; Troskie et al., 2014a) Amino acid supplemented cultures were used to produce two different mixtures of tyrocidine analogues. The tryptophan supplementation would yield a Trc C analogue rich extract, specifically Tpc C, contrary to the Phe supplemented culture extract since it normally contains more Trc A. Both are different to Trc mix which contains a mixture of the main Trcs: Trc A/A1, Trc B/B1 and Trc C/C1. The direct comparison of the chromatogram for each of these extracts (Figure S3.1) shows the shifts in the type of analogue produced. The relative purity of the

fractions and the percentage contribution of each of the tyrocidine analogues were calculated by determining the peak area of each of the peptides (Table S3.1).

Table S3.1: Percentage contribution of each of the tyrocidines and tyrocidine analogues as found in the commercial Trc mix, non-supplemented (Trc complex), Trp- and Phe-supplemented culture extracts (Trp-rich and Phe rich peptide complexes). The predominant tyrocidines are indicated in bold.

Peptide Identity	Sequence	M_r [c] (Theoretical)	% Contribution			
			Trc mix	Trc complex	Trp rich	Phe rich
Trc C1	*cyclo*-(fPWwNQYVKL)	1361.8404 (1361.6921)	12.0	4.6	3.0	1.5
Trc C	*cyclo*-(fPWwNQYVOL)	1347.9304 (1347.6764)	**13.9**	8.9	8.8	3.4
Tpc C1	*cyclo*-(fPWwNQWVKL)	1384.6404 (1384.7080)	1.6	2.8	**26.5**	1.2
Tpc C	*cyclo*-(fPWwNQWVOL)	1370.6844 (1370.6924)	1.9	5.1	**43.5**	2.9
Trc B1/B1’	*cyclo*-(fPFwNQYVKL)	1322.5864 (1322.6812)	**19.7**	**13.2**	<1	5.9
Trc B/B’	*cyclo*-(fPWfNQYVOL)	1308.6164 (1308.6555)	**18.4**	**22.9**	1.6	**15.2**
Tpc B1/B1’	*cyclo*-(fPWfNQWVKL)	1346.6901 (1345.6971)	1.1	3.6	5.5	<1
Tpc B/B’	*cyclo*-(fPFwNQYVOL)	1331.5744 (1331.6815)	3.4	**12.3**	10.7	4.2
Trc A1	*cyclo*-(fPFfNQYVKL)	1283.6464 (1283.6703)	**14.6**	**9.2**	<1	**17.3**
Trc A	*cyclo*-(fPFfNQYVOL)	1269.6684 (1269.6538)	12.3	9.8	<1	**30.2**
Tpc A	*cyclo*-(fPFfNQWVOL)	1292.6644 (1292.6479)	1.1	7.7	<1	6.3
Phc A	*cyclo*-(fPFfNQFVOL)	1253.6782 (1253.6597)	<1	<1	<1	**11.0**

[a] Trc - tyrocidine, Tpc – tryptocidine, Phc – phenycidine.

[b] [a]Peptide sequences, as previously described (Tang, Thibault and Boyd, 1992) where the amino acids are represented by conventional one-letter abbreviations except for Ornithine which is represented by O. The L-amino acids are in uppercase and the D-amino acids in lowercase

[c] The identity of the peptides were confirmed with high resolution mass spectrometry, with experimental Mr (top value) a representative analysis determined on the commercial Trc mixture

[d] Percentage contribution was calculated by determining the peak area as determined with LCMS for each analogue. The percentage contribution to peak area was calculated assuming equal response factors for each of the analogues.

The bulk of the peptides present in the Trp-supplemented extract (Table S3.1) are Tpc C (43.5% contribution), Tpc C1 (26.5%) and Tpc B (10.7%). A small amount of Trc C/C1 (11.8%) was produced, with very little Trc B/B1 (±2%) and a negligible amount of Trc A and Trc A

analogues. The main peptides detected in the Phe-supplemented extract were Trc A (30.2%), Trc A1 (17.3%), Trc B (15.2%) and Phc A (11%). The latter was not detected in either Trc mix or the Trp-supplemented culture extract. There remaining 30% of the extract comprised of a mixture of tyrocidines and tryptocidines. The main peptides found in the non-supplemented extract were predominantly Trc B (22.9%), Trc B1 (13.2%) and Tpc B/B' (12.3%). Followed by Trc A (9.8%), Trc A1 (9.2%) and Trc C (8.9%).

The difference in profile, however, between the supplemented extract and Trc mix is due to the variability of the tyrocidine structure at positions 3,4 and 7. The polyenzyme unit that is responsible for the production of these peptides have low selectivity when incorporating structurally similar amino acids at these positions (Fujikawa et al., 1968a; Mach and Tatum, 1964; Ruttenberg and Mach, 1966). Thus, supplementation of Trp into the growth media leads to an increased incorporation of Trp into the dipeptide unit at position 3 and 4 leading to an increase of production for Trc B- and Trc C-analogues. It also increases the incorporation of Trp at position 7 resulting the in the increased production of the tryptocidines (Tpcs). The opposite is true for Phe supplementation resulting in the increased production of Trc A analogues. The profile shifts that were obtained for the supplemented cultures aligned with the amino acid-induced shifts reported in literature (Fujikawa et al., 1968a; Mach and Tatum, 1964; Ruttenberg and Mach, 1966; Vosloo et al., 2013).

3.7.2 Optimisation of fluorescence parameters

Previous studies on the binding of Tyrocidines and tyrocidine analogues to various solid surfaces used changes in UV before and after incubation as the main method of determining peptide binding at 230, 256 and 280nm selecting for peptide bonds, aromatic rings and tryptophan (van Rensburg, 2015). The major drawback with this method was the occurrence of an increase in UV-signal after incubation of the peptide and some of the solid surfaces due to a release of compound from the solid surface. As a result, the amount of peptide bound to the solid surfaces could not be calculated. This was especially true for cellulose containing solid surfaces and more so for cellulose/paper. Thus, the method of detection moved from UV to fluorescence, making use of the naturally occurring fluorophores within the peptides namely Trp and Phe; and Tyr at position 3&4 and 7 respectively. The first step in optimising this method was to determine where the fluorescence peaks would occur on the emission spectra and if any of the peaks of the three amino acids overlapped. Equimolar amounts of Trp, Tyr Phe were tested to mimic the average occurrence of these amino acids within the tyrocidine

structure in terms of the three main analogues: Trc A ($F^3F^4Y^7$), Trc B ($F^3W^4Y^7$ or $W^3F^4Y^7$) and Trc C ($W^3W^4Y^7$).

All three amino acids were excited at Ex_{260}, Ex_{275} and Ex_{295}, for Phe, Tyr/Trp and Trp respectively (Figure S3.2). At Ex_{260}, scanning for emission between 290 nm to 360 nm (Figure S3.2: A), the fluorescence detected for Phe was similar to that of the background signal and therefore negligible. Tyr fluorescence alone was detected between 355-360 nm and Trp fluorescence at 300-302 nm. Overall the fluorescence detected was much lower in comparison to that observed at Ex_{275} and Ex_{295}. Excitation at 275 nm, scanning from 300-360 nm, though used in the detection of Tyr also excites Trp. Therefore, any excitation of a protein or peptide between 275-280 nm, would more correctly detect both Tyr and Trp residues. This can be seen with the overlapping fluorescence detected for Tyr and Trp at Ex_{275} (Figure S3.2: B). The signal for Phe was once again the same as the background and negligible. At Ex_{290}, scanning emission from 320-370 nm, predominantly Trp was detected as was expected. The signal for Tyr and Phe was negligible.

Based on the observed fluorescence, four parameters were selected: Ex_{275}/Ems_{324} (high Tyr fluorescence); Ex_{275}/Ems_{342} (high Trp fluorescence); Ex_{290}/Ems_{342} (highest signal intensity) and Ex_{290}/Ems_{350} (previously used in single fluorescence experiments)(Spathelf, 2010). It was observed that excitation at 290nm (Figure S3.3: A&B) gave better linearity especially at low peptide concentrations in comparison to excitation at 275nm (Figure S3.3: C&D). Also, the fluorescence at Ex_{290}/Ems_{342} (Figure: A) gave a better fit over the entire curve compared to that observed for Ex_{290}/Ems_{350} (Figure S3.3: B).

For the purpose of studying the behaviour of the Trcs in different environments Ex_{280} and $Ems_{300\text{-}400}$ was selected since it would detect both Trp and Tyr residue fluorescence. As for following the association and dissociation of the peptide Ex_{290} and Ems_{342} was selected as it was the most sensitive and could detect smaller changes in signal. This limits detection to only Trc C and Trc B analogues, but the assumption for this study was that all the analogues would associate and dissociate to the cellulose similarly. This assumption is based on that the organism produces the mixture of peptides close to sporulation to bind to the spore capsule (saccharide based) and therefore would bind in a similar manner to cellulose. Calculations on the amount of peptide bound to the various surface was done by making use of a standard curve of Trc mix in 5% acetonitrile (Figure S3.4), under the same conditions as the peptide incubation with the materials.

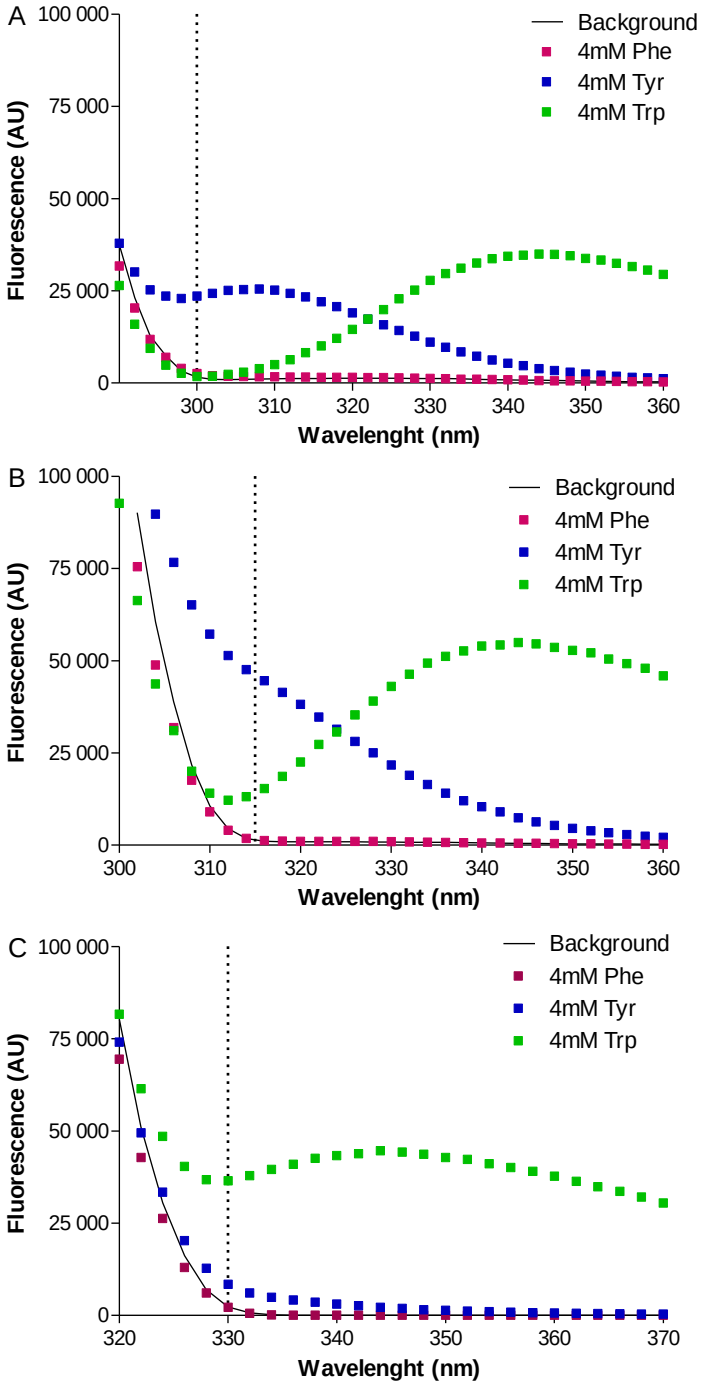

Figure S3.2: The fluorescence of 4mM Phe, Tyr and Trp as detected at excitation **(A)** Ex_{260} **(B)** Ex_{275} **(C)** Ex_{290}. The dotted line indicates at which point the background signal is zero. The data is representative of only one technical repeat.

At one hour of incubation, the limit of detection was at 5 µg/mL (S/N>2, 0.5 µg Trc mix) and the limit of quantification was at 10 µg/mL (S/N>10, 1 µg Trc mix). The limit of linearity was at 50 µg/mL, which was the highest concentration tested in the standard curve, but also the

concentration used for treatment of the solid surfaces. A fit of R^2 >0.99 was found and the amount of peptide bound calculated by using the linear equation presented on the graph.

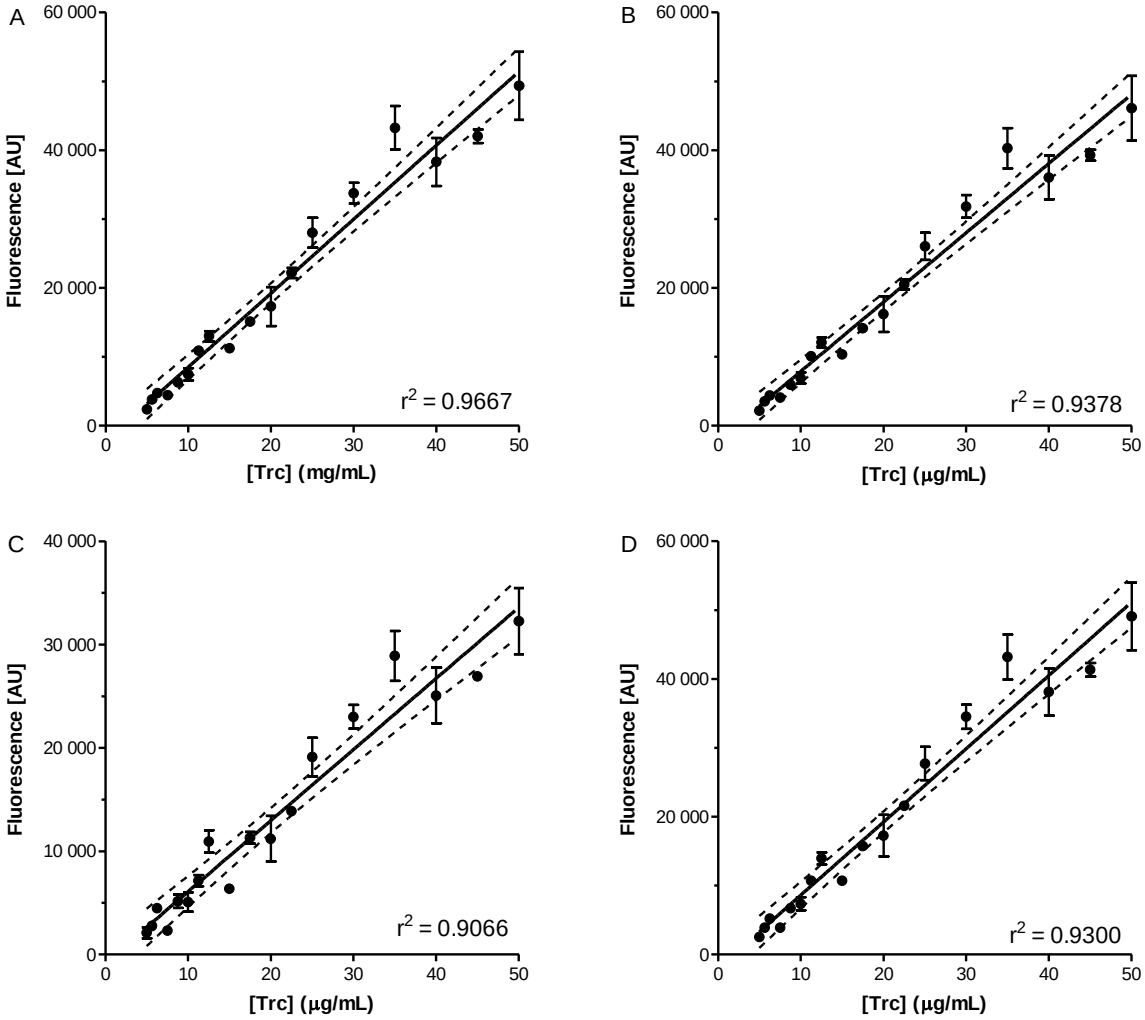

Figure S3.3: Standard curves of Trc mix in 5% ACN at **(A)** Ex_{290}/Ems_{342} **(B)** Ex_{290}/Ems_{350} **(C)** Ex_{275}/Em_{324} **(D)** Ex_{275}/Em_{342}. Linear regression was used to fit the curves (R^2>0.95). Each datapoint is the average of triplicate determinations with error bars showing the standard error of the mean (SE). The dotted lines show the 95% confidence interval (CI) for the fitted curve (solid line).

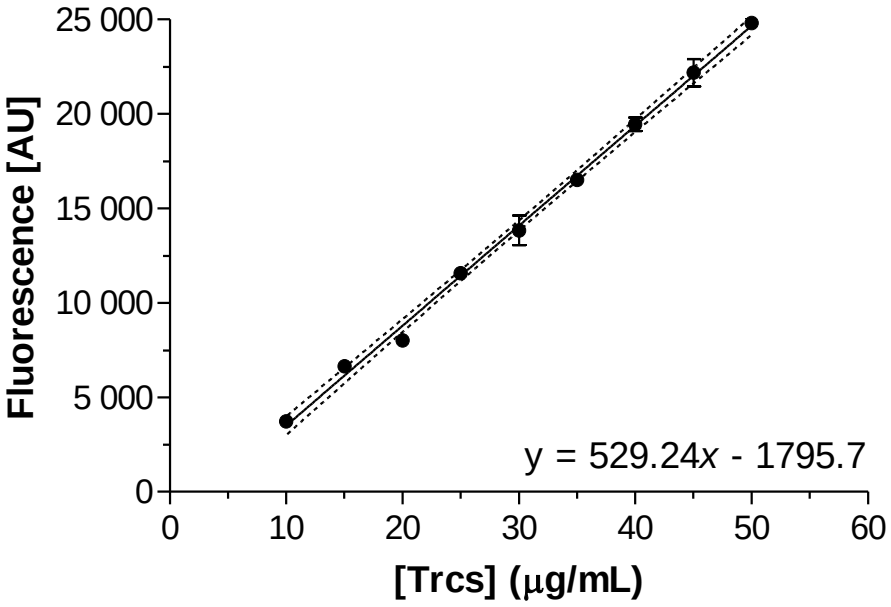

Figure S3.4: Standard curve (at Ems $_{290}$/Ex$_{342}$) of Trc mix in 5% acetonitrile used to calculate the amount of peptide remaining in the incubation solution by using linear regression to fit the curve (R^2>0.99). Each datapoint is the average of quadruplicate determinations with error bars showing the SE. The dotted lines show the 95% CI for the fitted curve (solid line).

3.7.3 Temperature stability of the Trc mix

Thermogravimetric analysis (TGA) was performed to determine the thermal stability of Trc mix (0.69 mg). TGA is used to determine the thermal stability of a compound by correlating changes in sample mass to an increase of temperature. Analysis was performed under nitrogen at a temperature range from 10ºC to 600 ºC, at a ramp rate of 20ºC/min with the use of TGA Q500 V6.7 Build 203 instrumentation.

Trc mix appears to remain stable up to 190ºC (Figure S3.5), which extends the temperature stability previously reported for tyrocidines (Appleby et al., 1947; Dubos, 1939; Hotchkiss, 1941). There appears to be three main degradation events at 190ºC – 240ºC, 250ºC – 290ºC and 300ºC - 350ºC which stabilises around 400 ºC. All three events can be attributed to the thermal degradation of the aromatic amino acids (Cuq et al., 1983; Cuq and Cheftel, 1983; Mello et al., 2015; Patron et al., 2008) The presence of both Tyr and Trp within Trc mix complicates the assignment of each of the peaks, however, it can be confirmed that the peptide is stable to 190ºC. This also correlates to the observed decrease in activity observed for the peptide treated cellulose after exposure to 200ºC.

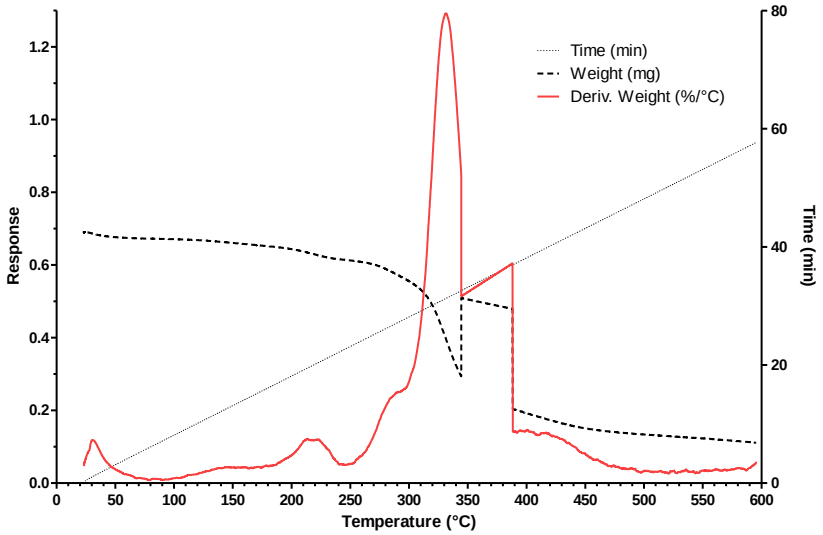

Figure S3.5: Thermogravimetric curve of Trc mix showing the change in sample mass over time and increasing temperature. Note the three main degradation points: 190ºC – 240ºC, 250ºC – 290ºC and 300ºC - 350ºC.

3.7.4 Summary of full statistical analysis

Table S3.2: Summary of statistical analysis between Trc mix and lab acquired materials for the activity against *L. monocytogenes* (Figure 3.3:A). Abbreviations: cellulose (CL), mixed cellulose filters GSWP (0.22 µm) and HAWP (0.45 µm); cellulose nitrate (CN – 0.4 µm), polycarbonate (PC – 0.4 µm), black polystyrene plate (BP), polypropylene round bottom plate (PPR), polystyrene round bottom plate (PSR) and polystyrene plate (AP). Statistical analysis was performed with One-way Anova (Bonferroni's multiple comparison test). ***P<0.001; **P<0.01; *P<0.05, ns – not significant

	CL	GSWP	HAWP	CN	PC	BP	PPR	PSR	AP
Trc mix	ns	*	***	**	***	***	***	***	***
CL		**	***	***	***	***	***	***	***
GSWP			ns	ns	ns	**	**	***	***
HAWP				ns	ns	*	ns	***	***
CN					ns	*	ns	***	***
PC						ns	ns	***	***
BP							ns	***	***
PPR								***	***
PSR									ns

Table S3.3: Summary of statistical analysis between Trc mix and commercial materials for the activity against *L. monocytogenes* (Figure 3.3:B). Statistical analysis was performed with One-way Anova (Bonferroni's multiple comparison test). ***P<0.001; **P<0.01; *P<0.05, ns – not significant

	Plastic tray	Tissue paper	Ripple carton	Paper Tray	Carton box	Meat paper – wax	Meat paper	White bag	Green bag	Cling film
Trc mix	ns	ns	ns	***	*	***	***	ns	ns	ns
Plastic tray		ns	ns	***	ns	***	***	ns	ns	ns
Tissue paper			ns	***	ns	***	***	ns	ns	ns
Ripple carton				***	ns	ns	***	ns	ns	ns
Paper tray					***	***	***	***	***	***
Carton box						ns	**	ns	ns	ns
Meat paper - wax							ns	**	**	**
Meat paper								***	***	***
White bag									ns	ns
Green bag										ns

Table S3.4: Summary of the statistical analysis between the activities observed for antibiotic treated cellulose against *L. monocytogenes* (Figure 3.11:A). Abbreviations: GD – Linear gramicidins, GS- gramicidin S. Statistical analysis was performed with One-way Anova (Bonferroni's multiple comparison test). ***P<0.001; ns – not significant

	Trc mix	GD	Trc Extract	GS	Magainin 2A	PGLa	Leucocin A	Melittin	Gentamycin
Tyrothricin	ns	***	ns	ns	***	***	***	***	***
Trc mix		***	ns	ns	***	***	***	***	***
GD			***	***	***	ns	***	***	***
Trc Extract				ns	***	***	***	***	***
GS					***	***	***	***	***
Magainin 2A						***	***	ns	***
PGLa							***	***	***
Leucocin A								***	ns
Melittin									***

Table S3.5: Summary of the statistical analysis between the activities observed for antibiotic treated cellulose against *E. coli* (Figure 3.11:B). Abbreviations: GD – Linear gramicidins, GS- gramicidin S. Statistical analysis was performed with One-way Anova (Bonferroni's multiple comparison test). ***P<0.001; ns – not significant

	Trc mix	GD	Trc Extract	GS	Magainin 2A	PGLa	Leucocin A	Melittin	Gentamycin
Tyrothricin	ns	ns	ns	***	***	***	***	***	***
Trc mix		**	ns	***	***	***	***	***	***
GD			*	***	***	***	ns	ns	***
Trc Extract				***	***	***	***	***	***
GS					***	***	***	***	***
Magainin 2A						***	***	***	***
PGLa							***	***	***
Leucocin A								ns	***
Melittin									***

Chapter 4
Elucidation of tyrocidine-cellulose interaction

4.1 Introduction

Antimicrobial surfaces and materials are regarded as the solution to various surface related problems such as infections related to medical implants, food processing industries, fresh foods and many others (Boatemaa et al., 2019; Noimark et al., 2009; Olanya et al., 2019; Ramsden et al., 2007; Srey et al., 2013). Self-sterilising or antimicrobial surfaces can either prevent adhesion by creating less favourable conditions for attachment or can carry compounds that either inhibit growth or kill pathogens by the release of antimicrobial compounds. Antimicrobial compounds are attached to base materials by means of three general methods: incorporation into the base material upon creation, 'graft-from' or 'graft-to' (Green et al., 2011). Incorporation into base materials are normally done during a swelling step for polymers before it is cast into films or electrospun into mats step (Green et al., 2011). 'Graft-from' relates to the synthesis of compounds directly from the base material (Felgueiras and Amorim, 2017). 'Graft-to' is the covalent attachment of already existing compounds to the base material by activating functional groups on the base material (Felgueiras and Amorim, 2017; Green et al., 2011). In the same category is the adsorption through non-covalent attachment through ionic bonds, hydrogen bonds, van der Waals bonds and hydrophobic interactions.

There are three main components considered in the development of active surfaces: the active compound, the method of attachment and the base material which is dependent on the final application. Cellulose and cellulose-derivatives have gained much attention for the use as a base material for slow release and contact killing active surfaces within the medical and food industries as wound dressings and active packaging (Barbiroli et al., 2012; Lin et al., 2003; Nguyen et al., 2008; Pivec et al., 2017; Son et al., 2004). Much of the attraction is due to the fact that it is low cost, non-polluting since it is biodegradable, edible, non-toxic and biocompatible (Cagri et al., 2004; Vásconez et al., 2009). Cellulose also has good barrier properties and is considered as a good carrier of antimicrobial compounds (Cagri et al., 2004; Vásconez et al., 2009). Cellulose derivatives, such as hydroxypropyl methylcellulose (HPMC) that is a renewable biodegradable polymer, can be used as a novel packaging material (Sanchez-Gonzalez et al., 2011). HPMC is already approved by the FDA and EU for food use (Burdock, 2007) and the application of cellulose-derived antimicrobial materials are as diverse as the scope of modified celluloses and active compounds.

Tyrocidines and tyrocidines analogues (Trcs) have been shown to associate to a range of laboratory and general commercial materials (plastics, biopolymers and paper), maintaining activity against *L. monocytogenes* although the amount of Trcs associated could not always be directly correlated to activity (Chapter 3)(Van Rensburg, 2015). Screening for residual antimicrobial activity on these materials, after washing steps, showed a selectivity of tyrocidines for cellulose association with the peptide-cellulose material being the most robust antimicrobial material. The association is not through covalent attachment but rather through an unknown mechanism of non-covalent attachment. It is therefore needed to elucidate the molecular descriptors in the association and dissociation of the Trcs with cellulose.

In this study the concentration dependency of the association of Trcs was first investigated. This was followed by activity studies against *Listeria monocytogenes* and red blood cells of Trc mix in conjunction with glucose, cellobiose and cellulose. The effect of glucose association, as a model cellulose monomer, on the peptide secondary structure and amino acids side chains was determined with circular dichroism (CD) and nuclear magnetic resonance (NMR). This work was part of a published article (Juhl et al., 2019)(Chapter 4 Addendum), and will only be discussed in brief. The ability of glucose and cellobiose to inhibit Trcs association and resulting activity against *L. monocytogenes* was also determined. Attenuated total reflectance Fourier transformed infrared spectroscopy (ATR-FTIR) was used to determine the molecular interactions between Trcs and sugars (glucose, cellobiose and hydroxypropyl cellulose) by drying the samples together providing a 'snap-shot' of the interaction. Lastly, (^{13}C,^{15}N) labelled Trc A was used to prove the association to microcrystalline cellulose with solid state NMR in an exploratory study.

4.2 Materials

D-cellobiose, resazurin sodium salt and KCl was supplied by Sigma (St. Louis, MA, USA). Acetonitrile (ACN), HPLC-grade far UV cut-off was supplied by Romil Ltd (Cambridge, UK). Merck (Darmstadt, Germany) supplied agar, yeast extract, tryptone, Na_2HPO_4, KH_2PO_4 and Merck (Wadeville, SA) supplied sodium chloride, brain heart infusion broth and black 96-well polystyrene plates. 96-well polystyrene plates were acquired from Corning (Kennebunk, ME, USA) and cellulose filters (Paper) (MN 615/No 1) were obtained from Macherey-Nagel (Düren, Germany). Packed erythrocytes (A^+) from anonymous donors (Western Cape Blood services) was washed twice with phosphate buffered saline (PBS) for haemolysis studies. The preparation of purified TrcA and uniformly (^{13}C,^{15}N)-labelled TrcA were purified from

Brevibacillus parabrevis culture extracts (refer supplementary data for details). Analytical grade water was obtained filtering water from a reverse osmosis plant through Millipore Milli-Q® water purification system (Milford, USA). Klucel™ E IND (KLU E) was obtained from Ashland Industries Europe GmbH (Rheinweg, Switzerland). All chemical structures were rendered by using ChemBioDraw Ultra and graphs were constructed utilising Prism 4.01 (GraphPad Software, Inc).

4.3 Methods

4.3.1 Creation of Trcs-containing cellulose

Peptides were dissolved in 50% *v/v* acetonitrile for a stock concentration of 2.00 mg/mL and was diluted to a concentration of 50.0 µg/mL in 5% *v/v* acetonitrile. This peptide solution (0.100 mL) was then transferred to a 96-well polystyrene plate containing cellulose disks and incubated for one hour to allow for interaction/adsorption. Following incubation, the peptide solution was removed, and the disks washed twice with 100 µL analytical quality water to remove remaining acetonitrile and free peptide. The disks were dried in a 40ºC oven and sterilized with chloroform vapour before testing.

Activity and haemolysis studies with glucose and cellulose entailed the creation of a 'solid surface' by drying peptide:saccharide solutions to the bottom of a well of a 96-well assay plate. Solutions of Trc mix and sugar were prepared at stock concentrations that would result in double dilution of peptide with 200 µg of sugar.

4.3.2 Fluorescence detection of tyrocidines and tyrocidine analogues

The emission (Ems) and excitation (Ex) parameters were optimised making use of the three possible fluorophores in the peptide as described in Chapter 3 – supplementary data. The fluorescence was read every 2 minutes for three hours at Ex_{290} and Ems_{342} as it delivered the most sensitive signal.

The fluorescence study of the influence of glucose and cellobiose on the association of Trc mix to cellulose was done by incubating 50 µg/mL Trc mix with a 0.5-32 mol:mol ratio of peptide and glucose or cellobiose. After an hour incubation, to ensure association based on the cellulose binding results, the solutions were transferred a 96-well black plate with cellulose and the fluorescence measured for two hours at Ex_{290} and Ems_{342}. The fluorescence readings were collected by using the Tecan Spark 10M Multimode Microplate Reader and controlled by the Spark Control™ software, both provided by Tecan Group Ltd (Mennedorf, Switzerland).

Following the incubation and fluorescence studies, the peptide solutions and control solutions were removed, and the cellulose disks washed twice with 200 µL analytical quality water to remove any remaining free peptide. The plates were then dried in a 40°C oven and used to study the effect the tested conditions have on the activity of the treated disks.

4.3.3 Antimicrobial activity detection

The effect of the change in environment on the activity of the created solid surfaces was determined with the use of the optimized resazurin assay (Chapter 2). *L. monocytogenes* B73 was streaked out from freezer stocks onto BHI agar plates (Brain Heart Infusion; 1.5% *w/v* agar) and incubated for 48 hours at 37°C until colonies were viable. A starter culture was prepared, by inoculating 1mL BHI media with 3-5 colonies and growing the cells overnight at 37 °C at an angle, shaking at 150 RPM. The starter culture was sub-cultured into fresh medium and grown until mid -exponential growth phase OD_{600} = 0.4 (±1.3 x 10^8 cells/mL). The culture was then pipetted (10 µL) onto the treated and untreated materials and incubated for one hour at 37°C. Following the incubation, 90 µL PBS (0.8% *w/v* NaCl, 0.04% *w/v* KCl, 0.144% *w/v* Na_2HPO_4, 0.02% *w/v* KH_2PO_4; pH 7.4) and 10 µL resazurin dye (0.03 mg/mL in PBS) was added and the plates incubated further at 37°C. The conversion of the resazurin was measured at Ex_{530} and Ems_{590} at 30 minutes, 1 hour, 2 hours and 3 hours of incubation using the Teacan Spark 10M Multimode Microplate Reader and controlled by the Spark Control™ software, both provided by Tecan Group Ltd (Mennedorf, Switzerland). The activity of the material was determined in terms of % inhibition by using the acquired fluorescence readings (F), calculated with the following formula:

$$\%\ \boldsymbol{Inhibition\ of\ Target\ organism} = \frac{\boldsymbol{F\ of\ well - F\ of\ average\ blank}}{\boldsymbol{F\ of\ growth\ control - F\ of\ average\ blank}}$$

4.3.4 Solid surface haemolysis activity

The haemolysis activity of Trc mix alone and in combination with 200 µg glucose or cellobiose, and cellulose disks was determined with the use of a previously optimised method for solid surface (Van Rensburg, 2015). In brief, analytical grade water (10 µL) and a 2% haematocrit solution in PBS (90 µL) were added to each of the wells and incubated at 37 ºC for two hours. Following the incubation, the plates were centrifuged for 10 minutes at 900 *xg* and the supernatant (10 µL) transferred into PBS (90 µL). Absorbance (A) was measured at 415nm using the Teacan Spark 10M Multimode Microplate Reader. Haemolytic activity was calculated using the following equation:

$$\%\ \boldsymbol{Haemolytic\ acitivity} = 100 \text{ x } \frac{\boldsymbol{A\ of\ well - avg.\ A\ of\ background}}{\boldsymbol{avg.A\ of\ fully\ lysed - avg.\ A\ of\ background}}$$

4.3.5 Circular dichroism (CD)

The circular dichroism data on the effect of glucose on the peptide backbone was published as part of the article added in Chapter 4 – Addendum (Juhl et al., 2019). Trc A was dissolved in 60% *v/v* acetonitrile, then diluted to glucose concentrations ranging from 0.025-6.25mM at a final peptide concentration of 250 µM. Spectra were acquired with the use of the Chirascan Plus CD spectropolarimeter (Applied Photophysics, UK) at ambient temperature (24 ± 1ºC) between 185-300nm at a bandwidth of 0.5nm in a quartz curvette (pathlength 0.5mm). Two repeats per sample in triplicate were performed and spectra were collected in a step wise manner over 0.2 seconds per 0.5nm. Percentage change in ellipticity (θ) at 206 and 216 nm was calculated with the following equation:

$$\%\ Change = \frac{B - A}{B}\ x\ 100$$

where *B* is the θ (molar ellipticity) of Trc A alone and *A* the θ of Trc A at the varying concentrations of glucose.

4.3.6 Fourier-transform infrared spectroscopy

Fourier-transform infrared spectroscopy (FTIR) analysis was performed on a Nicolet™ iS™ 20 FTIR Spectrometer (ThemoScientific) coupled with an ATR (attenuated total reflectance) for surface analysis at the Department of Polymer Science, University of Stellenbosch. Trc mix, and sugars (glucose, cellobiose and KLU E) were incubated together for one hour and then freeze-dried to remove all solvents. Spectra were recorded for each of the samples plus controls over a wavenumber range of 4000 cm^{-1} to 650 cm^{-1} with a 0.5 cm^{-1} bandwidth. The data was collected and manipulated with the basic OMNIC software package (ThermoScientific).

4.3.7 Solid-state NMR spectroscopy

The solid state nuclear magnetic spectroscopy (NMR) was done in collaboration with the group of Prof. Burkhard Bechinger at Strassbourg University utilising the methodology descibed below.

An aliquot of uniformly (^{13}C,^{15}N)-labelled TrcA (200 µg) was dissolved in 50% ACN at 2.5 mg/mL before 10 mg of microcrystalline cellulose was added. The sample was diluted to obtain a 10% ACN concentration. After 4 hours of incubation, the samples were centrifuged at

13,000 x*g* for 30 minutes and the supernatant removed. The pellet was washed once in analytical quality water prepared through a MilliQ system and subsequently packed into a 1.3 mm rotor for magic angle spinning solid-state NMR.

Magic-angle spinning (MAS) solid-state NMR spectra were measured at a magnetic field of 17.6 T, corresponding to a 1H frequency of 750 MHz, on a Bruker spectrometer equipped with an Avance III consol. The experiments were conducted using a 1.3 mm probe in ^{1}H, ^{13}C, ^{15}N triple resonance mode at 60 kHz sample spinning. The sample temperature was kept around 45°C. Cross-polarization was achieved with 50 kHz irradiation on ^{1}H and 10 kHz irradiation on 13C using a 1.5 ms contact time. Relaxation delays were set to 1s.

The sample for dynamic nuclear polarization (DNP) signal-enhanced solid-state NMR was prepared in a similar manner with 100 μg of uniformly (^{13}C,^{15}N)-labelled TrcA incubated with 10 mg of microcrystalline cellulose. After the final wash, the sample was left on the table over night to dry before 16 μL 15 mM AMUPOL in glycerol-d8/D_2O/H_2O 60/30/10 *v/v/v*) was added. The entire sample was stirred thoroughly and packed into a 3.2 mm sapphire MAS rotor with Teflon insert. The sample without peptide was prepared following the same procedure.

DNP solid-state NMR spectra were measured at a magnetic field of 18.8 T, corresponding to ^{1}H and electron Larmor frequencies of 800 MHz and 527 GHz, respectively. The DNP-enhanced NMR experiments were carried out at ISA-CNMR site (Lyon, France) on a Bruker Avance III solid-state NMR spectrometer equipped with a cooling unit using liquid nitrogen, and a 3.2-mm triple-resonance (^{1}H/^{13}C/^{15}N) low temperature MAS probe. The spectra were measured at the temperature of 99 K under MW irradiation of 9 W at the rotor and MAS rotation of 12.5 kHz. An adiabatic CP pulse sequence was used for ^{13}C spectra with a spectral width of 50 kHz and acquisition, cross-polarization contact, and recycle delay times of 20.5 ms, 2 ms, and 10 s, respectively. The ^{1}H π/2 pulse, CP contact and spinal64 heteronuclear decoupling field strengths B1 corresponded to a nutation frequency of 106, 64 and 96 kHz. To equilibrate the system before acquisition the sample was exposed to 4 dummy scans. An exponential line-broadening of 50 Hz was applied before Fourier transformation. For ^{15}N CP a spectral width of 59.5 kHz and acquisition, cross-polarization contact, and recycle delay times of 17.2 ms, 0.5 ms, and 10 s, were used. The DNP signal enhancement was determined as a ratio in the integral signal intensity of MW ON versus MW OFF spectra obtained with identical parameters.

4.4 Results

The research on tyrocidine association in this study focussed on cellulose due to its potent and robust antimicrobial activity. Therefore, cellulose was also chosen as the model material to study the interaction of Trcs to surfaces with the use of fluorescence, NMR, CD and ATR-FTIR.

4.4.1 Kinetics of tyrocidine association to cellulose as model material

It was previously found that the Trp fluorescence signal decayed when Trc mix at 50 µg/mL (approximately 38 µM) was monitored over 2-3 hours. This fluorescence decay over time of Trc mix alone (Figure 4.1: A) can be fitted to a one phase exponential decay which can be described by the following equation:

$$y = plateau + (Yo - plateau)^{-Kx}$$

where *y* is the fluorescence signal, Y_O is the starting/original fluorescence signal, *x* is the time elapsed and the fitted parameter indicated as *plateau* is the change (decay) endpoint where the difference between *y* and Y_O remains constant over time. *K* is a fitted decay constant.

The observed decay can be caused by two factors: self-assembly and association to the surface of the plastic plate used in the assay. The latter was confirmed in Chapter 3 by the activity against *L. monocytogenes* of the residual peptide that remain in the wells of the BP (black plate). The Trcs inclination to form self-assembly structures based on environmental changes and concentration has been widely studied (Appleby et al., 1947; Loll et al., 2014; Munyuki et al., 2013; Paradies, 1979; Williams et al., 1972). The formation of higher order structures over time could lead to quenching of the Trp residue fluorescence if these residues interact by aromatic stacking, with polar moieties in the peptide and/or with the polar solvent molecules due to conformational changes (Chattopadhyay and Raghuraman, 2004; Chen and Barkley, 1998; Lakowicz, 2013). Alternatively, if already formed peptide oligomers associate with surfaces, removing them from solution, it would also lead to a decrease of fluorescence signal. This assumption that a decrease of fluorescence is related to peptide association is based on the fact that peptide treated cellulose has no detectable fluorescence in the presence of water or and without water (dried treated disks). It has been previously shown that water washes do not remove the Trc from cellulose filters.

The fluorescence decay of 50.0 µg/mL Trc mix with cellulose (Figure 4.1: A) was best fitted to a two phase exponential decay (as statistically compared to a one-phase exponential decay

fit in Prism 4.01) with a fast initial decay occurring within the first 30 minutes of exposure. The equation used to fit the data is as follows:

$$y = plateau + (span_{fast})^{-K_{fast} \cdot x} + (span_{slow})^{-K_{slow} \cdot x}$$

where y is the fluorescence signal, *plateau* is the value of y at infinite time points, $span_{fast}$ and $span_{slow}$ is the range at which the fast and slow decay occurs expressed in the units of y, x is the time elapsed and K_{fast} and K_{slow} is fitted decay constants.

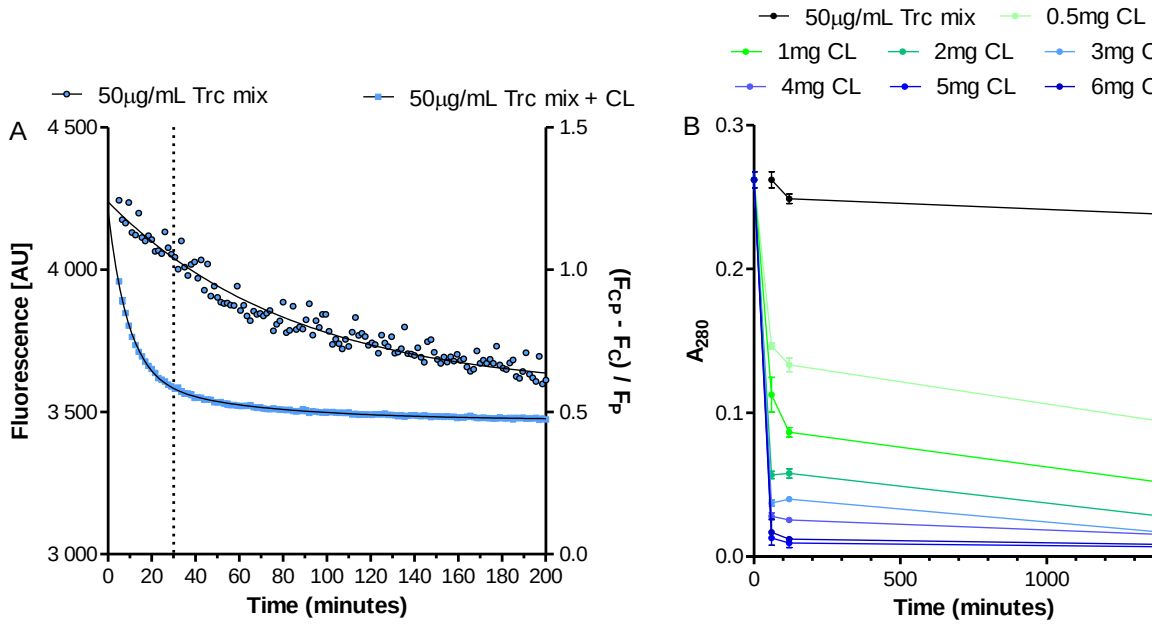

Figure 4.1: Fluorescence and UV monitoring of Trc mix association with cellulose **(A)** Decrease in fluorescence signal of 50.0 µg/mL Trc mix over time on the left y-axis vs. decrease in fluorescence signal of 50µg/mL Trc mix over time in the presence of cellulose (CL) on the right y-axis. F_{CP} is the fluorescence detected for the peptide and cellulose, F_C the fluorescence detected for the cellulose and F_P the fluorescence detected for the peptide alone. **(B)** Decrease in absorbance signal over time of 50.0 µg/mL Trc mix with the addition of increasing amounts of microcrystalline CL.

This initial rate/decrease can be attributed to the association of the peptide to cellulose. This was further verified by a separate experiment with monitoring of absorbance at 280 nm (Figure 4.1: B), using microcrystalline cellulose (MCC) and glass vials for the incubation step. MCC did not result in the same background signal with absorbance previously reported for cellulose paper and glass allows for much lower surface binding of the peptide. Thus, the influence of cellulose on the peptide signal could be studied without influence of environmental surfaces. It was observed that an increase of MCC resulted in an increase in the initial binding rate confirming what was observed with the fluorescence decay. The second decay in the black 96-

well plates can possibly be attributed to a combination between cellulose association, plate association and self-assembly.

From the fluorescence and UV spectrometry studies it is clear that there is a rapid interaction between cellulose and the Trcs, followed by a gradual association over time as seen with the gradual second fluorescence decay. This two-phase association holds similarity to the aggregation pattern of the Trcs, quickly forming dimers followed by a much slower aggregation into larger oligomers (Paradies, 1989). In the light of the high propensity of the tyrocidines to form oligomers the potential is that the cellulose surface could be covered by many layers of nanostructures or peptide networks, without being saturated. This could have been further studied with surface plasmon resonance; however, a suitable soluble cellulose model surface was not available. Therefore, the methods used in this study focussed on fluorescence and ATR-FTIR.

To study this, we followed the kinetics of binding to cellulose at different Trc mix concentrations, in 5% *v/v* ACN. The association of Trcs to cellulose was determined by direct correlation between a decrease in fluorescence as a decrease in available peptide within the solution. Fluorescence decrease was determined by comparing the background subtracted fluorescence of each concentration of Trcs expressed as a function of the Trcs fluorescence over time. Regardless of the concentration of peptide tested, all concentrations tested showed rapid binding in which a plateau was reached within 60 minutes (Figure 4.2: A). A two-phase exponential decay curve fit was found to best describe the data as noted in Figure 4.1: A for a single peptide concentration. This would suggest that there is a fast, initial association of the peptide to the cellulose, followed by a gradual self-association and stacking of layering forming higher order oligomers and possibly nano-spheroids and peptide sheets. The peptides can form higher order oligomers in the absence of any surface, however the influence of oligomerisation of the peptide on the peptide-cellulose association will be discussed in more detail in Chapter 5.

Comparing the fluorescence of all the Trcs concentrations over 270 minutes (Figure 4.2: B; left y-axis), at which point a plateau was reached assuming maximum association, about half (0.5) of the signal remains for 50 µg/mL (approx. 40 µM) and higher. At the lower concentrations the ratio of remaining peptide is 0.6 and 0.8 for 25 µg/mL and 12.5 µg/mL respectively. Comparing the initial binding rates (Figure 4.2: B), calculated from the first 5-11 minutes of association, there is a lower association rate for the two low concentrations followed by a peak

association rate around 50-75 µg/mL, which then slowly decreases with an increase in peptide concentration. As previously mentioned, the decrease in fluorescence can be described with the use of a two-phase exponential decay equation.

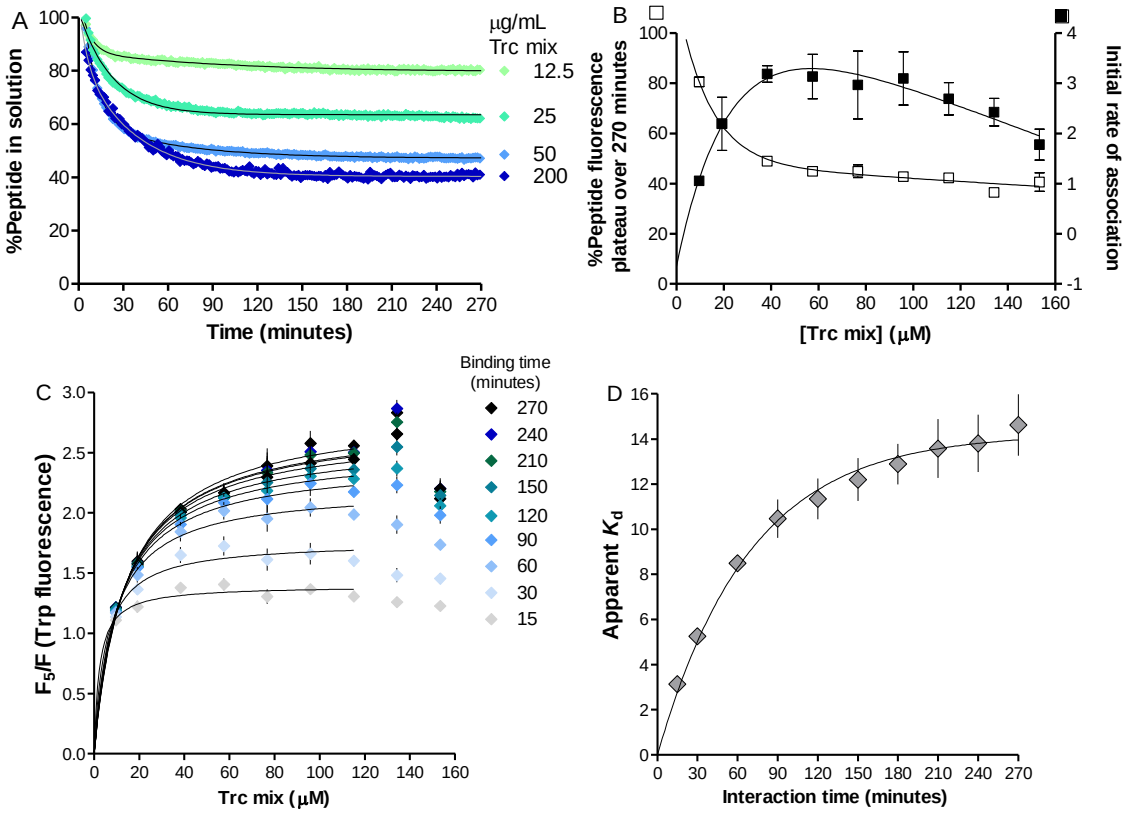

Figure 4.2: Following the binding of Trc mix to cellulose using Trp fluorescence **(A)** Background subtracted peptide fluorescence signal, at Ex_{290} and Ems_{342}, in the presence of cellulose expressed as a function of the fluorescence of peptide alone, the data was fitted two phase exponential decay (R^2>0.99) **(B)** Comparison of florescence at plateau for each concentration with the rate of association determined within the first 5-11 minutes of Trcs to cellulose exposure **(C)** Comparison of hyperbolic binding curves (R^2>0.99) over time and from 9.6-115 µM . Data points were calculated from ratio between initial fluorescence detected for Trcs+cellulose (F_5, average fluorescence for the first 5 minutes) over the fluorescence detected at different time points. **(D)**. The variation of the apparent K_d from the hyperbolic binding curves over time. An exponential curve (R^2 >0.99) was fitted to data to determine K_d plateau. All data represents quadruplicate repeats with standard error of the mean.

Inspection of the fluorescence change at incremental time-points (F_t) in relation to the initial fluorescence over the first 5 minutes (F_5) (Figure 4.2: C) exhibited a similar result as was seen previously. At the two lower concentrations, and two higher concentrations: too low peptide

concentration results in too low aggregation which leads to little association and high concentrations lead to large aggregates that hamper association. At 50 µg/mL (approx. 38 µM) to 115 µM a similar association (ratio) is observed from 15-60 minutes of incubation (Figure 4.2: C).

The smaller changes observed in the ratio between time points from 150-270 minutes, indicated further aromatic stacking or arrangement of Trcs onto the existing layers or nanostructures of peptide. This Trp quenching is more pronounced at the higher concentrations (80-120 µM) which shows that once the initial seeding interaction is associated, the peptide will continue to form larger oligomers on the cellulose until an equilibrium is reached between bound peptide and free peptide. Proposing that full absorption of peptide from the solution will only be observed if the number of possible binding sites are increased for the initial association, as seen with Trc mix and MCC. The apparent dissociation constant (K_d^{app}) between cellulose and Trc mix was found to drift over time. The first 60 minutes has a low K_d^{app} which translates to fast association, which reaches a turning point between 60 and 90 minutes of incubation, and plateauing between 90 and 270 minutes with K_d^{app} =14.2±0.3 µM for the reaction: **Trc-Cellulose** ↔ **Trc+Cellulose** (Figure 4.2: D). However, such an estimation is an oversimplication of a complex set of binding and dissociation reactions with various parameters that would be diffiult to determine.

Further comparison between the fast/initial decay constant (K_{fast}) of the two-phase exponential decays showed no difference between the concentration ranges (results not shown), indicating a simple reaction kinetics. However, comparison between the slow/secondary decay constant (K_{slow}) showed three distinct changes in the decay rate (Figure 4.3) the two low concentrations (12.5 µg/mL and 25 µg/mL), followed by 50 and 75 µg/mL and then the remaining higher concentrations. This indicated complex and dynamic reaction kinetics that are highly sensitive to peptide concentration. As the decay constants describe the percentage change in the fluorescence that would occur within a time range, a high *K*-value would translate to more change and thus faster association, either with other peptide molecules or with both surfaces and other peptide molecules. Considering the changing rate in the more dynamic second phase of association, the remaining peptide in the solution probably dictates the oligomerisation in solution and on the surfaces. From this result the optimal peptide concentration for association was deduced to between 38-60 µM (50-75 µg/mL).

In view of these results and the known aggregation/oligomerisation character of the Trcs (Munyuki et al., 2013; Salgado et al., 2001; Williams et al., 1972) it would suggest that there is an optimal aggregation state or oligomer size for association. Lower concentrations of peptide result in oligomers too small for optimal interaction, whereas higher concentrations lead to large oligomers and hinders optimal association to cellulose. However, the amount of peptide bound (percentage peptide bound) indicates that regardless of the slower association rate at higher concentrations, at least half of the peptide available in solution still binds to the cellulose regardless of concentration by comparing 50 µg/mL to 200 µg/mL of peptide. Thus, the determining factor for the association of Trcs to cellulose in terms of concentration, is a high enough concentration to form optimal size oligomers. It has been reported that dimerization and subsequent higher order oligomer formation is highly dependent on the concentration of peptide (Appleby et al., 1947; Paradies, 1979; Munyuki et al., 2013) which can be reversed with dilution (Williams et al. 1972) supporting the hypothesis that a critical level of aggregation must be achieved to allow for optimal association. The role of peptide oligomerisation will be further explored in Chapter 5.

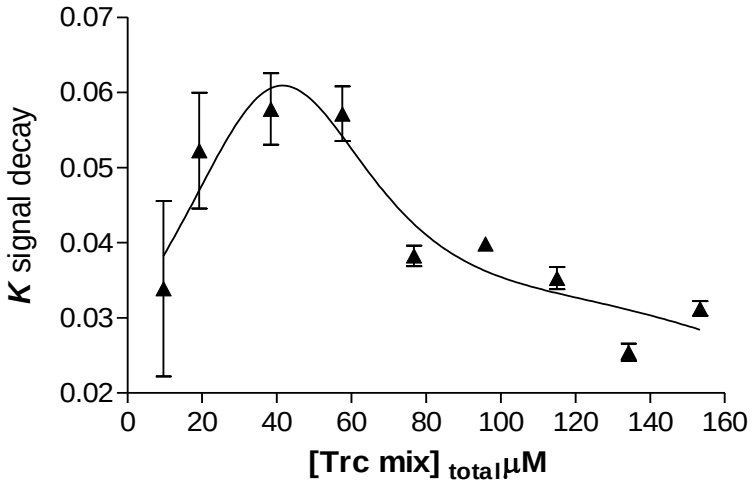

Figure 4.3: Change of the K_{slow} signal decay parameter over the Trc mix concentration range. The K_{slow} parameter for each Trc mix concentration was determined from the data in Figure 4.2 A that were fitted to a two-phase exponential decay of fluorescence signal at Ex_{290}/Ems_{342}. The data points are an average of quadruplicate repeats with SD fitted to a "sum of two Lorentzians" curve.

4.4.2. Trcs association with simple saccharides units from cellulose

Cellulose is a complex structure containing variable amounts of glucose moieties but is also not easily soluble which is needed for most analyses. Therefore, cellulose subunits or building

blocks which are easily soluble were used to probe the Trcs-cellulose interaction. Subunits included glucose, cellobiose (two glucose moieties) and cellotetraose (four glucose moieties) (Figure 4.4). KLU E is hydroxypropyl cellulose and acts as a soluble cellulose model.

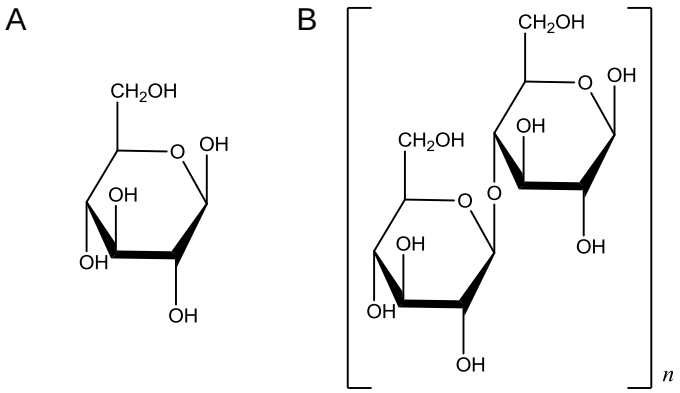

Figure 4.4: Structures of **(A)** glucose **(B)** general template glucose oligomers of two β-glucose molecules linked via a β(1→4) bond. Cellobiose *n* = 1, cellotetrose n = 2, cellulose *n* = *n*. The range of *n* for cellulose is unknown. Hydroxypropyl cellulose (KLU E) has the same structure as cellulose with one or more of the hydroxyl groups being replaced with $-OCH_2CH(OH)CH_3$.

In a dose response experiment with changing amounts of Trc mix with a constant 200 µg/well simple sugars (glucose and cellobiose)(Figure 4.5: A) it was found that though the dose response maintained the overall shape, that the addition of glucose, cellobiose and KLU E decreased the MIC from 1.0 µg/disk to 0.5 µg/disk (Figure 4.5: C&D). Furthermore, the KLU E increased the activity of Trc mix as seen with low amounts of peptide still resulting in inhibition. The presence of both simple sugars and KLU E therefore changed the peptide conformation which increased the overall activity. KLU E does have some inhibitory effect on the growth of *L. monocytogenes*, however, it is not as pronounced as the effect of cellulose. This inhibitory effect was included in the activity calculation. In the same experiment cellulose was incubated with a concentration range of Trc mix to compare the effect of concentration on activity mediated by association. Compared to the peptide control the cellulose treated with 2.0 µg/disk of Trc mix had comparable activity, 1.0 µg/disk showed a decrease in activity from full inhibition to 90% inhibition of *L. monocytogenes* and 0.5 µg/disk showed a decrease in activity from 70% to 20% inhibition (Figure 4.5: C&D). The three concentrations, 2 µg/disk, 1 µg/disk and 0.5 µg/disk, corresponds to 20 µg/mL, 10 µg/mL and 5 µg/mL incubation concentrations, respectively. We found that a decrease in Trc mix concentration resulted in

lower total association and association rates (previously discussed). Therefore, the difference in activity between the Trc mix-cellulose and Trc mix alone, especially at 0.5 µg/disk, can be attributed to the fact that only half the peptide associated than what was available.

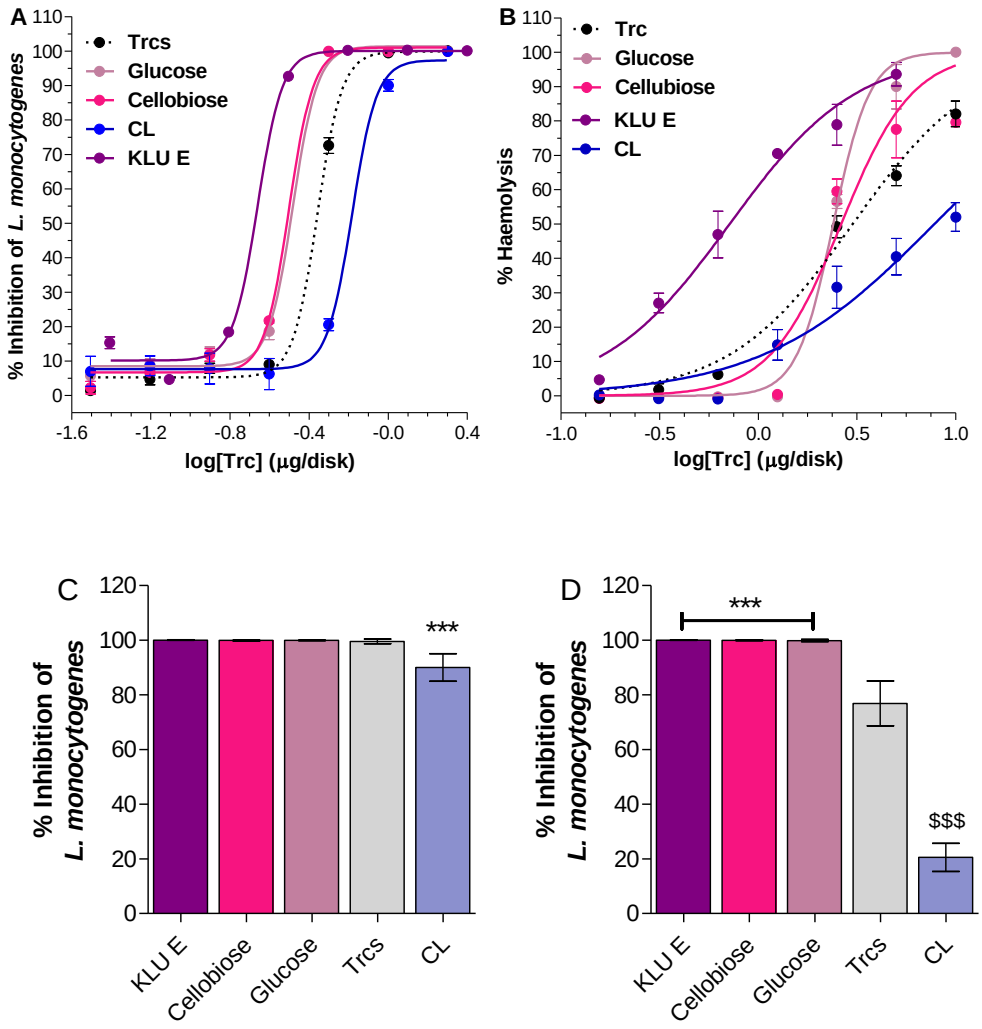

Figure 4.5: Dose-response against **(A)** *L. monocytogenes* and **(B)** red blood cells in the presence of simple sugars (glucose, cellobiose), modified cellulose (KLU E) and cellulose. The activity, expressed as percentage inhibition of *L. monocytogenes* or % haemolysis, of Trc mix was done in combination with 200 µg glucose, 200 µg cellobiose, 200 µg KLU-E and cellulose disks dried in each well before analysis. Each data point is the mean and standard error of the mean of 3-9 repeats. Percentage inhibition against *L. monocytogenes* for cellulose and cellulose models at **(C)** 1.0 µg Trcs/cm^2 and **(D)** 0.5 µg Trcs/cm^2. Data represents error of the mean of 6-9 repeats. Statistical analysis was performed with One-way Anova (Bonferroni's multiple comparison test) ***/$^{\$\$\$}$P<0.0001 to Trcs as control

In a similar experiment against red blood cells (Figure 4.5:B) it was observed that Trc mix and Trc mix-treated cellulose had a similar slope shape, however, the peptide-cellulose had a lower

haemolytic activity corresponding to the lower amount of peptide present. In contrast the slope shape for Trc mix and glucose/cellobiose changed, pointing to a change mode of activity and possibly conformation. Furthermore, the addition of glucose at the highest amount of peptide (10.0 µg) resulted in a higher haemolytic activity than that of the peptide control but completely removed the activity at lower peptide concentrations. KLU E had a similar activity slope shape to Trc mix but was much more haemolytic which could be due KLU E stabilising toxic aggregates or conformations. This change in conformation could be linked to the increased activity against *L. monocytogenes*. From this result it is clear that simple moieties from cellulose also can interact with the peptides in Trc mix and that it is not only a polymeric surface interaction. We therefore studied the interaction of these soluble saccharides with the Trcs using CD, NMR and fluorescence to elucidate some of the molecular interactions.

Collaborative research with the group of Prof. Burkhard Bechinger at Strassbourg University studied a simpler model of the interaction between glucose and a pure peptide from Trc mix namely TrcA utilising liquid NMR and CD (Juhl et al., 2019). As this NMR study focussed on specific interactions between the Trcs and glucose, the use of Trc mix would complicate analysis, since the difference in variable residues possibly influences the interactions. Therefore purified Trc A from Trc mix was chosen as a model peptide representing all the tyrocidines.

In 30% ACN, the CD spectrum of Trc A with the addition of glucose (Figure 4.6: A) was most influenced at 197 nm and 188 nm, which is the pi→pi* interactions of the p-electrons of C=O (Juhl et al., 2019). This indicates the involvement of glucose in hydrogen bonding, due to the changes in hydrogen-bonded structures. There are two types of hydrogen-bonds found within the Trcs structure: intramolecular bonds to stabilize the β-sheet structure (Beyer et al., 1974; Gibbons et al., 1975; Kuo and Gibbons, 1980) and those needed for sideways stacking to form higher order oligomers (Munyuki et al., 2013). However, it was observed with NMR analysis that only amino acids where the amide hydrogens are exposed to the solvent (Loll et al., 2014; Munyuki et al., 2013) were affected by the addition of glucose (Juhl et al., 2019). D-Phe^{4} and Orn^{9} were the most affected, followed by D-Phe^{1}, Val^{8}, Asn^{5} and Tyr^{7}, with Phe^{3} and Leu^{10} remaining unaffected. Therefore, the observed interaction of glucose with the hydrogen-bonded structures is possibly related to interference of the stacking of the peptide. The dissociation constant calculated from the CD and NMR data reported K_d=263 µM and K_d=215 µM repectively based on a one-site binding model fit (Juhl et al., 2019). The NMR

analysis of Trc A in the presence of cellotetraose gave a K_d= 50 µM supporting the model of four available binding sites due to four glucose units (Juhl et al., 2019).

The CD spectra of Trcs cannot be compared with those of proteins and peptides with natural L-amino acids, because these cyclic decapeptides contain two D-amino acids, that influence the detected ellipticity. However, secondary structures within the peptide namely β-turns and β-sheets can be still be detected at 206 nm and 216 nm, respectively (Laiken et al., 1969) with the ratio of $\theta_{206}/\theta_{216}$ being a measure of a change in conformation (Spathelf, 2010; Vosloo, 2016). Is was observed that the increased glucose concentration gradually decreased the observed conformation stabilising around 0.25-1.0 mM (Figure 4.6: B). Furthermore, upon inspection of the percentage change of θ_{206} over the percentage change over θ_{216} (Figure 4.6: C) in comparison with Trc A without gluocse it was observed that θ_{216} was affected the most at the low concentrations of glucose. Therefore, the β-sheet structure may be more affected by the addition of glucose, indicating an influence on hydrogen bonds (H-bonds) correlating with our NMR studies (Juhl et al., 2019).

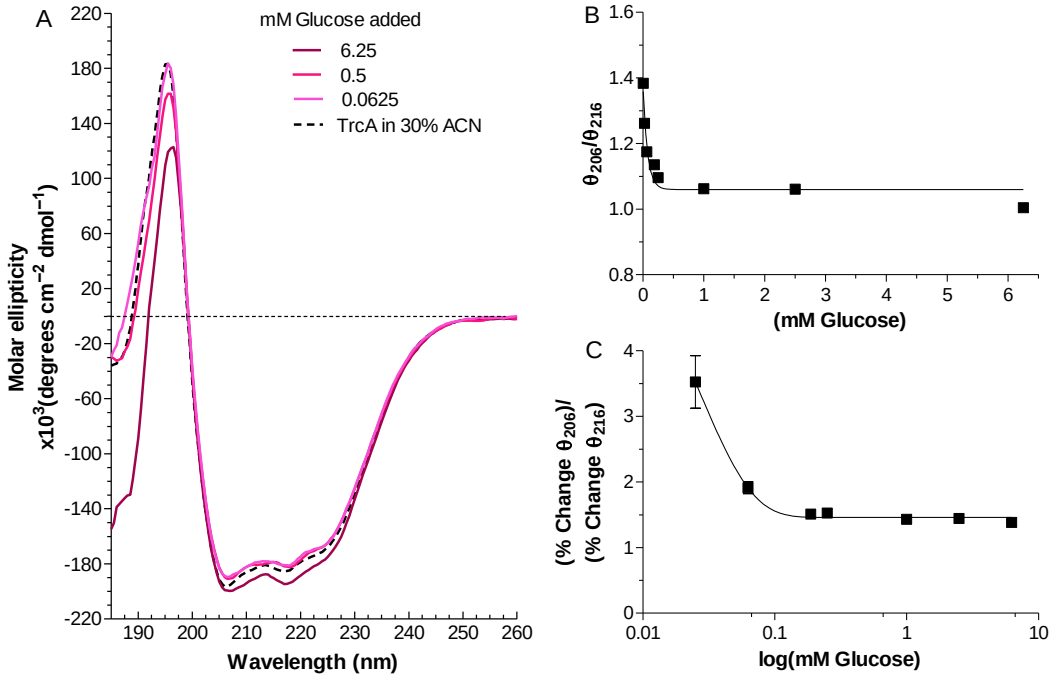

Figure 4.6: **(A)** CD spectra depicting the influence of glucose (0.06, 0.5 and 6.25 mM) on the overall ellipticity of 250µM Trc A in 30% acetonitrile (ACN). Each spectrum represents six background corrected repeats with smoothing performed over six neighbours. **(B)** Ratio between $\theta_{206}/\theta_{216}$ and **(C)** The ratio in percentage change of $\theta_{206}/\theta_{216}$. The x-axis is depicted in log scale to ease observations at the lower concentrations of glucose.

As discussed above, it is evident from the results that simple sugars bind to the Trcs and that they do positively affect the peptide activity, which begged the question of whether glucose (cellulose 'monomer') and cellobiose (cellulose 'disaccharide') could outcompete peptide association to cellulose. To challenge the interactions, we included the sugars with cellulose in our assessments. Trc mix (50.0 µg/mL) was incubated with increasing amounts of mol:mol ratio of glucose or cellobiose for one hour to ensure association. The peptide:sugar mixture was then transferred to cellulose and the change in fluorescence observed.

Binding curves for each of the ratios between Trcs and glucose/cellobiose were obtained (data not shown) and the fluorescence decay calculated for each. The summary of the time constants (K) (Figure 4.7:A) showed a 'tipping' point at 2:1 and 4:1 mol:mol ratio for cellobiose and glucose respectively. This correlates to what has been found with circular dichroism and nuclear magnetic resonance studies that the peptide associates in a of 4:1 and 1:1 association for glucose and cellotetraose respectively (Juhl et al., 2019). The large error bars observed can possibly be attributed to the peptide in solvent being a dynamic system that orders and re-orders based on the environment (Thies and Paradies, 1997).

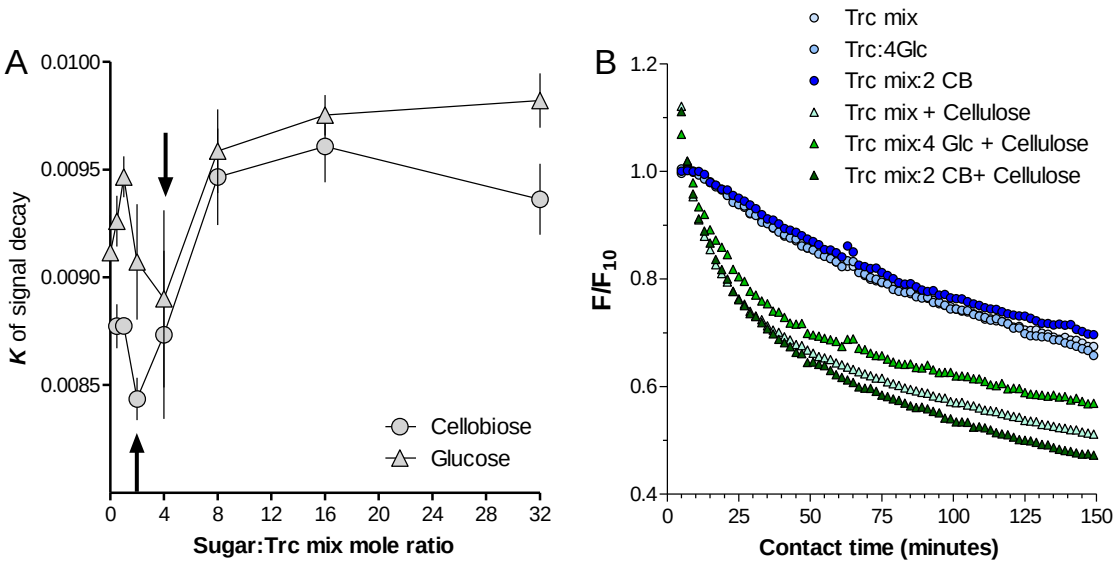

Figure 4.7: **(A)** K-value for the one phase decay fits of the fluorescence decrease over time for Trc mix (50 µg/mL) with increasing amounts of peptide:sugar mol ratio with glucose and cellobiose. The 'tipping' point is highlighted with an arrow **(B)** Fluorescence at set time point (F) in terms of the initial fluorescence (F_{10}) for Trc mix, sugars and the effected association over time. Data points are the mean of 4 determinations with standard error of the mean showed in A.

The full fluorescence-detected binding curves of Trc mix with glucose and cellobiose at a 4:1 and 2:1 showed (Figure 4.7: B) the glucose having minimal influence on the fluorescence decay, whereas the cellobiose showed a slightly slower decay. Trc mix association with cellulose was slowed down in the presence of glucose but seem to be higher in the presence of cellobiose. This could be that cellobiose interacts in the same way as cellulose with the peptides in Trc mix leading to quenching.

When antimicrobial activity against *L. monocytogenes* on the treated cellulose was assessed, the sugars had little effect, except at very high cellobiose concentrations (Figure 4.8: A&B). This maintenance of antimicrobial activity of cellulose treated with Trc mix, in the presence of glucose and cellobiose, does not correlate to the results observed with the fluorescence. This indicated that the peptide interaction with cellulose leading to the availability of active peptide moieties does not directly involve the aromatic amino acids, but rather secondary conformational changes that affect the aromatic amino acids. The ability of cellobiose to influence the Trc mix-cellulose interaction at higher cellobiose concentrations, point to cellobiose being a better model molecule than glucose to cellulose to study the Trc-mix-cellulose interaction. This can also be extended to cellotetrose and other soluble cellulose derivates.

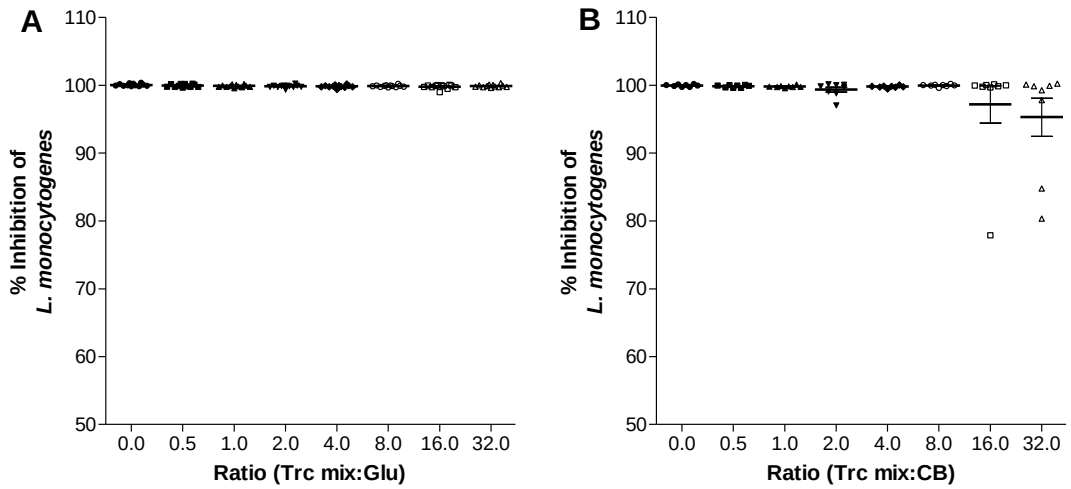

Figure 4.8: Antimicrobial activity of Trc mix treated cellulose in the presence of increasing amounts of peptide:sugar mol ratio of **(A)** glucose and **(B)** cellobiose. The data represents the mean and standard deviation of four technical repeats with three biological repeats for glucose and two biological repeats for cellobiose

4.4.3 Molecular descriptors of Trc-saccharide interaction

The analysis of Trc in the presence of sugars and cellulose performed with fluorescence, UV, NMR and CD were done in solution, which supports a dynamic interaction system. The aggregation, oligomerisation and peptide interactions with the environment/sugar molecules are dynamic and could order and rearange over time (Thies and Paradies, 1997). Therefore, ATR-FTIR of dried samples was used as a 'snap-shot' of the interaction between Trc mix and sugars (glucose, cellobiose and KLU E). KLU E is a commercial hydroxypropyl cellulose and acts as a soluble cellulose model. ATR mode of FTIR was utilised since is allows for the surface analysis of samples and therefore the samples could be dried limiting any residual solvent effect. FTIR spectra are electromagnetic absoption spectra that measure the movement/vibration in molecules. Movement in certain molecules can be grouped together e.g. C=O at 1700-1800 cm^{-1} creating a fingerprint that can be identified. Changes in interaction and bonds with these groups would constrain the movement decreasing the observed band intensity (Barth, 2000; Krimm, 1983). The full ATR-FTIR spectra of Trc mix with glucose (Figure 4.9: A), cellobiose (Figure 4.9:B) and KLUE (Figure 4.9: C) show the three main absorption regions: amide A&B, amide I&II and a C-O bond regions. Amide I&II only shows the effect of the interaction on the peptide, whereas the C-O region shows the interaction with the sugar. The amideA&B is a very complex region, shows the N-H streching and is very sensitive to the strength of the H-bonds (Kong and Yu, 2007). Comparing this region among the three saccharide samples, it is clear that glucose influences the H-bonding between N-H groups within the peptide. This correlates to the increased CD spectral intensity around 197 nm and 188 nm observed with the addition of glucose.

The second region observed (amide I&II) is ideal to study the effect of the sugar on the peptide since no overlapping signal with the respective sugars are involved. The absorption spectra (Figure 4.10: A) shows the amide I band to be around 1700-1600 cm^{-1} (Kong and Yu, 2007; Surewicz and Mantsch, 1988; Susi and Byler, 1983). It depends on the hydrogen bonding which is influenced by backbone conformation associated with the C=O stretching vibration, and C-N bonds (Kong and Yu, 2007; Surewicz and Mantsch, 1988; Susi and Byler, 1983). It is used to determine secondary structures of peptides and proteins (Kong and Yu, 2007; Surewicz and Mantsch, 1988; Susi and Byler, 1983). The second region, amide II, is around 1480 and 1580 cm^{-1} and detects N-H bending, C-N and C-C stretching (Kong and Yu, 2007). However is it much more complex than Amide I because of the overlaps in peaks and therefore great care must be taken when assigning peaks (Kong and Yu, 2007).

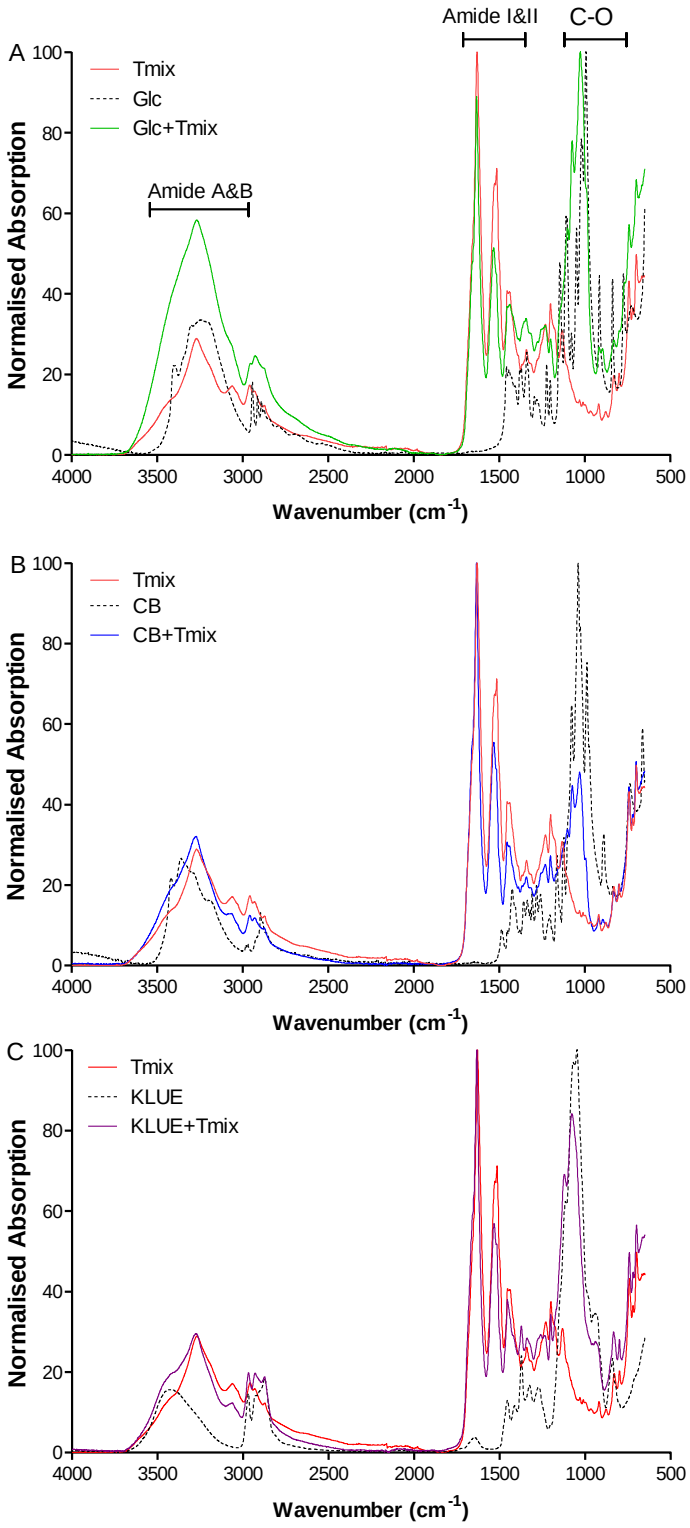

Figure 4.9: Full FITR spectra for from 4000 cm^{-1} – 650 cm^{-1} of Trc mix, sugar and Trc mix-sugar combined observed for **(A)** glucose **(B)** cellobiose and **(C)** KLU E. The Main regions of interest are annotated on the (A) glucose spectra: Amide A&B, Amide I&II and the far UV C-O regions.

The FTIR absorption spectra have very low resolution, however, 2nd derivative analysis of the spectra can be used to improve resolution and identify bands that occur within one band (Kong and Yu, 2007; Owen, 1995; Susi and Byler, 1983). The 2nd derivative analysis is used for increased sentivitiy though this makes the analysis more complex since the amount of bands visible is given by the degree of derivatisation plus one (Kong and Yu, 2007; Owen, 1995; Susi and Byler, 1983). The 2nd derivative analyis of amide I and amide II regions (Figure 4.10: B&C) shows clear valleys that are to be assigned . A further complication with our FTIR analysis was the use of a mixture of peptides in Trc mix in the ATR-FTIR analysis. However, it is assumed that the backbone structure remains constant and that at least 7/10 amino acids in the major group, the tyrocidines, are identical. The mole contribution of each amino acid to the Trc mix are given in Table 4.1. It is also compared to that of the analogous peptide gramicidin S (GS), which were used as model to assign some of FTIR bands.

Table 4.1: Molar contribution of the amino acid residues to tyrocidine mixture (as calculated from percentage abundance of each Trcs analogue) in comparison with GS

Type of residue	Amino acid	Trc mix	GS
Aliphatic	Val	1	2
	Leu	1	2
	Pro	1	2
Aromatic	Phe	2	2
	Tyr	0.9	0
	Trp	1.1	0
Cationic/Basic	Orn	0.5	2
	Lys	0.5	0
Acid amide	Asn	1	0
	Gln	1	0

The summary of the assignments can be found in Table 4.2 and 4.3 with possible assignments made from literature (Krimm, 1983; Naik et al., 1984; Venyaminov and Kalnin, 1990) and using a comparison with GS as guide for the assignment of amino acids in the VOLfP peptide moiety, β-sheets and β-turns. The detailed assignments, particularly of amino acids in the variable pentapeptide moiety, are therefore only suggestive. One thing to note is that FTIR cannot fully distinguish between parallel and antiparallel β-sheets (Buchet et al., 1996; Surewicz and Mantsch, 1988). However, antiparallel β-sheets have a strong band near 1630 cm^{-1} with a secondary weaker band at 1685 cm^{-1}, whereas parallel β-sheets have their main

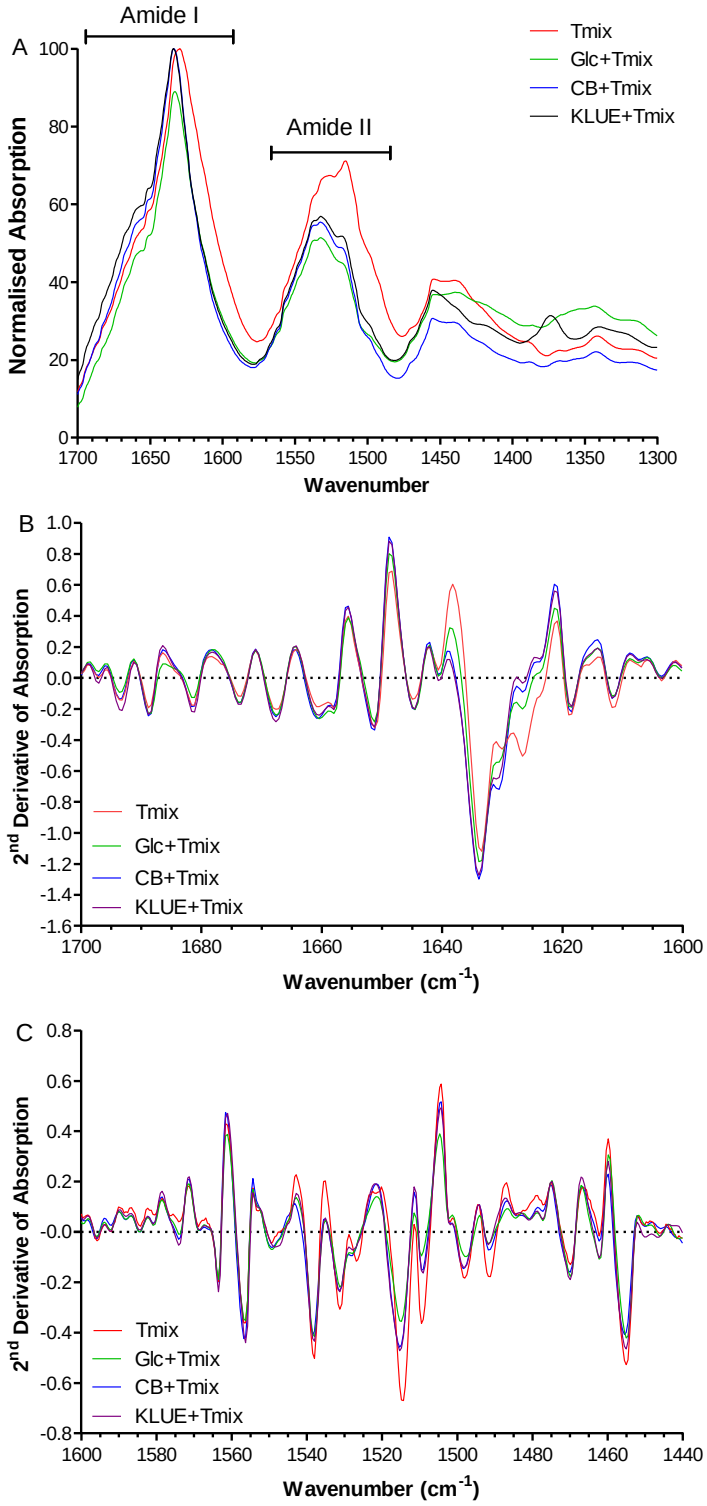

Figure 4.10: ATR-FTIR of the peptide specific regions. **(A)** Normalised spectra of Trc mix, and sugars (glucose/cellobiose and KLU E) indicating the Amide I and Amide II peaks. 2nd derivative spectra of the **(B)** amide I and **(C)** amide II FTIR regions.

absorption at higher wavenumbers than antiparallel β -sheets (Barth, 2007). The difference in the two can be as little as 4 cm^{-1} (Chitnumsub et al., 1999). The peptides in Trc mix possibly form three different types of β-sheets (Table 4.2): antiparallel intrapeptide, antiparallel interpeptide and parallel interpeptide β-sheets. Each of the detected structures have an amide I and amide II band corresponding to C=O stretching and N-H bending respectively. It is expected that there should be two types of β-turns with two peaks in amide I and two peaks in amide II. The peak assignments that correlate with the GS model is type II' β-turns, with the remaining β-turn assignments, that of β-turn type I, both correlating with the Trc A and Trc C models of Munyuki et al.(2013).

Table 4.2 ATR-FTIR analysis of Trc secondary structures in comparison with gramicidin S (GS) and change in absorption in the presence of selected saccharides. The data in bold font highlights the correlation with the FTIR done on the analogous GS by Naik et al. (1984). The change in absorption is indicated with a heat map with blue showing a decrease in absorption and red an increase in absorption.

Predicted Secondary structure	IR	Wavenumber (cm^{-1})			Change in absorption [c]		
	Group	Model [a]	GS[b]	Trc	Glc	CB	KLU E
β -sheet	Stretching C=O (amide I)	**1701**	**1700**	**1705**	-0.36	-0.08	0.26
		1695	**1700**	**1697**	-0.32	-0.04	0.28
		1694		1693	-0.26	-0.01	0.28
	Bending N-H (amide II)	1534		1538	-0.18	-0.12	-0.10
		1534	**1532**	**1532**	-0.22	-0.16	-0.14
		1523		1527	-0.27	-0.21	-0.19
β-turn	Stretching C=O (amide I)	**1656**	**1655**	**1652**	-0.10	0.05	0.11
		1640	**1643**	**1640**	-0.06	0.10	0.12
		1630		1630	-0.14	-0.06	-0.06
		1631/2		1634	-0.08	0.04	0.04
	Bending N-H (amide II)	**1559**	**1563**	**1563**	-0.16	-0.14	-0.11
		1559		1556	-0.15	-0.10	-0.08
		1546/1547	**1546**	**1548**	-0.15	-0.09	-0.07
		1575		1574	-0.20	-0.23	-0.19

[a] Krimm et al. (1983); [b]Naik et al. (1984), data shown in bold,
[c] Fractional change in IR absorption from the free peptide alone to a 1:1 mixture with saccharide

Inspection of the change in absorption due to the peptide interaction with saccharides showed decrease in absorption for glucose which can be attributed to glucose competing for the hydrogen-bonds in the β-sheets and having a chaotropic effect on oligomerization. This is contradictory to the solution interaction of Trc A and glucose which suggested from the CD analysis that glucose increased peptide hydrogen-bonded interactions, particularly β-sheets. This could be due to the difference between "dry interactions" and interaction in an aqueous environment. Although FTIR could have been performed in an aqueous environment to better

correlate with other experiments in solution, the use of ATR-FTIR was used to provide a better understanding of the peptide-cellulose interaction on a dry material and to limit variability due to the dynamic nature of Trcs in solvent systems. In solution the glucose hydroxyl groups would interact with water, effectively lowering the number free water molecules that can compete with peptide H-bonds. Cellobiose had a limited influence, whereas KLU E possibly supports β-sheets into certain conformations as C=O stretching were more pronounced. This could be due to the propyl groups in KLU E interacting with aliphatic amino acids constraining the arrangement of the interpeptide β-sheets. This corroborates the change in activity, especially the haemolysis, due to possible conformational changes observed in the presence of KLU E in comparison to glucose and cellobiose. The β-turns were minimally influenced, most probably due to the rigidity of the decapeptide ring structure. This corroborated the results from CD analysis, where the addition of glucose had less influence on the β-turns.

The three saccharides had a similar influence on the aromatic amino acid side chains except for the Tyr hydroxyl group. The decrease in absorption could be due to chaotropic disruption of aromatic stacking by direct dipole-induced dipole interactions (Trp and Phe rings) and dipole-dipole interaction (Tyr ring). The possible influence on Orn increases with the increase in saccharide size. The influence on Phe and Orn^{9} is corroborated by our NMR analysis with glucose which showed that D-Phe^{4} and Orn^{9} side chains were affected the most (Juhl et al., 2019). This correlates to the increase in activity observed as D-Phe^{4} and Orn^{9} are in the same plane of the peptide active structure (Beyer et al., 1974; Gibbons et al., 1975) and both are key factors in the activity of Trcs (Danders et al., 1982; Rautenbach et al., 2007; Spathelf and Rautenbach, 2009). The presence of saccharides could therefore change the peptide conformation to increase the activity. Assignments of Lys^{9} bands are uncertain due to overlapping IR bands, therefore the influence of the saccharides on Lys^{9} could not be determined, but it can be assumed that it would be in line of that of Orn^{9}. Both glucose and KLU E appear to have a similar influence on the aliphatic amino acids Val^{8}, Leu^{10} and Pro^{2}. This influence could possibly be ascribed to effect of glucose and KLU E decreasing interaction with water before drying whereas cellobiose might have a slight chaotropic effect on hydrophobic driven oligomerisation. NMR studies showed that the amide group of Val^{8} was affected, while this group of Leu^{10} was not affected (Juhl et al., 2019). Pro^{2} amide cannot be detected with ^{1}H-NMR due to the absence of the Pro amide hydrogen.

Table 4.3 ATR-FTIR analysis of amino acids found in the peptides in Trc mix in comparison with GS and change in absorption presence of selected saccharides. The amino acids and data in bold font highlight the correlation with the FTIR done on the analogous GS by Naik et al. (1984). The change in absorption is indicated with a heat map with blue showing a decrease in absorption and red an increase in absorption. Assignments in corresponding colour fonts and italics are uncertain because of overlapping bands. (na, not applicable; –, no data)

Amino acid residue side chain	IR assignment	Wavenumber (cm^{-1})			Change in absorption [d]		
		Model [a]; Literature [b,c]	GS[a]	Trc mix	Glc	CB	KLU E
Asn	Bending NH_2	1612-1622	na	1612	-0.31	-0.34	-0.32
		1626-1629		*1626*	-0.15	-0.08	-0.09
	Stretching C=O	1677-1678	na	*1674*	-0.13	0.07	0.22
Gln	Bending NH_2	1586-1610	na	*1596*	-0.32	-0.38	-0.34
	Stretching C=O	1668-1687	na	1689	-0.20	0.02	0.26
				1681	-0.18	0.03	0.24
Pro	Bending CH_2	1447-1472	-	1470	-0.13	-0.31	-0.11
	Stretching C-N	1435-1465	-	1455	-0.10	-0.25	-0.07
	Bending C-H	**1387**	-	*1388*	0.18	-0.20	0.04
Leu	Stretch, asym CH_3	1445, **1451**	**1451**	**1439**	-0.07	-0.27	-0.17
	Bending C-H	**1395**	**1390**	*1388*	0.18	-0.20	0.04
		1370	**1369**	**1370**	0.39	-0.12	0.37
		1345	***1342***	***1341***	0.29	-0.16	0.09
		1310	**1314**	**1313**	0.33	-0.15	0.11
Val	Bending C-H	**1336-1342**	***1342***	***1341***	0.29	-0.16	0.09
Lys	Bending sym NH_3^+	1526	na	*1532*	-0.22	-0.16	-0.14
	Bending asym NH_3^+	1626		*1624*	-0.22	-0.20	-0.20
Orn	Bending NH_3^+	**1672, 1673**	-	*1674*	-0.13	0.07	0.22
		1667	-	1668	-0.10	0.08	0.19
		1660	-	1661	-0.09	0.07	0.14
		1659	***1655***	**1658**	-0.09	0.06	0.13
		1647	***1643***	**1645**	-0.07	0.09	0.12
Phe	Stretching C-C ring	1602	-	1603	-0.33	-0.38	-0.34
		1585	-	1585	-0.27	-0.33	-0.30
		1494	-	1492	-0.42	-0.48	-0.39
Trp	Stretching C-C rings Bending C-H	1487-1496	na	1498	-0.44	-0.46	-0.39
	Bending N-H, C-H, C-N	1509	na	1509	-0.44	-0.41	-0.36
Tyr	Stretching C-C Bending C-H	1616-1621	na	1619	-0.27	-0.28	-0.27
	Stretching C-C ring	1594-1602	na	*1596*	-0.32	-0.38	-0.34
	Vibration C-C ring Bending C-H	1516-1518	na	1515	-0.38	-0.33	-0.29
	Stretching C-OH	1169-1260	na	1172	-0.35	-0.26	0.16

[a] Naik et al. (1984), data shown in bold, [b] Venyaminov & Kalin (1990); [c] Barth (2007), [d] Fractional change in IR absorption from the free peptide alone to a 1:1 mixture with saccharide

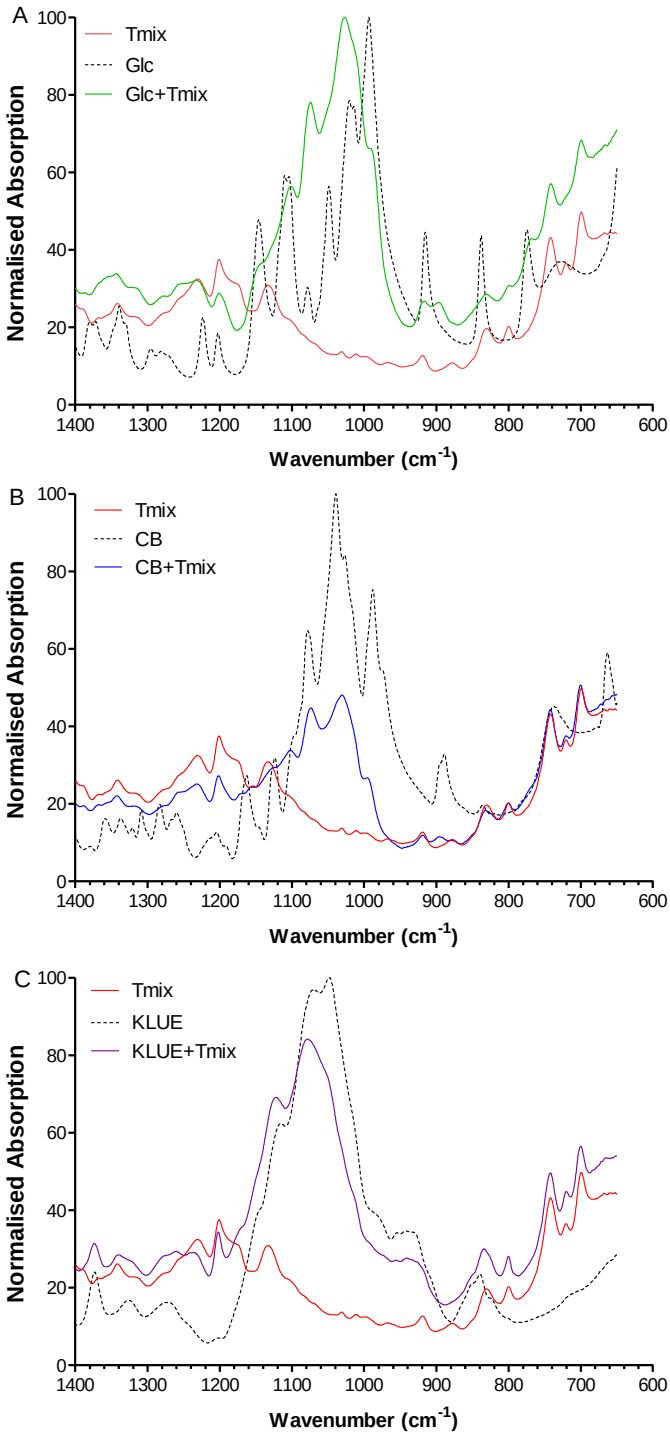

Figure 4.11: FTIR spectra of the C-O region from wavenumbers 1100 – 900cm^{-1}, indicating the saccharide contribution in the FTIR spectra.

The three saccharides had a similar effect on the amino group in the acid amide side chain of Asn^{5} and Gln^{6} (uncertainty due to band overlap in latter), possibly forming hydrogen bonds with the amino groups. The effect of glucose on Asn^{5} and Gln^{6} was reported with the NMR

studies in which that of Asn^5 was correlated to solvent exposure. Similarly, the side chain of Gln^6 is also exposed to the solvent environment (Kuo and Gibbons, 1980). The influence on the C=O stretching in the amide side chain of both amino may be dependent on the size of the saccharide with glucose being more chaotropic that the other saccharides.

The last region between 1100-900 cm^{-1} is associated with C-O stretching and was very prominent in spectra of the three saccharides (Figure 4.11). The spectra of all three saccharides are influenced by either a decrease in signal or shifting proposing that the primary groups of interaction between peptides and cellulose/saccharides are the hydroxyl groups.

To further study the molecular interaction of the Trcs with cellulose we utilised solid state nuclear magnetic resonance spectroscopy (SS-NMR). For this we produced (^{13}C,^{15}N)-labelled Trcs in culture and purified the labelled TrcA (Supplementary data). The work done regarding the SS-NMR study of Trcs-cellulose interaction was completed in collaboration with Prof. Burkhard Bechinger at the University of Strasbourg. Parameters regarding Trcs association to cellulose were determined with Trc mix and microcrystalline cellulose (MCC) (refer to Figure 4.1). MMC was used since it was better suited to the solid surface NMR experimental setup compared to cellulose paper. The results discussed above showed that the cellulose can be saturated with TrcA at high cellulose:peptide ratios and that cellulose can remove almost all peptide from a solution at the right ratio (Figure 4.1). Based on the binding assay, a sample of 1:100 TrcA:cellulose (*m/m*) was prepared for structural characterization of uniformly (^{13}C,^{15}N)-labelled TrcA bound to MCC. As the cellulose used in this study is microcrystalline, the molar ratio between cellulose and TrcA could only be estimated as 1:45 (assuming that MMC contains one reducing end per 18 residues of glucose moieties).

The sample was firstly subjected to fast magic angle spin (MAS) solid-state NMR. The ^{13}C CP spectrum recorded at 17.6 Tesla with a MAS spinning speed of 60 kHz was predominantly showing the natural abundance resonances of the cellulose, but a few signals from aromatic carbons of TrcA were observed (not shown). These signals were more pronounced in a 2D ^{1}H-^{13}C CP-HSQC experiment due to the better resolution (data not shown).

The TrcA coated MCC was subjected to surface dynamic nuclear polarization (DNP) solid-state NMR spectroscopy (Lesage et al., 2010), a technique where transfer of polarization from unpaired electron spins to the NMR nuclei enhance the signal intensities for use in structural studies. Signals of nuclei that are in close proximity to the biradicals, added to the glass-forming solvent, are specifically enhanced. Thus, using this technique a better enhancement of

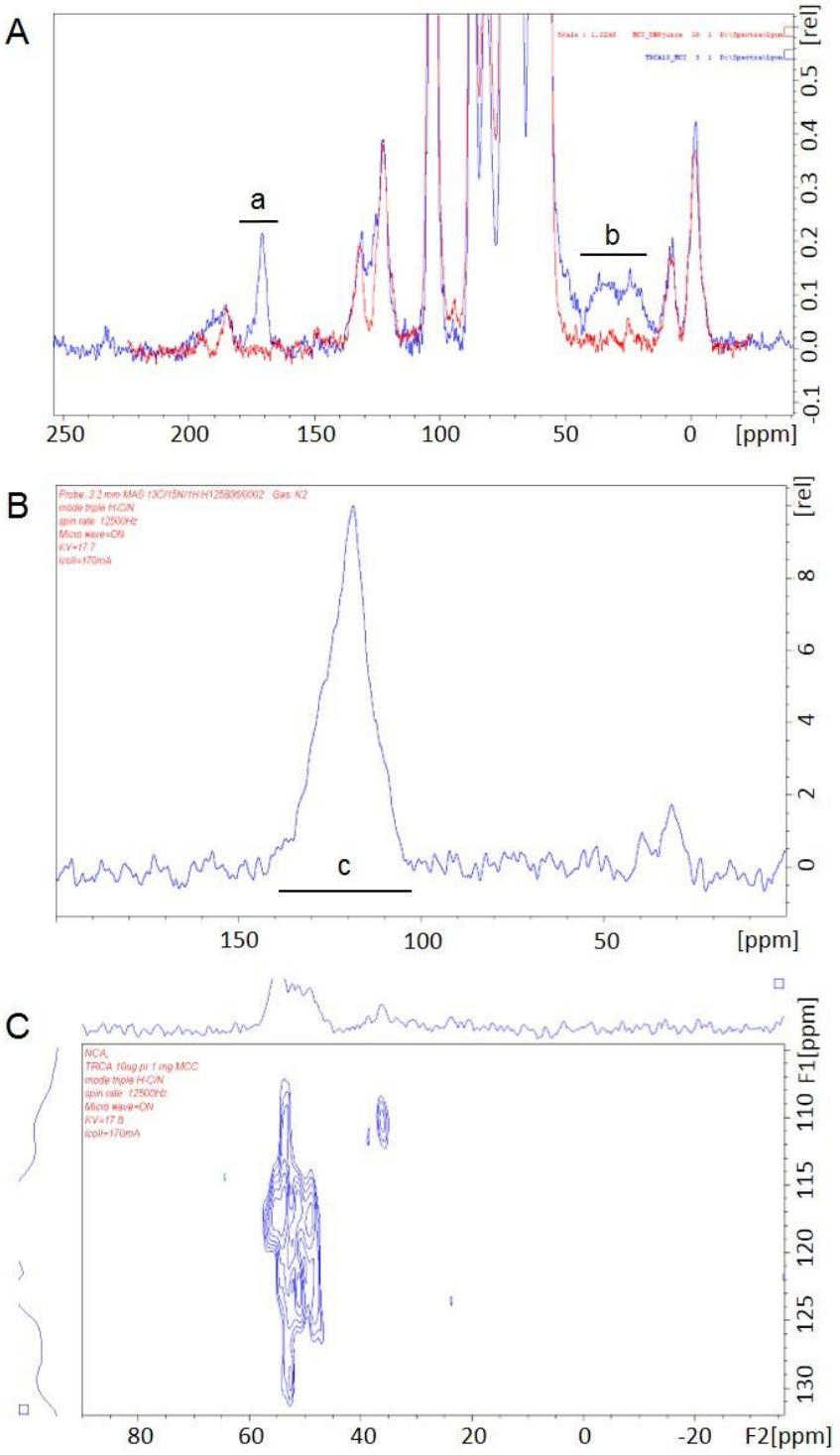

Figure 4.12: **(A)** Proton-decoupled ^{13}C solid state NMR/DNP spectra of 10 mg microcristalline cellulose before (red) and after (blue) incubation with 200 µg of uniformly (^{13}C,^{15}N)-labelled TrcA with (a) carbonyl and (b) aliphatic groups **(B)** ^{15}N spectra of the same sample with (c) amide nitrogens. **(C)** A two-dimensional NCA correlation spectrum. The sample was dispersed in glycerol-d8/D_2O/H_2O 60/30/10 (*v/v/v*) in the absence or in the presence of 15 mM AMUPOL and the spectra recorded at 99K under MAS at 12.5 kHz.

the surface-associated peptide is obtained compared to the bulk of the cellulose. The enhancement factor of the 200 MHz ^{13}C spectrum is about 30-fold and reveals several ^{13}C resonances originating from TrcA in the aliphatic (40-10 ppm) and carbonyl regions (180-165 ppm) (Figure 4.12: A). The one-dimensional ^{15}N spectrum shows a largely unresolved intensity of the amide nitrogens (Figure 4.12: B) at 105-140 ppm, which were slightly better resolved in a two-dimensional NCA (intra-molecule) experiment (Figure 4.12: C).

This is the first reported data indicating that enough peptide can be associated with cellulose to allow for further investigation of the peptide by solid-state NMR spectroscopy. However, analysis of peptide-cellulose interaction would still be complex due to the low resolution caused by the low concentration associated to the cellulose. An increase in peptide concentration at the incubation step would not resolve this issue, since it would result in more peptide-peptide interactions (due to stacking) and would overshadow the peptide-cellulose interaction. As a result, research is currently limited to fluorescence, FTIR and NMR with soluble cellulose derivatives to further elucidate the peptide-cellulose interaction.

4.5 Conclusions

Tyrocidines adsorb to cellulose in a concentration dependent manner in two-phases: a fast, initial association followed by a slower association, with the latter possibly involving stacking and oligomerisation. The primary focus of this chapter was on the initial/seeding step mediated by the interaction between the peptide and cellulose. The role of peptide conformation and oligomerisation for association will be discussed in Chapter 5. Activity studies on Trc mix and sugars (glucose, cellobiose and cellulose) showed that both glucose and cellobiose increased the activity against *L. monocytogenes* and the addition of glucose made the peptide much more haemolytic in comparison with cellobiose and cellulose. The glucose possibly influences peptide aggregates/oligomers in a manner that both favours antimicrobial activity and haemolysis. This increase in both antimicrobial activity and haemolysis was observed to a greater extent for KLU E, especially an increase in haemolysis which points to the stabilization of toxic Trcs oligomers by KLU E. Investigation of the ability of glucose and cellobiose to inhibit the association of Trcs to cellulose showed that glucose and cellobiose interacts with Trcs in a 4:1 and 2:1 mol:mol ratio confirming the results observed with NMR. However, glucose could not hamper Trcs association and activity to cellulose whereas cellobiose could to some degree at high mol:mol ratios. This indicates that cellobiose interacts with the peptides in Trc mix in the same way as cellulose leading to competitive binding. From this it is proposed

that further studies should be done with cellobiose or cellotetrose as either one may be a better model to cellulose than glucose. Analysis of the interaction between (^{13}C,^{15}N)-labelled Trc A and MCC with dynamic nuclear polarization (DNP) solid-state NMR spectroscopy, showed that the cellulose associated peptide could be detected.

Inspection of the effect of glucose on Trc A with CD, showed that the β-sheets are most influenced compared to the β-turns. FTIR, however, showed glucose had a different effect on the β-sheets compared to cellobiose and KLU E. This confirms that glucose may not be the best model unit to study the peptide:cellulose interaction. Furthermore, the glucose caused disruption of the hydrogen bonded structures in dry samples, but supported it in aqueous samples, indicating the major role of environment on the interaction and peptide conformation. This, however, supports the hypothesis that the addition of glucose influences oligomerisation since the Trcs have been reported to form hydrogen bonds in side-way stacking (Munyuki et al., 2013). This chaotropic effect of glucose was further supported with the increase in signal intensity in the AmideA&B regions in the FTIR analysis. KLU E had a marked influence on the C=O of the β-sheets which supports conformational changes that resulted in the increased activity and haemolytic activity.

It was found with NMR analysis that only amino acids where the amide protons are exposed to the solvent (Loll et al., 2014; Munyuki et al., 2013) were affected by the addition of glucose. (Juhl et al., 2019). The amides of D-Phe^{4} and Orn^{9} was the most affected, followed by D-Phe^{1}, Val^{8}, Asn^{5} and Tyr^{7}, with Phe^{3} and Leu^{10} remained unaffected. FTIR confirmed that the aromatic amino acid side chains were affected, however, due to Trc mix being analysed in FTIR no differentiation could be made between the three Phe residues. The influence on Orn^{9} increased with the increase in saccharide size which could point to conformational changes induced by the saccharides which increases overall activity. The influence of Lys could not be determined due to the overlapping of IR peaks complicating the assignment. Both glucose and KLU E had a similar influence on the aliphatic amino acids Val, Leu and Pro possibly caused by glucose and KLU E decreasing interaction with water before drying whereas cellobiose might have a slight chaotropic effect. The effect of the saccharides on Asn and Gln increased with the increase in size for the saccharides possibly forming hydrogen bonds with the amino groups. Lastly, changes in the C-O regions for all the sugars proposes that primary point of interaction between peptide and cellulose are the hydroxyl groups. The current hypothesis of Trc interaction with cellulose is therefore that Trcs associates quickly to cellulose hydroxyl groups mediated by the amide side chains of Asn^{5} and Gln^{6} , the hydroxyl group of Tyr^{7}, the

amino group of the Trp residues and amino group of Orn^9/Lys^9 from our ATR-FTIR studies, as well as the peptide bond groups of residues 1, 4 and 9, and possibly 7 and 8 from NMR studies. Once associated the peptide undergoes secondary structural changes that select for further peptide attachment and increase antimicrobial activity. In this the aromatic and aliphatic amino acid residues possibly play a secondary role in hydrophobic interactions and aromatic stacking. A more detailed study on peptide association/oligomerisation will be discussed in Chapter 5, in combination with the conclusions in Chapter 6 on cellulose-Trc interactions.

4.6 References

Appleby, J.C., Knowles, E., Pearson, J., White, T., 1947. A preliminary study of the formation, assay and stability of tyrothricin. J. Gen. Microbiol. 1, 137–44.

Barbiroli, A., Bonomi, F., Capretti, G., Iametti, S., Manzoni, M., Piergiovanni, L., Rollini, M., 2012. Antimicrobial activity of lysozyme and lactoferrin incorporated in cellulose-based food packaging. Food Control 26, 387–392.

Barth, A., 2007. Infrared spectroscopy of proteins. Biochim. Biophys. Acta 1767, 1073–1101.

Barth, A., 2000. The infrared absorption of amino acid side chains. Prog. Biophys. Mol. Biol. 74, 141–173.

Beyer, C.F., Gibbons, W.A., Craig, L.C., Longworth, J.W., 1974. Heterogeneous tryptophan environments in the cyclic peptides tyrocidines B and C. Phosphorescence studies. J. Biol. Chem. 249, 3204–3211.

Boatemaa, S., Barney, M., Drimie, S., Harper, J., Korsten, L., Pereira, L., 2019. Awakening from the listeriosis crisis: Food safety challenges, practices and governance in the food retail sector in South Africa. Food Control 104, 333–342.

Buchet, R., Tavitian, E., Ristig, D., Swoboda, R., Stauss, U., Gremlich, H.U., de La Fournière, L., Staufenbiel, M., Frey, P., Lowe, D.A., 1996. Conformations of synthetic β peptides in solid state and in aqueous solution: relation to toxicity in PC12 cells. Biochim. Biophys. Acta -Molecular Basis Dis. 1315, 40–46.

Burdock, G.A., 2007. Safety assessment of hydroxypropyl methylcellulose as a food ingredient. Food Chem. Toxicol. 45, 2341–2351.

Cagri, A., Ustunol, Z., Ryser, E.T., 2004. Antimicrobial edible films and coatings. J. Food Prot. 67, 833–848.

Chattopadhyay, A., Raghuraman, H., 2004. Application of fluorescence spectroscopy to membrane protein structure and dynamics. Curr. Sci. 87, 175–180.

Chen, Y., Barkley, M.D., 1998. Toward understanding tryptophan fluorescence in proteins. Biochemistry 37, 9976–9982.

Chitnumsub, P., Fiori, W.R., Lashuel, H.A., Diaz, H., Kelly, J.W., 1999. The nucleation of monomeric parallel β-sheet-like structures and their self-assembly in aqueous solution. Bioorg. Med. Chem. 7, 39–59.

Danders, W., Marahiel, M.A., Krause, M., Kosui, N., Kato, T., Izumiya, N., Kleinkauf, H., 1982. Antibacterial action of gramicidin S and tyrocidines in relation to active transport, in vitro transcription, and spore outgrowth. Antimicrob. Agents Chemother. 22, 785–790.

Felgueiras, H.P., Amorim, M.T.P., 2017. Functionalization of electrospun polymeric wound dressings with antimicrobial peptides. Colloids Surfaces B Biointerfaces 156, 133–148.

Gibbons, W.A., Beyer, C.F., Dadok, J., Sprecher, R.F., Wyssbrod, H.R., 1975. Studies of individual amino acid residues of the decapeptide tyrocidine A by proton double-resonance difference spectroscopy in the correlation mode. Biochemistry 14, 420–429.

Green, J.D., Fulghum, T., Nordhaus, M.A., 2011. A review of immobilized antimicrobial agents and methods for testing. Biointerphases 6, MR13–MR28.

Juhl, D.W., Rensburg, W., Bossis, X., Vosloo, J.A., Rautenbach, M., Bechinger, B., 2019. Tyrocidine A interactions with saccharides investigated by CD and NMR spectroscopies. J. Pept. Sci. 25, e3163.

Kong, J., Yu, S., 2007. Fourier transform infrared spectroscopic analysis of protein secondary structures. Acta Biochim. Biophys. Sin. (Shanghai). 39, 549–559.

Krimm, S., 1983. Vibrational analysis of conformation in peptides, polypeptides, and proteins. Biopolym. Orig. Res. Biomol. 22, 217–225.

Kuo, M.-C., Gibbons, W.A., 1980. Nuclear Overhauser effect and cross-relaxation rate determinations of dihedral and transannular interproton distances in the decapeptide tyrocidine A. Biophys. J. 32, 807–36.

Laiken, S., Printz, M., Craig, L.C., 1969. Circular dichroism of the tyrocidines and gramicidin S-A. J. Biol. Chem. 244, 4454–4457.

Lakowicz, J.R., 2013. Principles of fluorescence spectroscopy. Springer Science & Business Media. 529-567.

Lesage, A., Lelli, M., Gajan, D., Caporini, M.A., Vitzthum, V., Miéville, P., Alauzun, J., Roussey, A., Thieuleux, C., Mehdi, A., Bodenhausen, G., 2010. Surface enhanced NMR spectroscopy by dynamic nuclear polarization. J. Am. Chem. Soc. 132, 15459–15461.

Lin, J., Qiu, S., Lewis, K., Klibanov, A.M., 2003. Mechanism of bactericidal and fungicidal activities of textiles covalently modified with alkylated polyethylenimine. Biotechnol. Bioeng. 83, 168–172.

Loll, P.J., Upton, E.C., Nahoum, V., Economou, N.J., Cocklin, S., 2014. The high resolution structure of tyrocidine A reveals an amphipathic dimer. Biochim. Biophys. Acta - Biomembr. 1838, 1199–1207.

Munyuki, G., Jackson, G.E., Venter, G.A., Kövér, K.E., Szilágyi, L., Rautenbach, M., Spathelf, B.M., Bhattacharya, B., Van Der Spoel, D., 2013. β-sheet structures and dimer models of the two major tyrocidines, antimicrobial peptides from *Bacillus aneurinolyticus*. Biochemistry 52, 7798–7806.

Naik, V.M., Krimm, S., Denton, J.B., Nemethy, G., Scheraga, H.A., 1984. Vibrational analysis of peptides, polypeptides and proteins: XXVII. Structure of gramicidin S from normal mode analyses of low-energy conformations. Int. J. Pept. Protein Res. 24, 613–626.

Nguyen, V.T., Gidley, M.J., Dykes, G.A., 2008. Potential of a nisin-containing bacterial cellulose film to inhibit Listeria monocytogenes on processed meats. Food Microbiol. 25, 471–478.

Noimark, S., Dunnill, C.W., Wilson, M., Parkin, I.., 2009. The role of surfaces in catheter-associated infections. Chem. Soc. Rev. 38, 3435–3448.

Olanya, O.M., Hoshide, A.K., Ijabadeniyi, O.A., Ukuku, D.O., Mukhopadhyay, S., Niemira, B.A., Ayeni, O., 2019. Cost estimation of listeriosis (*Listeria monocytogenes*) occurrence in South Africa in 2017 and its food safety implications. Food Control 102, 231–239.

Owen, A.J., 1995. Uses of derivative spectroscopy, Application Note, Agilent Technologies, Waldbronn.

Paradies, H.H., 1989. Structure of tyrocidine micelles in isotropic aqueous solution. J. Pharm. Sci. 78, 230–234.

Paradies, H.H., 1979. Aggregation of tyrocidine in aqueous solutions. Biochem. Biophys. Res. Commun. 88, 810–817.

Pivec, T., Hribernik, S., Kolar, M., Kleinschek, K.S., 2017. Environmentally friendly procedure for in-situ coating of regenerated cellulose fibres with silver nanoparticles. Carbohydr. Polym. 163, 92–100.

Ramsden, J.J., Allen, D.M., Stephenson, D.J., Alcock, J.R., Peggs, G.N., Fuller, G., Goch, G., 2007. The design and manufacture of biomedical surfaces. CIRP Ann. 56, 687–711.

Rautenbach, M., Vlok, N.M., Stander, M., Hoppe, H.C., 2007. Inhibition of malaria parasite blood stages by tyrocidines, membrane-active cyclic peptide antibiotics from *Bacillus brevis*. Biochim. Biophys. Acta - Biomembr. 1768, 1488–1497.

Salgado, J., Grage, S.L., Kondejewski, L.H., Hodges, R.S., McElhaney, R.N., Ulrich, A.S., 2001. Membrane-bound structure and alignment of the antimicrobial β-sheet peptide gramicidin S derived from angular and distance constraints by solid state ^{19}F-NMR. J. Biomol. NMR 21, 191–208.

Sanchez-Gonzalez, L., Pastor, C., Vargas, M., Chiralt, A., Gonzalez-Martinez, C., Chafer, M., 2011. Effect of hydroxypropylmethylcellulose and chitosan coatings with and without bergamot essential oil on quality and safety of cold-stored grapes. Postharvest Biol. Technol. 60, 57–63.

Son, W.K., Youk, J.H., Lee, T.S., Park, W.H., 2004. Preparation of antimicrobial ultrafine cellulose acetate fibers with silver nanoparticles. Macromol. Rapid Commun. 25, 1632–1637.

Spathelf, B.M., 2010. Qualitative structure-activity relationships of the major tyrocidines , cyclic decapeptides from Bacillus aneurinolyticus. Stellenbosch University, Department of Biochemistry, Stellenbosch, South Africa. PhD.Thesis, http://scholar.sun.ac.za/handle/10019.1/4001.

Spathelf, B.M., Rautenbach, M., 2009. Anti-listerial activity and structure-activity relationships of the six major tyrocidines, cyclic decapeptides from *Bacillus aneurinolyticus*. Bioorganic Med. Chem. 17, 5541–5548.

Srey, S., Jahid, I.K., Ha, S. Do, 2013. Biofilm formation in food industries: A food safety concern. Food Control 31, 572–585.

Surewicz, W.K., Mantsch, H.H., 1988. New insight into protein secondary structure from resolution-enchanced infrared spectra. Biochim. Biophys. Acta 952, 115–130.

Susi, H., Byler, D.M., 1983. Protein structure by Fourier transform infrared spectroscopy: second derivative spectra. Biochem. Biophys. Res. Commun. 115, 391–397.

Thies, M., Paradies, H.H., 1997. Self-Assembly of tyrocidines in nanotubular structures. MRS online Proc. Libr. Arch. 489.

Troskie, A.M., Rautenbach, M., Delattin, N., Vosloo, J.A., Dathe, M., Cammue, B.P.A., Thevissen, K., 2014. Synergistic activity of the tyrocidines, antimicrobial cyclodecapeptides from *Bacillus aneurinolyticus*, with amphotericin B and caspofungin against *Candida albicans* biofilms. Antimicrob. Agents Chemother. 58, 3697–3707.

van Rensburg, W., 2015. Characterization of natural antimicrobial peptides adsorbed to different matrices. Stellenbosch University, Department of Biochemistry, Stellenbosch, South Africa. MSc.Thesis, http://scholar.sun.ac.za/handle/10019.1/97929.

Vásconez, M.B., Flores, S.K., Campos, C.A., Alvarado, J., Gerschenson, L.N., 2009. Antimicrobial activity and physical properties of chitosan–tapioca starch based edible films and coatings. Food Res. Int. 42, 762–769.

Venyaminov, S.Y., Kalnin, N.N., 1990. Quantitative IR spectrophotometry of peptide compounds in water (H_2O) solutions. I. Spectral parameters of amino acid residue absorption bands. Biopolym. Orig. Res. Biomol. 30, 1243–1257.

Vogt, T.C.B., Schinzel, S., Bechinger, B., 2003. Biosynthesis of isotopically labeled gramicidins and tyrocidins by *Bacillus brevis*. J. Biomol. NMR 26, 1–11.

Vosloo, J.A., 2016. Optimised bacterial production and characterisation of natural antimicrobial peptides with potential application in agriculture. Stellenbosch University, Department of Biochemistry, Stellenbosch, South Africa. PhD.Thesis, http://scholar.sun.ac.za/handle/10019.1/98411

Vosloo, J.A., Stander, M.A., Leussa, A.N.N., Spathelf, B.M., Rautenbach, M., 2013. Manipulation of the tyrothricin production profile of *Bacillus aneurinolyticus*. Microbiology 159, 2200–2211.

Williams, R.C., Yphantis, D.A., Craig, L.C., 1972. Noncovalent association of tyrocidine B. Biochemistry 11, 70–77.

4.7 Supplementary data

Purification of the TrcA and labelled peptides was performed with an established RP-HPLC method (Spathelf and Rautenbach, 2009). Isotopically labelled peptide was produced using an amalgamation of the method used by Vogt *et. el* (Vogt et al., 2003) and the production of unlabelled tyrocidines (Vosloo et al., 2013). Production media contained 3% *w/v* glucose (^{13}C labelled) and 85% *v/v* $^{13}C^{15}N$ Celltone media. Cultures were grown for 15 days, after which the peptides were extracted from the biomass pellet with 80% *v/v* ACN. Characterization and purity determination of the peptide complexes and purified labelled peptides was performed with a UPLC-MS method previously described (Spathelf and Rautenbach, 2009; Troskie et al., 2014; Vosloo et al., 2013)

4.7.1 Purification of tyrocidines and analogues from commercially obtained tyrothricin and amino acid supplemented cultures

The linear gramicidins, produced with tyrocidines as the peptide complex tyrothricin, were removed from commercially obtained peptide with the use of an organic solvent extraction to obtain a tyrocidine extract, which is referred to as Trc mix. The six major tyorcidines Trc C1 (1361.6785), Trc C (1347.6694), Trc B1/B1' (1322.6669), Trc B (1308.6517), Trc A1 (1283.6587) and Trc A (1269.6412) constitute >75% of the peptide complex (Figure S4.1) and peptide purity >90%. Refer to the discussion in supplementary data of Chapter 3, specifically Table S3.1.

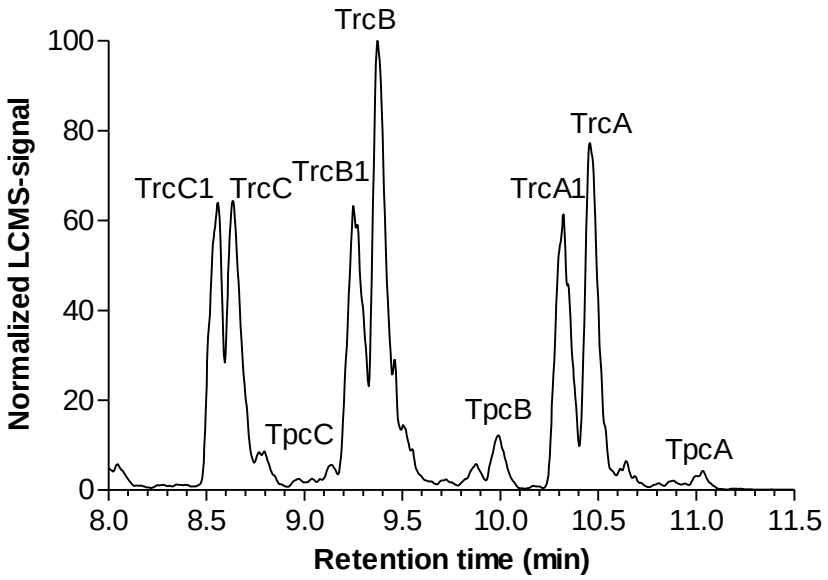

Figure S4.1: UPLC-MS chromatogram showing in analogues present in Trc mix, the major tyrocidines groups are indicated.

4.7.2 Production and purification of isotopically labelled peptide

Labelled tyrocidines were produced with the use of $^{15}N^{13}C$ labelled culture media over a period of 15 days. The growth of the producer was deterred, showing the effect of the media on the growth of the producer organism. A similar effect is seen with tryptophan supplementation, which can be rectified with a longer culturing period (Vosloo et al., 2013). Upon completion of production, the cell pellet was resuspended in 80% *v/v* acetonitrile, extracted overnight, and freeze-dried. Following extraction, a yellow/orange pigment was found to associate with the peptide. Upon resuspension in 50% *v/v* acetonitrile distinct layers where observed. The lighter top layer yielded a white powder when freeze-dried, whereas the bottom darker layer yielded a yellow sugary compound and some white powder. This process was repeated until no more white powder was observed with the sugary compound after freeze-drying. The combined fractions of all the purification steps were further purified with the use of RP-HPLC. The HPLC chromatogram of the labelled peptide was overshadowed by remnants of the pigment (Figure S4.2: A, indicated with *). However, closer inspection of the chromatogram produced peaks like those observed for unlabelled produced peptide (Figure S4.2:B) and separated accordingly. Only a small amount of peptide was produced, most of which was Trc A, it was therefore decided to purify only the labelled Trc A for further biophysical studies.

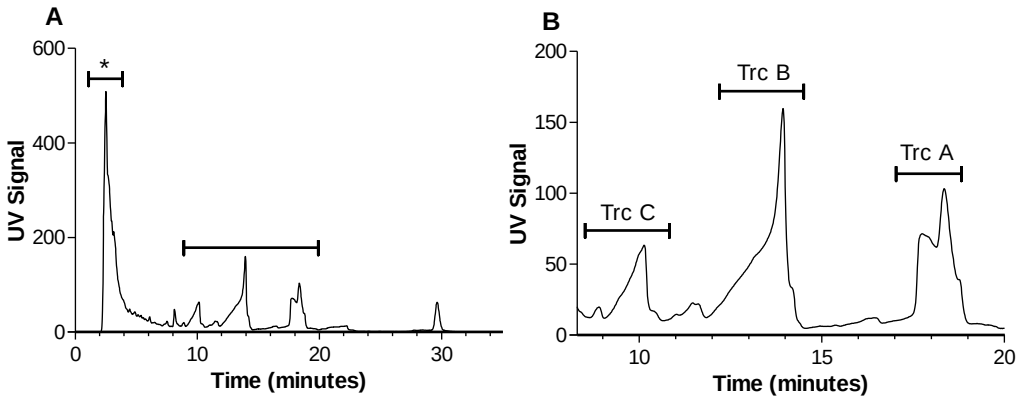

Figure S4.2: RF-HPLC chromatogram of labelled tyrocidines extract **(A)** Full chromatogram with the contaminating pigment indicated (*). **(B)** Chromatogram from 8-20 min showing the expected peak identity based on separation observed for the unlabelled peptide. The asymmetrical peaks, shoulders and double peaks are due to the extensive aggregation of the peptides, especially in the presence of the C_{18} matrix and high %acetonitrile.

After separation with RP-HPLC the purity of the labelled Trc A was confirmed with UPLC-MS. An unlabelled Trc A was also analysed for comparison, to confirm the identity of the labelled peptide. Both unlabelled and labelled Trc A had a retention time of 11.10 and 11.06 minutes, respectively (Figure S4.3: A-B). The labelled Trc A chromatogram did however have a second peak at 11.16 minutes which also contained labelled Trc A. The reason for the second peak is unknown. ESI-MS analysis confirmed the presence of unlabelled Trc A (1270.6570 – protonated M_r)(Figure S4.3:C) and labelled Trc A (1347.8372 – protonated M_r) (Figure S4.3:D). Similar oligomer formation patterns were observed of monomer, dimers, tetramers and pentamers for both labelled and unlabelled peptides. The lower oligomerisation observed for the labelled peptide can be attributed towards lower concentration used in the analysis.

The M_r of 1346.8293 as calculated with the MaxEnt 3 algorithm for the labelled Trc A correlated with what was expected (Table S4.2) for a peptide with all the nitrogens labelled and 65/67 carbons labelled. However, when the Mr was calculated from the ion spectrum (Figure S4.4: A), using the *m/z* value of the highest isotope of the doubly charged molecular ions (Figure S4.4: B) we found a M_r of 1348.8404, correlating to a uniformly labelled TrcA. This discrepancy is because MaxEnt considers all the isotopes in the calculation and the oligomerisation complicates the spectra, specifically as the oligomer peaks overlap in with the singly charged ion signals (Figure S4.4:C). The labelling was deemed sufficient and the overall purity of the combined TrcA fractions was higher than 90%, which made it acceptable for further biophysical analyses.

Table S4.2: Expected monoisotopic M_r values for the $^{15}N^{13}C$ labelled major tyrocidine analogues

Peptide	Monoisotopic M_r	Uniformly labelled ($^{15}N^{13}C$)	Minus ^{15}N	Minus ^{13}C	Minus 2x ^{13}C
Trc A	1269.6547	1348.8409	1347.8439	1347.8375	1346.8308
$TrcA_1$	1283.6703	1363.8565	1362.8595	1362.8532	1372.8506
TrcB	1308.6656	1390.8555	1389.8585	1389.8522	1388.8455
$TrcB_1$	1322.6812	1405.8712	1404.8741	1404.8678	1414.8652
TrcC	1347.6765	1432.8702	1431.8731	1431.8668	1430.8601
$TrcC_1$	1361.6921	1447.8858	1446.8888	1446.8825	1456.8799

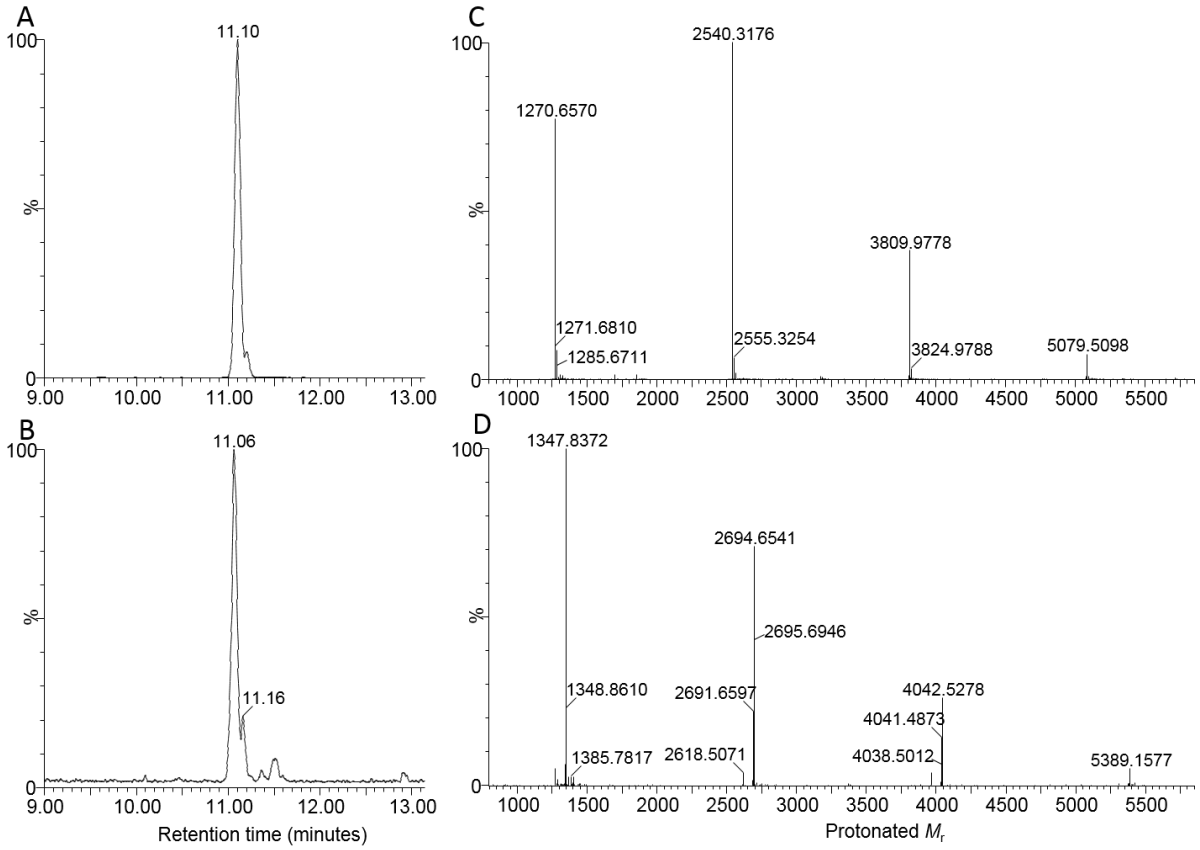

Figure S4:3 UPLC-chromatogram **(A)** Trc A and **(B)** labelled Trc A with detected peaks at 11.10 and 11.06/11.16 minutes. MaxEnt 3 analysis of **(C)** Trc A and **(D)** labelled Trc A showing the detected oligomers

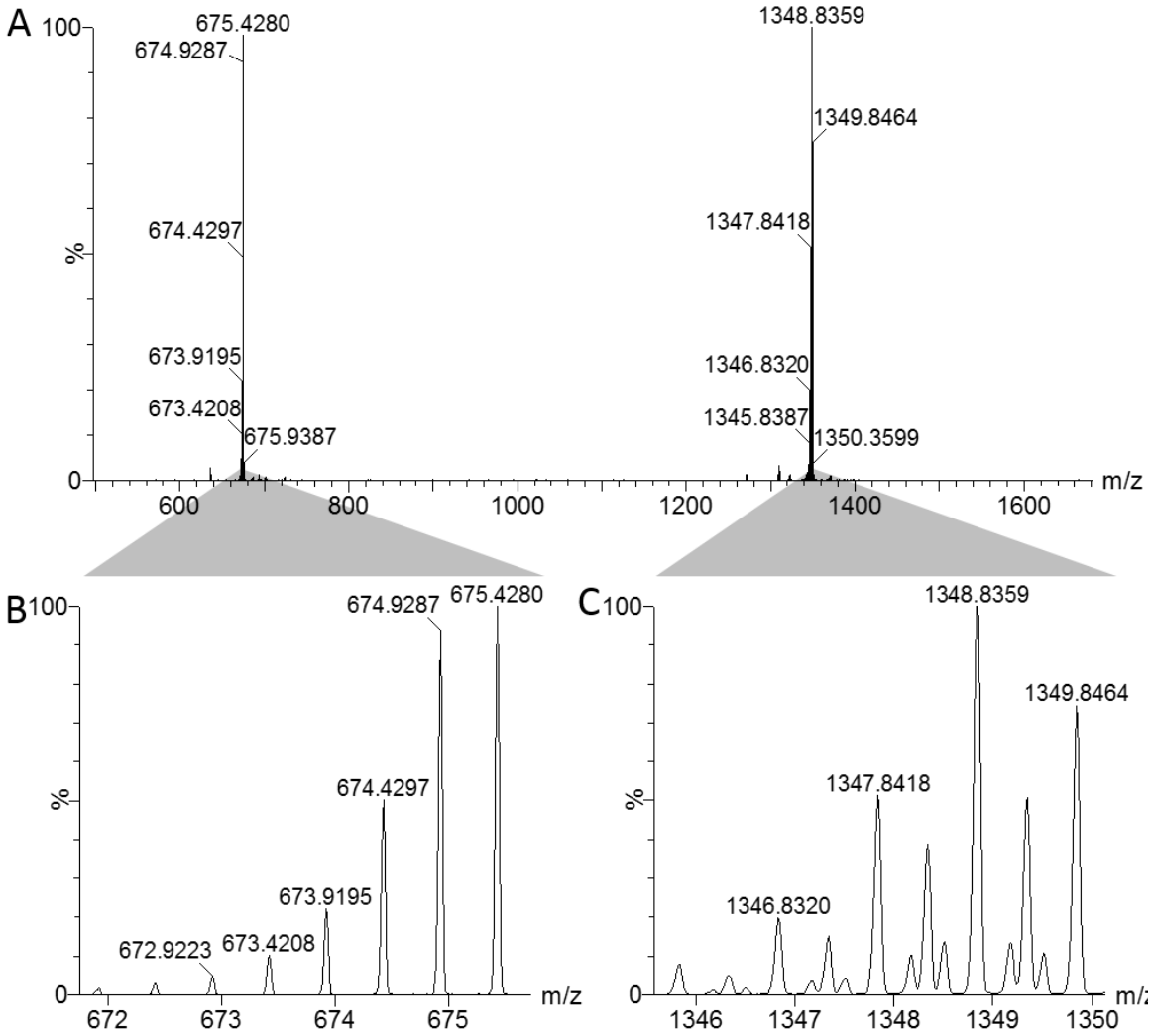

Figure S4:4: ESI-MS *m/z* spectrum of **(A)** labelled Trc A showing the doubly charges and singly charged species. Closer inspection of the singular isotopes of the **(B)** doubly charges $[M+2H]^{2+}$ and **(C)** singly charged $[M+H]^{+}$ species.

Addendum (Chapter 4)

Tyrocidine A interactions with saccharides investigated by CD and NMR spectroscopies

Addendum to Chapter 4 was published in the *Journal of Peptide Science*, Volume 25, Issue 5, p.e3163. This article was published as part of a collaboration between the Prof. M. Rautenbach and Prof. B. Bechinger and their respective research groups, forming part of two PhD projects. The contribution of each of the authors where as follows: first author D.W. Juhl (NMR studies, data analysis and writing of article), co-authors W. van Rensburg (CD experiments, peptide purification and knowledge transfer in terms of handling the peptides to X. Bossis), X. Bossis (NMR studies), J.A. Vosloo (CD experiments), M. Rautenbach (critical evaluation of data, co-writer and editing), B. Bechinger (critical evaluation of data, co-writer and editing). This article, as published, is included as Addendum Chapter 4 of this thesis.

Received: 19 November 2018 | Revised: 10 February 2019 | Accepted: 12 February 2019

DOI: 10.1002/psc.3163

SPECIAL ISSUE ARTICLE

WILEY Journal of PeptideScience

Tyrocidine A interactions with saccharides investigated by CD and NMR spectroscopies

Dennis Wilkens Juhl[1] | Wilma van Rensburg[2] | Xavier Bossis[1] | J. Arnold Vosloo[2] | Marina Rautenbach[2] | Burkhard Bechinger[1]

[1] Université de Strasbourg/CNRS, Strasbourg, France

[2] BIOPEP Peptide Group, Department of Biochemistry, University of Stellenbosch, Matieland, South Africa

Correspondence
Burkhard Bechinger, Faculté de Chimie, Institut le Bel, 4, rue Blaise Pascal, 67070 Strasbourg, France.
Email: bechinge@unistra.fr

Marina Rautenbach, BIOPEP Peptide Group, Department of Biochemistry, University of Stellenbosch, Private Bag X1, 7602 Matieland, South Africa.
Email: mra@sun.ac.za

Funding information
Hubert Curien Campus France, Grant/Award Number: Protea 33948; Institut Universitaire de France; RTRA International Center for Frontier Research in Chemistry; South African Agency for Science and Technology Advancement, Grant/Award Number: Protea FSTR14061870171; CNRS; University of Strasbourg; Agence Nationale de la Recherche Région Grand-Est; South African National Research Foundation, Grant/Award Number: CSUR14073083174

Tyrocidines are a family of cyclic decapeptides produced by the soil bacterium, *Brevibacillus parabrevis*. These antibiotic peptides can be used to prevent infections in agriculture and food industry but also to prepare antimicrobial lozenges, creams, and dressings for medical applications. It has been observed that the tyrocidines interact with saccharides such as cellulose from their soil environment, as well as sugars in culture media and glycans in fungal cell walls. Here, we investigated the interactions of tyrocidines with glucose, sucrose, and cellotetraose (as cellulose model) in a quantitative fashion utilising CD and NMR spectroscopy. The CD and NMR spectra of tyrocidine A (TrcA) were analysed as a function of solvent composition, and the spectral properties agree with the formation of oligomeric structures that are governed by β-sheet secondary structures once the acetonitrile content of the solvent is increased. Saccharides seem to also induce TrcA spectral changes reverting those induced by organic solvents. The CD spectral changes of TrcA in the presence of glucose agree with new ordered H-bonding, possibly β-sheet structures. The amides involved in intramolecular H-bonding remained largely unaffected by the environmental changes. In contrast, amides exposed to the exterior and/or involved in TrcA intermolecular association show the largest ^{1}H chemical shift changes. CD and NMR spectroscopic investigations correlated well with TrcA-glucose interactions characterized by a dissociation constant around 200 μM. Interestingly, the association of cellotetraose corresponds closely to the additive effect from four glucose moieties, while a much higher dissociation constant was observed for sucrose. Similar trends to TrcA for binding to the three saccharides were observed for the analogous tyrocidines, tyrocidine B, and tyrocidine C. These results therefore indicate that the tyrocidine interactions with the glucose monosaccharide unit are fairly specific and reversible.

KEYWORDS

antimicrobial coating, antimicrobial peptide, cell wall interactions, cyclodecapeptide, dressings, glucose, gramicidin S, tyrothricin

Abbreviations: ACN, acetonitrile; AMP, antimicrobial peptide; Br. parabrevis, *Brevibacillus parabrevis*; CD, circular dichroism; ESMS, electrospray mass spectrometry; Glc, glucose; NMR, nuclear magnetic resonance spectroscopy; Orn, O, ornithine; Trc/s, tyrocidine/s; TrcA, tyrocidine A; UPLC, ultraperformance liquid chromatography; UPLC-MS, ultraperformance liquid chromatography linked to mass spectrometry; UV, ultra violet

Chapter 5
Does oligomerisation dictate interaction and stability of the tyrocidine-treated celluloses?

5.1 Introduction

The tyrocidines and tyrocidine analogues (Trcs) have a history of binding to various materials without any clear relationship between material and probability of attaching, while maintaining activity against target organisms (Chapter 3)(Van Rensburg, 2015). Previous research has shown the selectivity of the peptides to bind to cellulose while maintaining activity, while not binding or not maintaining activity on mixed cellulose (cellulose acetate and nitrocellulose). Furthermore, the only conditions that could remove or influence peptide association based on a decrease in activity was 1% *m/v* SDS and 70% *v/v* acetonitrile (Chapter 3) pointing to a possible influence of amphipathic dimers and higher order oligomer formation.

Trcs activity is directly correlated to the amphipathic character of peptide in the complex (Salgado et al., 2001) which in turn is linked to the dimerization of the peptides. Trcs are only amphipathic in certain dimeric conformations (e.g. parallel stacking) and not in any of the monomer conformations (Loll et al., 2014; Munyuki et al., 2013). Loss of cyclic structure resulted in a loss in antimicrobial activity, highlighting the importance of the inter- and intrapeptide β-sheet secondary structure and resulting amphipathic character (Ruttenberg et al., 1965; Stern et al., 1969; Williams et al., 1972). Dimerization is concentration and time dependent (Appleby et al., 1947; Munyuki et al., 2013; Paradies, 1979), but can also be reversed, to some extent, with dilution (Williams et al., 1972). However, the aggregation/oligomerization needed for the tyrocidines to elicit an antimicrobial response is dependent on a 'critical concentration' (Laiken et al., 1971) since a too high concentration can lead to the loss of activity also due to aggregation (Appleby et al., 1947). Temperature only affects dimerization at very high concentrations (Appleby et al., 1947; Paradies, 1979).

Studies into the contribution of the constituent amino acid of tyrocidines to aggregation showed that neither Orn^9/Lys^9 or Tyr^7 is responsible for aggregation since aggregation still occurred after alkylation and acylation of these residues were performed (Ruttenberg et al., 1965). Hydrogenation of the sidechains of the aromatic amino acids did not affect aggregation/oligomerisation, showing that intermolecular π-bonds through the aromatic amino acids were not a major contributor to aggregation (Ruttenberg et al., 1966). However, recent studies indicated that oligomers are stabilized by the aromatic amino acids (Munyuki et al.,

2013). It is therefore possible that aggregation/oligomerisation is partially dependent on the different aromatic amino acids in the analogues, as well as on a common backbone structure (Laiken et al., 1969) or specific peptide conformation that drives aggregation/oligomerisation based on hydrophobic interactions (Ruttenberg et al., 1965).

The shape of the larger aggregates varies between the solvent system used and method of analysis, ranging from tubular (Paradies, 1979; Thies and Paradies, 1997) to micellular or spheroid structures (Helle et al., 1992; Ruttenberg et al., 1966). Chromatographic assessment of aggregation showed that there is a quick initial aggregation, followed by a much slower aggregation into larger aggregates (Paradies, 1989). Based on the time dependency, it was suggested that tyrocidines aggregate with two different mechanisms resulting respectively in smaller micelles and larger proposed prolate ellipsoid formation (Paradies, 1989). Two different types of aggregation have also been observed: sideways aggregation which is mediated by hydrogen bonding opposed to stacking which is mediated by hydrophobic interactions, primarily between aromatic amino acids (Munyuki et al., 2013). It has been hypothesised that tyrocidines could order and re-order based on the environment, pH, and rate at which the environment changes pointing to a dynamic aggregation/oligomerisation system rather than one aggregation/oligomeric state (Thies and Paradies, 1997).

As dimerization is hypothesised to play a key role in the peptide activity, it is probably a key contributor to the association of Trcs to surfaces resembling target cell walls and membranes. Acetonitrile was already shown to influence the dissociation of Trcs from cellulose (Chapter 3) and was therefore chosen as solvent to study the oligomerisation of Trcs. Acetonitrile is expected to dissolve oligomeric structures dependent on hydrophobic interaction but could support hydrogen bonds and other polar/electrostatic interactions. This switch between interactions was studied by ion-mobility mass spectroscopy, an *in vacuo* technique which selects for strong polar/electrostatic interactions and hydrogen bonds by removing any solvent influence, and circular dichroism, an *in solutio* technique that detects secondary structures which are stabilised by hydrogen bonding.

The formation of hydrophobic cavities, linked to the formation of oligomers stabilized by hydrophobic interactions, was studied using fluorescence and 8-anilinonaphthalene-1-sulfonic acid (ANS), a dye whose fluorescence intensifies in hydrophobic environments (Kumar and Mishra, 2015). The fluorescence of the Trcs has been mainly used to study the association of Trcs to materials (Chapter 3) but can also be employed to gain insight into the peptide

behaviour with a change in environment. Of the three available residues only Trp and Tyr are used since fluorescence from Phe is rarely observed in proteins due to its low quantum yield (Lakowicz, 2013). The extinction coefficient and quantum yield for Trp is much higher than that of Tyr and normally overshadows the fluorescence seen for Tyr (Lakowicz, 2013). Tyr remains relatively unaffected by environmental changes, whereas the indole ring of Trp is highly sensitive to solvent changes and peptide conformational changes (Chattopadhyay and Raghuraman, 2004; Chen and Barkley, 1998; Lakowicz, 2013). As each Trp gives information about the environment around this fluorophore, an increase in the number of Trp residues would complicate interpretation. As the Trc mix contains Trc B/B1 and Trc C/C1, with the tryptocidines as minor contribution to the Trp content, only the average fluorescence of what is occurring on a structural level can be deduced (Lakowicz, 2013). Local environment changes can include conformational changes, subunit binding/association, denaturing of a peptide/protein or solvent changes and are detected as either spectral shifts or quenching (Lakowicz, 2013). Spectral shifts are caused by a change in polarity surrounding the fluorophore: polar environments result in red shifts and a decrease in environment polarity resulting in blue shifts (Lakowicz, 2013). Quenching of the Trp-residue fluorescence can be due to ground state complex formation, excited state reactions and collisional quenching (Lakowicz, 2013). In Trcs, quenching by ground state complex formation can be expected with an increase in self-assembly due to the interaction between aromatic amino acids contributing to the stabilising of higher order oligomers in aqueous solutions (Munyuki et al., 2013). Excited state interactions can be due to electron transfer between the excited-state indole ring of the Trp-residues to the peptide backbone, Lys/Orn amino group and amide groups of Asn and Gln (Chen and Barkley, 1998; Lakowicz, 2013). Collisional quenching is dependent on the solvent accessibility of the fluorophore and therefore be determined by the degree of self-assembly and peptide conformation. The change in fluorescence of these fluorophores can highlight how the peptide conformation changes in response to the changing environment.

In order to challenge the stability of the Trc-oligomers/aggregates thermo-degradation studies were done to selectively melt certain structures/conformations of higher order oligomers. Thermo-degradation studies are typically done as a quality control to detect any mutations in proteins that would destabilise secondary structures of proteins (Brown et al., 2002). Lastly, scanning electron microscopy was used to visualise nanostructures that form on cellulose and in the presence of glucose and cellobiose to assess oligomer/aggregate formation after initial association to form a seeding layer.

5.2 Materials

Acetonitrile, HPLC-grade far UV cut-off was supplied by Romil Ltd (Cambridge, UK). Merck (Darmstadt, Germany) supplied agar, yeast extract, tryptone, Na_2HPO_4, KH_2PO_4 and Merck (Wadeville, SA) supplied sodium chloride. The 96-well polystyrene plates were acquired from Corning (Kennebunk, ME, USA) and Whatman Filter paper 1 from GE Healthcare Life Sciences supplied by Sigma-Aldrich (Darmstadt, Germany). Analytical grade water (milliQ) was obtained filtering water from a reverse osmosis plant through Millipore Milli-Q® water purification system (Milford, USA).

5.3 Methods

5.3.1 Acetonitrile influence on Trc oligomerisation

5.3.1.1 Mass spectrometry and Ion-mobility study

Electrospray ionisation mass spectrometry (ESI-MS) was used to determine the identity of the peptides present within the purified peptide fractions and the crude produced extracts (refer to supplementary data, Chapter 3, Figure S3.1, Table S3.1. Trc mix (0.250 mg/mL) was analytically prepared of which 3.0 µL was injected for analysis. ESI-MS analysis was done using a Waters Synapt G2 quadrupole TOF mass spectrometer with electrospray ionisation source (Milford, MA, USA). Samples were subjected to a cone voltage of 15V, capillary voltage of 3.0 kV and source temperature of 120 ºC. The desolvation gas was set as nitrogen (650 L/hour) with a desolvation temperature of 275 ºC. All data was collected in the positive mode scanning over a *m/z* range of 300-2000.

Analysis on the aggregation of Trcs was studied by using ion-mobility mass spectrometry (IM-MS) based on studies done by Rautenbach *et. al.* (2017) and Ruotolo *et. al.* (2008). Trc mix (0.100 mg/mL) was incubated in a range of acetonitrile concentrations in analytical quality water (5-90% *v/v*) for 24 hour and 48 hours. Samples (3.0 µL) was injected into the ESI-MS at a flow rate of 0.300 mL/min. Solvent conditions of 20% (*v/v*) acetonitrile was used, as 50% and 80% (*v/v*) acetonitrile lead to a general decrease of observed signals detected between samples. The parameters used for the ion-mobility included an extraction cone voltage at 4 V, 180 mL/min helium cell gas flow, 90 mL/min N_2 as ion mobility buffer, 4 V trap collision energy, a trap release period of 200 µs, a mobility trap and extract height at 15 V and 0 V respectively, wave height ramp (100%) from 8 to 20 V and the weight height linear velocity ramp (20%) of 200 m/s from 1 000 to 650 m/s. All data was collected in the positive mode scanning over a *m/z* range of 300-2100 at a rate of 0.2 scans per second. Driftscope v2.9

software (Milford, MA, USA) and Waters MassLynx V4.1 software (Milford, USA) were used for the data analysis. Cross collisional surfaces (CCS) for the major peptides in the Trc mix was obtained from the BIOPEP™ data base in which the CCS was determined utilising a poly-Ala calibration as described by Rautenbach *et. al.* (2017).

5.3.1.2 Circular dichroism of tyrocidines in acetonitrile

The circular dichroism data on the effect of acetonitrile (ACN) on the peptide backbone was published as part of the article added in Chapter 4 – Addendum (Juhl et al., 2019). Trc A was dissolved in 60% *v/v* acetonitrile, then diluted to acetonitrile concentrations ranging from 15%-85% at a final peptide concentration of 250 µM. A sample of Trc A in trifluoroethanol (TFE) was also prepared at the ratio of TFE:ACN:water as 50:30:20 as a membrane mimicking model. Spectra were acquired with the use of the Chirascan Plus CD spectropolarimeter (Applied Photophysics, UK) at ambient temperature (24 ± 1ºC) between 185-300 nm at a bandwidth of 0.5 nm in a quartz curvet (pathlength 0.5 mm). Two repeats per sample in triplicate were performed and spectra was collected in a step wise manner over 0.2 seconds per 0.5 nm.

5.3.1.3 Fluorescence study on peptide behaviour, adsorption and desorption

The change in peptide oligomerisation/aggregation was tested by incubating Trc mix in different acetonitrile concentrations for one hour, after which the solution was transferred to a black 96-well plate. Fluorescence emission scans from 300-400 nm ($Em_{300-400}$) were done with excitation at 280 nm (Ex_{280}) utilising a Varioscan™ Multimode reader (Thermo Scientific) controlled by SkanIt Software 2.4.1 (Thermo Electron).

The emission and excitation parameters were optimised making use of the three possible fluorophores in the peptide as described in the Supplementary data of Chapter 3. The single wavelength fluorescence was read every 2 minutes for an hour at Ex_{290} and Em_{342} as it delivered the most sensitive signal. Fluorescence readings were collected by using the Tecan Spark 10M Multimode Microplate Reader and controlled by the Spark Control™ software, both provided by Tecan Group Ltd (Mennedorf, Switzerland).

The effect of change in solvent on the adsorption of Trc mix to cellulose was determined in a similar fashion as to how it is created. A solution of Trc mix (100 µL of 50.0 µg/mL) containing a range of percentage acetonitrile concentrations (5-95%, *v/v*) was incubated with cellulose for 2 hours. For peptide desorption, cellulose disks pre-treated with Trc mix were treated with different acetonitrile concentrations for 2 hours to allow for passive desorption. Following the

incubation, the solutions were removed, and the samples washed two times with 100 µL sterile analytical quality water and dried in a 40°C oven for 2 hours before it was used for antibacterial tests.

5.3.1.4 Oligomerisation monitoring with 8-anilinonaphthalene-1-sulfonic acid

The peptide was dissolved in 50% *v/v* acetonitrile to a stock concentration of 2.00 mg/mL before it was transferred to different ranges of acetonitrile (5% - 95% *v/v* acetonitrile) at a final concentration of 50.0 µg/mL. 8-Anilinonaphthalene-1-sulfonic acid (ANS) was dissolved in 50% *v/v* acetonitrile at a stock concentration of 16 mM and centrifuged at 14 000*xg* for 20 minutes to remove any particulate matter. Following an incubation step of the peptide solutions for 30 minutes, the ANS was added to the peptide solutions to a final concentration of 80 µM. The peptide-ANS solutions were incubated a further 30 minutes to ensure that full association of ANS to the peptide occurred as well as that the peptide aggregates have stabilized. The solutions were then transferred to 96-well black plates (100 µL) and the fluorescence scan read at Ex_{355} and $Ems_{450\text{-}550}$ using the Tecan Spark 10M Multimode Microplate Reader and controlled by the Spark Control™ software, both provided by Tecan Group Ltd (Mennedorf, Switzerland).

5.3.1.5 Temperature study

The effect of temperature on the oligomerisation and aggregation of Trc mix (0.100 mg/mL) in solution was determined for a range of percentage *v/v* acetonitrile (5-95%). The samples were incubated for one hour before 10.0 µL was carefully transferred to capillary tubes, sealed to limit evaporation and subjected to an incremental temperature increase over 60 minutes in the Prometheus NT.48 (Nanotemper, USA). For each sample, 23 fluorescence measurements were taken with 1°C temperature intervals over a temperature range from 20 °C to 95 °C with Ex_{280} and Em_{350}; Em_{330}. Light scattering measurements were conducted simultaneously with 23 measurements over a 1°C change. The technology is optimized to not allow evaporation, therefore any change observed is due to changes in conformation/oligomerisation and aggregation.

5.3.2 Visualisation of Trc oligomers

TrcA was dried on mica alone and on cellulose, as well as in the presence of glucose (1:1) and cellobiose (1:1) to study the peptide behaviour with scanning electron microscopy (SEM). Trc mix was also dried on mica. Untreated cellulose was also included in the analysis as a control.

Samples were dried overnight to ensure the removal of any moisture that could interfere with the SEM signal and was kept under vacuum for transport. In preparation the samples were mounted with double sided carbon isolation tape onto stubs and coated with gold to increase the conductivity of the surface of the sample. Sample analysis was done at the Central Analytical Facility at Stellenbosch University with a Zeiss EVO MA15VP Scanning Electron Microscope. Images of Trc A were recorded with high resolution SEM dual beam system (NOVA 450 NANOLAB, FEI) operating at WD 5.1 mm and 20 kV at the Sophisticated Instrument Centre (SIC)-Dr Harisingh Gour Central University Sagar, India.

5.3.3 Activity against Listeria monocytogenes

A freezer stock of *Listeria monocytogenes* B73 was streaked out onto BHI agar plates (brain heart infusion) and incubated at 37ºC for 48 hours until colonies were visible. Overnight starter cultures were made by selecting three to five colonies of the target organism and inoculating 1mL of growth media. From the starter culture a subculture was made into 6mL of fresh media and grown to mid exponential growth phase. All cultures were incubated at 37 ºC by shaking at 150 RPM at an angle. Mid-log and cell concertation were determined with classical plate counts for *L. monocytogenes* at OD_{620} = 0.4 (1.3 x 10^8 cells/mL). The solid phase antimicrobial activity was determined with the resazurin assay as described in Chapter 2.

5.4 Results

Results from Chapter 4 showed that the association of Trc mix to cellulose was influenced by the concentration of the peptide present within the incubation solution and that an optimal concentration exists for association. This was attributed to the peptides' activity being dependent on a 'critical point' of dimerization or oligomerization (Laiken et al., 1971) and high concentrations of peptide could lead to extensive aggregation which leads loss of activity (Appleby et al., 1947). Results from Chapter 3 showed that of all the conditions tested, only 70% *v/v* acetonitrile and 1% *m/v* SDS could remove enough peptide to influence the activity of Trc mix pre-treated cellulose. Moreover, SDS had a greater effect on the association compared to dissociation. SDS is an anionic detergent with membrane mimetic properties (Ovchinnikova et al., 2008; Tulumello and Deber, 2012), while 70% acetonitrile creates a more amphipathic environment. The question is therefore whether peptide aggregation/oligomerisation is key for the association of Trcs to materials, and specifically cellulose. The behaviour of Trcs in changing acetonitrile concentrations (as denaturant) was studied to determine the changes that

occur within the peptide arrangement as environments change between polar vs. amphipathic environments.

In our studies we regularly analysed the commercial Trc mix to assess the purity and in particular to determine if it is free from gramicidins. In our group we always observe oligomeric species, regardless of the purity, concentration or organic solvent modifier. Mass spectroscopy analysis by Munyuki *et al*. (2013) have shown that oligomerisation up to trimers and pentamers can be observed, depending on the analogue. An example of ESI-MS stable oligomers, up to heptamers detected for the Trc mix in this study can be seen in Figure 5.1: A. Dimers formed the major group of oligomers followed by monomers.

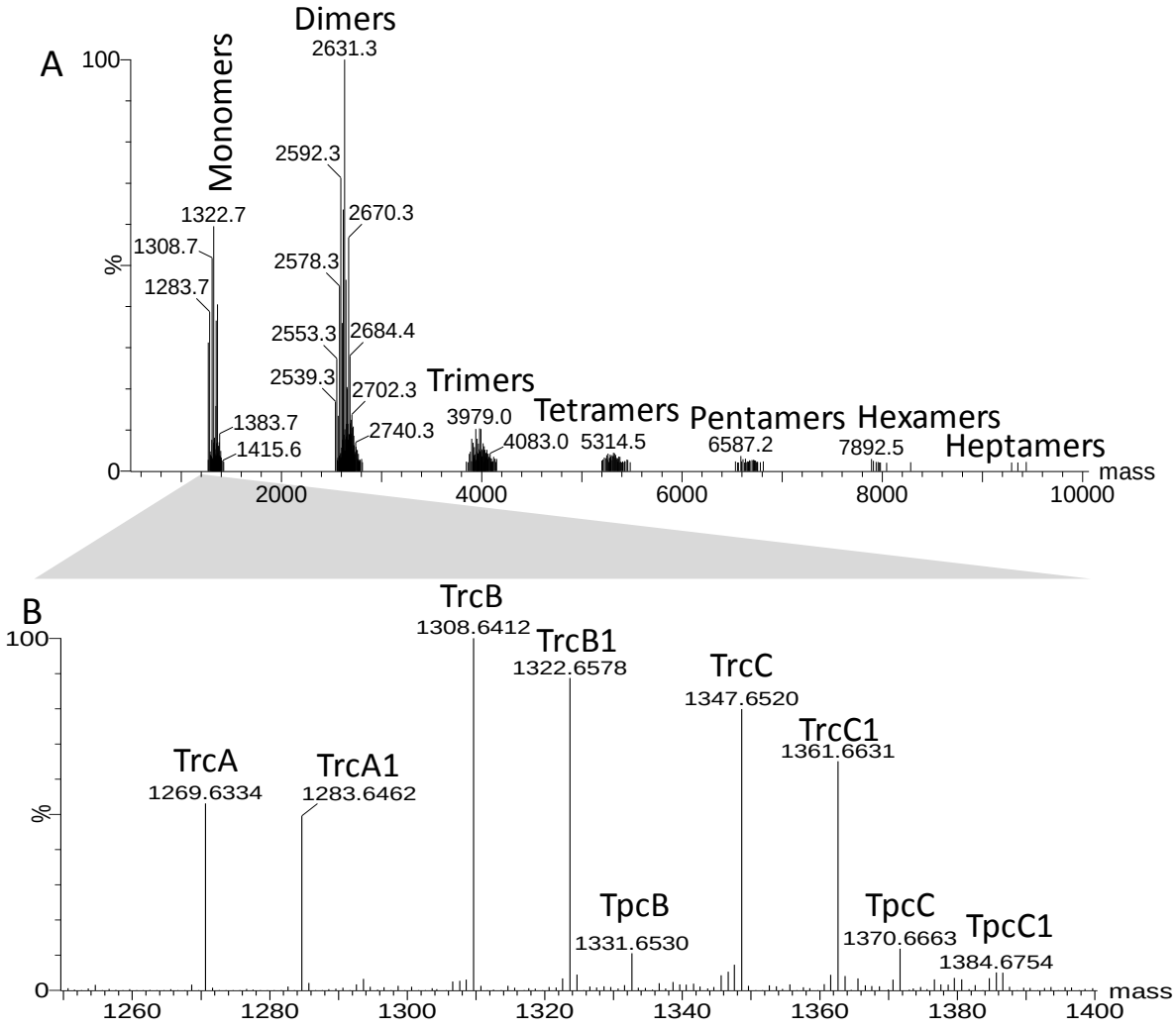

Figure 5.1: ESI-MS analysis of Trc mix **(A)** Max Ent 3 analysis showing the monomers, dimers, and higher oligomers of the major tyrocidines and tryptocidines. **(B)** Mass spectrum of the monomeric species showing the tyrocidine and tryptocidine analogues present in the sample.

The mass spectra of the monomeric species in Figure 5.1 B show the six main tyrocidines and three tryptocidines: Trc A (1269.6385), Trc A1 (1283.6592), Trc B (1308.6508), Trc B1 (1322.6615), Trc C (1347.6705), Trc C1 (1361.6777) with Tpc A (1292.6454), Tpc B (1331.6632), Tpc C (1370.6812) and Tpc C1 (1384.6754). The Trcs readily forms homo-and hetero-dimers based on the peptide analogues present in the peptide extract.

5.4.1 Probing the Trc oligomerisation with acetonitrile

5.4.1.1 Ion-mobility mass spectrometry of oligomers in acetonitrile

High resolution ESI-MS is not only used to confirm the identity of compounds but can be used to detect the formation of higher order oligomers as depicted in Figure 5.1: A. ESI-MS coupled with ion-mobility (IM-MS) allows for the separation of these oligomers so that the formation, size and conformation (cross collisional surface, CCS) thereof can be studied. To better study the self-assembly that occurs with the increase of acetonitrile, the percentage contribution to the total signal was calculated for the monomer, dimer and oligomer species. Table 5.1 shows a summary of the possible *m/z* values of dimeric species that can be observed within a Trc mix sample. Singly charged monomeric species $[M + H]^+$ will have a similar *m/z* value as doubly charged homo-dimeric species $[2M + 2H]^{2+}$. However, these two species are separated within the IM-MS profile and can therefore be distinguished from each other.

Table 5.1: Summary of possible doubly charged dimeric species $[2M + 2H]^{2+}$ of the six major tyrocidines found with in Trc mix. Also note the overlapping *m/z* values of doubly charged dimeric species $[2M + 2H]^{2+}$ (indicated in bold font).

	Trc A (1270.66)	Trc A1 (1284.68)	Trc B (1309.67)	Trc B1 (1323.69)	Trc C (1348.68)	Trc C1 (1362.70)
Trc A	1270.62					
Trc A1	1277.67	1284.68				
Trc B	1290.17	**1297.18**	**1309.67**			
Trc B1	**1297.18**	1304.18	**1316.68**	**1323.69**		
Trc C	**1309.67**	**1316.68**	1329.18	**1336.19**	1348.68	
Trc C1	**1316.68**	**1323.69**	**1336.19**	1343.19	1355.69	1362.70

There is an overlap between the doubly charged dimeric species $[2M + 2H]^{2+}$ were 11/22 combinations of the six major tyrocidines result in similar *m/z* values and cannot be differentiated e.g. Trc B:Trc B and Trc A:Trc C (Table 5.1, Figure 5.2). Many of the dimeric

species could be separated, but some of the major dimers such as Trc B-Trc B and Trc A-Trc C both with *m/z* = 1309.67 had similar ion mobility drift times (Figure 5.2). Important to note is that the IM-MS profiles are expressed in percentage signal and therefore a ratio between the signal detected for the monomer and dimer specie at each *m/z* range. Therefore, no direct comparisons can be made between each *m/z* range based on the peak height of each of the species. Furthermore, with the formation of higher order oligomers the overlapping *m/z* values increases, complicating the correct identification of tyrocidines and analogues present in the oligomer. Due to the complexity of the peptide complex and the range of possible tyrocidine combinations that could be present within the oligomers, all the species were studied as a grouping rather than looking at each individual combination of analogues.

The 48-hour incubation of Trc mix in 80% ACN is shown as a representative example of the IM-MS analysis of oligomerisation in Figure 5.3. The peak area of each species was determined by acquiring the peak area from the chromatogram of a calculated *m/z* range as was observed from the IM-MS profile (Figure 5.3: A). The doubly charged monomer $[M+2H]^{2+}$ (*m/z* = 634.781 to 695.20)(Figure 5.3: B) yielded a drift peak at 3.41 (CCS =377-394 Å) with a MS spectrum showing the six main analogues present in Trc mix (expected/observed): Trc A (634.8275/634.8200, CCS = 377 Å), Trc A1 (641.8354/641.8310, CCS = 380 Å), Trc B/B' (654.3330/654.3353, CCS = 385 Å), Trc B1/B' (661.3408/661.3405, CCS = 386 Å), Trc C (673.8384/673.8393, CCS = 386 Å) and Trc C1 (680.8463/680.8450, CCS = 394 Å). The singly charged monomers $[M + H]^{+}$ and doubly charged dimers $[2M + 2H]^{2+}$ were detected by using the same set of parameters (*m/z* = 1270.50 to 1364.85) which yielded an ion profile with drift peaks at 6.82 (CCS = 550 - 569 Å) and 11.22 (CCS = 377 - 394 Å) (Figure 5.3: C). The spectra for the singly charged monomers showed the six main analogues present in Trc mix (expected/observed): Trc A (1269.6546/1269.6572, CCS = 377 Å), Trc A1 (1283.6703/1283.6735, CCS = 380 Å), Trc B/B' (1308.6655/1308.6791, CCS = 385 Å), Trc B1/B' (1322.6812/1322.6858, CCS = 386 Å), Trc C (1347.6764/1347.6816, CCS = 386 Å) and Trc C1 (1361.6921/1361.7014, CCS = 394Å). Comparison of the MS spectra obtained for the doubly charged dimers showed the presence of the major tyrocidines and species that represents the heterodimers formed within the sample. Triply charged tetramers were also detected at *m/z* = 1693.5 to 1802.00 with a peak at 7.15 (CCS = 827 - 899 Å) (Figure 5.3: E) and doubly charged trimers and quadruply charged hexamers at *m/z* = 1905.30 to 2026.70 with peaks at 6.82 (CCS = 676 - 724 Å) and 10.67 (CCS = 1086 - 1262 Å), respectively (Figure 5.3: F). The size of the oligomers that were supplied, was determined with the use of peptide standards and

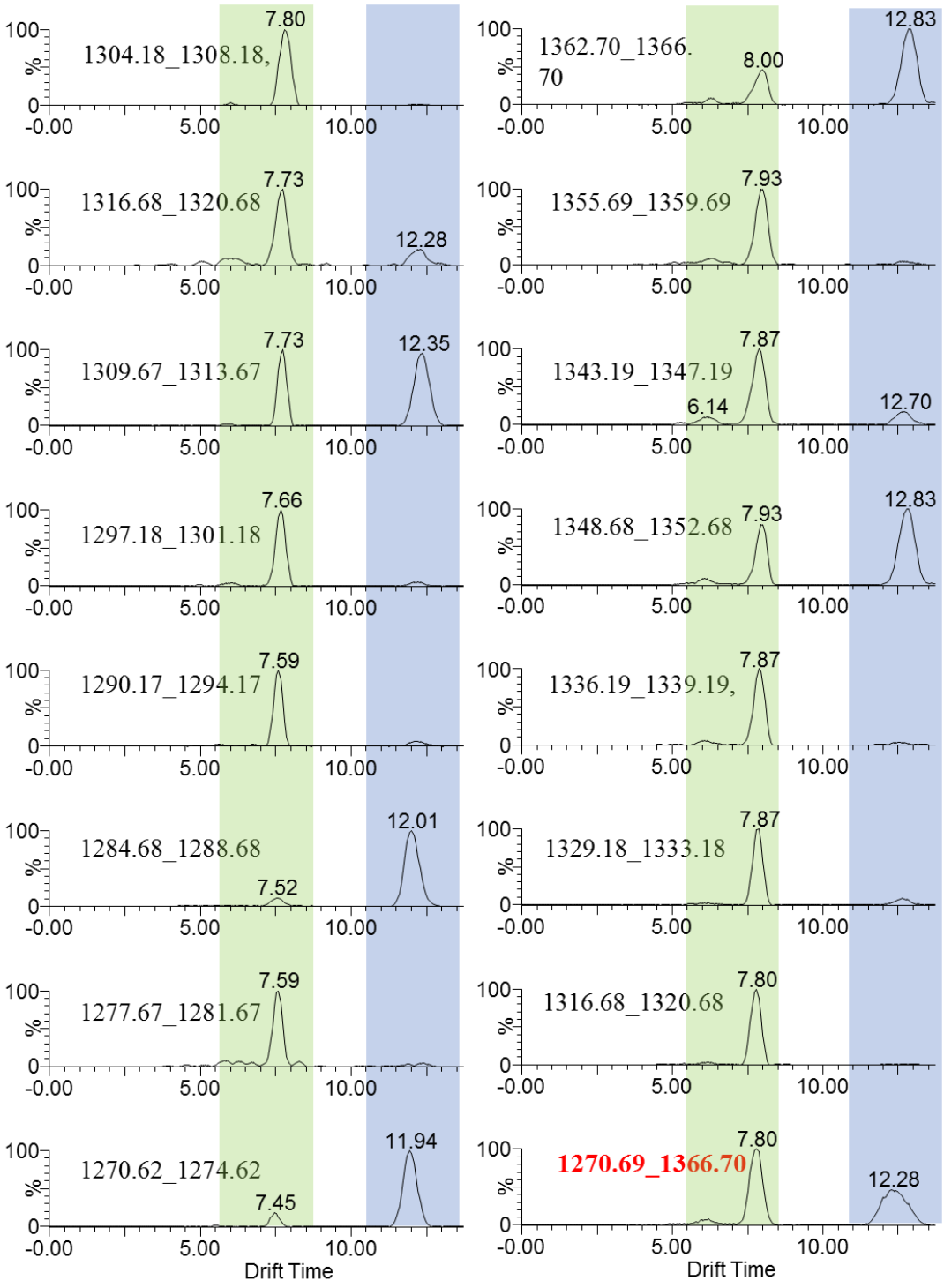

Figure 5.2: IM-MS profiles of the Trcs oligomerisation as a practical visualisation of Table 5.1. The green band shows the dimers, blue the detected monomers and the numbers next to the profiles are the *m/z* range of the extracted molecular ion profiles. The final profile in red is the sum of all the monomers and dimers of the six major tyrocidines. Profiles were compiled from a Trc mix sample in 30% *v/v* acetonitrile.

the size expressed as cross collisional surface (CCS). Typically, poly-alanine is used as the protein standard and even though it is a linear peptide, it has been successfully used to determine the CCS of cyclic peptides, gramicidin S and those in the surfactin complex (Rautenbach et al., 2017) and to set up a BIOPEP^{TM} database of CCS values of the peptides and oligomers in the Trc mix.

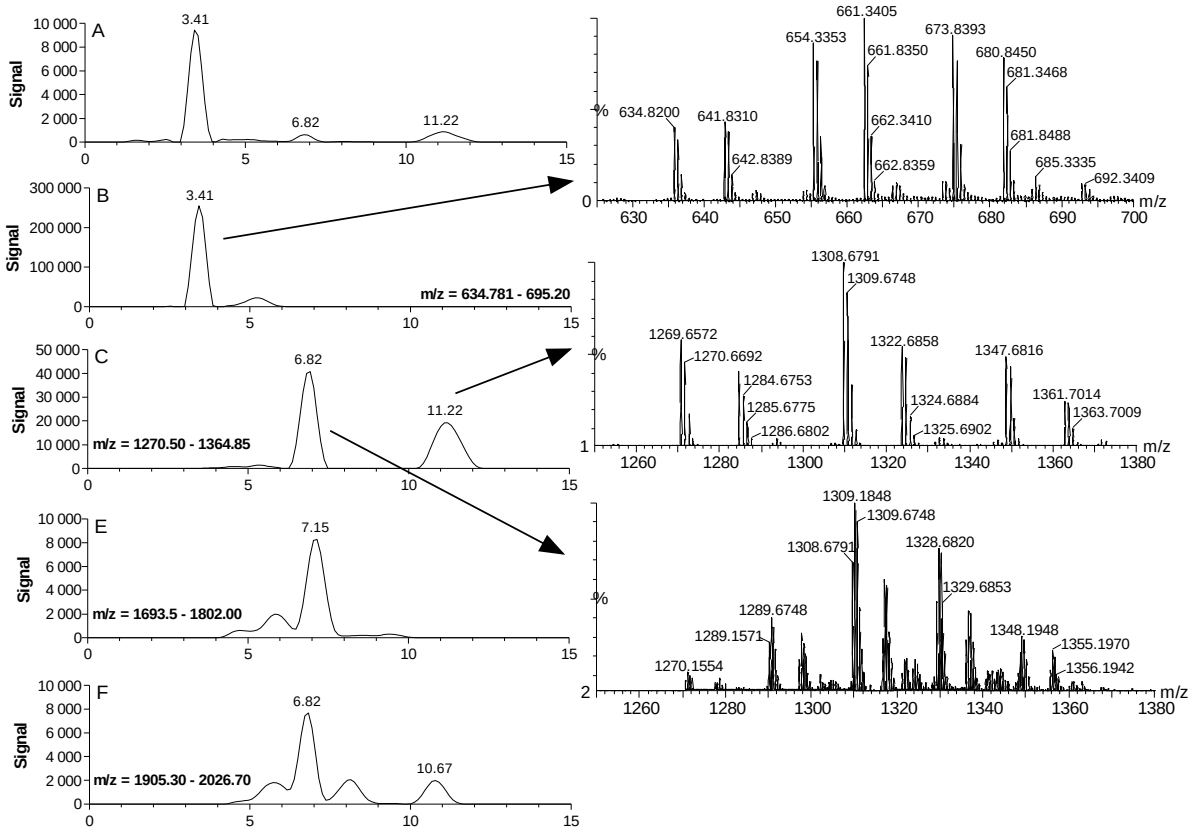

Figure 5.3: IM-MS profile of the species detected for (**A)** Trc mix (0.100 mg/mL) in 80% acetonitrile, (**B)** doubly charged monomeric Trc mix, $[M+2H]^{2+}$ (**C)** singly charged monomeric Trc mix, $[M+H]^{+}$, and doubly charged dimeric Trc mix $[2M + 2H]^{2+}$ and (**E&F)** oligomeric species. The ESI-MS spectra of the monomeric and dimeric species are shown with its corresponding ion profiles.

CCS is used to determine the conformation and 'tightness' of an oligomer and the association between subunits of the oligomer. IM-MS in this study was primarily used to study the formation of oligomers, rather than the size of the oligomers, therefore, the CCS values will only be discussed briefly. It is interesting to note that CCS values do not double from monomer to dimer to tetramer but there is an incremental increase that indicates a tight packing and association of the peptide molecules in an oligomer. This and the fact that the oligomers survive

the harsh conditions in the mass spectrometer could also relate to their thermal stability discussed in Chapter 3 and hereafter.

To study the influence of ACN on the stable oligomers formed by Trcs further, Trc mix (0.1 mg/mL) was incubated in a range of acetonitrile concentrations (5-90%) for 24 hours (Figure 5.4). Direct comparison of the Driftscope profiles of 5% and 50% acetonitrile showed the effect of both acetonitrile and time on the formation of oligomers. At 5% acetonitrile (Figure 5.4: A) the major observed species was (a) singly charged monomers (b) doubly charged dimers and (c) doubly charged monomers. However, at 50% acetonitrile (Figure 5.4: B) higher order oligomers (d-f) where detected, of which the signal intensified after an increased incubation time (data not shown). A 3D representation of the profile observed for 50% acetonitrile (Figure 5.4: C) shows the signal intensity of the singly charged monomers, doubly charged dimers and doubly charged monomers. A summary of the percentage contribution of the species found for all the acetonitrile concentrations after the 24-hour incubation period can be found in Figure 5.4: D. At 24 hours (Figure 5.4: D) an increase in doubly charged dimers and singly charged monomers were observed with a decrease in doubly charged monomers. Both reached a plateau at 50% acetonitrile. Signals of larger oligomers significantly increased around 40% acetonitrile and higher, and the percentage contribution remained stable throughout the remaining acetonitrile concentrations. It is important to note that during IM-MS analysis all solvent molecules are removed, enhancing the polar interactions (dipole- and ionic-interactions, as well as hydrogen bonds) and negating the hydrophobic effect (Bich et al., 2010; Daniel et al., 2002; Wu et al., 1997). Therefore, the IM-MS results are assessed based on what is not present rather than what can be detected in the solution. There were very low levels of oligomers detected at 5 - 30% acetonitrile. The reason for this can be that that most of the oligomers were lost due to the loss of the hydrophobic effect *in vacuo,* the oligomers settled out of solution or they were too big to detect with the IM-MS method parameter set. The tyrocidines are known to aggregate in aqueous solutions (Munyuki et al., 2013) presumably through hydrophobic interactions which would not survive the process of IM-MS analysis. Thus, the absence of very low abundance of oligomers at 5 - 30% acetonitrile, suggests that the bulk of oligomerisation/aggregation that does occur in more aqueous solvents is mediated through hydrophobic interactions.

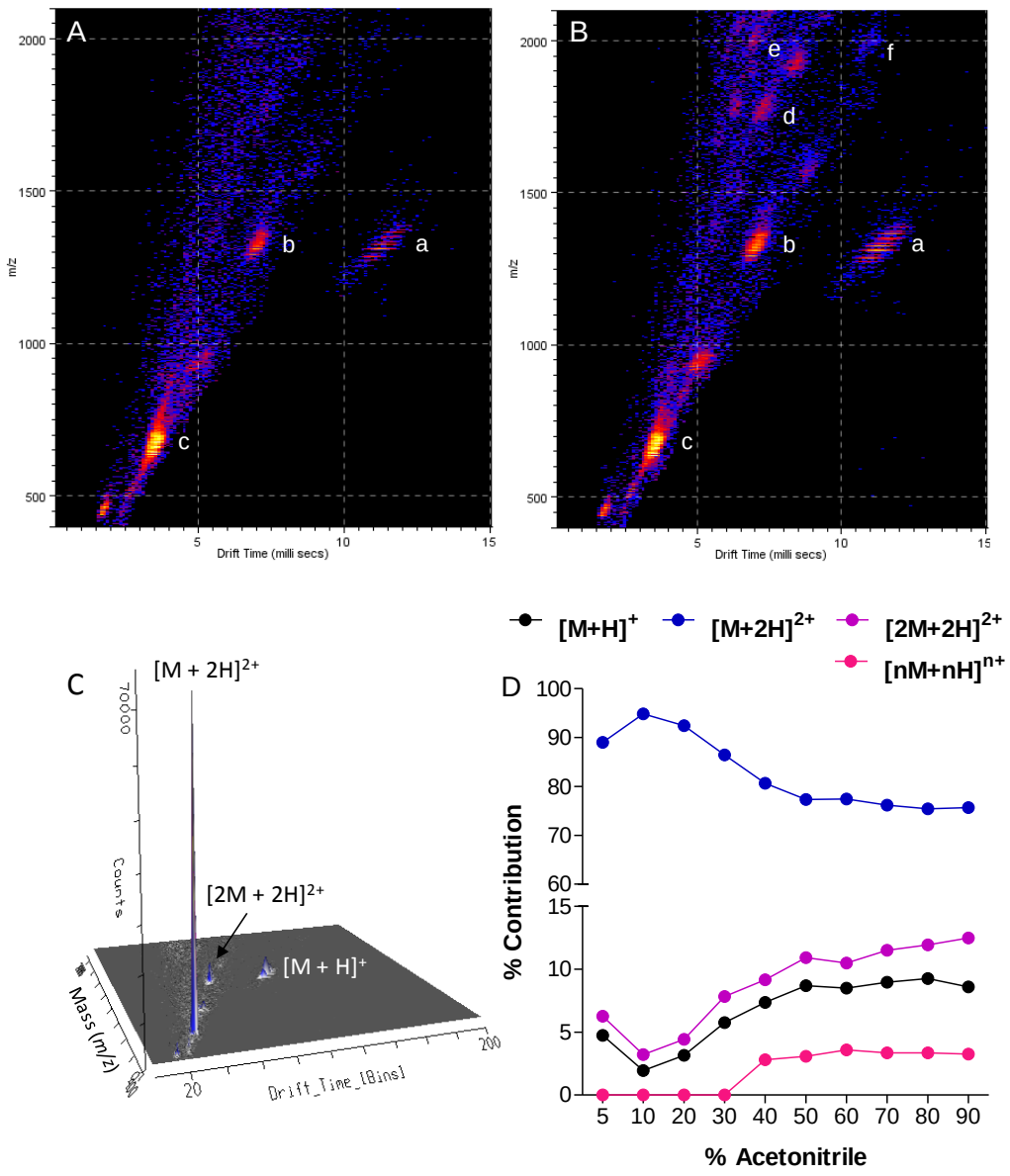

Figure 5.4: IM-MS of Trc mix in different concentrations of acetonitrile. Driftscope profiles with the x-axis of drift time (milli seconds) and y-axis of *m/z*. The profiles represent Trc mix (0.100 mg/mL) incubated in **(A)** 5% acetonitrile for 24 hours **(B)** 50% acetonitrile for 24 hours. Observed species (a) singly charged monomeric $[M+H]^+$ (b) doubly charged dimeric $[2M + 2H]^{2+}$ (c) doubly charged monomeric $[M+2H]^{2+}$ and (d-f) oligomeric species. **(C)** 3D profile of 0.100 mg/mL Trc mix in 50% acetonitrile with drift time on the x-axis, *m/z* on the y-axis and signal intensity (counts) on the z-axis. **(D)** Summary of the percentage contribution of each of the oligomer species observed after 24-hour incubation of Trc mix (0.100 mg/mL) in different acetonitrile concentrations.

5.4.1.2 Circular dichroism to follow hydrogen bonding in oligomers

Collaborative research was done with Prof. Burkhard Bechinger at the Strassbourg University on the structural changes that occur with Trc A with the increase of organic solvents (Juhl et al., 2019)(Chapter 4 – Addendum). It was observed with circular dichroism (CD) (Figure 5.5:

A) that the addition of organic solvents leads to an increase in hydrogen-bonded structures as seen with the deepining of the ellipticity signals at 206 nm and 216 nm, and increase in ellipticity at 196 nm. The spectra of Trc A in 15% *v/v* acetonitrile shows a loss of ellipticity pointing to loss of structure or peptide falling out of solution due to the formation of large aggregates/oligomers. This correlates to the lack of oligomers visible with IM-MS at low acetonitrile concentrations. Furthermore, it was observed that 60% *v/v* acetonitrile had a similar spectrum to trifluororethanol (TFE) which is a membrane mimetic solvent (Rajan and Balaram, 1996) that supports hydrogen bonding. Closer inspection of the ratio between 206 nm and 216 nm, as a β-turn and β-sheet respectively (Laiken et al., 1969), shows a change in aggregation/oligomerisation with the increase in organic solvent (Figure 5.5: B) with specific effect on the β-turns at 206 nm as seen with the lower $\theta_{206}/\theta_{216}$ ratio at low concentrations of organic solvent.

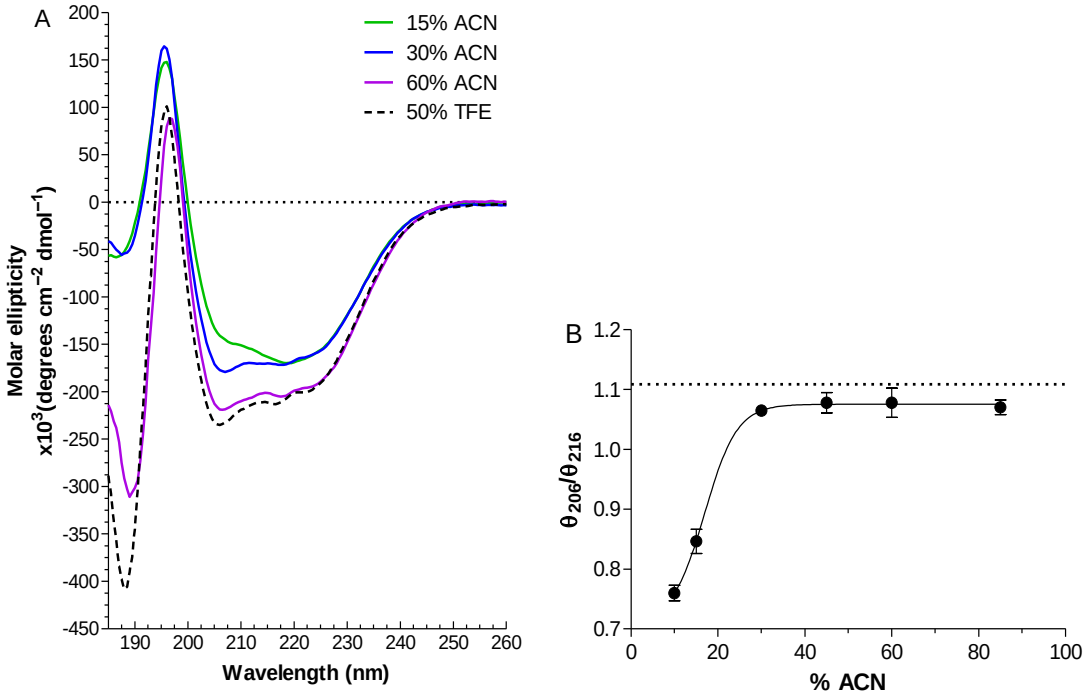

Figure 5.5: **(A)** CD spectra depicting the influence of percentage *v/v* acetonitrile (% ACN) (15%, 30%, 60%) and 50% *v/v* trifluoroethanol (TFE) on the overall ellipticity of 250 µM Trc A. Each spectrum represents the average of six background corrected spectra with smoothing performed over six neighbours. **(B)** Ellipticity ratio of $\theta_{206}/\theta_{216}$ of TrcA as influenced by the %ACN in the peptide solution.

5.4.1.3 Fluorometric analysis of the effect of acetonitrile on peptide behaviour

Fluorescence scans were taken of the aromatic amino acids at Ex_{280} and $Ems_{300\text{-}400}$ of the peptide complex (Trc mix, 50 µg/mL) incubated with a range of acetonitrile concentrations at room temperature for one hour. The spectra obtained (Figure 5.6: A) clearly show a gradual red shift and quenching of fluorescence signal with reference to 50% *v/v* acetonitrile. The same is observed for the higher acetonitrile concentrations (Figure 5.6: B), where a gradual blue shift and quenching is observed with reference to the 50% acetonitrile sample. To ease the comparison between each of the acetonitrile concentrations the percentage quenching and shift in wavelengths were summarised in one graph (Figure 5.6: C). Based on the quenching of the peptide signal and the shift in λ-max the peptide behaviour can be grouped into three stages. First, slight de-quenching or no-change compared to the 50% acetonitrile signal was observed for the 60% and 70% acetonitrile samples respectively. The second stage, 5% to 40% acetonitrile, shows a gradual signal quenching up to half of the signal lost and red shift. The last stage, 80 to 95% acetonitrile showed some quenching and a blue spectral shift.

The red shift and quenching observed for 5% to 40% acetonitrile can be attributed to the collisional quenching occurring between the solvent (water) and excited indole group of the Trp-residue (Chattopadhyay and Raghuraman, 2004; Chen and Barkley, 1998; Lakowicz, 2013). Furthermore, it has been shown that the Trcs aggregates/oligomerises in aqueous solutions and are stabilized by the π-bonds between the aromatic amino acid residues (Munyuki et al., 2013). This could result in a decrease in fluorescence due to ground state complex formation. Increased quenching therefore shows increased interaction between the aromatic amino acids, which translates to the increase in the formation of higher order oligomers driven by hydrophobic interactions with the decrease in acetonitrile concentration. Previously the interaction between aromatic residues was not thought to be directly responsible for aggregation (Ruttenberg et al., 1966), but our IM-MS and fluorescence studies indicate that the aromatic residues have a major role in oligomerisation in aqueous solvents. The blue shift observed for 80% to 95% acetonitrile can be attributed to the decrease in solvent polarity with the increase in acetonitrile concentration (Lakowicz, 2013). The quenching that occurs with the increase in acetonitrile could be due to a rearrangement of the peptide aggregates/oligomers with aromatic residues being in more hydrophobic environment, but in proximity to a quenching group.

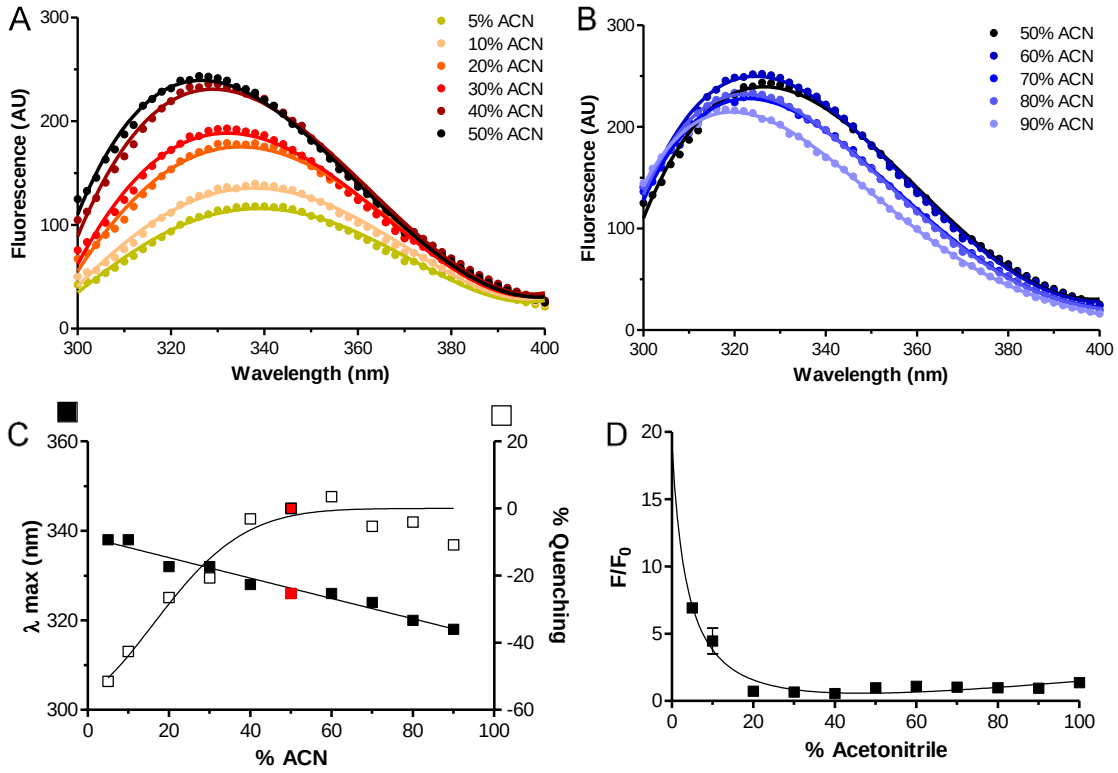

Figure 5.6: Monitoring the influence of acetonitrile on the fluorescence of Trc mix. Fluorescence scans of 50 µg/mL Trc mix at Ex_{280} and $Ems_{300-400}$ incubated in **(A)** 5 - 50% *v/v* acetonitrile and **(B)** 50 - 95% *v/v* acetonitrile. The data has been background fluorescence subtracted and are the average of four technical repeats. **(C)** Relationship between percentage change in RFU (right y-axis) and the wavelength shift of the peptide spectra (λ-max)(left y-axis) after incubation in a range of acetonitrile concentrations. The red block in both graphs indicate 50% *v/v* acetonitrile as reference for the 'optimal conditions'**(D)** The aggregation/oligomerisation of Trc mix (50 µg/mL) in different acetonitrile concentrations as studied by the incorporation of ANS into the hydrophobic areas of the self-assembled structures. The data represents the mean and SD of

The aggregation of Trc mix was also studied by incubating the peptide with ANS in acetonitrile, ranging from 5 - 95%, and determining the change in fluorescence. ANS works on the basis that when it inserts into hydrophobic pockets of a protein or aggregate, a shift in maximum fluorescence (λ-max) is combined with an increase in total fluorescence signal (Kumar and Mishra, 2015). Additionally, an increased hydrophobic environment such as higher concentrations of acetonitrile would also result a λ-max shift and increased fluorescence of the ANS itself. Therefore, the fluorescence detected for the peptide was expressed as a function of the background ANS fluorescence (F/F_0)(Figure 5.6: D). It was observed only at 5 and 10% acetonitrile that there was a marked increase in fluorescence of the ANS indicating notable aggregate formation/self-assembly. The increase of fluorescence is dependent on both the incorporation of ANS and the sensitivity of the detection and therefore does not exclude

aggregation formation at the higher acetonitrile concentrations, but merely highlights the extent of aggregation formation and hydrophobic driven aggregation. The formation of aggregates driven by hydrophobic interaction at low concentrations of acetonitrile confirms what was observed with fluorescence quenching at the same concentration of acetonitrile. It also correlates with IM-MS hypothesis, that the oligomers formation in the aqueous solvents is based primarily on hydrophobic interactions.

5.4.1.4 Temperature effect on peptides and oligomers in acetonitrile

We previously found that the Trc mix and peptide treated cellulose is highly heat stable up to nearly 200ºC (Chapter 3). The thermal stability of Trc mix oligomers was determined over a range of acetonitrile concentrations. As the boiling point of water at sea level is 100ºC and acetonitrile is 82ºC, we were unable to proceed above 95ºC and only considered the fluorescence detected melting curve up to 80ºC in Figure 5.7: A. The melting curves were atypical (Mondini et al., 2011) and showed a gradual decrease in signal for 50.0 µg/mL Trc mix in 95% and 90% acetonitrile, followed by a sharp increase in signal with a complete loss of signal at 36ºC and 48ºC for 95% and 90% acetonitrile respectively (Figure 5.7: A). It is interesting to note that the change in a more hydrophobic solvent system is close to 37ºC, which may have relevance to the oligomerisation or dissociation within membranes of living cells. Similar results were observed for 50-80% acetonitrile, with the loss of signal occurring around 70-74ºC (Figure 5.7: A). No sudden increase or loss in signal was observed for 5-40% acetonitrile but the melting profile only showed a gradual decrease in signal, as previously also found for the samples at room temperature (refer to discussion later). Nearly identical profiles for the Trc mix in different acetonitrile concentrations was observed at Em_{320} (results not shown). Temperature is known to influence fluorescence intensity (Lakowicz, 2013) and would therefore explain the gradual decrease in signal with increase in temperature. Only the complete loss of signal is considered as a temperature induced change in oligomerisation. The observed sudden loss of signal could be the full dissociation of oligomers leading quenching due to exposure of the Trp and Tyr residues to water or water-acetonitrile clusters in the environment (Lakowicz, 2013). However, an anomalous increase in fluorescence was seen before the signal loss at 50-95% acetonitrile, which in combination with the total loss of signal may indicate another type of event, namely precipitation. This was further analysed by assessing the light scatter of the samples over the temperature ramp (Figure 5.7: C and D). Comparison of fluorescence signal intensities at each of the acetonitrile concentrations at set temperature points (Figure 5.7: B), ranging from 20ºC to 95ºC, showed three transitions in terms of stability.

The first is 5-40% acetonitrile, followed by 50-80% acetonitrile and last 90-95% acetonitrile. Inspection of light scattering of the Trc mix in different acetonitrile concentrations over 20-95^{o}C (Figure 5.7: C) showed the stability of the oligomer size (no change in light scattering) in 5-40% acetonitrile, whereas from 50-95% there was an increase in light scattering at the high temperatures. This light scattering correlated with the results in Figure 5.7: A and indicated that rather than dissociating the peptides, high acetonitrile concentrations combined with temperature increase induces the formation of large aggregates leading to light scatter.

As discussed in Chapter 3, the peptide is heat stable to 190ºC therefore none of the changes observed can be due to peptide degradation. Previous studies done in aqueous solutions, showed that aggregation is not effected by temperature unless a high peptide concentration is used (Appleby et al., 1947; Paradies, 1979). This confirms the stability observed for both the fluorescence and light scattering of the 5-40% acetonitrile samples. IM-MS detected very low amounts of larger oligomers for the Trc mix in 5-30% acetonitrile. As this *in vacuo* analysis removes all oligomers formed via hydrophobic interactions (Bich et al., 2010; Daniel et al., 2002; Wu et al., 1997), we can assume that the bulk of oligomers were dependent on hydrophobic interactions, possibly aromatic stacking. The fluorescence and ANS study confirmed the formation of oligomers formed based on hydrophobic interactions which has been reported in literature (Ruttenberg et al., 1965). The decay in fluorescence detected for 50-80% acetonitrile with increasing temperatures is characteristic for precipitation which also correlates to the increased light scattering observed. IM-MS showed increased formation of hydrogen-bonded oligomers which is characteristic for the Trcs at higher concentrations of organic solvent (Juhl et al., 2019; Munyuki et al., 2013). These results confirm two distinct types of oligomerisation/aggregation: the one driven by hydrophobic interactions which is stabilized by aromatic amino acid stacking and aliphatic amino acid interactions, which is much more thermostable compared to the second type of the hydrogen-bonded oligomers.

As we were unable to use classical analysis of the atypical thermal melting curves, we considered acetonitrile as a denaturant. These transitions can be better observed when the 50% change in light scattering over the temperature range is correlated with the concentration of acetonitrile (Figure 5.7: D). There are three transition temperatures that result in a change in light scattering: minor transitions at 36.2ºC and 49.6ºC, and major transition at 72.9 ºC, with the latter between 45% and 85% acetonitrile.

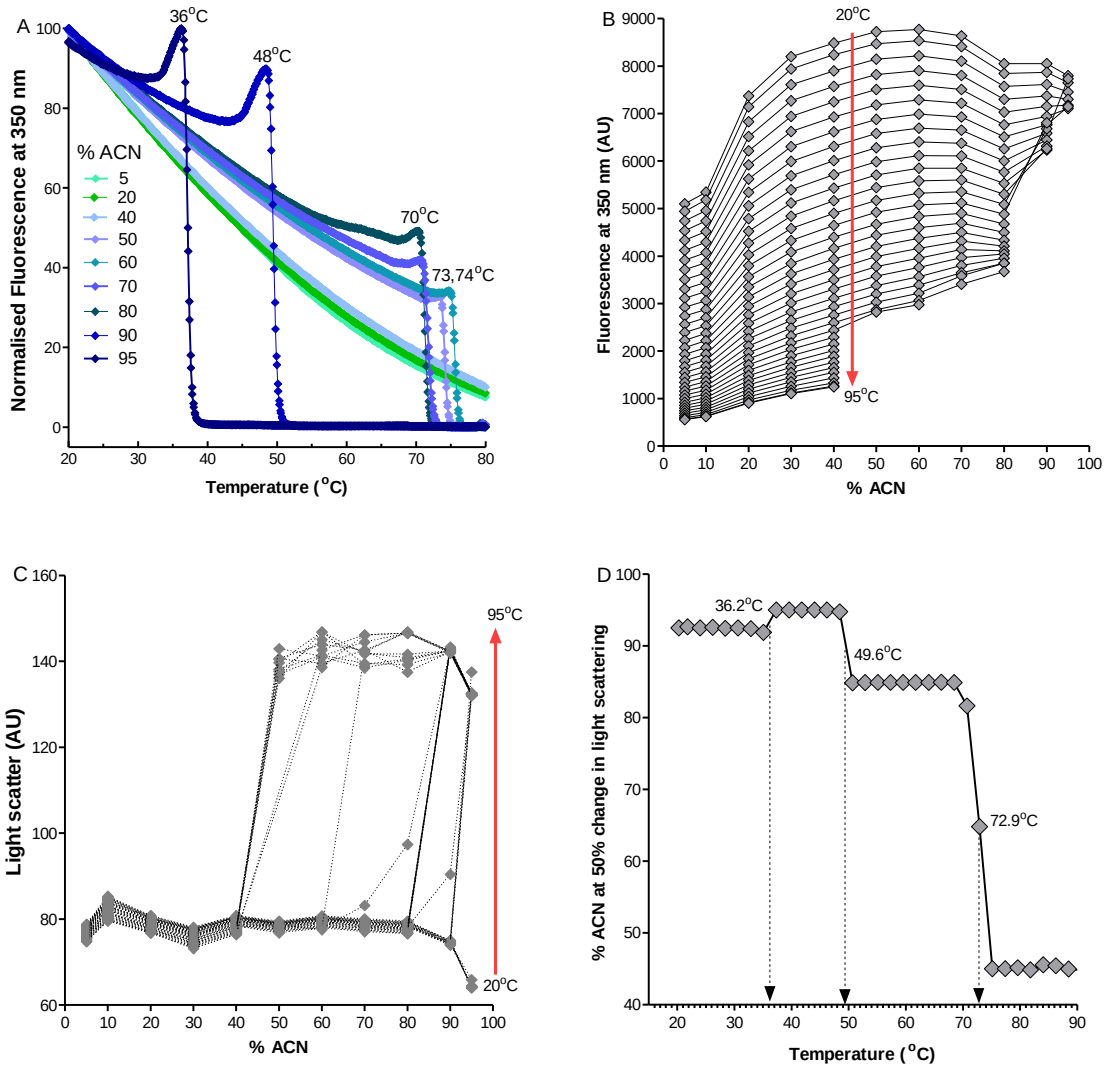

Figure 5.7: Thermal stability of oligomers in Trc mix (0.100 mg/mL) at different acetonitrile concentrations **(A)** Melting curves as normalised fluorescence monitored at 350 nm over temperature form 20 ºC to 80 ºC **(B)** Change in fluorescence at 350 nm for each of the acetonitrile concentrations at set temperatures with 20ºC as the top fluorescence values, through to 95ºC as the lowest fluorescence detected. Only datapoints where fluorescence was observed are shown. Each datapoint is the average of 23 fluorescence measurements over 1 ºC temperature change. **(C)** Changes in light scatter detected for each of the acetonitrile concentrations over time. Each datapoint is the average of 23 measurements over 1 ºC temperature change. **(D)** Acetonitrile profile for 50% change in light scatter over the set temperature changes showing three thermal events. Data to determine the acetonitrile concentration for 50% light scatter were derived from sigmoidal curve fits to the light scatter data in C.

The hydrophobic force driving aromatic stacking would be less in high acetonitrile concentrations and therefore the majority of oligomers are proposed to be hydrogen-bonded in correlation with our IM-MS and CD studies. The first two transitions may therefore be the loss of interpeptide hydrogen bonds and weak polar interactions, possibly those that side chains (i.e. Orn, Lys, Gln, Asn, Tyr and Trp) participate in. As we analysed a mixture of peptides different in aromatic amino acids, those with Tyr and to lesser extent Trp would have an extra group that could participate in polar bonds possibly leading to the two transitions. The third transition may be related to all the peptides as β-sheet type hydrogen bonds, as indicated by CD (see above) and IR analysis (Chapter 4). It has been shown that β-sheets unfold around 60-70ºC (Brown et al., 2002; Wu et al., 1992) which can shift depending on the effect that the environment/solvent system has on the β-sheet stability (Markovic-Housley and Garavito, 1986). The loss of β-sheet structures between 85% and 45% acetonitrile at high temperatures and the stability of the structures in the lower acetonitrile concentrations correlates to what has been reported with CD under the same acetonitrile concentrations. This shows a change in the hydrogen bonded structures that occur within the peptide oligomerisation at high acetonitrile concentrations to more hydrophobic self-assembled oligomers at low acetonitrile concentrations which appears to be more temperature stable.

5.4.2 Probing Trc-cellulose interaction with acetonitrile

5.4.2.1 Trc-cellulose dissociation and desorption by acetonitrile

The study on the dissociation of the peptide was done by incubating cellulose disks pre-treated with 50.0 µg/mL with the same range of acetonitrile as was tested for the association study. Any change in fluorescence signal at Ex_{290}, Em_{342} was directly correlated to peptide being released from the cellulose. The parameters are optimised to detect tryptophan which was the most sensitive and gave the best linear relationship between fluorescence and peptide concentration (Chapter 3 – Supplementary data). Even though there are two other fluorophores, the assumption is that the different tyrocidines would associate and dissociate in a similar fashion. This assumption is based on desorption of Trc mix from cellulose in 50% acetonitrile that yielded similar ratios of each of the tyrocidine and tyrocidine analogues present in the peptide fraction used to treat the cellulose (Van Rensburg, 2015). Furthermore, Phe has a very low quantum yield in a peptide (Lakowicz, 2013), and was not observed above the background in Trc mix dilutions (data not shown).

Two observations where made from the desorption curves obtained (Figure 5.8: A&B). First, the plateau or maximum release of peptide was reached within 15 minutes of incubation for all the conditions, and second this plateau was followed by a decrease in signal. This decrease is either due to aggregation, association to the plate or re-association to the cellulose. Direct comparison of the fluorescence signals showed a gradual increase of peptide release (Figure 5.8: C) and rate of release with an increase of acetonitrile (Figure 5.8: D) peaking at 60% *v/v* acetonitrile. Whereas, 5%, 10% and 95% *v/v* acetonitrile can be concluded as not resulting in desorption, or negligible levels of desorption. When comparing the rates of desorption, there is a clear grouping of conditions that cause desorption (40-80% acetonitrile) and conditions that do not (5-20% and 90-100% acetonitrile). The rate of fluorescence decay at 20ºC to 37ºC (Figure 5.8: D), from the Figure 5.7:A before any thermal events, shows a similar curve with slower rates of decay for 5-10% and 90-95% acetonitrile. This correlates to the decrease in signal observed for the desorption study (Figure 5.8: A&B) after the initial desorption. Considering that the thermal study was completed in glass in the absence of any cellulose, it is possible that the decrease is due to aggregation which also suggests that the decrease observed in the desorption study would also be as a result of aggregation rather than association to the plate or cellulose.

Assessing the remaining antimicrobial activity of these acetonitrile treated cellulose disks against *L. monocytogenes* (Chapter 3) showed 70% *v/v* acetonitrile as the only statistically significant disruption of activity, with possible disruption occurring at 60% *v/v* acetonitrile. This compares well with what was seen with the desorption as determined with fluorescence. The amount of peptide bound to each cellulose disk can be determined to some degree but is not exact and therefore the desorption of peptide was only determined as an increase of fluorescence signal. The peptide signal at 70% *v/v* acetonitrile is compared to 50% and 60% *v/v* acetonitrile and therefore the amount of peptide desorbed (as detected in Figure 5.8: C) at 60% and 70% *v/v* acetonitrile could be equal or more. Thus, more peptide could have been removed that what was originally observed.

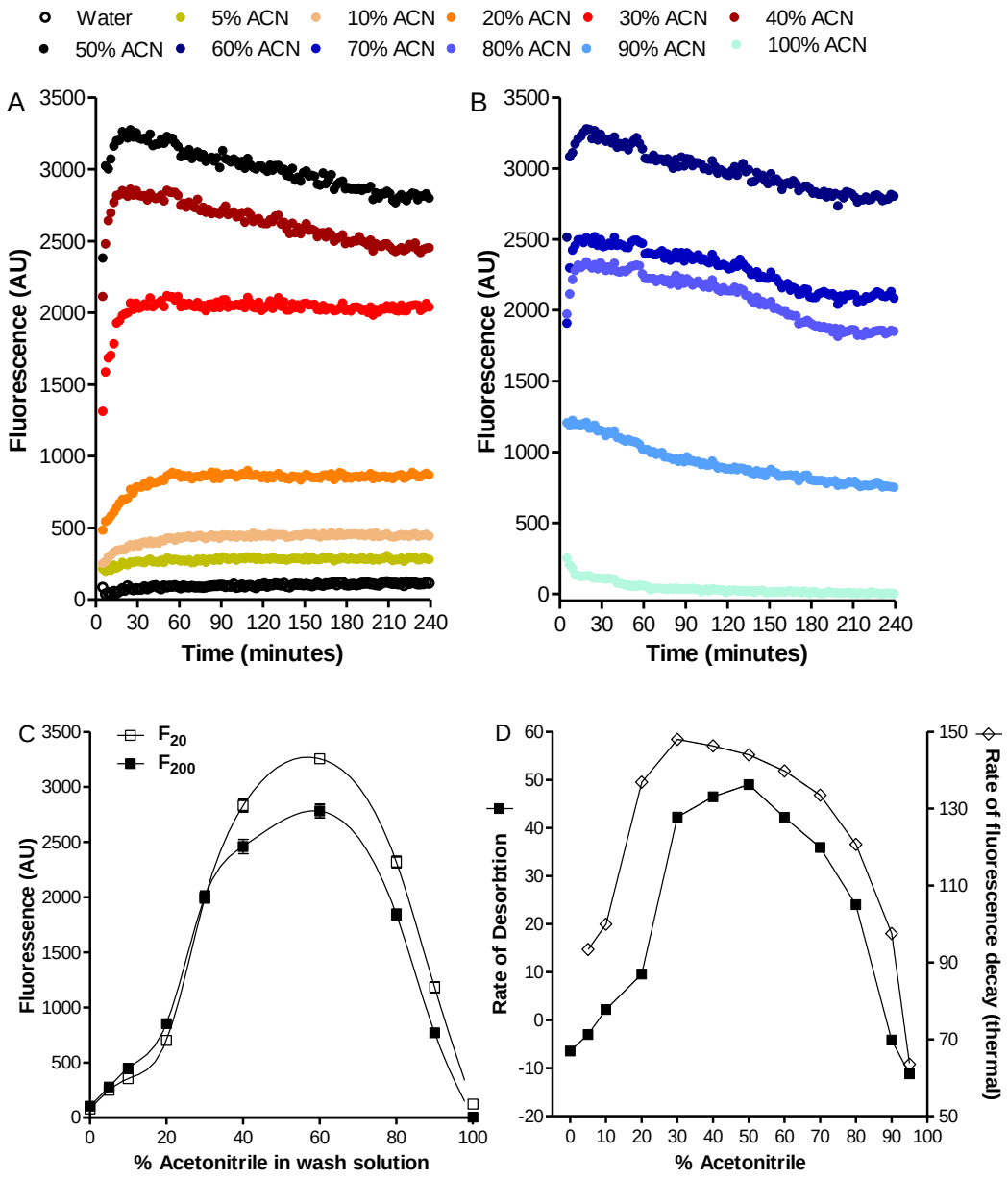

Figure 5.8: Influence of acetonitrile on Trc dissociation/desorption. Increase in fluorescence at Ex_{290}, Ems_{342} of cellulose pre-treated with Trc mix in the presence of **(A)** 5%-50% *v/v* acetonitrile and **(B)** 60%-95% *v/v* acetonitrile. Each data set is the average of four technical repeats and blank/background subtracted. **(C)** Comparison of fluorescence at 20 minutes (F_{20}) and 200 minutes (F_{200}) of 5% - 95% acetonitrile **(D)** Rate of peptide desorption in comparison with the rate of fluorescence thermal decay of the free peptide. The peptide desorption rate was calculated from the slope (first 15 minutes of incubation) of the binding curves of cellulose pre-treated with Trc mix in the presence 5-95% *v/v* acetonitrile. The rate of fluorescence thermal decay of the free peptide was calculated over 20-37°C from data in Figure 5.7: A. All the other data are the average of four technical repeats and blank subtracted.

5.4.2.2 Trc-cellulose association influenced by acetonitrile concentration

The peptide (50 µg/mL) was incubated with range of acetonitrile concentrations (5-95%) and incubated with cellulose disks. It was observed that at 5% and 10% acetonitrile the peptide readily binds to the cellulose which starts to slow down at 20% (Figure 5.9: A). At 30% and 40% acetonitrile only 10% of the available peptide is binding to the cellulose. Anything higher than 50% acetonitrile, the peptide does not bind to the cellulose or at least not according to the change in detectable fluorescence (Figure 5.9: B). At 95% acetonitrile a decrease in fluorescence can be observed, followed by an increase in fluorescence signal. This could be due to a combination between peptide association to the cellulose, dequenching of the Trp and/or acetonitrile evaporation. Assessing the activity of these treated cellulose disks against *L. monocytogenes* (Figure 5.9: C) there is a noteworthy change in activity between 50-90% acetonitrile samples, with 60-90% acetonitrile samples showing statistically significant changes. Interestingly there is inverted bell shape trend in the disruption of activity with 80% acetonitrile as the point of the most disruption and this weakest association with cellulose. Drawing comparison between the antimicrobial activity and fluorescence decease (Figure 5.9: D), expressed as a ratio between the initial (F_5) and final (F_{200}) fluorescence, the peptide binding conditions can be grouped into optimal (5-20% acetonitrile), intermediate (30-50% acetonitrile) and low-binding (60-90% acetonitrile). This correlates to the low levels of oligomers observed with IM-MS for 5-30% acetonitrile with the highest signal detected with ANS at 5-10% acetonitrile, suggesting that an oligomer formed driven by hydrophobic interactions would result in the fast association of peptide to cellulose. However, this does not disqualify any of the other conditions as seen with the activity for 50% acetonitrile samples as very low levels of peptide on the cellulose surface are required for full inhibition of *L. monocytogenes* (Chapter 4). Therefore, any intermediate conformation between fully hydrophobic driven oligomers and more hydrogen-bonded oligomers still allowing for some association of the peptide to cellulose would elicit some antimicrobial response.

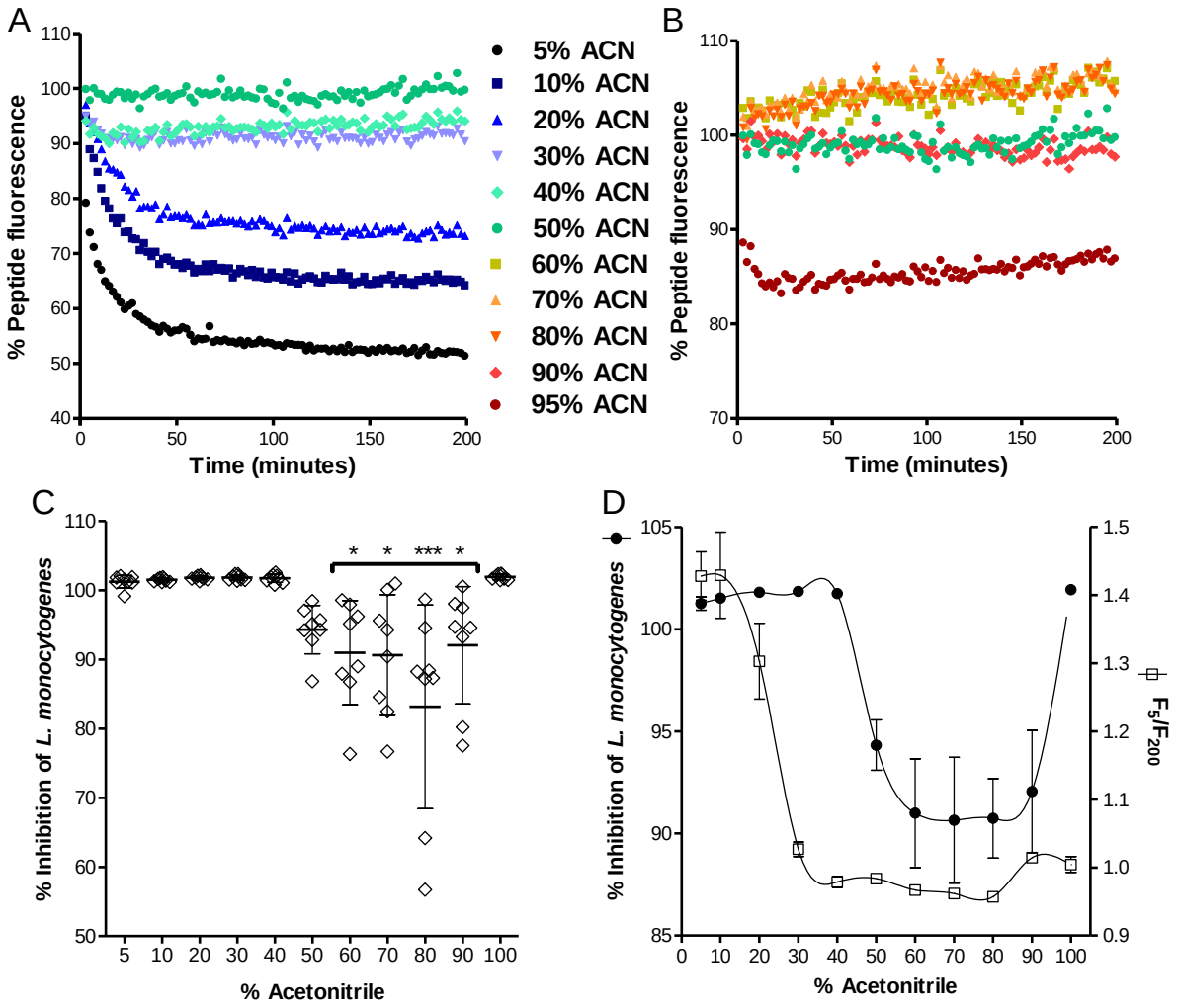

Figure 5.9: Percentage fluorescence signal (F/F_0) of peptide in the presence of acetonitrile (ACN) ranges **(A)** 5-50% and **(B)** 50-95%; showing a decrease in signal with the association to cellulose. Each data set is the average of four technical repeats and blank subtracted. **(C)** Antimicrobial activity of cellulose, expressed in percentage metabolism inhibition against *L. monocytogenes*, treated with peptide in ranges of percentage (*v/v*) acetonitrile. Each data set is the standard deviation of the mean of two biological and four technical repeats. Statistical analysis between 5% acetonitrile as control and the other conditions were determined with One-way Anova and Bonferroni's Multiple comparison post-test; *P<0.05; ***P<0.001 **(D)** Comparison between the decrease in fluorescence at the beginning (5 minutes) and end of incubation (200 minutes)(F_5/F_{200}) showing peptide association and the resulting antimicrobial activity of the treated cellulose against *L. monocytogenes.*

5.4.3 Visualisation of tyrocidine oligomers

The aggregation of Trcs on cellulose was inspected visually with the use of scanning electron microscopy (SEM). SEM images of untreated cellulose showed a fibrous mat (Figure 5.10: A&B) that upon closer inspection had a rough surface area (Figure 5.10: C).

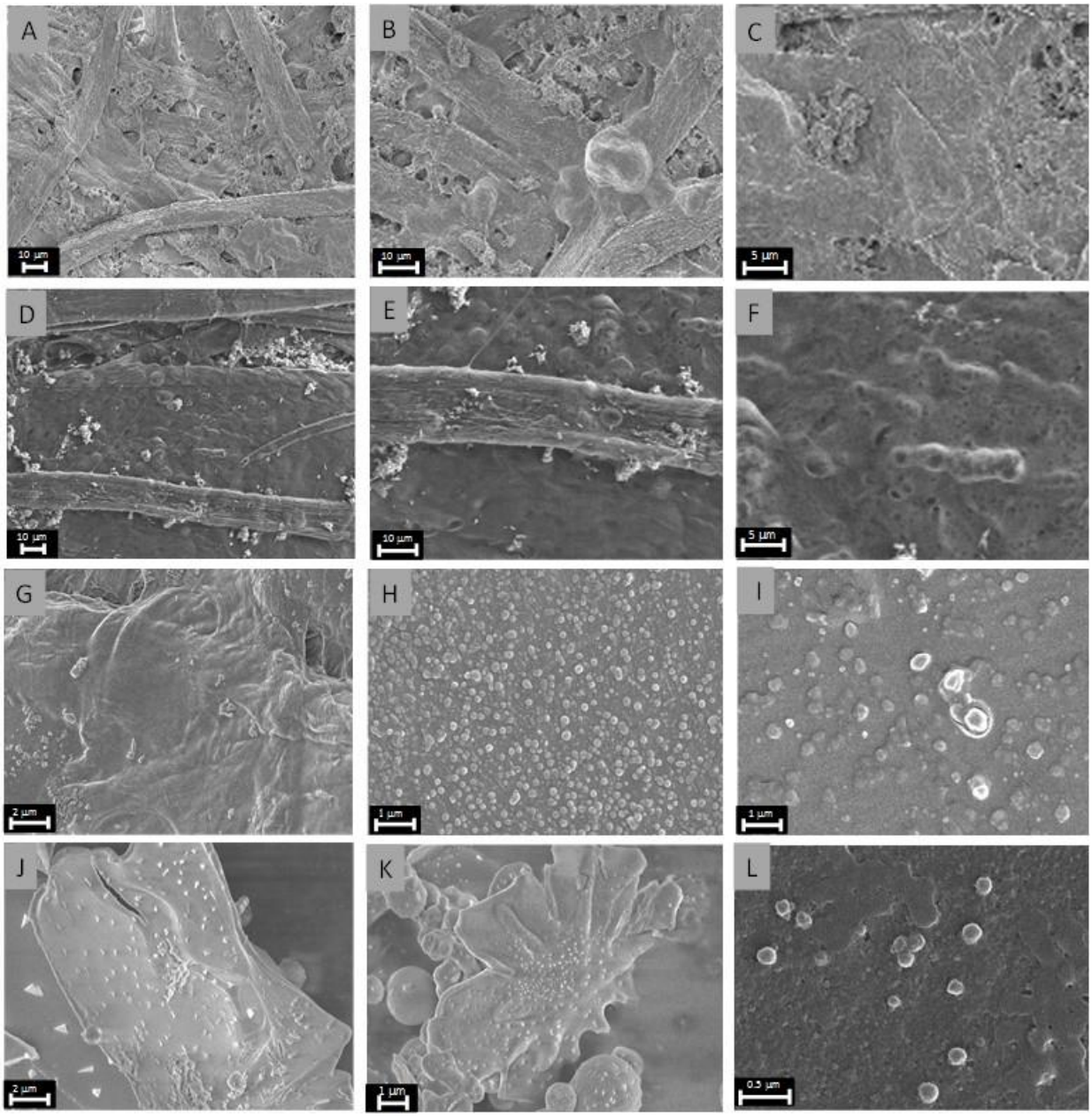

Figure 5.10: Scanning electron microscopy images of **(A-C)** untreated cellulose **(D-G)** cellulose treated with purified Trc A, glucose:Trc A (1;1) on mica **(H)** cellobiose:Trc A (1;1) on mica **(I),** Trc mix on mica **(J, K)** and pure TrcA on mica **(L)**. Micrographs (A-K) were acquired with a Zeiss EVO MA15VP SEM and (L) with high resolution NOVA 450 NANOLAB, FEI dual beam SEM. Micrograph (L) was provided by Dr V Kumar from a parallel study on Trc A nanostructures.

In comparison, cellulose treated with Trc A still had an overall fibrous structure, but it appeared smoother with more swollen fibres, as well as some crystal-type structures (Figure 5.10: D&E). However, closer inspection of the smoother surface areas indicated knobbly structures not seen in the untreated cellulose (Figure 5.10: F). Other areas on the Trc A-treated cellulose showed more sheet-like structures (Figure 5.10: G). When Trc A was mixed with glucose at 1:1 molar ratio, it resulted in spheroid nanostructures with 100-300 nm in diameter, as well as much smaller spheres (Figure 5.10: H). Cellobiose:Trc A (1:1) mixtures also led to the formation of spheroids, but with much higher polymorphism and diameters ranging from about 20-600 nm (Figure 5.10: I). Trc A on its own also presented nanospheroids with a diameter of about 200 nm with smaller nanospheres interspersed sheet-like structures (Figure 5.10: L). Visualisation of the Trc mixture alone (Figure 5.10: J&K) presented a sheet-like covering of the surface with smaller balls/structures visible within the sheet, including crystal-type structures. The visualised peptide nanostructures such as spheroids, spheres and sheets are the consequence of a complex peptide oligomerisation and aggregation that are dependent on the attachment surface environment, peptide and solvent system. If the simpler models with glucose and cellobiose are considered certain structures are also found on the cellulose. If the structures of the peptide alone, Trc mix and TrcA are considered the sheet structures, spheroids and smaller structures were observed on the peptide treated cellulose (Figure 5.10: G).

5.5 Conclusions

The aggregation or self-assembly of Trc mix was studied with various techniques to correlate the conditions required for aggregation or that needed for association. Previous research has proposed that self-assembly occurs based on common backbone structure (Laiken et al., 1969) or peptide conformation (Ruttenberg et al., 1965) that favours hydrophobic interactions. However, it has been proposed that self-assembly is more a dynamic system than just one aggregation state (Thies and Paradies, 1997). Our results support this hypothesis that the oligomerisation is a highly dynamic and complex process that is further complicated by environment, temperature, solvent system and many other parameters, as well as the sensitivity and selectivity of the technique to follow the process.

A summary of the results is presented in Table 5.2 as a heat map to ease the comparison between the different techniques employed in this study. Larger oligomers could not be reliably detected at 5-30% acetonitrile with IM-MS pointing to the formation of oligomers based on hydrophobic interactions due to the method removing all solvent, negating the hydrophobic

effect (Bich et al., 2010; Daniel et al., 2002; Wu et al., 1997). This was confirmed with fluorescence analysis showing increased quenching from 5-40% acetonitrile, with optimal fluorescence conditions around 50-80% acetonitrile. Fluorescence analysis with ANS only showed detectable hydrophobic pockets forming at 5-10% acetonitrile further confirming the formation of oligomers by hydrophobic interactions. CD analysis showed an almost complete loss of hydrogen-bonded structures at low concentrations of acetonitrile. Interestingly the spectrum of Trcs in 50% *v/v* TFE, a membrane mimicking solvent, was similar to the spectrum observed for 60% acetonitrile indicating that the hydrogen-bonded self-assembly structures may be favoured for membranolytic activity of these peptides. Temperature analysis of the self-assembly structures showed that the hydrophobic driven structures are far more stable confirming the robustness observed in Chapter 3. Furthermore, the melting curve of Trc mix in 85-45% acetonitrile was similar to melting curves observed for β-sheets, confirming the CD and IR results of the presence of hydrogen bonded structures. The interplay between the hydrogen-bonded structures and structures driven by hydrophobic interactions could best be observed between association and dissociation. Association of the peptide to cellulose was influenced more by the acetonitrile concentration with 50-90% acetonitrile preventing association and activity. Whereas, only 60% and 70% could remove enough peptide to affect the activity against *L. monocytogenes*. This correlates with 1% SDS having a greater influence on association compared to dissociation as seen in Chapter 3. SEM analysis of Trc A with cellobiose and glucose showed the formation of spherical/spheroid nanostructures whereas a combination of sheet structures and spheroids were observed with Trc A and Trc mix alone. Analysis of peptide-cellulose showed a combination of these structures pointing to an initial seeding layer of peptide forming upon association followed by continued self-assembly as seen with the smaller structures formed on top of the seeding layers.

Though a more detailed hypothesis of Trc association with cellulose will be discussed in Chapter 6, in conjunction with Chapter 4 to highlight the amino acids involved in the association, a few conclusions can be made. Trcs have two very distinct self-assembly modes: one mediated by hydrogen-bonding (60-80% acetonitrile) and one mediated hydrophobic interaction (5-10% acetonitrile). Depending on the environment the peptide will modulate its self-assembly to either favour one form of self-assembly or intermediates thereof. However, from these studies we hypothesise that the aggregates formed by hydrophobic interactions are favoured for association to cellulose. Once associated to cellulose it appears that only detergents or amphipathic solvents can remove the peptide.

Table 5.2: Summary of the effect of acetonitrile on the oligomerisation of Trc mix and its association/dissociation to cellulose. Pink represents the formation of hydrophobic driven oligomers whereas blue represents hydrogen-bonded oligomers. Grey represents results that differ from the hydrogen-bonded oligomers (blue), however no commentary can be given on proposed self-assembly type formed. As the conditions for CD were different the respective percentage acetonitrile is noted.

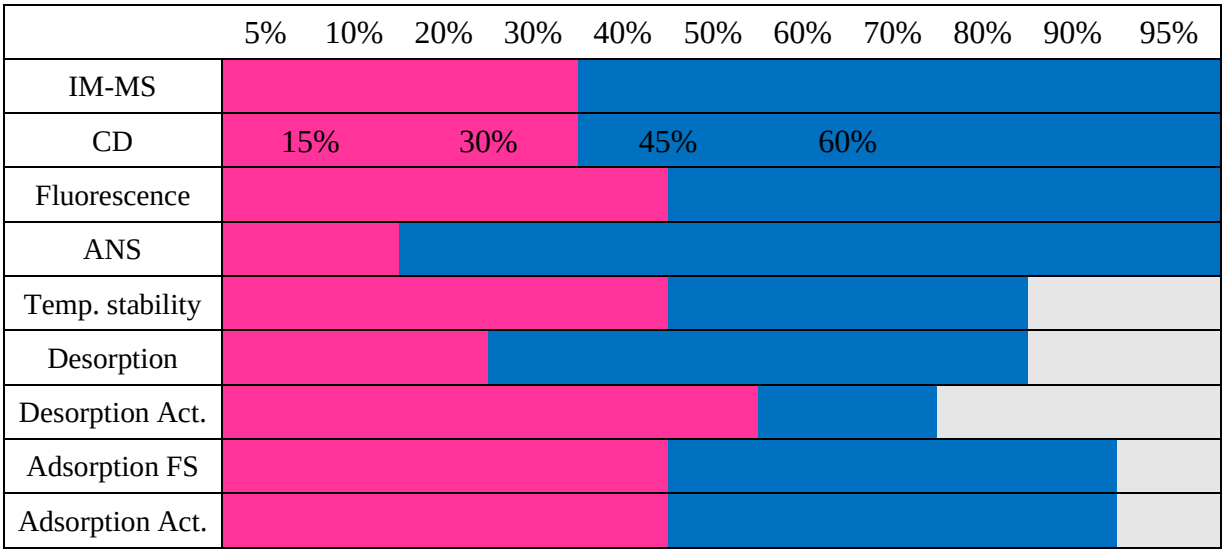

5.6 References

Appleby, J.C., Knowles, E., Pearson, J., White, T., 1947. A preliminary study of the formation, assay and stability of tyrothricin. J. Gen. Microbiol. 1, 137–44.

Bich, C., Baer, S., Jecklin, M.C., Zenobi, R., 2010. Probing the hydrophobic effect of noncovalent complexes by mass spectrometry. J. Am. Soc. Mass Spectrom. 21, 286–289.

Brown, L.J., Singh, L., Sale, K.L., Yu, B., Trent, R., Fajer, P.G., Hambly, B.D., 2002. Functional and spectroscopic studies of a familial hypertrophic cardiomyopathy mutation in Motif X of cardiac myosin binding protein-C. Eur. Biophys. J. 31, 400–408.

Chattopadhyay, A., Raghuraman, H., 2004. Application of fluorescence spectroscopy to membrane protein structure and dynamics. Curr Sci 87, 175–180.

Chen, Y., Barkley, M.D., 1998. Toward understanding tryptophan fluorescence in proteins. Biochemistry 37, 9976–9982.

Daniel, J.M., Friess, S.D., Rajagopalan, S., Wendt, S., Zenobi, R., 2002. Quantitative determination of noncovalent binding interactions using soft ionization mass spectrometry. Int. J. Mass Spectrom. 216, 1–27.

Helle, S.S., Zandstra, P.W., Cooper, D.G., 1992. Unusual surface tension behavior of an aqueous solution of gramicidin S. J. Colloid Interface Sci. 151, 130–135.

Juhl, D.W., Rensburg, W., Bossis, X., Vosloo, J.A., Rautenbach, M., Bechinger, B., 2019. Tyrocidine A interactions with saccharides investigated by CD and NMR spectroscopies. J. Pept. Sci. 25, e3163.

Kumar, K., Mishra, A.K., 2015. Application of partial least square (PLS) analysis on fluorescence data of 8-anilinonaphthalene-1-sulfonic acid, a polarity dye, for monitoring water adulteration in ethanol fuel. J. Fluoresc. 25, 1055–1061.

Laiken, S., Printz, M., Craig, L.C., 1969. Circular dichroism of the tyrocidines and gramicidin S-A. J. Biol. Chem. 244, 4454–4457.

Laiken, S.L., Printz, M.P., Craig, L.C., 1971. Studies on the mode of self-assosiation of tyrocidine B. Biochem. Biophys. Res. Commun. 43, 595–600.

Lakowicz, J.R., 2013. Principles of fluorescence spectroscopy. Springer Science & Business Media. 529-567.

Loll, P.J., Upton, E.C., Nahoum, V., Economou, N.J., Cocklin, S., 2014. The high resolution structure of tyrocidine A reveals an amphipathic dimer. Biochim. Biophys. Acta - Biomembr. 1838, 1199–1207.

Markovic-Housley, Z., Garavito, R.M., 1986. Effect of temperature and low pH on structure and stability of matrix porin in micellar detergent solutions. Biochim. Biophys. Acta - Protein Struct. Mol. Enzymol. 869, 158–170.

Mondini, L., Nachit, M.M., Porceddu, E., Pagnotta, M.A., 2011. Mondini, L., Nachit, M.M., Porceddu, E. and Pagnotta, M.A. Plant Genet. Resour. 9, 166–169.

Munyuki, G., Jackson, G.E., Venter, G.A., Kövér, K.E., Szilágyi, L., Rautenbach, M., Spathelf, B.M., Bhattacharya, B., Van Der Spoel, D., 2013. β-sheet structures and dimer models of the two major tyrocidines, antimicrobial peptides from *Bacillus aneurinolyticus*. Biochemistry 52, 7798–7806.

Ovchinnikova, T.V., Shenkarev, Z.O., Balandin, S.V., Nadezhdin, K.D., Paramonov, A.S., Kokryakov, V.N., Arseniev, A.S., 2008. Molecular insight into mechanism of antimicrobial action of the β-hairpin peptide arenicin: Specific oligomerization in detergent micelles. Biopolym. Orig. Res. Biomol. 89, 455–464.

Paradies, H.H., 1989. Structure of tyrocidine micelles in isotropic aqueous solution. J. Pharm. Sci. 78, 230–234.

Paradies, H.H., 1979. Aggregation of tyrocidine in aqueous solutions. Biochem. Biophys. Res. Commun. 88, 810–817.

Rajan, R., Balaram, P., 1996. A model for the interaction of trifluoroethanol with peptides and proteins. Int. J. Pept. Protein Res. 48, 328–336.

Rautenbach, M., Vlok, N.M., Eyéghé-Bickong, H.A., van der Merwe, M.J., Stander, M.A., 2017. An electrospray ionization mass spectrometry study on the “In Vacuo” hetero-oligomers formed by the antimicrobial peptides, surfactin and gramicidin S. J. Am. Soc. Mass Spectrom. 28, 1623–1637.

Ruotolo, B.T., Benesch, J.L.P., Sandercock, A.M., Hyung, S.J., Robinson, C.V., 2008. Ion mobility – mass spectrometry analysis of large protein complexes. Nat. Protoc. 3, 1139.

Ruttenberg, M.A., King, T., Craig, L.C., 1965. The use of the tyrocidines for the study of conformation and aggregation behavior. J. Am. Chem. Soc. 87, 4196–4198.

Ruttenberg, M.A., King, T.P., Craig, L.C., 1966. The chemistry of tyrocidine. VII. Studies on association behavior and implications regarding conformation. Biochemistry 5, 2857–2864.

Salgado, J., Grage, S.L., Kondejewski, L.H., Hodges, R.S., McElhaney, R.N., Ulrich, A.S., 2001. Membrane-bound structure and alignment of the antimicrobial β-sheet peptide gramicidin S derived from angular and distance constraints by solid state ^{19}F-NMR. J. Biomol. NMR 21, 191–208.

Stern, A., Gibbons, W.A., Craig, L.C., 1969. Effect of assosiation on the nuclear magnetic resonance spectra of tyrocidine B. J. Am. Chem. Soc. 91, 2794–2796.

Thies, M., Paradies, H.H., 1997. Self-Assembly of tyrocidines in nanotubular structures. MRS online Proc. Libr. Arch. 489.

Tulumello, D.V., Deber, C.M., 2012. Efficiency of detergents at maintaining membrane protein structures in their biologically relevant forms. Biochim. Biophys. Acta (BBA)-Biomembranes 1818, 1351–1358.

van Rensburg, W., 2015. Characterization of natural antimicrobial peptides adsorbed to different matrices. Stellenbosch University, Department of Biochemistry, Stellenbosch, South Africa. MSc.Thesis, http://scholar.sun.ac.za/handle/10019.1/97929.

Williams, R.C., Yphantis, D.A., Craig, L.C., 1972. Noncovalent association of tyrocidine B. Biochemistry 11, 70–77.

Wu, J., Yang, J.T., Wu, C.S.C., 1992. β-II conformation of all-β proteins can be distinguished from unordered form by circular dichroism. Anal. Biochem. 200, 359–364.

Wu, Q., Gao, J., Joseph-McCarthy, D., Sigal, G.B., Bruce, J.E., Whitesides, G.M., Smith, R.D., 1997. Carbonic anhydrase-inhibitor binding: From solution to the gas phase. J. Am. Chem. Soc. 119, 1157–1158.

Chapter 6
Conclusions and future studies

6.1 Introduction

The main goal of this project was to screen commercial surfaces to determine the commercial viability of tyrocidine-materials, determine the robustness of the active materials and elucidate the interactions between tyrocidine (Trc) and cellulose that allow for its unique association and activity. In order to reach this goal, the cyclodecapeptides first had to be produced and/or purified, and second, characterised in terms of composition and behaviour in different environments namely *in vacuo*, at high temperatures, in dried form and in various solutions. Third, the different antimicrobial materials and surfaces had to be created by optimised exposure to the characterised peptide mixture, denoted Trc mix. The amount of peptide bound to the surfaces and materials was then determined utilising Trp fluorescence. Fourth, we had to confirm that antimicrobial materials/surfaces were created, followed by selection of the most promising material for further characterisation. To characterise the antimicrobial activity a solid surface antimicrobial assay was developed and optimised to allow for high throughput activity determination. From these studies, cellulose was selected as the most promising material for creation of a Trc-functionalised antimicrobial material. The Trc mix treated cellulose was then characterised in terms of kinetics (binding and association) in different solvents compositions, as well as by challenging the antimicrobial cellulose with high temperatures, detergents, water washes, a broad pH range, organic solvent washes and a range of bacterial concentrations. Finally, the molecular descriptors of Trc interaction with cellulose, using simple saccharides as models, were investigated in terms of the roles of the side chains of amino acid residues in interactions, as well as the role of oligomerisation, specifically the formation of β-sheet type structures, on association with cellulose.

6.2 Experimental Conclusions

6.2.1 Production and purification of tyrocidines and tyrocidine analogues

As tyrocidines and analogues were the focus of this study, certain peptide fractions had to be produced and/or purified. Trc mix was purified from commercial tyrothricin, the purity confirmed with UPLC linked to ESI-MS (>90%) and the percentage contribution of each analogue found to be comparable to what has been previously reported (Tang et al., 1992; Troskie et al., 2014). Trcs and Trc analogues were produced in non-supplemented and amino

acid supplemented media to obtain peptide extracts that contained predominantly tyrocidines (non-supplemented), tryptocidines and Trp-rich cyclodecapeptides (Trp-supplemented) and Phe-rich cyclodecapeptides (Phe-supplemented). Subsequent to ESI-MS analysis the successful production of the different extracts were confirmed (cyclodecapeptide contribution >90%) and the production profile shift occurring due to the amino acid supplementation could be correlated to previous results (Fujikawa et al., 1968; Mach and Tatum, 1964; Ruttenberg and Mach, 1966; Vosloo et al., 2013). Isotopically labelled tyrocidines were produced based on an amalgamation between the optimised method for unlabelled production (Vosloo et al., 2013) and a method published by Vogt *et al.* (2003). The method made use of 3% *w/v* glucose (^{13}C labelled) and 85% *v/v* $^{13}C^{15}N$ Celltone media and produced uniformly ($^{13}C^{15}N$)-labelled tyrocidines of which Trc A was purified, based on abundance. We did not make use of an acid precipitation step during this production and found that the peptides associated tightly with a pigment in the culture extract, which took multiple extractions to remove. This tight association with a sugary pigment possibly pointed to the natural internal storage of the peptides and may relate to the association with saccharides.

The isotopically labelled peptide was used to study the interaction between tyrocidines and microcrystalline cellulose with the use of solid surface NMR. This has not been previously done due the low amounts of peptide associating to cellulose, lower than what is detectable by most biophysical methods. Therefore, future studies would include further optimisation of the production of ($^{13}C^{15}N$)-labelled tyrocidines to not only increase the overall yield but also to enable purification of enough of the other tyrocidines (Trc B and Trc C) to be included in solid-state NMR studies. Furthermore, production of ($^{13}C^{15}N$)-labelled media using cheaper starter labelled nutrients should be considered due to the high cost of Celltone^{TM} media which currently limits labelled peptide production.

6.2.2 Development of high-throughput solid surface assay

The development and screening of novel/optimised active materials is limited by current screening methods which are time consuming, costly and laborious. We developed and optimized a resazurin based solid surface assay and compared it to disc diffusion, commonly used with material development research (Abou-Yousef and Kamel, 2015; De Moura et al., 2012; Gemili et al., 2009; Imran et al., 2010; Isquith et al., 1972; Rouabhia et al., 2014; Sayanjali et al., 2011), and a modified version of JIS Z 2801, which is a Japanese industrial standard and best performing solid surface method (van de Lagemaat et al., 2017). The novel

method and disk diffusion were tested against *Escherichia coli*, *Pseudomonas aeruginosa*, *Staphylococcus aureus* and *Listeria monocytogenes*, whereas the JIS Z 2801 was only tested with *P. aeruginosa* and *L. monocytogenes.* Active materials were created by direct treatment of cellulose disks (without washing) with gentamicin, bacitracin, ampicillin, gramicidin S and tetracycline. It was found that disk diffusion is better suited to the detection of slow release material where the active compound is polar (Elshikh et al., 2016; Sánchez and Kouznetsov, 2010) and can easily diffuse through agar. The JIS Z 2801 could detect the true surface activity as previously reported (van de Lagemaat et al., 2017). Our novel assay utilising resazurin detected the same trend in results as the JIS Z 2801 method within a shorter time and due to the high-throughput design, we could perform more technical and biological repeats at lower cost.

Future studies should include optimization with other target organisms prone to contaminate solid surfaces or forming biofilms such as Enterobacteria, yeasts and fungi. The latter is of great importance since there is currently no high-throughput screening method to test the prevention of surface contamination by yeasts such as *Candida albicans* before *in vivo* testing, which can become costly in the development phase. Further optimisations should include more types of materials since the current methods, JIS Z 2801 and the novel method discussed in Chapter 2, only allow to test thin flat materials which is not always possible with polymeric materials in their development phase production. As for the commercial application of the method, it can be optimised for the detection of microbial contamination in environments that have limited infrastructure. Since conversion of resazurin to resorufin can be visibly assessed without the use of expensive instrumentation, the method can be adapted to detect threshold cell numbers in set time points based on observable colour changes.

6.2.3 Creating robust antimicrobial materials with sticky tyrocidines

The antimicrobial activity of Trc mix treated laboratory and commercial materials were tested against *L. monocytogenes*. It was found that though all the surfaces resulted in at least 80% growth inhibition; the cellulose, plastic tray, tissue paper, ripple carton, white plastic, green plastic and cling film resulted in full inhibition. This points to great promise for the application of the technology in commercial materials since the activity was not limited to laboratory materials. Furthermore, the overall performance of cellulose and cellulose based materials suggests possible application of peptide treated wound dressings and textiles (cotton, wool, nylon). Inspection of the amount of peptide associated the with materials, with the use of a

developed fluorescence assay, showed two groupings of amount of peptide association vs. resulting activity. The materials resulting in full inhibition showed association of 5-8 µg/cm^2 of peptide whereas the remaining materials showed a linear trend between peptide associated and activity (85-100% inhibition). It appears as if the peptide conformation alters to adapt and associate to different surfaces, since both groups contained various types of materials, namely cellulose based materials, plastics, hydrophilic and hydrophobic materials. Further testing of cellulose, as the laboratory-controlled surface, showed a robustness of activity being able to totally inhibit the growth of 10^6 cells/cm^2 and inhibit >90% growth of 10^7 cells/cm^2 after only 10 minutes of exposure. This rapid activity correlates to the rate of activity reported of tyrocidines alone (Mach and Slayman, 1966; Spathelf and Rautenbach, 2009). The stability of the peptide association was evaluated with heat exposure and solvent exposure. The activity of the peptide treated cellulose remained stable in 'wet' temperatures up to 100ºC and dry heat up to 175ºC and one-minute exposure up to 200ºC. The decrease in activity was related to Trp/Tyr breakdown indicated by thermogravimetric analysis. The stability of these peptides on cellulose as also determined through exposure to heat, pH ranges, salt solutions, acidic solutions, acetonitrile, multiple water washes and the surfactant, sodium dodecyl sulphate (SDS). The only two solvents that had any effect on association was 1% *m/v* SDS and 70% *v/v* acetonitrile, pointing to the possible disruption of self-assembled structures related to the amphipathic nature of the peptide (Loll et al., 2014; Munyuki et al., 2013; Ruttenberg et al., 1965; Stern et al., 1969; Williams et al., 1972). Furthermore, adsorption was more effected than desorption pointing to a secondary occurrence to association that locks the seeding layer of peptide into place on the cellulose. As the drying step is the only difference between association and desorption; the Maillard reaction between Orn, Lys, Asn , Gln, Tyr and Trp and the reducing ends of the cellulose can result in the stability of the peptide once dried to the cellulose (Dubinina et al., 2002; Mottram et al., 2002; Nagaraj et al., 1996; Niquet and Tessier, 2007; Zhuang and Sun, 2013). Although the Maillard reaction typically takes place at high temperatures, the 16-hour exposure to 60 °C during the drying step could in theory be enough for the reaction to take place. In brief, the process occurs in three stages: the initial interaction between the amine group and reducing sugar moiety, followed by rearrangement to stabilize the interaction and the formation of stable Maillard products that is accompanied with some browning (Dubinina et al., 2002; Nagaraj et al., 1996; Zhuang and Sun, 2013). Amines in general are susceptible to this process, but Lys is reported to be the most sensitive (Zhuang and Sun, 2013). As the Maillard reaction results in covalent bonds between the sugar moiety (cellulose) and amines (amino acid side chains of the peptide), and the amino acids most

affected are key to the activity of Trcs (Danders et al., 1982; Rautenbach et al., 2007; Spathelf and Rautenbach, 2009); the seeding layer of peptide would possibly lose all activity. However, this initial seeding layer could provide a more favourable binding surface, compared to cellulose alone, since the peptide favours self-assembly (Munyuki et al., 2013; Williams et al., 1972).

Lastly, the uniqueness of the tyrocidine-cellulose interactions was compared to the activity of cellulose treated with other antimicrobial peptides. The only other antimicrobial compound that showed some promise was gramicidin S (GS) since it was both active against Gram-positive and Gram-negative bacteria. The activity of GS-treated cellulose can possibly be attributed to the similarities to tyrocidines: GS shares a sequence similarity with tyrocidines in the VOLfP-moiety, is also cyclic and produced by a spore forming soil bacterium pointing to an evolutionary adaptation for the peptide to be retained on the spore coating, which is similar to cellulose (Kondejewski et al., 1996).

Further studies should include commercial trials with the commercial materials to determine whether the peptide would survive the material creation process, to optimise the point of introduction and to determine the active materials activity as an application. As the filtering experiment showed to be useful in the robustness testing, the same methodology can be used to determine the minimum time required for the activity of tyrocidine-treated materials and further robustness testing. Furthermore, the method can be optimised for a high-throughput method to determine the activity of polymeric materials not suited for the resazurin assay. Since the cells are captured by the filter plate, the materials can be exposed to a small volume of culture (to ensure only surface activity), following a washing step to remove cells at which point the material can be removed and the remaining cells determined as was done with the robustness experiment. Further studies on the heat stability of the peptide should include thermogravimetric analysis (TGA), ESI-MS analysis after heat exposure and broth/cellulose activity studies with purified peptides such as Tpc C, Phc A and Tyr A. The peptides selected range from most affected to least affected as suggested in the dry heat exposure of cellulose study. Moreover, the use of single analogues should prevent overlap in the TGA and ESI-MS analysis.

Optimisation of the current Trc-derived antimicrobial materials could include the incorporation of GS with the Trcs to be effective against Gram-positive, Gram-negative bacteria and fungi. Furthermore, considering the similarity of origin, structure, and activity on cellulose between

GS and tyrocidines, future studies could include other peptides from spore forming soil bacteria in the creation of active surfaces.

6.2.4 Hypothesis on peptide-cellulose interaction

The general Trcs structure consists of *cyclo*-(f[1]P[2]X[3]x[4]N[5]Q[6]X[7]V[8]O[9]L[10]) that forms antiparallel β-sheets between Trp[3]-Asn[5] and Val[8]-Leu[10] which is separated by a type I (Gln[6]-Tyr[7]) and type II' β-turn (D-Phe[1]-Pro[2]) (Kuo and Gibbons, 1980, 1979). The β-sheets are stabilised with Phe[3] O-NH Leu[10] and Asn[5] NH-O Val[8], also Phe[3] NH-O Leu[10] and Asn[5] O-NH Val[8] (Beyer et al., 1974; Gibbons et al., 1975; Kuo and Gibbons, 1980). Should the peptide be split along the β-sheet, Phe[4] and Orn[9] can be found in the same plane (Beyer et al., 1974; Gibbons et al., 1975) and Gln[6] exposed to the solvent (Kuo and Gibbons, 1980). This conformation (Beyer et al., 1974) and the peptides' ability to aggregate (Munyuki et al., 2013; Williams et al., 1972) is the basis of its amphipathic character (Loll et al., 2014; Munyuki et al., 2013) and antimicrobial activity (Loll et al., 2014; Munyuki et al., 2013; Salgado et al., 2001). Furthermore, the initial interaction needed between target organism membrane and peptide for the activity of Trcs have been attributed to Orn[9], and the dipeptide unit at position 3 and 4 (Danders et al., 1982; Rautenbach et al., 2007; Spathelf and Rautenbach, 2009).

Trcs are only amphipathic in their dimeric form (Loll et al., 2014; Munyuki et al., 2013) and therefore dimers are at the base of the dynamic self-assembly and re-assembly observed for Trcs (Helle et al., 1992; Paradies, 1979; Ruttenberg et al., 1966; Thies and Paradies, 1997). Closer inspection of the directional hydrogen-bonded dimer (based on work published by Munyuki *et. al.*, 2013) shows a clear hydrophobic region of the dimer (in blue) from Val[8]-Trp[4] and a hydrophilic head of the dimer (in grey) from Asn[5]-Tyr[7] (Figure 6.1). The only exception to the homogeneity of the hydrophobic region is the occurrence of Orn[9] between Leu[10] and Val[8], however this allows for the electrostatic interaction of Orn[9] to the cell membrane lipid head groups and the burrowing of Trp[4] into the lipid bilayer for the peptide to elicit its antimicrobial response (Loll et al., 2014; Munyuki et al., 2013).

Structure activity studies have shown that as long as the structural topography of the hydrophobic and hydrophilic regions is not disrupted, the peptide will remain active (Danders et al., 1982). Since the ability of the peptide to form amphipathic dimers, followed by self-assembly into oligomers are needed for its activity, it is expected to play a key role in the Trcs-cellulose interaction. The effect of Trcs self-assembly was studied in the presence of acetonitrile as it can be a partial detergent for the hydrophobic interactions and supporting

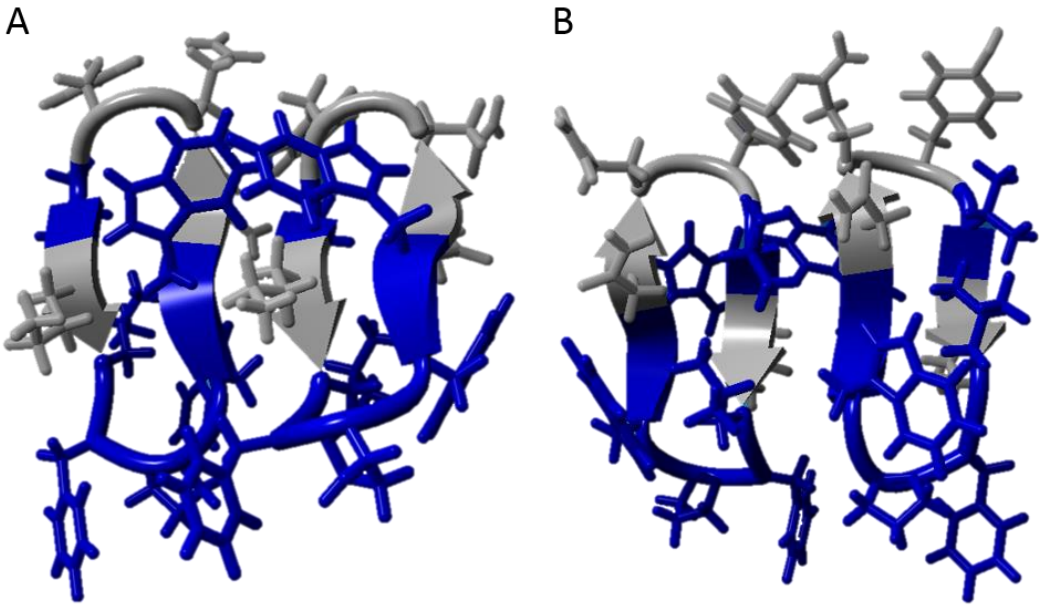

Figure 6.1: Trc C homodimer as modelled from the results published by Munyuki et. al. (2013). The hydrophobic amino acids are in blue and the polar amino acids in grey. The peptide is split in the **(A)** front and **(B)** back view to better show the hydrophobic and hydrophilic regions within the dimer.

solvent for polar/electrostatic and hydrogen bonds (latter was indicated with CD and NMR). The Trcs self-assembly has been proposed to be regulated by common backbone structure (Laiken et al., 1969) or peptide conformation (Ruttenberg et al., 1965) that favours hydrophobic interactions. However, IM-MS results showed the formation of two distinct self-assembly structures. The first correlated with literature by favouring hydrophobic interactions due to the aqueous environment possibly forcing the Trcs into micellar structures to shield the hydrophobic amino acids. The second is stabilized by the amphipathic solvent environment and possibly hydrogen bonds forming between the side chains of the polar amino acid residues. The formation of hydrophobic pockets to shield the hydrophobic amino acids was confirmed by the intercalation of ANS at low acetonitrile concentrations. This was further confirmed by the fluorescence quenching observed at low concentrations of acetonitrile as the shielded aromatic amino acids would result lower fluorescence. Furthermore, the formation of multi-layered micellar structures would better shield the hydrophobic amino acids from the polar solvent but also increase the quenching. These micellar structures could possibly contain a combination of side-by-side peptide interaction and stacked self-assembled structures. CD analysis showed a loss of detectable secondary structures at low concentrations of acetonitrile pointing to the formation of large oligomers. Comparison between the CD spectra of 50% *v/v* trifluoroethanol, a membrane mimicking solvent that supports hydrogen bonding, and 60% *v/v*

acetonitrile showed similarity confirming that the second type of oligomer formed is stabilised through hydrogen bonding. What is interesting is the change in self-assembly type between an aqueous environment used in biological assays and microbial membrane activity (based on the results of TFE) from hydrophobic to hydrogen-bonded structures.

Temperature studies showed that the hydrophobic self-assembly structures were stable up to 95ºC confirming stability observed in Chapter 3, suggesting the peptide aggregates formed on the cellulose might be in the hydrophobic self-assembly form. Furthermore, melting curves resembled those of β-sheets in the presence of 45-85% acetonitrile, confirming the FTIR and CD results on secondary structure. Association of Trcs to cellulose was further studied with acetonitrile and found that 50-90% acetonitrile could prevent association to some extent, whereas 60% and 70% could remove enough peptide to affect the activity of the peptide. This is a strong indication that the possible interaction of the Trcs to the cellulose to be dependent on hydrophobic/amphipathic self-assembly structures and that an optimal amphipacity could change the conformation of the peptide to that of the hydrogen-bonded self-assembly. Furthermore, if the peptide is already in the hydrogen-bonded self-assembly conformation, association appears to be lessened. Therefore, it can be suggested that the peptide needs to be in the hydrophobic self-assembly form to form hydrogen bonds with cellulose similar to its initial interaction with the cell wall of a target organism.

Scanning electron microscopy analysis showed peptide layers with larger self-assembly structures correlating with the behaviour of the peptides on their own when dried on different surfaces. This was confirmed with the two-phase exponential decay observed for the association of Trcs to cellulose at an optimal concentration of 50-75 µg/mL. The decrease in association at high and low concentrations was attributed to the formation of large aggregates that hampered association or not forming big enough oligomers, both preventing the formation of a seeding layer of peptide that can initiate further self-assembly. It is proposed that the Trcs form oligomers that ‘melt’ into a seeding layer upon contact with the cellulose, from which further self-assembly structures can be formed.

Antimicrobial and haemolytic activity studies with Trc mix and saccharides (glucose, cellobiose, KLU E, cellulose) showed that glucose, cellobiose and KLU E increased the antimicrobial activity and haemolysis activity of Trc mix pointing to conformational changes. Continuing on the hypothesis that the hydrophobic self-assembled structures are required for the initial association to cellulose, it can be deduced that a hydrophobic-driven

oligomer/aggregate would be decorated with a polar surface, with Orn[9]/Lys[9], Asn[5], Gln[6] and possibly Tyr[7] decorating the oligomer/aggregate surface. This would allow these amino acids to interact with the hydroxyl-groups on the surface of cellulose, forming hydrogen bonds, as well as dipole-dipole and ion dipole interactions in the initial seeding layer. It could explain the reason why glucose is unable to prevent association of Trcs to cellulose as the increased formation of hydrophobic self-assembly structures would increase association (as seen with better association at 5% acetonitrile compared to 40% acetonitrile). Cellobiose at high concentrations could prevent association to cellulose, possibly by associating to Trcs in a similar manner as Trcs associating to cellulose thereby having competitive binding. In a more amphipathic environment, such as 70% acetonitrile and SDS, hydrogen-bonded self-assembled structures are formed trapping the polar amino acids in unfavourable environment in the self-assembly structure thereby limiting association to cellulose. It is important to note that only two conformations are proposed but that the peptide could possibly arrange and re-arrange its self-assembled structures based on the environment which would affect the association to cellulose as seen with the range of acetonitrile association and dissociation experiments.

Inspection of the effect of glucose on Trc A with CD, showed that the β-sheets are most affected compared to the β-turns which, was confirmed with FTIR. There was a marked difference between the influence of glucose and cellobiose/KLU E on the β-sheets, as observed with FTIR. NMR analysis showed that only amino acids where the amide protons are exposed to the solvent (Loll et al., 2014; Munyuki et al., 2013) were affected by the addition of glucose. D-Phe[4] and Orn[9] were the most affected, followed by D-Phe[1], Val[8], Asn[5] and Tyr[7], with Phe[3] and Leu[10] remaining unaffected. FTIR analysis confirmed the NMR results that the amino acids side chains exposed to the solvent were most affected: Asn[5], Gln[6], Orn[9], Phe[1,3,4], Trp[3,4] and Tyr[7] (in no specific order). Lastly, changes in the C-O regions for all the sugars, proposes that primary point of interaction between peptide and cellulose could be the hydroxyl groups.

The experimental data was compared to a pilot study of 67 possible docking models constructed with Yasara V11.3.2 using two conformers of a Trc C dimer as receptor and two conformers of cellotetraose as ligand (courtesy of M. Rautenbach). The cellotraose:TrcC-dimer models predicted a similar influence on the peptide bonds, except for Val as detected for TrcA in the presence of glucose by liquid-state ^{1}H NMR spectroscopy (Juhl et al., 2019)(Figure 6.2: A). It was surprising that such a good correlation was found as the models and NMR study utilised different peptides and sugars. The models could also predict the influence on Pro[2] and Gln[6] which could not be done with NMR. The models predicted similar influences on the amino

acid side chains of Trp[3,4], Asn[5] and Gln[6] (C=O) as was observed with FTIR for Trc mix and KLU E (Figure 6.2: B). An overprediction of the hydrogen bond preference for Gln[6] (N-H), Tyr[7] and Orn[9] was found with the models, versus what was observed with FTIR, but this is probably due to the use of a Trc mixture, different saccharides and limited number of models. The proposed association from the model between cellotetraose and Trcs (Figure 6.3) shows the formation of three hydrogen bonds, correlating with the lower K_d found for cellotetraose in our NMR studies (Juhl et al., 2019).

It is hypothesised that in an aqueous solution the peptide would form self-assembly structures driven by hydrophobic interactions, shielding the hydrophobic amino acids from the polar solvent environment. This would result in an oligomer with Orn[9]/Lys[9], Asn[5], Gln[6] and Tyr[7], as well as Phe[4]/Trp[4] exposed to the environment. It is assumed that Trcs binds to cellulose in a similar fashion as to a target cell wall, based on the importance/effect observed of Orn[9]/Lys[9] and Phe[4]/Trp[4] as well as the probable switch between amphipathic dimers to hydrogen bonded oligomers.

Therefore, residue 9 (Orn[9]/Lys[9]) peptide bond and amino group in the side chain, with Asn[5], Gln[6] could initiate the association followed by hydrogen bonds with Trp[4] and Tyr[7]. It is also these amino acid side chains that would be involved in the Maillard reaction upon drying/heating of the cellulose after treatment. Following this association, it proposed that the oligomers 'melt' into a seeding layer on the cellulose which would require re-assembly of the hydrophobic core of the oligomer resulting in the changes observed with D-Phe[1], Pro[2] and to some extent Val[8] peptide bonds. The seeding layer can consist of two, or multiples of two layers of peptide with Orn[9]/Lys[9], Phe[4]/Trp[4], Asn[5], Gln[6] and Tyr[7] attached to the cellulose and exposed to the environment, if we consider that dimer are the dominant conformer driving oligomerisation. The exposed residues will then be available for further self-assembly structures or to interact with target organism cell membranes.

Since the peptide appears to form hydrophobic self-assembly structures in solution that change to hydrogen-bonded structures within a membrane (based on 50% TFE results), which also leads to dissociation of Trcs from cellulose (60-70% acetonitrile results) future work should include robustness testing by continually washing the Trcs-treated cellulose with a bacterial culture to determine whether it would remove peptide but also if the peptide could be rendered ineffective by cellular debris. Furthermore, unilamellar lipid vesicles mimicking bacterial (anionic) and erythrocytes (neutral) membranes can be used to quantify the amount of peptide

removed for the treated cellulose after exposure to these model lipid targets. As 1% SDS was able to remove Trcs from cellulose and prevent association, CD analysis should be done with SDS to determine the effect on secondary structures.

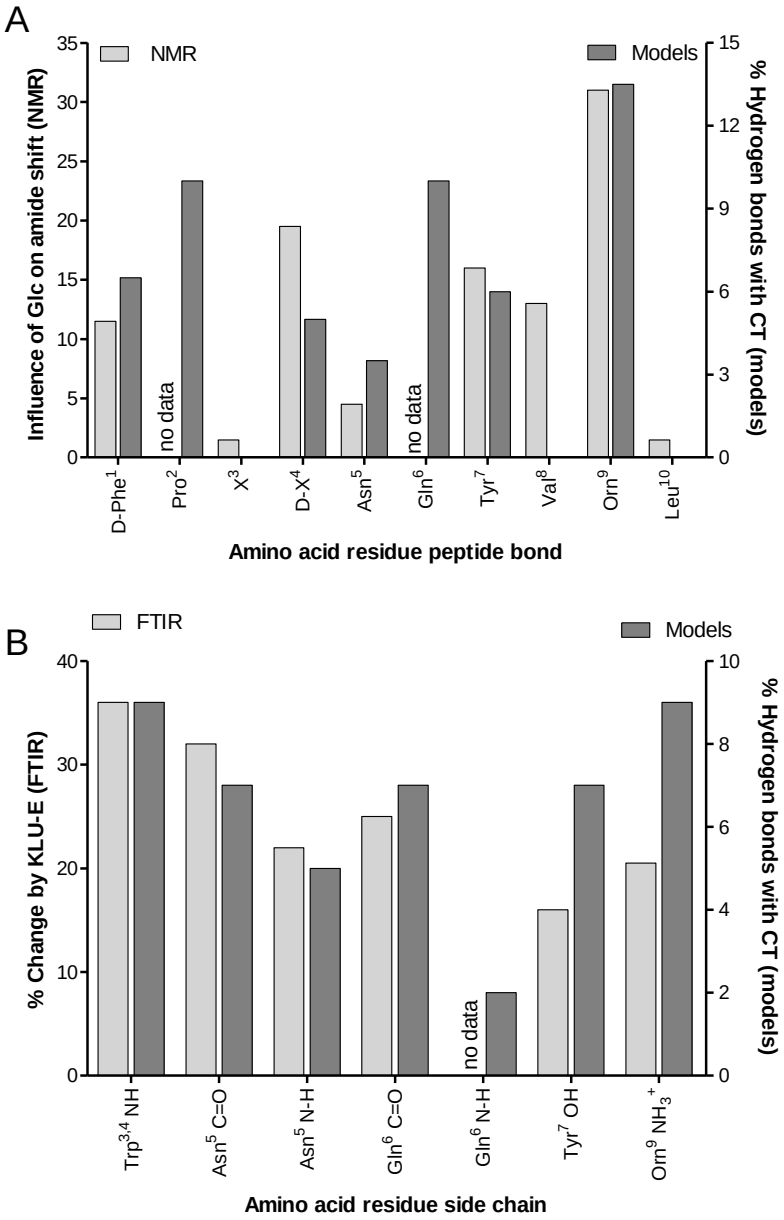

Figure 6.2: Comparison of the tendency of hydrogen bonds between Trc C dimer and cellotetrose according to the 67 molecular models derived from a docking experiment and parameters from biophysical analyses: **(A)** amide shift of TrcA in the presence of glucose as detected with liquid-state ^{1}H NMR spectroscopy (Juhl et al., 2019) and **(B)** percentage change in the side chain absorption of Trc mix in the presence of KLU E as observed with FTIR.

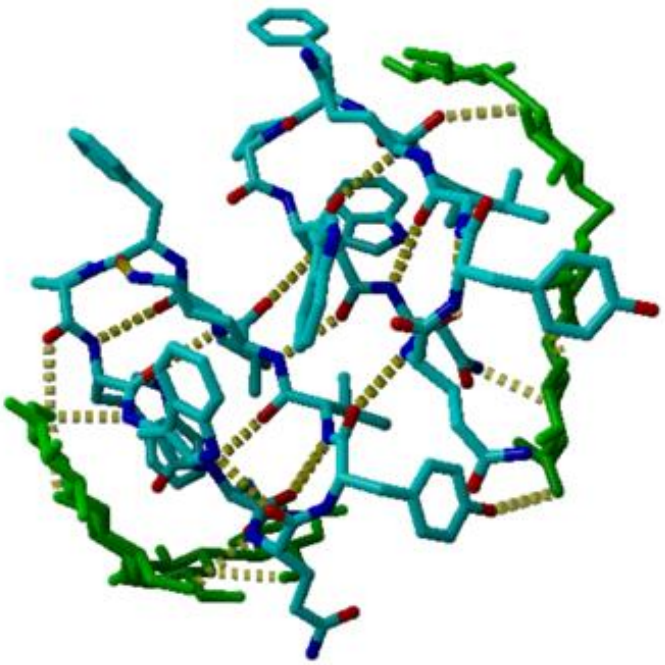

Figure 6.3: An example of a docking model showing a proposed hydrogen bonded interaction between cellotetraose and Trc C dimer (model courtesy M. Rautenbach)

CD and detailed NMR analysis should also be done with purified Trcs and cellobiose, cellotetrose and KLU E, as was done with glucose, as more appropriate models to the Trcs-cellulose interaction. Furthermore, since cellobiose was able to inhibit some of the association of Trcs to cellulose, future work should include KLU E and cellotetraose to confirm the hypothesis of competitive binding. Further FTIR analysis using purified Trc with cellobiose, cellotetrose and KLU E could further clarify the role of the aromatic amino acids and Lys in the interactions. Considering the Maillard reactions, this could be followed with FTIR and NMR over time and with temperature exposure. Finally, in order to fully elucidate the Trc saccharide interactions more comprehensive modelling with NMR constraints must be done.

6.3 Last word

During this study the question arose if the association of Trcs to cellulose is designed to protect its producer, *Brevibacillus parabrevis*, considering its biological activity and rich composition of high value amino acids. Trcs are produced in the late-logarithmic growth phase and involved with spore formation. During the spore phase of the producer, Trcs (or then tyrothricin) would be released by a subset of "suicidal" producers and eliminate competing organisms. The Trcs would then adhere to the spore capsule of the sporulating organisms and surrounding environment, minimising any competition for the nutrients once the conditions become

favourable. As this occurs in an aqueous or moist soil environment, the conformation of peptide would favour hydrophobic self-assembly structures that would quickly associate to the spore capsule and any surrounding materials, such as plant material. Therefore, our hypothesis is that Trcs forms hydrophobic self-assembly structures in an aqueous solution that displays Asn^5, Gln^6 and Orn^9 and probably Tyr^7 for association to target cell walls and hydroxyl groups on cellulose. Once associated the peptide continues to form new self-assembly structures in a concentration depended manner, leading to either target cell death or an antimicrobial surface enriched with peptides with high value amino acids, such as Trp, Tyr, Phe, Asn, Gln and Lys and Orn. As the association with cellulose is robust and water-resistant the peptide will sterilise the environment until the amino acids are release by the protease action of the producer for the next generation of bacterial growth and colonisation.

We can learn from this strategy of survival and utilise these peptides in various applications, as the rising resistance of pathogens to known antibiotics is of great concern, especially due to its continual occurrence in the medical and food processing industries. A possible solution would be the incorporation of antimicrobial materials to limit surface colonisation thereby curbing the continual pathogenic infections. Trcs and analogues hold great promise for application in the creation of solid surfaces since it has a broad spectrum of activity and the development of resistance is unlikely due to its multiple modes of action. Trcs adsorbs to various commercial surfaces and is robust in activity and stability. The methods employed to create the surfaces are very basic and make use of the natural conformational changes and self-assembly of the peptide that favours surface association. This process is more environmentally friendly since the peptide can be produced economically in gram amounts and no harsh chemicals are needed to create the Trc-derived antimicrobial materials and surfaces.

6.4 References

Abou-Yousef, H., Kamel, S., 2015. High efficiency antimicrobial cellulose-based nanocomposite hydrogels. J. Appl. Polym. Sci. 132, 1–9.

Beyer, C.F., Gibbons, W.A., Craig, L.C., Longworth, J.W., 1974. Heterogeneous tryptophan environments in the cyclic peptides tyrocidines B and C. Phosphorescence studies. J. Biol. Chem. 249, 3204–3211.

Danders, W., Marahiel, M.A., Krause, M., Kosui, N., Kato, T., Izumiya, N., Kleinkauf, H., 1982. Antibacterial action of gramicidin S and tyrocidines in relation to active transport, in vitro transcription, and spore outgrowth. Antimicrob. Agents Chemother. 22, 785–790.

De Moura, M.R., Mattoso, L.H., Zucolotto, V., 2012. Development of cellulose-based bactericidal nanocomposites containing silver nanoparticles and their use as active food packaging. J. Food Eng. 109, 520–524.

Dubinina, E.E., Gavrovskaya, S.V., Kuzmich, E.V., Leonova, N.V., Morozova, M.G., Kovrugina, S.V., Smirnova, T.A., 2002. Oxidative modification of proteins: oxidation of tryptophan and production of dityrosine in purified proteins using Fenton's system. Biochem. 67, 343–350.

Elshikh, M., Ahmed, S., Funston, S., Dunlop, P., McGaw, M., Marchant, R., Banat, I.M., 2016. Resazurin-based 96-well plate microdilution method for the determination of minimum inhibitory concentration of biosurfactants. Biotechnol. Lett. 38, 1015–1019.

Fujikawa, K., Sakamoto, Y., Suzuki, T., Kurahashi, K., 1968. Biosynthesis of tyrocidine by a cell-free enzyme system of *Bacillus brevis* ATCC 8185. II. Amino acid substitution in tyrocidine. Biochim. Biophys. Acta 169, 520–533.

Gemili, S., Yemenicioglu, A., Altinkaya, S.A., 2009. Development of cellulose acetate based antimicrobial food packaging materials for controlled release of lysozyme. J. Food Eng. 90, 453–462.

Gibbons, W.A., Beyer, C.F., Dadok, J., Sprecher, R.F., Wyssbrod, H.R., 1975. Studies of individual amino acid residues of the decapeptide tyrocidine A by proton double-resonance difference spectroscopy in the correlation mode. Biochemistry 14, 420–429.

Helle, S.S., Zandstra, P.W., Cooper, D.G., 1992. Unusual surface tension behavior of an aqueous solution of gramicidin S 151, 130–135.

Imran, M., El-Fahmy, S., Revol-Junelles, A.M., Desobry, S., 2010. Cellulose derivative based active coatings: Effects of nisin and plasticizer on physico-chemical and antimicrobial properties of hydroxypropyl methylcellulose films. Carbohydr. Polym. 81, 219–225.

Isquith, A.J., Abbott, E.A., Walters, P.A., 1972. Surface-bonded antimicrobial activity of an organosilicon quaternary ammonium chloride. Appl. Environ. Microbiol. 24, 859–863.

Juhl, D.W., Rensburg, W., Bossis, X., Vosloo, J.A., Rautenbach, M., Bechinger, B., 2019. Tyrocidine A interactions with saccharides investigated by CD and NMR spectroscopies. J. Pept. Sci. e3163.

Kondejewski, L.H., Farmer, S.W., Wishart, D.S., Hancock, R.E., Hodges, R.S., 1996. Gramicidin S is active against both Gram-positive and Gram-negative bacteria. Int. J. Pept. Protein Res. 47, 460–466.

Kuo, M.-C., Gibbons, W.A., 1980. Nuclear Overhauser effect and cross-relaxation rate determinations of dihedral and transannular interproton distances in the decapeptide tyrocidine A. Biophys. J. 32, 807–36.

Kuo, M.-C., Gibbons, W.A., 1979. Determination of individual side-chain conformations, tertiary conformations, and molecular topography of tyrocidine A from scalar coupling constants and chemical shifts. Biochemistry 18, 5855–5867.

Laiken, S., Printz, M., Craig, L.C., 1969. Circular dichroism of the tyrocidines and gramicidin S-A. J. Biol. Chem. 244, 4454–4457.

Loll, P.J., Upton, E.C., Nahoum, V., Economou, N.J., Cocklin, S., 2014. The high resolution structure of tyrocidine A reveals an amphipathic dimer. Biochim. Biophys. Acta - Biomembr. 1838, 1199–1207.

Mach, B., Slayman, C.W., 1966. Mode of action of tyrocidine on *Neupospora*. Biochim. Biophys. Acta 124, 351–361.

Mach, B., Tatum, E.L., 1964. Environmental control of amino acid substitutions in the biosynthesis of the antibiotic polypeptide tyrocidine. Proc. Natl. Acad. Sci. 52, 876–884.

Mottram, D.S., Wedzicha, B.L., Dodson, A.T., 2002. Food chemistry: acrylamide is formed in the Maillard reaction. Nature 419, 448–449.

Munyuki, G., Jackson, G.E., Venter, G.A., Kövér, K.E., Szilágyi, L., Rautenbach, M., Spathelf, B.M., Bhattacharya, B., Van Der Spoel, D., 2013. β-sheet structures and dimer models of the two major tyrocidines, antimicrobial peptides from *Bacillus aneurinolyticus*. Biochemistry 52, 7798–7806.

Nagaraj, R.H., Shipanova, I.N., Faust, F.M., 1996. Protein cross-linking by the Maillard reaction: Isolation, characterization, and *in vivo* detection of a lysine-lysine cross-link derived from methylglyoxal. J. Biol. Chem. 271, 19338–19345.

Niquet, C., Tessier, F.J., 2007. Free glutamine as a major precursor of brown products and fluorophores in Maillard reaction systems. Amino Acids 33, 165.

Paradies, H.H., 1979. Aggregation of tyrocidine in aqueous solutions. Biochem. Biophys. Res. Commun. 88, 810–817.

Rautenbach, M., Vlok, N.M., Stander, M., Hoppe, H.C., 2007. Inhibition of malaria parasite blood stages by tyrocidines, membrane-active cyclic peptide antibiotics from *Bacillus brevis*. Biochim. Biophys. Acta - Biomembr. 1768, 1488–1497.

Rouabhia, M., Asselin, J., Tazi, N., Messaddeq, Y., Levinson, D., Zhang, Z., 2014. Production of biocompatible and antimicrobial bacterial cellulose polymers functionalized by RGDC grafting groups and gentamicin. ACS Appl. Mater. Interfaces 6, 1439–1446.

Ruttenberg, M.A., King, T., Craig, L.C., 1965. The use of the tyrocidines for the study of conformation and aggregation behavior. J. Am. Chem. Soc. 87, 4196–4198.

Ruttenberg, M.A., King, T.P., Craig, L.C., 1966. The chemistry of tyrocidine. VII. Studies on association behavior and implications regarding conformation. Biochemistry 5, 2857–2864.

Ruttenberg, M.A., Mach, B., 1966. Studies on amino acid substitution in the biosynthesis of the antibiotic polypeptide tyrocidine. Biochemistry 5, 2864–2869.

Salgado, J., Grage, S.L., Kondejewski, L.H., Hodges, R.S., McElhaney, R.N., Ulrich, A.S., 2001. Membrane-bound structure and alignment of the antimicrobial β-sheet peptide gramicidin S derived from angular and distance constraints by solid state ^{19}F-NMR. J. Biomol. NMR 21, 191–208.

Sánchez, J.G.., Kouznetsov, V.V., 2010. Antimycobacterial susceptibility testing methods for natrual products reseach. Brazilian J. Microbiol. 41, 270–277.

Sayanjali, S., Ghanbarzadeh, B., Ghiassifar, S., 2011. Evaluation of antimicrobial and physical properties of edible film based on carboxymethyl cellulose containing potassium sorbate on some mycotoxigenic *Aspergillus species* in fresh pistachios. LWT - Food Sci. Technol. 44, 1133–1138.

Spathelf, B.M., Rautenbach, M., 2009. Anti-listerial activity and structure-activity relationships of the six major tyrocidines, cyclic decapeptides from *Bacillus aneurinolyticus*. Bioorganic Med. Chem. 17, 5541–5548.

Stern, A., Gibbons, W.A., Craig, L.C., 1969. Effect of assosiation on the nuclear magnetic resonance spectra of tyrocidine B. J. Am. Chem. Soc. 91, 2794–2796.

Tang, X.J., Thibault, P., Boyd, R.K., 1992. Characterisation of the tyrocidine and gramicidin fractions of the tyrothricin complex from *Bacillus brevis* using liquid chromatography and mass spectrometry. Int. J. Mass Spectrom. Ion Process. 122, 153–179.

Thies, M., Paradies, H.H., 1997. Self-Assembly of tyrocidines in nanotubular structures. MRS online Proc. Libr. Arch. 489.

Troskie, A.M., de Beer, A., Vosloo, J.A., Jacobs, K., Rautenbach, M., 2014. Inhibition of agronomically relevant fungal phytopathogens by tyrocidines, cyclic antimicrobial peptides isolated from *Bacillus aneurinolyticus*. Microbiology 160, 2089–2101.

van de Lagemaat, M., Grotenhuis, A., van de Belt-Gritter, B., Roest, S., Loontjens, T.J.A., Busscher, H.J., van der Mei, H.C., Ren, Y., 2017. Comparison of methods to evaluate bacterial contact-killing materials. Acta Biomater. 59, 139–147.

Vogt, T.C.B., Schinzel, S., Bechinger, B., 2003. Biosynthesis of isotopically labeled gramicidins and tyrocidins by *Bacillus brevis*. J. Biomol. NMR 26, 1–11.

Vosloo, J.A., Stander, M.A., Leussa, A.N.N., Spathelf, B.M., Rautenbach, M., 2013. Manipulation of the tyrothricin production profile of *Bacillus aneurinolyticus*. Microbiology 159, 2200–2211.

Williams, R.C., Yphantis, D.A., Craig, L.C., 1972. Noncovalent association of tyrocidine B. Biochemistry 11, 70–77.

Zhuang, Y., Sun, L., 2013. Antioxidant activity of maillard reaction products from lysine-glucose model system as related to optical property and copper (II) binding ability. African J. Biotechnol. 10, 6784–6793.